Small Break Critical Discharge -- The Roles of Vapor and Liquid Entrainment in a Stratified Two-Phase Region Upstream of the Break

Prepared by V. E. Schrock, S. T. Revankar, R. Mannheimer, C-H. Wang

Lawrence Berkeley Laboratory

NOTICE

Availability of Reference Materials Cited in NRC Publications

Most documents cited in NRC publications will be available from one of the following sources:

1. The NRC Public Document Room, 1717 H Street, N.W.
   Washington, DC 20555

2. The Superintendent of Documents, U.S. Government Printing Office, Post Office Box 37082, Washington, DC 20013-7082

3. The National Technical Information Service, Springfield, VA 22161

Although the listing that follows represents the majority of documents cited in NRC publications, it is not intended to be exhaustive.

Referenced documents available for inspection and copying for a fee from the NRC Public Document Room include NRC correspondence and internal NRC memoranda; NRC Office of Inspection and Enforcement bulletins, circulars, information notices, inspection and investigation notices; Licensee Event Reports; vendor reports and correspondence; Commission papers; and applicant and licensee documents and correspondence.

The following documents in the NUREG series are available for purchase from the GPO Sales Program: formal NRC staff and contractor reports, NRC-sponsored conference proceedings, and NRC booklets and brochures. Also available are Regulatory Guides, NRC regulations in the *Code of Federal Regulations*, and *Nuclear Regulatory Commission Issuances*.

Documents available from the National Technical Information Service include NUREG series reports and technical reports prepared by other federal agencies and reports prepared by the Atomic Energy Commission, forerunner agency to the Nuclear Regulatory Commission.

Documents available from public and special technical libraries include all open literature items, such as books, journal and periodical articles, and transactions. *Federal Register* notices, federal and state legislation, and congressional reports can usually be obtained from these libraries.

Documents such as theses, dissertations, foreign reports and translations, and non-NRC conference proceedings are available for purchase from the organization sponsoring the publication cited.

Single copies of NRC draft reports are available free, to the extent of supply, upon written request to the Division of Technical Information and Document Control, U.S. Nuclear Regulatory Commission, Washington, DC 20555.

Copies of industry codes and standards used in a substantive manner in the NRC regulatory process are maintained at the NRC Library, 7920 Norfolk Avenue, Bethesda, Maryland, and are available there for reference use by the public. Codes and standards are usually copyrighted and may be purchased from the originating organization or, if they are American National Standards, from the American National Standards Institute, 1430 Broadway, New York, NY 10018.

Small Break Critical Discharge -- The Roles of Vapor and Liquid Entrainment in a Stratified Two- Phase Region Upstream of the Break

Prepared by
V. E. Schrock, S. T. Revankar, R. Mannheimer, C-H. Wang

Lawrence Berkeley Laboratory
University of California
Berkeley, CA 94720

MASTER

ABSTRACT

The analysis of small break loss of coolant accidents is an essential part of light water reactor safety assessment. In these analyses the discharge of primary coolant must be calculated accurately in order to track the primary coolant inventory. In the case of a small break situated on a large horizontal pipe carrying stratified two-phase flow, the effective stagnation state driving the critical discharge depends upon the proximity of the interface in the upstream region to the entrance of the break channel. Vapor pull through and liquid entrainment will determine the inlet quality and hence have a major effect upon the critical flow out the break. This report describes the results of an experimental investigation of steam-water discharge from a stratified upstream region through small diameter break channels oriented at the bottom, top and side of the main channel. The main pipe was 102mm in diameter and the break tubes were 4, 6 and 10mm in diameter and 123mm in length. Both air-water and steam-water were used at pressures up to 1.07 MPa.

The results of this investigation showed that the interface level for incipient gas pull through is not the same for air-water as for steam-water in the same apparatus. This fact pointed up the need to include surface tension and liquid viscosity in a generalized correlation of this phenomenon. A new correlation form involving the relationship between the dimensionless interface level and Froude, Bond and Viscosity numbers, has been shown to accurately represent both the air-water and steam-water data of the present experiments as well as recent air-water data obtained at KfK (Kernforschungszentrum Karlsruhe) in larger scale and steam-water data obtained at INEL (Idaho National Engineering Laboratory) at high pressure and larger scale.

Incipient levels for liquid entrainment were found insensitive to the physical properties (surface tension and liquid viscosity). These results are well correlated in terms of Froude number alone. Quality of the fluid entering the break (following onset of pull through or entrainment) has been correlated in terms of the ratio of interface level at incipient two-phase flow. Use of the new correlations in small break critical discharge evaluations is discussed. In addition the critical discharge data reported here for small diameter tubes adds significantly to the data base for two-phase critical flow.

CONTENTS

APPENDICES

ILLUSTRATIONS

Illustrations (continued)

Illustrations (continued)

NOMENCLATURE

Symbol	Description	Dimension
A	Cross-sectional area of break tube	L^2
Bo	Bond number ($d\sqrt{g\Delta\rho/\sigma}$)	
C_D	Orifice plate discharge coefficient	
D	Inside diameter of test pipe	L
d	Break tube diameter	L
d_o	Air-water separator discharge fitting diameter	L
d_1	Pipe diameter connecting orifice meter	L
d_2	Orifice plate diameter	L
f	Friction factor	
Fr	Froude number ($V/\sqrt{gd}$)	
G	Mass flux	$ML^{-2}t^{-1}$
g	Acceleration due to gravity	Lt^{-2}
h	Liquid gas interface height from break centre	L
h_ℓ	Liquid enthalpy	Lt^{-2}
h_g	Vapor enthalpy	Lt^{-2}
h_{fg}	Latent heat of evaporation	Lt^{-2}
h_L	Liquid height from the bottom of test pipe	L
j	Superficial velocity	Lt^{-1}
L	Length of the break tube	L
LC1	Load cell number 1	
LC2	Load cell number 2	
m	Mass	M
$\dot{m}$	Mass flow rate	Mt^{-1}
N_μ	Viscosity number ($\mu_\ell/(\sigma\rho_\ell\sqrt{\sigma/g\Delta\rho})^{0.5}$)	

NOMENCLATURE (Continued)

Symbol	Description	Dimension
p	Pressure	$ML^{-1}t^{-2}$
Δp	Differential pressure	$ML^{-1}t^{-2}$
Re	Reynolds number	
S_g	Ratio of specific volume of gas with air	
T	Temperature	T
t	Time	t
V	Velocity	Lt^{-1}
v	Volume	L^3
w	Weight of the tank	M
x	Break entrance quality	
Y	Compressibility factor	
z	Length variable	L

Greek Letters

Symbol	Description	Dimension
α	Void fraction	
β	Ratio d_2/d_1	
Γ	Circulation	L^2t^{-1}
γ	Specific heat ratio	
δ	Error	
Δ	Difference	
ε	Surface roughness	L
μ	Viscosity	$ML^{-1}t^{-1}$
ϕ	Phase (1ϕ, single phase, 2ϕ two phase)	
ν	Kinematic viscosity	L^2t^{-1}
ρ	Density at saturation	ML^{-3}

Subscripts

b	Beginning of gas or liquid pull through
c	Critical
cond	Condensation due to heat loss
f	Liquid
g	Gas or saturated vapour
gin	Gas entering test pipe
gout	Gas leaving test pipe
ℓ	Liquid
man	Manometer
o	Pipe stagnation condition or initial
or	Orifice
p	pipe
r	Recirculation loop
T	Total
t	At time t
w	Water

Index

'	Evaluated at pipe inlet from reservoir vessel
"	Evaluated at pipe inlet from recirculation loop

1. INTRODUCTION

1.1 Critical Flow in Nuclear Safety

A knowledge of two-phase critical flow rate is essential for the prediction of effluent rates from an accidental break in a nuclear reactor. The discharge flow rate, resulting from a loss of coolant accident (LOCA) represents a loss of inventory in the cooling system. This coolant loss controls the heat transfer in the core and the depressurization rate of the coolant system.

Phenomena of a large break (e.g., a sheared pipe which contains a flowing fluid) are well defined, though the flow rates from the large breaks may be difficult to predict accurately. On the other hand phenomena of a small break (characterized by a large main channel flow diameter to break flow diameter ratio; $D/d \gg 1$), tend to be more ill-defined. The accident at Three Mile Island (TMI) brought attention of researchers on many aspects of a small break LOCA. The need for small break LOCA flow regime studies lies in the need to predict the spectrum of reactor behavior in small break accidents, where break size and locations are variable.

1.2 Background

Recent studies on large scale small break LOCA experiments LOFT L3-5 [1,2] have revealed that the critical flow rate models incorporated in the computer codes, such as TRAC and RELAP-5, do not adequately predict the loss of coolant or pressure measured. Comparison of the experimental data of LOFT L3-5 test with RELAP-5 and TRAC results, shown in Figure 1-1, indicate that the break mass flow rate is severely overpredicted in early transient. This overprediction will in turn affect the timing of all other events in an accident scenario. Thus a proper and accurate modelling of the small break LOCA is necessary for better prediction of experimental data. Hence investigation of small break simple separate effects experiments are needed where the break has well defined size and location. This has been one motivation for the present experimental program.

Contrary to a large break or severed duct (where the reactor coolant flows through the entire cross section), when a small break LOCA occurs in a pipe the geometry of the system at the break as well as the flow pattern in the vicinity of the break is of great concern. Because of slow depressurization rates which would accompany a small break LOCA, the steam and water can separate and lead to a stratified two-phase flow in the horizontal sections of the system [3]. Under these conditions the position of the break relative to the steam water interface governs the flow pattern which in turn greatly affects the amount of coolant leaving the system through the break. The various two-phase phenomena
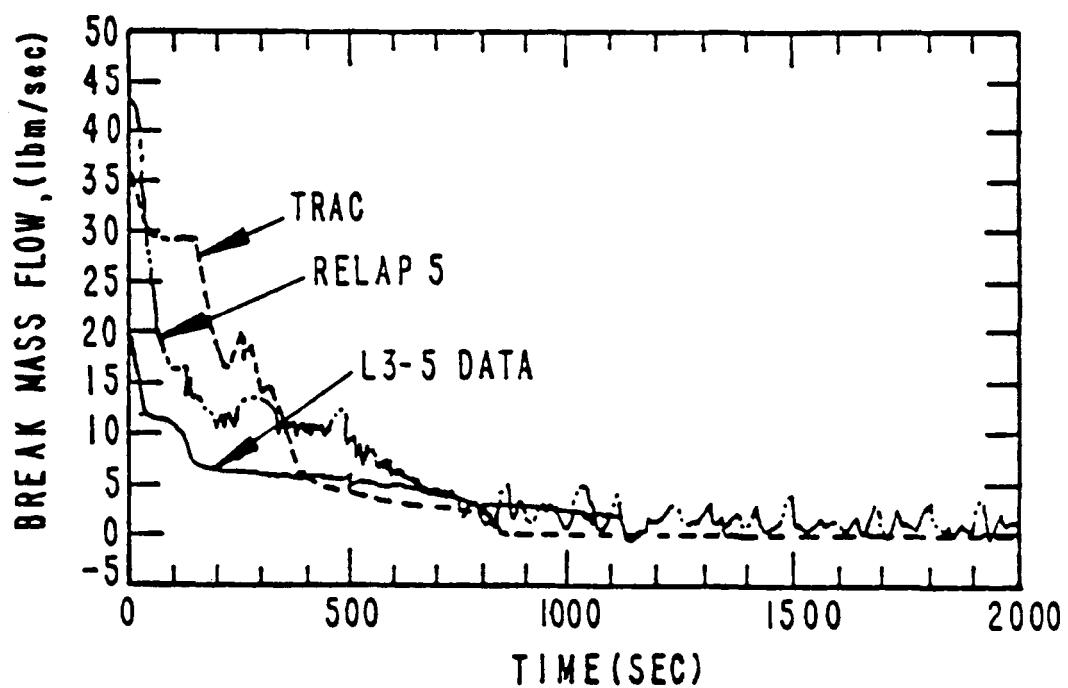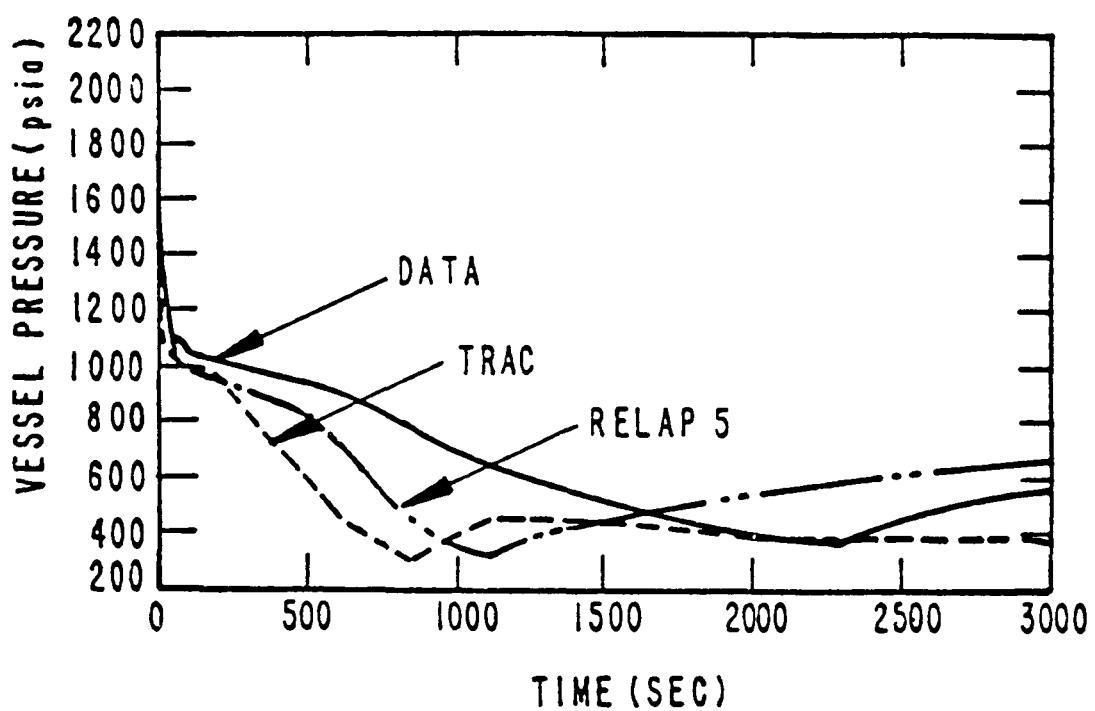
Figure 1-1   Comparison of Calculated and Measured Behavior for
LOFT Test

which may occur in horizontal pipes during a small break LOCA have been discussed by Zuber [4].

In the steam generator steam may be condensed and produce liquid which flows back to the vessel through the hot leg. This can cause a counter-current stratified flow in the hot leg. The mass flow through the break will then depend on the geometry of the fluid at the break. When a small break or fracture occurs below the liquid level in a horizontal pipe which is carrying a two-phase stratified flow a vortex accompanied by vapor pull-through may establish itself at the entrance to the break as shown in Figure 1-2 for bottom oriented break. The quality entering the break depends on the height of the liquid-vapor interface above the break. With the break located above the horizontal interface, liquid can be entrained due to vapor acceleration (Bernoulli effect). For the break at the level of vapor liquid interface, the flow pattern at the break may take the combined features of top and bottom break flow explained above.

In the published literature few data are available on critical flow from small break in a pipe with stratified two-phase flow that are pertinent to reactor accident situations. Recently for such flow geometries, critical flow experiments were performed by Crowley and Rothe [5] for side, top and bottom breaks, by Reimann and Smoglie [6,7,8] for top and side oriented break, and by Reimann and Khan [9] for bottom oriented break. The data of Reimann et al. [6,7,8,9] will be referred as KfK data in this report. These works were performed with air-water flow. Series of steam-water tests were carried out by Anderson [10] at the Idaho National Engineering Laboratories (INEL) for side and bottom oriented branches of a horizontal pipe. These data cover a pressure range of 3.4 - 6.2 MPa. However, there are no other data available on steam-water flow system for such flow geometries, except the data from INEL [10].

1.3 Objectives

The main objective of this research program was to perform an experimental investigation on the phenomena of two-phase critical flow through small break from a horizontal pipe which contained a stratified two phase flow. Stagnation conditions investigated were saturated steam-water, and air-cold water at pressures ranging from 0.37 MPa to 1.07 MPa. The small breaks employed were cylindrical tubes of diameters 3.96 mm, 6.32 mm, and 10.1 mm with sharp-edged entrance. For breaks resulting from a small hole in a primary coolant pipe or in a small pipe, a sharp-edged orifice or a sharp-edged tube can be the approximation. The specific purposes of this research programs were to:

• Measure and correlate to system variables the interface level for incipient entrainment of the second phase at the entrance to bottom, side and top branch (breaks) lines.
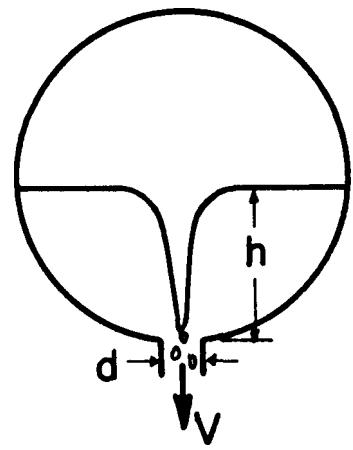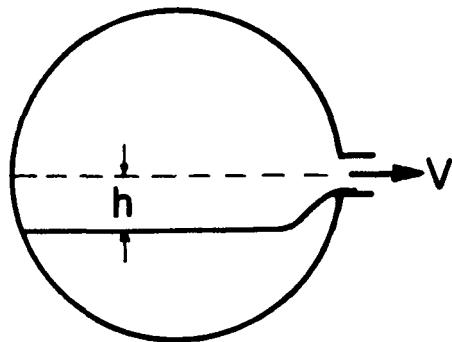
Bottom Break   **Side Break**   **Top Break**
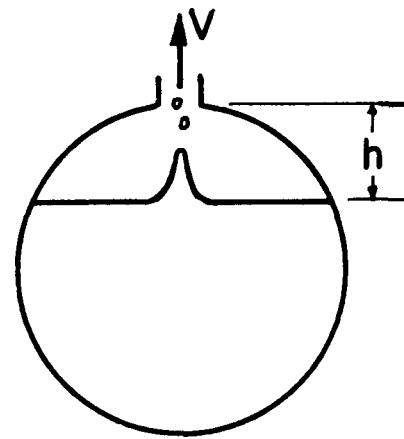
Figure 1-2   Schematic of Pull-Through and Entrainment from Stratified Region

- Measure gas/vapor and liquid flow rates and hence flow quality at the break entrance with stratified flow in horizontal pipe, and relate the measured quantities to the stratified level and the thermohydraulic conditions in the main line for bottom, side and top break orientations.

- Observe and document the flow patterns for various break orientations.

- Establish a data base for steam-water flow for all the system geometries described above for the pressures up to 1 MPa.

- Establish a general relationship relating discharge rate and the level in the mainline using present,' KfK and INEL data.

1.4 Experimental Program

The preliminary experimental study was carried out with a glass test section for ease of visual observations. Ten runs were carried out on this system to evaluate and calibrate the instrument under operation and to set a procedure of operation for the rest of the test runs. Because the glass system failed a metallic test section with windows was used for the rest of the experiments. A series of tests were conducted with bottom, side and top oriented break for single phase and two phase, air-water and steam-water flows. Run numbers for tests were assigned in the order that they were carried out. Inception data for gas pull-through and liquid entrainment were collected for all the three orientations for steam-water and air-water flows. In case of two-phase flows, for each stagnation pressure at least three different heights of liquid-gas interface level were used to study liquid entrainment and gas pull-through phenomena. Run numbers for bottom oriented break studies were assigned from 1 to 200, for top oriented break studies from 201 - 300 and for side oriented break from 301 - 400.

2. PREVIOUS RESEARCH

As summaries on studies of two phase critical flow are available in recent literature [11,12] only those works, which are directly relevant to the topic of present experimental study are considered for discussion in the present chapter.

Zuber [4] has discussed the important nonhomogeneous two-phase flow phenomena which may occur in a horizontal pipe during a small break LOCA. He also presented a summary of the existing experimental work and correlations for the onset of vapor pull-through and liquid entrainment. Crowley and Rothe [5] performed air-water experiments at a system pressure of 0.3 MPa in a horizontal 66.6 mm ID pipe with a 6.3 mm ID orifice break. They obtained data for the side, bottom and top oriented flow configurations with short nozzle and orifice as break at the pipe wall. Subsequently Reimann and Smoglie [6] studied liquid entrainment from a top oriented break with stratified air-water flow in a 206 mm mainline pipe and 3 different break tube of diameters, 6, 12 and 20 mm. These same break and pipe sizes were used by Reimann and Khan [9] to study vapor pull-through phenomena in a bottom oriented break at a systems pressure of 0.5 MPa and for various differential pressures across the break tube. Also Smoglie [7] studied liquid entrainment and vapor pull-through phenomena for side branch configurations and presented all the KfK data for the three break tube orientations. The experimental investigations carried out at INEL [10] for the phenomena of liquid entrainment and vapor pull-through provided data for steam water flows at system pressures of 3.4, 4.4 and 6.2 MPa. The INEL experiments used 284 mm ID mainpipe with the branch line of 34 mm ID, and had a nozzle installed at the downstream part of the branch line to give the location of choking.

2.1 Liquid Entrainment

Several mechanisms may cause liquid entrainment with steam through small breaks in pipes with stratified steam-water flow. Vapor acceleration in the vicinity of the break, liquid flashing and bubble bursting or interfacial shearing, any one or combination of these mechanisms may lead to entrainment of liquid. An expression obtained through experimental study of the formation of the non-circulatory waterspouts was presented by Rouse [13], for air-water and freshwater-saline water systems, with pipes of different diameters (13.7 mm, 38.1 mm and 78 mm). Data were fit by the relationship for the onset of liquid entrainment from a large reservoir through a pipe situated at a distance h above the liquid surface given as

$$Fr_g \left[\frac{\rho_g}{\Delta\rho} \right]^{0.5} = 5.67 \left(\frac{h_b}{d} \right)^2 \tag{2.1}$$

and no capillary or viscous effects were observed. A similar correlation for onset of liquid entrainment through side orifices derived by Craya [14], and verified by Gariel [15] and by Crowley and Rothe [5] is given by

$$Fr_g \left[\frac{\rho_g}{\Delta\rho} \right]^{0.5} = A \left(\frac{h_b}{d} \right)^{2.5}$$

(2.2)

with A = 3.25.

KfK data of onset of liquid entrainment when expressed in terms of equation (2.2) gave the value of the constant A as 0.35 for top oriented break and 3.22 for side oriented break. The KfK data also showed that the superimposed velocities on either phase of the stratified two-phase system may affect the value of constant A and the exponent on RHS of equation (2.2). As has been suggested by Zuber [4], in the available correlations the constant A and/or the exponent on RHS of equation (2.2) may be different for PWR conditions. However, these correlations show that the break location with respect to the interface level and the break geometry have an important effect on the correlations predicting onset of liquid entrainment through breaks. The effect of water flashing and interfacial shearing or slug formation due to high velocity steam, on the liquid entrainment through breaks have been discussed by Hardy and Richter [16]. The INEL liquid entrainment data for a side oriented branch were obtained based upon extrapolation of the mean flow quality versus mainline liquid level for three sets of data. These three data when correlated with equation (2.2) gave approximately A = 4.21.

2.2 Vapor Pull-Through

When the break is located below the horizontal interface, vapor can reach the break by being pulled through with a vortex or vortex free flow. For vapor pull-through due to vortex formation near the drain at the bottom of large vessel, Daggett and Keulegan [17] presented a correlation;

$$\frac{h_b}{d} = 35 \times 10^{-3} \; \Gamma/\nu_\ell \quad \text{for} \quad \frac{Vd}{\nu_\ell} < 5 \times 10^4$$

(2.3)

$$\frac{h_b}{d} = 150 \; \frac{\Gamma}{Vd} \quad \text{for} \quad \frac{Vd}{\nu_\ell} \geq 5 \times 10^4$$

(2.4)

These correlations were obtained for axisymmetric geometries with defined circulation Γ. Studies [18-20] on the vortex formation at intakes in conventional pump sumps have suggested a correlation for onset of pull-through as

$$Fr_\ell \left[\frac{\rho_\ell}{\Delta\rho}\right]^{0.5} = B \left(\frac{h_b}{d}\right)^C \qquad (2.5)$$

where B was dependent on the intake geometry and the exponent C was a positive constant.

Studies [21-24] carried out on the vapor pull-through from the free surface of the liquid draining from a cylindrical tank through a axisymmetric drain, showed that the vapor pull-through was caused by large-amplitude deformation of the liquid surface with vortex free gas ingestion.

Lubin and Springer [22] matched their experimental data using equation (2.5) with constants B = 3.22 and C = 2.5. Experimental studies of Lubin and Hurwitz [23], showed a strong dependence on the viscosity of the lower fluid on the vapor pull-through phenomena. Subsequent theoretical analysis by Easton and Catton [24], considered the surface tension effect and the pull-through height was correlated with Froud number and Bond number, however, the effect of viscosity was neglected.

Reiman and Khan [9] studied in detail the formation of a vortex at the break during gas pull-through for three type of flow geometries: (a) the symmetric in flow, which exists when a large liquid flow rates are available on either side of break, (b) the inflow to break from one side, which exists when one end of pipe is closed and (c) stratified flow in the horizontal main pipe at a rate greater than the break flow rate. For the case (c) a resultant liquid flow perpendicular to the break axis exists whereas for case (a) and (b) it does not. In the latter cases the situation favors the formation of vortex flow. Reimann and Khan observed vortex induced vapor pull-through for cases (a) and (b). They fitted their experimental data for vortex induced pull-through with the correlation given by equation (2.5), with constants B = 0.2 and C = 2.5. Crowley and Rothe [5] also used equation (2.5) to reproduce their air-water experimental results for bottom oriented breaks in pipes. In case of flow geometry (c), Reimann and Khan observed vortex free vapor pull-through and proposed a correlation in this case as

$$Fr_\ell \left[\frac{\rho_\ell}{\Delta\rho}\right]^{0.5} = B \left(\frac{h_b}{d}\right)^{2.5} \qquad (2.6)$$

with B = 0.94 for inception of first bubble pull-through and B = 1.1 for onset of continuous gas pull-through.

In the case of side breaks, KfK data when correlated with equation (2.6) gave the value of B = 2.61. The INEL data for onset of vapor pull-through were obtained based on the response of a pressure transducer connected between the main pipe and the break, where the onset of first bubble was identified by a sharp increase in the noise level on the pressure transducer response and the onset of continuous

2-3

pull-through was identified by an abrupt drop in the level of pressure drop. Because of the small number of data (three data points) no attempt was made to find an independent correlation for incipient pull-through. Instead equation (2.6) was used to find the constant B. Thus the values of B obtained in case of a side break was 2.09 and in case of a bottom oriented break B = 1.27.

2.3 Break Flow Rate and Quality

Crowley and Rothe [5] presented water and air flow rate data (at pipe pressure of 282 kPa, d = 6.35 mm and D = 76 mm) as a function of liquid level in the pipe for the side break and found agreement between measured and calculated single phase flow rates. The KfK data were presented in terms of quality as a function of nondimensional interface level for side, top and bottom oriented branches for air-water flows. For the side break the results were correlated by

$$x = x_0^{\left(1+C\frac{h}{h_b}\right)} \left[1 - \frac{1}{2}\frac{h}{h_b}\left(1+\frac{h}{h_b}\right) x_0^{\left(1-\frac{h}{h_b}\right)}\right]^{0.5} \qquad (2.7)$$

where x_0 = 0.075, the value of quality at h = 0

and C = 1   for $h/h_b \le 0$ (Liquid entrainment)

= 1.09 for $h/h_b > 0$ (Vapor pull-through).

For the bottom break, the correlation for quality was

$$x = \left(\frac{1.15}{1+\sqrt{\rho_\ell/\rho_g}}\right)^{2.5\frac{h}{h_b}} \left[1 - \frac{1}{2}\frac{h}{h_b}\left(1+\frac{h}{h_b}\right)\left(\frac{1.15}{1+\sqrt{\rho_\ell/\rho_g}}\right)^{\left(1-\frac{h}{h_b}\right)}\right]^{0.5} \qquad (2.8)$$

For the top oriented branch the quality correlation was

$$x = 1 - \left(\frac{1.15}{1+\sqrt{\rho_\ell/\rho_g}}\right)^{2\left(\frac{h}{h_b}\right)} \left[1 - \frac{1}{2}\frac{h}{h_b}\left(1+\frac{h}{h_b}\right)\left(\frac{1.15}{1+\sqrt{\rho_\ell/\rho_g}}\right)^{\left(1-\frac{h}{h_b}\right)}\right]^{0.5} \qquad (2.9)$$

INEL data were presented in terms of branch mass flux, quality and void fraction as a function of liquid level for side and bottom oriented branches for steam-water flows at system pressures of 3.4, 4.4 and 6.2 MPa. From observations of data trends, the correlations

for quality were presented using exponential relations. For side oriented breaks, the branch line quality was given as,

$$
x = \begin{cases} 0 & \text{for} \quad h > h_1 \\[2ex] \exp\left[C_x \left(\dfrac{h-h_1}{h_1-h_2} \right) \right] & \text{for} \quad h_2 \le h \le h_1 \\[2ex] 1 & \text{for} \quad h < h_2 \end{cases} \tag{2.10}
$$

where C_x is -3.8 for 3.4 MPa, -3.6 for 4.4 MPa and -3.4 for 6.2 MPa, and h_1 and h_2 are the incipient heights for vapor pull-through and liquid entrainment, respectively, observed in INEL tests at each pressure.

For bottom flow the INEL quality correlation was

$$
x = \begin{cases} 1 & \text{for} \quad h < a \\[2ex] \exp\left[C_{vx} \left(\dfrac{h-a}{h_1} \right) \right] & \text{for} \quad a \le h \le h_1 \\[2ex] 0 & \text{for} \quad h > h_1 \end{cases} \tag{2.11}
$$

where a = 1.7cm and C_{vx} = -4.7.

Using the incipient heights h_1 and h_2 from INEL experiments, the KfK correlation given by equation (2.7), when compared against INEL quality vs liquid level data for the side break configuration, showed discrepancies in quality corresponding to liquid level h = D/2 of 200% for 6.2 MPa, 170% for 4.4 MPa and 150% for 3.45 MPa. For vertical down flow configuration the KfK correlation given by equation (2.8) showed a poor agreement ($\sim$1000% error in quality) when compared against INEL data.

3. DESCRIPTION OF THE EXPERIMENTAL FACILITY

Major components of the experimental apparatus are, a water reservoir vessel, a horizontal test pipe, a recirculation loop, and a discharge section with tee. A schematic of the test facility is shown in Figure 3-1. The main objective in the design of the apparatus was to provide constant water and steam (or air) flow rates in the horizontal test pipe, and to maintain steady stagnation state of the fluid entering the break.

The flow of the water from the reservoir to test pipe was controlled using regulating needle valve. Steam regulating valves were used to control the air/steam flow in to and out of the test pipe which also regulated the pressure in the pipe. For air-water tests under 650 kPa, compressed air from laboratory supply lines was used to pressurize the reservoir and supply air to the test section. Because the laboratory air supply pressure was limited, compressed nitrogen cylinders were used for higher pressure (650 to 1065 kPa) air-water test runs. The gas pressure supplied to the reservoir was controlled by a standard pressure regulator. The steam/air leaving the test pipe was discharged to a quench tank. In the case of saturated steam-water tests the water in the reservoir vessel was heated using electric heaters in order to maintain the desired pressure while generating the desired steam flow-rate. Saturation pressures from 15 to 35 kPa above the desired test pipe stagnation conditions were maintained in the reservoir vessel. The temperature within the vessel and at the vessel wall was monitored with thermocouples during the heatup period and during the test runs. The pressure and temperature data were collected using an automatic data collection system.

In Figure 3-2 a photograph of the experimental facility is shown. In the following sections the descriptions of each of the components of the equipment are presented.

3.1 Reservoir Vessel

The reservoir vessel served as both the reservoir for saturated water and steam. The vessel was constructed from a 2.743 m length of 12" IPS Schedule 5 stainless steel pipe. The inside diameter of the pipe is nominally 31.54 cm with wall thickness of 0.419 cm. Both ends of the pipe were welded on to 12" IPS Schedule 10 pipe caps. To the top cap, 1" and 1/4" IPS couplings were welded and to the cap at the bottom end, couplings of 2.5", 0.5" and 0.25" IPS were welded. At the height of 10" from the bottom end another coupling of 1.5" IPS was welded on to the pipe wall. All the couplings used were Schedule 150, 304 stainless steel threaded pipe fittings.

A heater unit was installed at the bottom of the reservoir vessel through the 2.5" coupling. This heater was a 12 kW tubular immersion

Reservoir Blowdown Line

Steam/Air
Feed Line

⊘ Pressure Guage
○ Thermocouple
▢ Pressure Transducer
▽ Load Cell

Reservoir

Water Return Line from Separator

Air Supply
Line

Water
Feed Line

Test Pipe

Test
Section

Top Water

To Drain
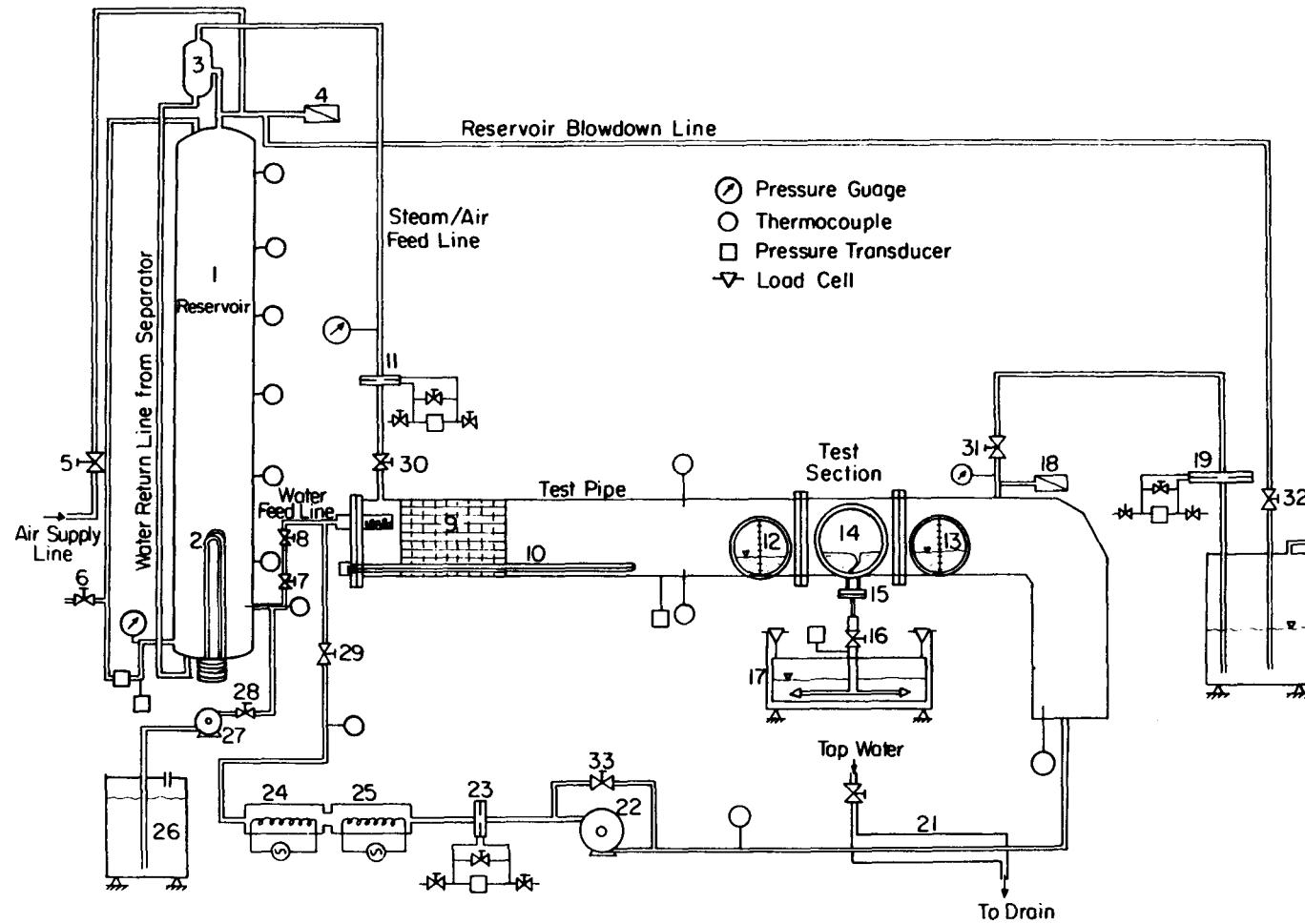
Figure 3-1 Schematic of Experimental Facility

TABLE 3-1

Key to Figure 3-1

Component Number	Description
1	Pressure Vessel Steam Water Reservoir
2	Pressure Vessel Immersion Heaters
3	Steam Separator
4	Reservoir Pressure Relief Valve
5	Air/Nitrogen Supply Shut-Off Valve
6	Vessel Vent Line Valve
7	Water Feed Regulating Valve
8	Water Feed Shut-Off Valve
9	Honeycombed Test Pipe Flow Homogenizer
10	Test Pipe Immersion Heater
11	Gas Entry Orifice Meter
12	Upstream View Window for Liquid Level Indicator
13	Downstream View Window for Liquid Level Indicator
14	Test Section Flow Entry View Window
15	Break Discharge Section
16	Break Discharge Gate Valve
17	Weigh Tank
18	Test Pipe Pressure Relief Valve
19	Gas Exit Orifice Meter
20	Quench Tank
21	Double Pipe Heat Exchanger
22	Water Recirculation Pump
23	Water Recirculation Orifice Meter
24	Water Recirculation Reheater
25	Water Recirculation Reheater
26	Distilled Water Storage Tank
27	Reservoir Fill Pump
28	Reservoir Fill Line Regulating Valve
29	Recirculation Rate Regulating Valve
30	Gas Entry Regulating Valve
31	Gas Exit Regulating Valve
32	Reservoir Blowdown Regulating Valve
33	Pump Bypass Line Regulating Valve
34	Heat Exchanger Cold Water Feed Regulating Valve
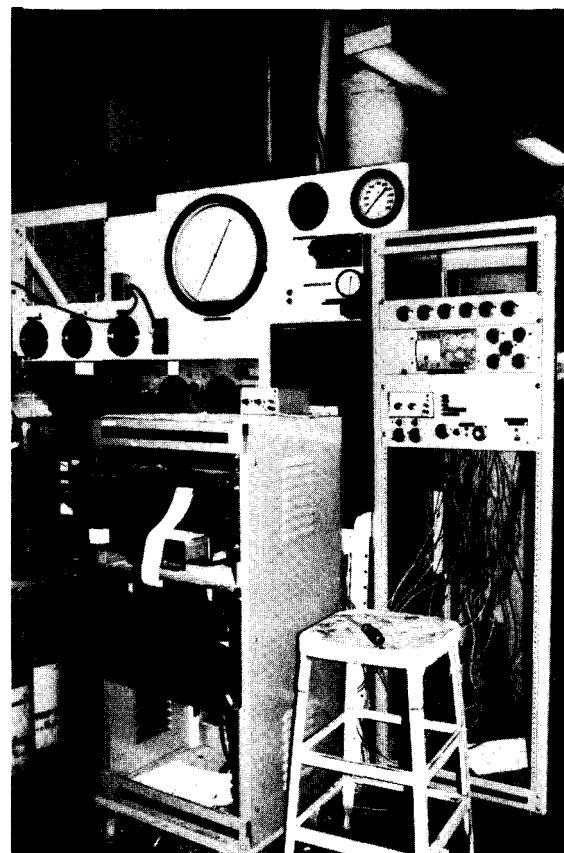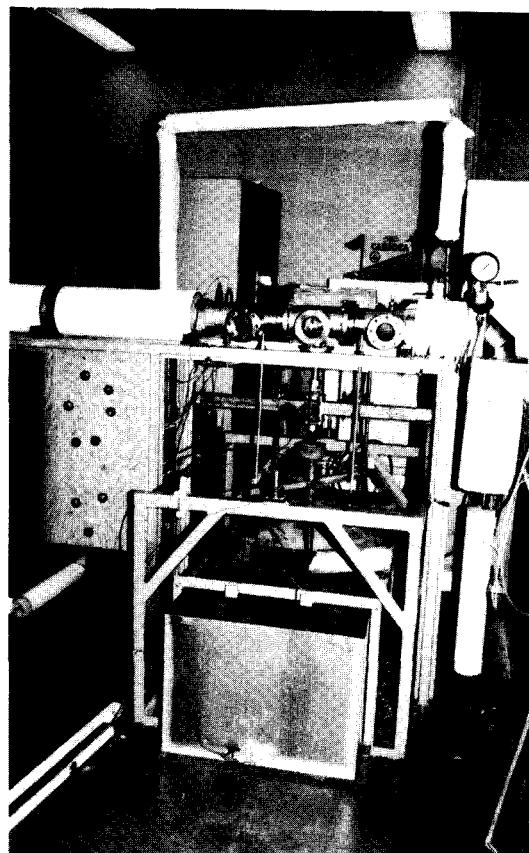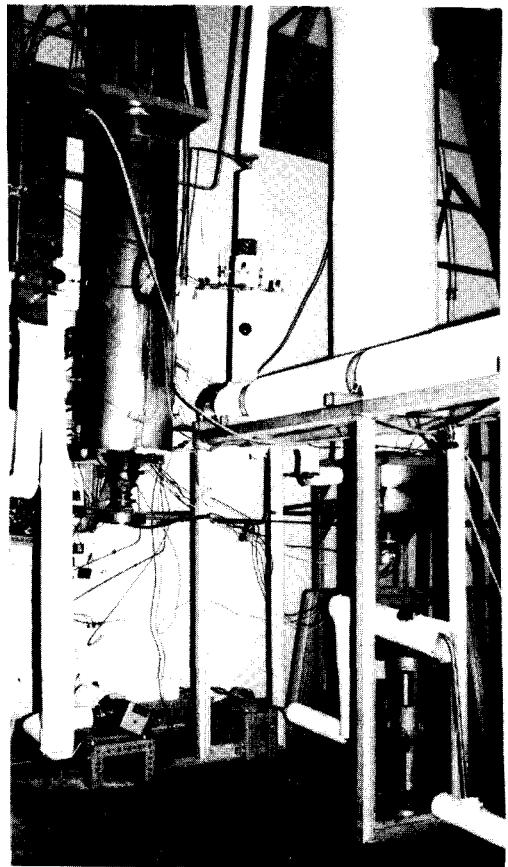
Figure 3-2 Photograph of Experimental Facility

heater comprised of three individually controlled 4 kW units. The heater sheaths were 1 cm in outer diameter and were made of stainless steel for corrosion resistance. The total length of heater was 33". The heater units were each hooked up to separate 220 V fixed and 120 V variable power lines. For fast heating the heaters could be switched to 220 V power. In this configuration the heaters provide the total power of 12 kW. When the water reached the required saturation temperature, the heaters were switched to the 120 V autotransformers, which enabled control of the power for each heater unit from 0-2 kW. For switching the heater to these power levels a 4-pole double-throw switch was used for each unit. The power lines were each provided with 5 Amper breakers for safety.

A water feed line of 1.27 cm diameter was connected to the reservoir vessel using a reducer bushing and Swagelok fittings. The water feed line included a flexible stainless steel hose of 0.6 m long to prevent flow disturbances propagating to the test pipe and to avoid thermal stresses. A needle valve was provided on the feed line for fine control of flow rate to the test pipe. A shut-off valve was connected in series with the needle valve.

A steam separator tank was connected to the top end of the vessel. From the top of the separator tank a steam feed line was connected to the test pipe. From this separator tank, a water return line was routed to the bottom end of the vessel. Stainless steel tubing of 1.27 cm O.D. was used for these lines. A pressure relief valve, set at 1.3 MPa was installed at the top of the vessel for safety. A separate line was routed to the steam quench tank from the top of the vessel to blow down the pressure whenever required. To provide a compressed air/nitrogen supply, a line was connected to the top of the reservoir vessel with a pressure regulator in the supply line.

The stagnation temperature and pressure were measured by the thermocouple and pressure tap located near the water feed line connection at the lower end of the vessel. To determine the water level in the reservoir vessel, a differential pressure transducer was used to measure the pressure head of the water in the constant area portion of the vessel. Stainless steel tubing of 0.63 cm O.D. was used for pressure sense lines. In addition to a Statham absolute pressure transducer, a precision pressure gauge (Heise) was also connected to the bottom of the vessel to monitor the vessel's absolute pressure. Six iron-constantan thermocouple junctions were soldered onto the reservoir vessel wall at equal distances along its length. The temperature measured by these thermocouples gave an estimate of the water temperature in the reservoir. To prevent excessive heat loss from the vessel, a 5 cm thick layer of fibre glass pipe insulation was applied to the outside surface of the reservoir. Also all the pipe and tube lines were covered with 2.5 cm thick fibre glass pipe insulation.

3.2 Test Pipe

3.2.1 Glass Test Pipe

Initially, to provide the best viewing facility for the two-phase
stratified flow and the flow pattern near the break, the test pipe was
made of glass. The glass test pipe was made of a nominal 4" beaded
pressure Corning pyrex glass pipe. It consisted of four sections of
pipe, one 183 cm, and three 35.5 cm long, all joined in series with
one-bolt couplings. One 35.5 cm long section had two 1" tees on
opposite sides in the middle region. To one of the tees a discharge
tube was connected. Onto the tees associated with other parts of the
test pipe, the steam/air feed line, steam exit line, pressure sense
lines were connected. The relative position of these connections were
similar to those explained in the following metal test pipe descrip-
tion. The end flange at the upstream end of the pipe is the same one
that has been used in metallic system. As the recirculation system
was not used with glass system the downstream end of horizontal pipe
was closed with a blind flange. The remaining features were as
explained in the metal pipe description. The glass test pipe failed
during a run carried out with air-water two phase discharge at 60 psig
stagnation pipe pressure. However, the glass pipe was provided with
a protective case of 0.64 cm thick lucite glass sheet cover that pre-
vented injury to the persons working with the equipment. As the
manufacturer had quoted 50 psig as the maximum working pressure on this
glass pipe with a generous safety factor, it had been decided to use
the system up to 75 psig. After the failure of the glass pipe, a
metallic test pipe was designed and fabricated capable of operating up
to 200 psig with glass windows to provide viewing of the fluid
interfaces.

3.2.2 Metal Test Pipe

The metallic test pipe consisted of three parts; an upstream section,
test section, and a downstream section. The test section is described
in the following section. The upstream and downstream parts of the
test pipe were constructed from 4" IPS Schedule 40 stainless steel
pipe. The inside diameter of the pipe is nominally 10.22 cm with wall
thickness of 0.602 cm. The upstream part of the pipe is 260 cm long
with a end flange connected to a blind flange at one end of the pipe.
The blind flange has been welded with a 2.5" threaded coupling to which
the water feed lines from the reservoir vessel and the recirculation
unit were connected with reducer bushing and Swagelok fittings. The
steam/air feed line was connected to the upstream part of the test
pipe near the water feed line. A tubular 4 kW electric heater was
placed inside parallel to the pipe axis and close to the bottom of the
pipe to maintain the fluid temperature and pipe pressure at required
steady value. The heater sheath was 0.66 cm in diameter and was made
of Incaloy. The heater had a minimum radius hairpin bend at its mid-
point with an overall length of 333 cm. The threaded bushings at the
base of heaters were welded to the blind flange that was connected to
the upstream pipe section. Along the length of the narrow U-shaped

heater several guard rings were provided for structural integrity. A honeycomb shaped flow homogenizer made of stainless steel plates was mounted inside the pipe near the fluid entry region. The flow homogenizer helped to get smooth stratified two-phase flow in the pipe.

To the other end of the upstream part of the test pipe a flange is welded that matches with the test section. Near this flange a viewing window is provided with the purpose of observing and recording the liquid/gas interface level upstream of the break. The window is made of a disc-shaped 2.5 cm thick and 7.62 cm diameter optical quartz glass. To provide the viewing facility a 6.35 cm hole was drilled in the test pipe, and a 5 cm long 6.35 cm ID stainless steel pipe was welded on to the pipe as a tee branch.. The other end of this pipe was flanged for mounting the window assembly. The mounting arrangement is such that the glass window is sandwiched with viton gaskets and flanges on either side to provide an arrangement of clamped-edge-mounting. An identical window is provided on the down stream part of the test pipe so that the liquid level downstream of the break can be measured. Two stainless steel rods of 0.16 mm diameter were machined and wire rings were installed at equal distances of 6.35 mm along its length. These rods were used to measure the water level inside the pipe. They were mounted vertically down inside the center of the pipe so that the rods can be viewed through the windows. For the earlier glass test pipe these level measuring rods were mounted at the top tee of test section, such that they were situated in a vertical position about 10 cm on either side of the break position.

The down stream part of the test section has a 46 cm long horizontal section, a 90^0 elbow and 51 cm long vertical downward oriented section. The bottom end of the vertical section is welded with a 1.25 cm thick stainless steel disc. This end plug disc has a coupling welded onto it through which a recirculation line is connected. Near the end of the horizontal portion of the test pipe a steam exit line is connected. It leads to the quench tank. A pressure relief valve, set at 1.1 MPa, is provided on the test pipe for safety. To measure the stagnation pipe pressure, pipe steam and liquid temperatures, pressure sense lines and thermocouples are provided on the upstream and downstream parts of the test section. The test pipe was insulated with 3.8 cm thick fibre glass pipe insulation except at the viewing windows which were insulated by a dead air space outside the windows.

3.3 Test Section

The test section is 58 cm long with flanges at both ends that match to the upstream and downstream parts of the test pipe. The test section has a 1" tee where the break tube is mounted. In order to have a clear view of the flow pattern at the discharge tube entrance, the test section has two quartz glass windows 7.6 cm in diameter installed on opposite sides of the test section. The windows are aligned vertically

off-centered toward the break so that the break entrance can be observed more clearly.

The small break sections are made of straight sections of stainless steel tubes with a flange that fits into the 1" tee branch of the test section. A break tube of 2.95 mm ID and 12.35 cm long was used for the tests carried out on the glass test pipe. Break tubes of 3.76 mm, 3.96 mm, 6.32 mm and 10.15 mm ID were constructed for experimental tests. The break tubes each have five pressure taps distributed along their length. The pressure tap locations and the mounting of the break tube onto the tee branch of test section is shown in Figure 3-3. The pressure transducer connections between the taps are also indicated in Figure 3-3. Table 3-2 gives the various test break tube systems used in the present experimental program. A photograph of the 6.32 mm ID break section is shown in Figure 3-4.

The test section can be mounted, in between the upstream and downstream parts of the test pipe for bottom, side and top orientation of the break tube with respect to the horizontal test pipe. The break tube discharges into a larger diameter discharge line which is fitted with a gate valve. The opening of the valve starts the discharge of the fluid from the break tube.

3.4 Recirculation Loop

To provide a component of flow velocity to the stratified fluid in the horizontal test pipe, a circulation loop was constructed. A centrifugal pump was used to pump the liquid from the downstream end of the test pipe back to test pipe water feed line. Because the saturation temperature of the water at operating pressures (up to 1 MPa) was higher than the temperature ($110^{\circ}C$) that the recirculation pump can handle, a double pipe heat exchanger cooled by a tap water was installed between downstream end of the test pipe and the pump. A bypass line was provided across the pump to keep the operating point within the pump performance range. Two 5 kW reheaters were installed in series in between the recirculation pump outlet and the test pipe water feed line to reheat the pumped water. The heaters are U shaped Incaloy sheathed tubular heaters encased in a 2.5" ID stainless steel pipe with threaded reducer fittings of 0.5" for the fluid inlet and outlet connections. The power to each of these two reheaters was controlled by 220 V variable autotransformer. A valve downstream of the heaters was used to control the flow rate of water in the recirculation system. The flow rate was measured with an orifice meter, installed between the recirculation pump and the reheaters, together with a differential pressure transducer. The temperature of the liquid entering the test pipe feed line was controlled by the heater power and heat exchanger cooling. Thermocouples were installed between the pump and heat exchanger and between the feed line and the reheaters. All the piping in the recirculation loop was 0.5" stainless steel pipe. The piping
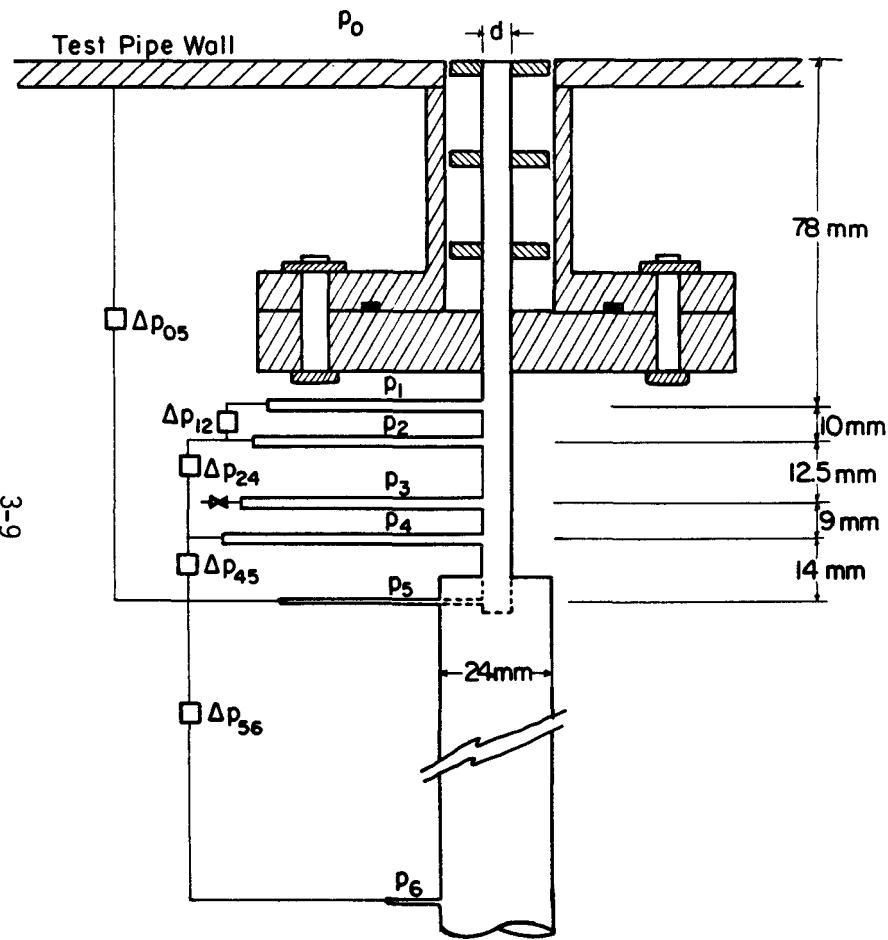
Figure 3-3   Test Section and Its
Mounting Onto Test Pipe
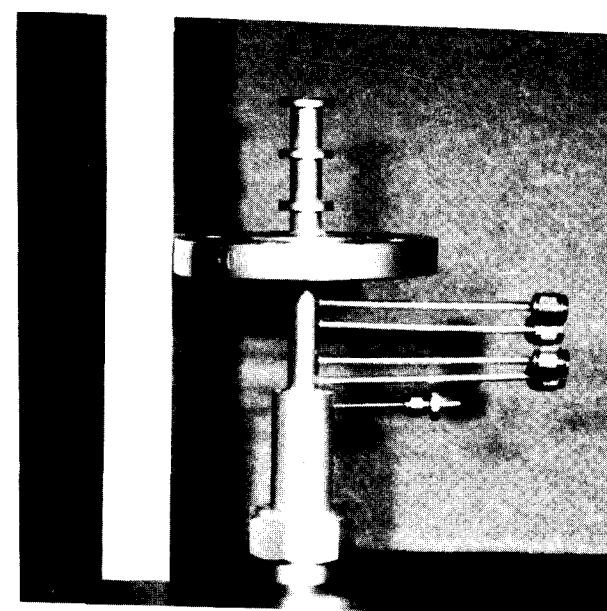
Figure 3-4   Photograph of Test Section,
Break ID d = 6.32 mm

TABLE 3-2

Break Geometry

Notation for Test Break Tube	d (mm)	L (cm)	Distance of pressure tap location from entrance (cm)				
			P_1	P_2	P_3	P_4	P_5
1G	2.95	12.35	7.8	8.8	10.05	10.95	12.30
1A	3.91 (3.62*)	12.35	7.8	8.8	10.05	10.95	12.30
1B	3.76	12.30	7.6	8.6	10.05	11.05	12.25
1	3.96	12.30	7.85	8.8	10.05	10.95	12.25
2	6.32	12.10	7.6	8.6	9.85	10.75	12.05
3	10.15	12.35	8.05	9.0	10.5	11.35	12.30

-DN, - SD, - UP, represent respectively downward, side and upward orientation of the discharge tube with respect to the horizontal test pipe.

*This discharge tube had a smaller diameter at entrance forming a smooth edged orifice with diameter 3.62 cm.

and heaters were all insulated with 2.5 cm thick fiber glass pipe insulation.

3.5 Water Supply

Water for the experiments was distilled in a single stage still and was stored in two tanks each with a capacity of 0.21 m^3. A small centrifugal pump with a capacity of two litres per minute under a 3 m head was used to pump water from the tanks to the reservoir vessel. For cold water test runs, the discharged water was collected in the weigh tank and was reused after passing it through a filter.

3.6 Weigh Tank and Steam Suppression System

The weigh tank and steam suppression system used in the present apparatus was taken from a earlier experimental facility (Amos and Schrock [25]). The piping downstream of the discharge tube was constructed of 2.5 cm OD brass tubing. A gate valve controls the opening and closing of the fluid discharge. In Figure 3-5 a photograph of the condensing nozzle system is shown. A gap of about 4 cm was allowed between the H-shaped nozzle system and the bottom of the weigh tank. The nozzles were kept submerged at least 5 cm below the surface of the water in the weigh tank. The weigh tank was suspended on load cells described in section 3.7.3.

3.7 Data Collection and Instrumentation

Data were collected with a Vidar AutoData Eight data collection system. The Auto-Data was operated in a continuous mode with printer on. In the experiments, 26 channels were used and the data was recorded on paper tape. The data were printed on paper tape at an average rate of 2.275 lines per second. Two measurement ranges were utilized: 100 mV and 10 V. All the signals were D-C inputs. Except for two Validyne transducers all the measurements were in the 0-100 mV range. Temperature measurements were made using thermocouple millivolt responses. Strain gauge type load cells were used to measure the weigh tank mass. All the differential and absolute pressure transducers used were strain gauge type except two Validyne transducers which were variable reluctance type.

3.7.1 Pressure Measurements

Three absolute and nine differential pressure transducers were used in the system. The stagnation pressure in the reservoir was measured using a model PA822-3M absolute pressure transducer which had a range
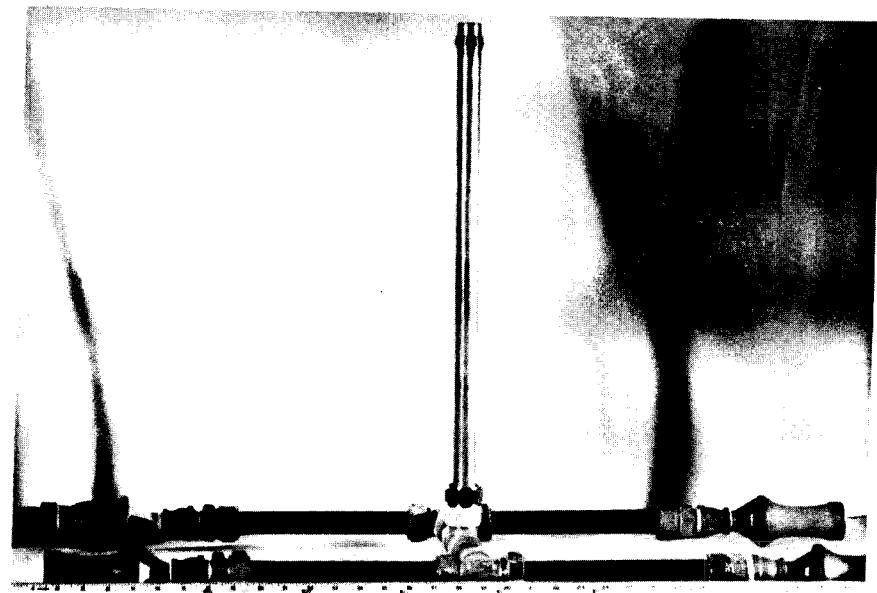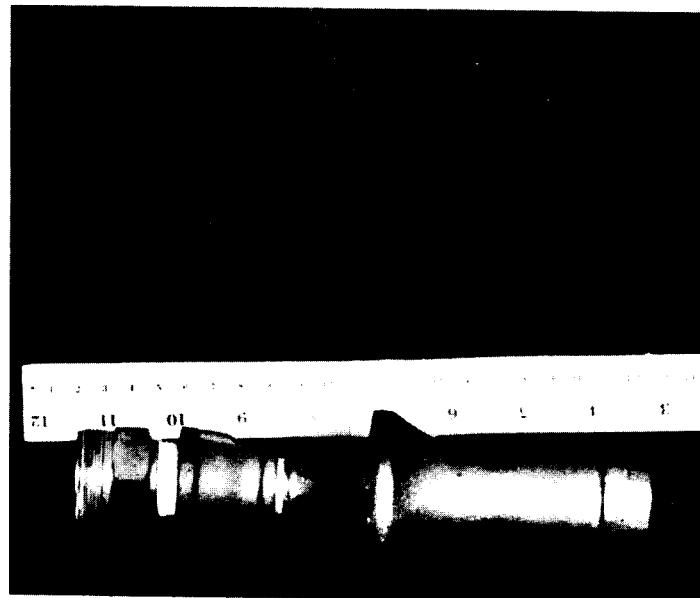
Figure 3-5   Photograph of Nozzle System

of 0 - 20.6 MPa. As this range was quite high for the operating ranges of present experiment (up to 1 MPa), a precision pressure gauge (Heise) was used to read the reservoir pressure in addition to this pressure transducer. The stagnation pressure in the test pipe was measured with a model PA822-100 absolute pressure transducer which had a range of 0-790 kPa. Since overpressure rating is 200 percent, for this transducer, pressure measurements up to 1065 kPa were made, without affecting the response characteristic of the transducer. Another model PA 822-100 transducer of range 0-790 kPa was used to measure the pressure downstream of the break discharge section. Transducer model PA822-3M had resolution of $\pm$4.3 kPa and the precision Heise pressure gauge had $\pm$1.7 kPa pressure. Transducers of model PA800-100 had $\pm$0.2 kPa resolution. All the three absolute transducers, manufactured by Gould-Statham, were powered by a bridge type DC power supply with adjustable zero setting dial. Five differential pressure transducers were used to measure the pressure profile at the break discharge section. Of these, three, manufactured by Data Sensor, Inc., were of 0-103 kPa range with resolution of $\pm$0.1 kPa. Two variable reluctance differential transducers manufactured by Validyne Engineering, Inc., were of model DP-15. These had a replaceable diaphragm system that allows different operating ranges with each diaphragm. In the present work a Validyne transducer with range $\pm$350 kPa was used to measure the differential pressure from the test pipe to the fifth tap of the discharge tube. The fifth tap is located just inside the exit plane. Between the fifth tap and the downstream expansion section a transducer with range $\pm$827 kPa was used. Both the Validyne transducers were powered by a standard Validyne demodulator unit. A typical pressure transducer arrangement used in steam-water two-phase discharge runs is shown in Table 3-3. As the pressure profiles were different for single phase cold water runs, and single phase saturated water runs, the pressure transducer arrangements at the discharge test section were made according to the need, so that better responses are obtained with the available ranges associated with each transducer.

Three differential pressure transducers, each of range $\pm$103 kPa, manufactured by Data Sensor Inc., were used to measure differential pressure across the orifice meters. Three sharp edged orifice meters were used: on steam/air feed line, on steam exit line and in the recirculation loop. A Gould-Statham PM8142$\pm$3.6 differential transducer was used to measure the differential pressure across the constant area portion of the reservoir vessel. This transducer had a range of $\pm$25 kPa. Arrangements were made to flush the pressure sense lines in the system. All the lines associated with pressure sensing were filled with water to improve the dynamic response.

3.7.2 Thermocouples

Two types of thermocouples, J-type (iron-constantan) and T-type (copper-constantan) were used in the experimental set up. The iron-constantan thermocouples were used to read wall temperature of the reservoir

TABLE 3-3

Pressure Transducer Connections

Measurement Locations (Tap No.)*	Designation	Transducer Used
0	absolute P_0 (stagnation)	Statham PA800-100 (s/n 21442)
1-2	differential ΔP_{12}	Data Sensor PB413B-17 (s/n 429)
2-4	differential ΔP_{24}	Data Sensor PB413B-17 (s/n 434)
4-5	differential ΔP_{45}	Data Sensor PB413B-17 (s/n 320)
0-5	differential ΔP_{05}	Valicyne DP-15 (s/n 50139)
5-6	differential ΔP_{56}	Validyne DP-15 (s/n 50140)
6	absolute P_6	Statham PA800-100 (s/n 21455)

*Refer to Figure 3-3 for pressure tap locations.

vessel from which approximate liquid temperature inside the reservoir could be estimated. A total of six copper-constant thermocouples were used to measure water temperature inside the reservoir and recirculation loop, and water and steam temperatures inside the test pipe. The data from the J-type thermocouples were recorded on a Honeywell, twenty-four channel chart recorder so that the temperature response of the vessel wall could be observed continuously during the heating period.

The copper-constantan thermocouple probes manufactured by Omega were made of 36 gauge wire in a 1.6 mm diameter stainless steel sheath. The time constant for these thermocouples was typically 3 seconds. The probes were mounted with single penetration fittings containing teflon seals. The thermocouples were installed such that the probe tips were aligned in the direction of fluid flow.

3.7.3 Load Cells

Strain gauge type load cells, manufactured by Gould-Statham, were used to measure the mass of the weigh tank. The load cells used were Universal Transducing Cell UC3 that can measure 0 to 60 grams in compression. With UC-4-500 adapters, these cells were used in the present setup to measure 0 to 250 kg in tension. The resolution of the load cell response was about ± 0.03 kg for the present set up and the nonlinearity plus hysteresis of the load cells as quoted by the manufacturer was 0.5 percent of full scale.

4. EXPERIMENT OPERATING PROCEDURE

Basically two types of test runs were carried out, air-cold water runs and saturated steam-water runs. For the first type of runs no heating was involved. For saturated steam-water runs initial preparation involved heating the water to the saturation temperature in the vessel and in the test pipe, and bringing the steam-water system to a steady state. In this chapter the theory and practice of operating the experimental set up for these two types of test runs are discussed.

Water for the test runs supplied by single stage distiller was stored in two tanks each of 0.21 m^3. A small centrifugal pump was used to fill the reservoir vessel. Air was vented into the room through the vessel vent line and as well through the vessel blow down line. The valve on the water fill line was closed when the vent line began to discharge water. The sense line for the vessel level pressure transducer was flushed and filled with water. The vessel level reading was checked against the calibrated value for a full vessel when the water passing through the vent line was stopped. The vent valve was then closed.

Water from the reservoir was then drained through water feed line to the test pipe until the test pipe was filled up to approximately 50 percent. The pressure sense lines at the test section were then flushed and filled with water. The power supplies to the pressure transducers, Validyne demodulators and the Auto Data were checked for correct operation. The zero readings for all the pressure transducers and thermocouples were recorded. These readings were checked with a table of calibrated zeroes to ensure the proper responses of each instrument. Before applying the pressure or starting the heating to the system, all the valves in the equipment were closed.

4.1 Air-Water Tests

For air-water test runs the reservoir water level was kept full and the pressure was applied by a compressed air/nitrogen supply. The pressure in the reservoir was maintained higher(15 to 35 kPa) than the required stagnation pipe pressure to drive the water from the reservoir to the test pipe. The pressure inside the test pipe was maintained slightly higher than the required pressure before opening the discharge valve. The gate valve at the discharge section was then opened and at the same time the shut-off valve and needle valve on the water feed line, and the steam/air feed valve were opened simultaneously and adjusted to get the required pipe pressure. The water level in the test pipe was adjusted by controlling the water flow rate using the needle valve. The pressure in test pipe was controlled by the control on the steam/air inlet and the steam/air exit valves. The valves were carefully handled to obtain a constant water level and a constant pressure inside the test pipe.

For the case of bottom and side oriented break, for inception of vapor-pull-through data, the liquid level in the test pipe was kept almost full. After establishing single phase flow, at a particular pipe pressure, the liquid level in the test pipe was decreased slowly (0.5 mm/s-0.25 mm/s) and the heights at which the first bubble pull-through and the onset of continuous pull-through occur were read by direct visual observation and recorded. The Auto-Data system recorded the responses from the various transducers during the flow. For the case of liquid entrainment data, first a particular liquid level was set in the test pipe. And then by adjusting steam/air inlet and out-let valves small single phase gas flow rate was maintained at parti-cular pipe pressure. Then slowly the gas discharge rate was increased while maintaining constant pipe pressure. When the inception of liquid entrainment was observed, the corresponding Auto-Data recordings were identified.

The two-phase flow with vapor pull-through or liquid entrainment data were recorded for a particular liquid level and pipe pressure. Once the required steady state conditions were achieved in the test pipe, the Auto-Data Eight was started and the data were recorded in continu-ous mode for about 2-4 minutes. Meanwhile, both water level readings in the test pipe were recorded at 30 second intervals by observation through viewing windows. The flow pattern near the break was visually observed and recorded. The runs were conducted for different stagna-tion pressures. For each pipe pressure at least three different liquid levels were studied for both the case of flows with liquid en-trainment and vapor pull-through.

Before the orifice meters were installed to measure gas/vapor flow rate, the discharged gas flow rate was read through an air-water separator-manometer system. This system was installed downstream of the dis-charge tube and was used in glass pipe tests. In these runs the mano-meter readings were read at 20 second intervals along with the water level readings. After 2-4 minutes of recording the Auto-Data was stopped and all the valves were then closed.

4.2 Steam-Water Tests

Additional procedures involved in the steam-water test were to heat the reservoir fluid to saturation and to maintain a saturation state in the test pipe during break discharge. The reservoir was filled to a level such that enough space was available for expansion of water when heated. This level was determined on the basis of a ratio of the saturated water density at the planned pressure and temperature and the density at 20°C temperature. Heating was first done at full power until satura-tion was achieved and was then reduced to give the desired steam flow-rate.

The temperature of the reservoir was monitored by the chart recorder and the Auto-Data. When the temperature of the reservoir water was

close to 100°C the water flow in the recirculation loop was started and the heaters in the test pipe and recirculation loop were put on to full power. This procedure was adopted because the heating of the water in the reservoir took a much longer time (~3 hours) to bring the water temperature to ~100°C. The recirculation flow rate was maintained to a constant value of approximately 0.5 GPM for most of the experiments. This value of flow rate was fixed with due consideration to the capabilities of the heat exchanger and the reheaters. As the heating proceeded the temperature and pressure were monitored carefully. Especially in the recirculation loops, the water temperature entering the recirculation pump was always kept less than 110°C and the temperature of the liquid entering the water feed line at the upstream of the test pipe was maintained as close to the desired saturation temperature as possible. Before starting a run, air inside the test pipe and the reservoir was purged by flowing steam from the vessel through the test pipe and through the blowdown line into the quench tank for about three minutes. The saturation pressure inside the reservoir was kept slightly higher (20-35 kPa) than the planned test pipe stagnation pressure, in order to drive water from the reservoir to the test pipe. For the runs involving liquid entrainment, the liquid level in the reservoir was maintained at half the vessel, since for liquid-entrainment experment, liquid discharge rate was quite small. This also reduced the heating time substantially during the initial preparation of the test run.

Once the required saturation temperature and pressure were reached inside the test pipe, the break discharge gate valve was opened and at the same time the shut-off valve and needle valve were opened for liquid flow into the test pipe. The power to the reservoir and test pipe heater were cut to 50 percent level. However, in some cases it was required to put the reservoir heaters to higher than this level whenever larger steam flow rates were required, e.g., in the case of small liquid level, with high vapor pull-through rate. The liquid level and pressure inside the test pipe were controlled as explained in the air-water test case. In addition the water and steam temperatures were also monitored carefully to assure maintainance of saturation conditions. The rest of the procedures follow those described for the air-water system. For one vessel filling, 3 to 4 runs were conducted for different water levels and a particular saturation pressure. The water level in the reservoir was checked in consecutive runs, so the heater elements were always submerged in water and the runs were concluded accordingly.

5. RESULTS

5.1 Presentation of Results

Results of all the test runs carried under this experimental program are presented in this chapter. Table 5-1 gives the brief test matrix of all the experimental runs included in this report. The reduced data are summarized for all runs in the tabular form in Appendix B. Test runs 1-10 were carried out on the system with the glass test pipe. The remaining experiments were carried out on the system with metallic test pipe. The details of the T/S mentioned in the first column of the Table 5-1 can be referred from Table 3-2. The discussion in the following sections details the results of the flow for each break orientation, bottom, side and top.

5.2 Flow Pattern at the Break

5.2.1 Downward Orientation (Bottom Break)

With the glass test pipe the test runs were carried out with downstream end of the test pipe closed with a blind flange. Recalling the review presented in section 2 concerning Reimann and Khan Experiments [9], we find that the flow geometry of the tests carried out with the glass test pipe correspond to their case (b). In this flow geometry, the tests carried out at basically two different stagnation pressures (∿356 kPa and 427 kPa) for different liquid interface levels, showed similar flow patterns as observed by Reimann and Khan [9], namely, the vortex flow was observed at the above certain liquid interface level and when the interface level was lowered, the water flow pattern changed to vortex-free flow. In Figure 5-1 a & b, photographs of the air-water flow at the break, in the glass pipe system with and without vortex are shown. Though the pipe curvature contracts the picture at the break entrance, still the vortex flow in Figure 5-1a and vortex free flow in Figure 5-1b can be identified for two different liquid levels.

In the metallic test pipe system, the flow in the recirculation loop provided a velocity component in the direction transverse to the break axis. This flow geometry corresponds to case (c), for which Reimann and Khan [9] observed in their experiments, that the flow field near the break was always vortex-free. In the present study with recirculating flow, however, vortex and vortex-free flow were both observed depending on the interface level as was observed in the glass test pipe system described above. A simple test was carried out to observe the vortex free and vortex flow near the break entrance and its dependence on the transverse flow component. First a two-phase flow with vortex was established with no recirculation flow in the system, for a typical height of liquid h = 20 mm with T/S: 2-DN. Then the

TABLE 5-1. Test matrix

T/S	Run No.	Fluids and Flow at Break Entry VP = Vapor Pull-through LE = Liquid Entrainment	p_o range (kPa)
Down Oriented Break			
1G-DN*	1-4, 8-10	Air-water, 2ϕ, VP	347-433
1G-DN*	5-7	Cold-water, 1ϕ	351-432
1A-DN	11-18	Cold-water, 1ϕ	374-1069
1A-DN	19-30	Air-water, 2ϕ, VP	376-647
1A-DN	31-38	Saturated-water, 1ϕ	375-1074
1-DN	39-55	Cold-water, 1ϕ	141-570
1-DN	55-66, 108, 112, 115 133, 135, 138	Saturated-water, 1ϕ	168-1065
1-DN	67-78, 109-111, 113 114, 116-118, 131, 132, 134, 136, 137, 139	Steam-water, 2ϕ, VP	367-980
2-DN	79-90, 191-197	Cold-water, 1ϕ	106-446
2-DN	91, 94, 102, 198, 182-190	Saturated-water, 1ϕ	107-448
2-DN	92, 93, 95-101, 103-107, 129, 130	Steam-water, 2ϕ, VP	314-683
3-DN	119-128	Steam-water, 2ϕ, VP	281-540
1B-DN	140-146, 174-179	Cold-water, 1ϕ	108-500
1B-DN	400-403	Air-water, 2ϕ, VP	149-151
1B-DN	148-173, 180, 181	Saturated-water, 1ϕ	107-947
Up Oriented Break			
1-UP	200-208	Air-water, 2ϕ, LE	350-584
1-UP	209-212, 214-222	Steam-water, 2ϕ, LE	369-508

TABLE.5-1 (continued) Test matrix.

T/S	Run No.	Fluids and Flow at Break Entry VP = Vapor Pull-through LE = Liquid Entrainment	P_0 range (kPa)
Up Oriented Break (cont'd)			
1-UP	213	Saturated-water, 1ϕ	550
1B-UP	240-243	Air, 1ϕ	404-608
1B-UP	223, 224, 228 230-239, 244-249 255-258	Air-water, 2ϕ, LE	270-647
1B-UP	225-227, 229, 250-254	Steam-water, 2ϕ, LE	275-523
Side Oriented Break			
1B-SD	300-324	Steam-water, 2ϕ, VP	263-820
1B-SD	325-336	Steam-water, 2ϕ, LE	149-284

*Test carried on glass test pipe.

(a)

(b)
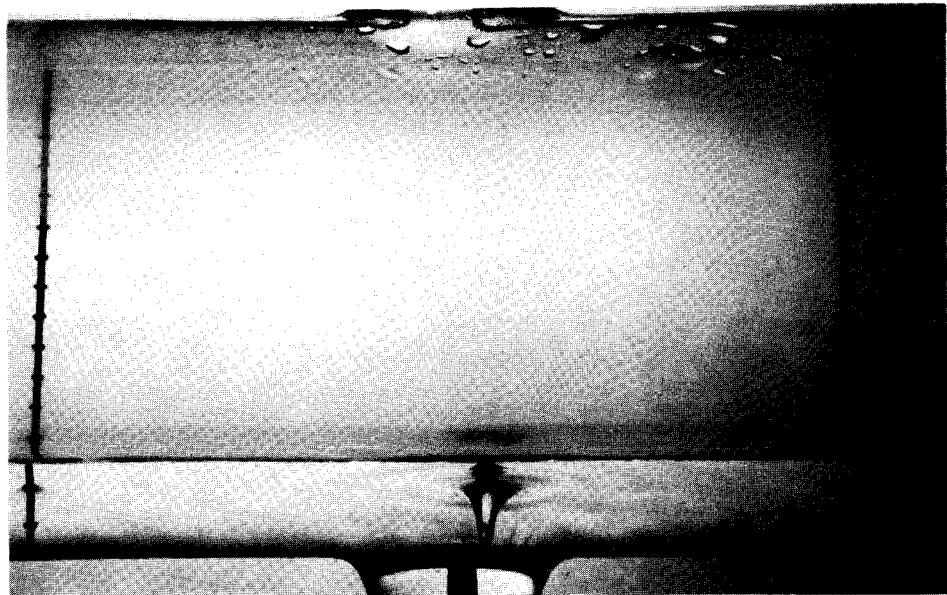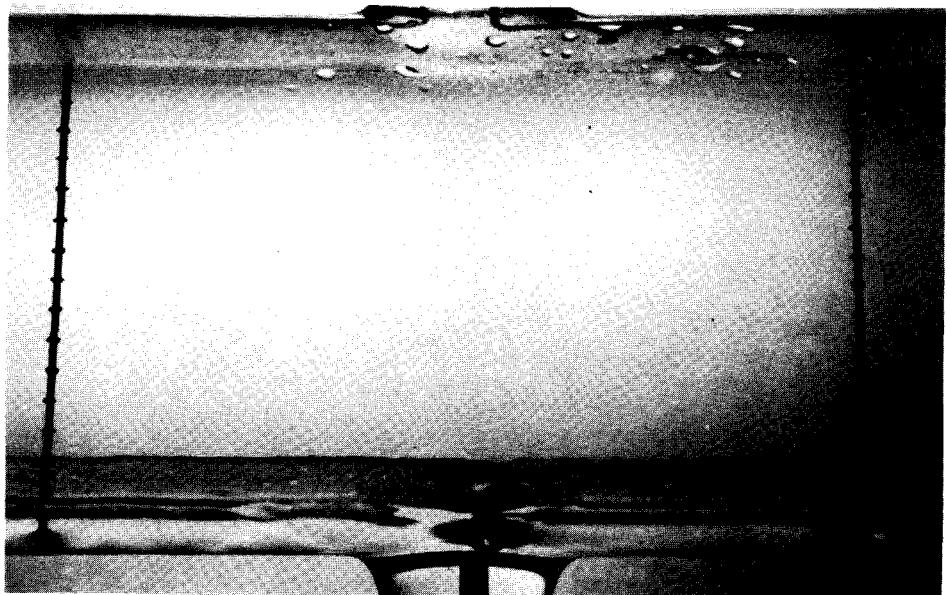
Figire 5-1   Two-phase Flow with Vapor Pull-Through (Glass Pipe
             System) Fluids: Air-Water, T/S: 1G-DN,
             p_0 = 356 kPa (a) Vortex Flow h = 20 mm
             (b) Vortex Free Flow h = 10.16 mm

recirculation flow was started and was increased in smaller steps
(0.1 GPM). Observation showed that the transverse component of
velocity in the fluid near the break retards the formation of the
vortex. With a recirculation flow rate greater than 1 GPM it was
found that the vortex was suppressed completely and vortex free flow
was observed. In Figure (5-2a & b) the photographs of steam-water
flow at break in metallic pipe system are shown for TS:2-DN. At
h = 19.6 mm, from picture we observe the effects of vortex
suppression in the vapor pull-through flow near the break. For inter-
face level h = 17.1 mm, the vortex is suppressed completely and the
flow is vortex free.

KfK results also showed that lowering the interface level below a cer-
tain value and increasing the superimposed liquid velocity above a
certain value, can cause the flow pattern near the break to change from
vortex flow to vortex free flow. The reason for the transition from a
vortex to a vortex free flow field was attributed to the increasing
influence of the wall friction with decreasing interface levels. Thus
the phenomena of vortex and vortex free flow near the break in general
is a function of the two-phase flow rate through the break, the inter-
face level and the superimposed liquid velocity.

In the present experiments, for all the three test sections used, both
vortex and vortex free vapor pull-through flow were observed depending
on the interface level and the stagnation pressure in the test pipe.
Oscillatory behavior of vapor pull-through was observed for certain
values of interface level as was observed by KfK experiments, and this
has been discussed in the last section (5-7).

5.2.2 Upward Orientation (Top Break)

For the upward oriented branch both steam-water and air-water two-phase
flows were studied with stratified smooth flow in the test pipe having
a superimposed fluid velocity due to flow in the recirculation loop.

The liquid entrainment phenomena observed was very similar to the ob-
servation of Smoglei's experiments [7]. The entrainment involved a
vortex formation in the entraining liquid spouts, and depending on the
gas discharge through the break and the interface level, the spout
height would vary. The process being intermittant, showed an
oscillatory behavior as was observed in Smoglie's experiments [7].

In Figure 5-3, the photographs taken through the viewing windows across
the break are shown. The liquid spout occur leading to entrainment at
about 1 cm downstream side of the break location. The gas flow in the
pipe was from left to right and there was also the superimposed liquid
velocity in the pipe, with flow direction from left to right. Due to
these flow directions, the liquid spout appear on the right side of the
break plane. The initiation of liquid entrainment always involved a
vortex in the fluid. Increase in gas flow rate in the pipe caused the
interface of the liquid to be wavy, especially for larger size test
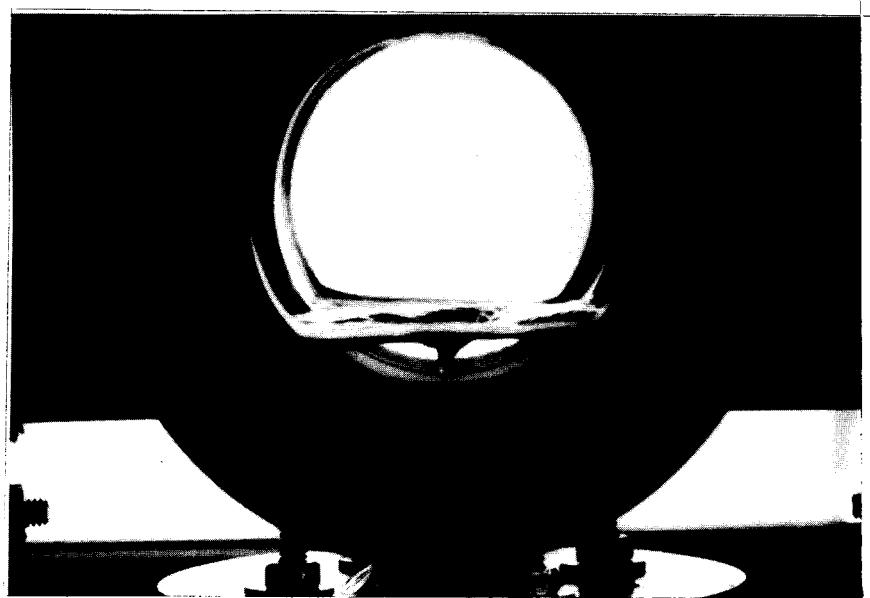
(a)
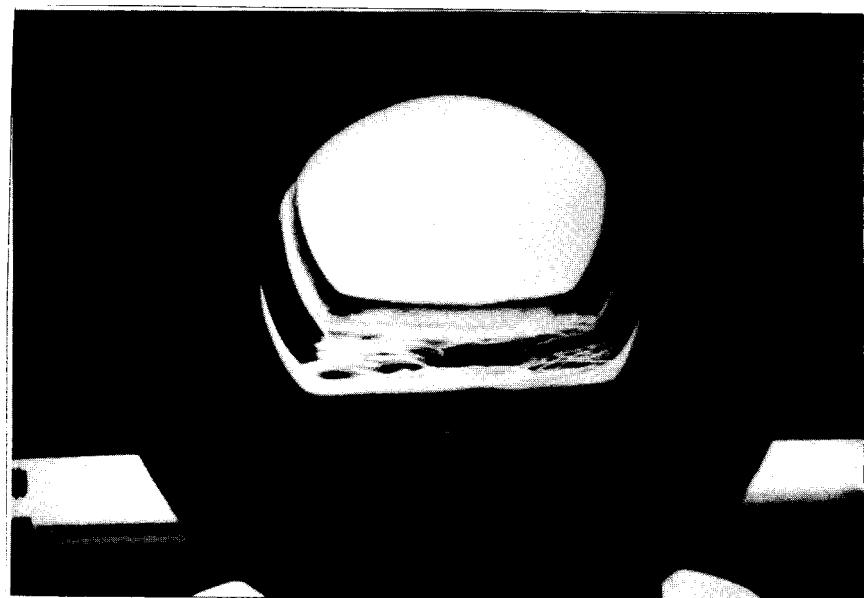
(b)

Figure 5-2   Two-phase Flow with Vapor Pull-Through (Metal Pipe
System)   Fluids: Steam-Water, T/S: 2-DN,
p_0 = 376 kPa (a) h = 19.6 mm, (b) h = 17.1 mm

(a)

(b)

(c)

(d)

Figure 5-3   Upward Oriented Break, Liquid Entrainment Fluids:
Air-Water   T/S: 1-UP, p_0 = 280 kPa, h = 1.5 cm

breaks for which the gas discharge rate is high. In such cases whenever the wavy interface is closer to the break, liquid entrainment would occur as shown in Figure 5-4. For wavy interfaces the entrainment was unstable and continuous two-phase flow through break could not be maintained.

Though the liquid entrainment starts with vortex induced flow, the continuous two-phase flow with liquid entrainment, tended to be vortex free as there was increase in amount of liquid entrained. In the experiments vortex free and intermittent vortex continuous two-phase liquid entrainment flows were observed. In Figure 5-5 the photographs of typical continuous two-phase flow with liquid entrainment flow are shown. In Figure 5-5(a) the flow is with intermittent vortex and Figure 5-5(b) the flow is vortex free.

5.2.3 Side Orientation

In the side oriented break, the vapor pull-through and the liquid entrainment flow patterns differed from those in bottom and top oriented break due to the side wall effect. Inception of vapor pull-through occurred with vortex induced flow. However, this vortex became suppressed as the initial gas hose reaches the break location. The continuous two-phase flow with vapor pull-through was vortex free, in general. However, for interface heights larger than a certain value for a given stagnation pipe pressure, the intermittent vapor pull-through involved a weak vortex and as the interface level was decreased or the pipe pressure was increased the flow tended to be vortex free. Similar observations were also found in KfK experiments.

For the interface level below the break location, the liquid entrainment observed in side oriented branch was vortex free. In the entrainment process a cone of liquid film was found to climb along the pipe wall until it gets dispensed into the break. When the interface level was increased or the pipe pressure was increased the two-phase flow with liquid entrainment became continuous.

5.3 Single Phase Entrance Condition

5.3.1 Cold Water Flow

Cold water ($\sim 20^\circ$C) mass flow rates were measured for various stagnation pressures in T/S: 1A-DN, 1-DN and 2-DN.

Single phase cold water data for T/S 1A-DN are summarized in Table 5-2. The liquid mass flux was correlated with the relation

$$G_\ell = C_D \sqrt{\Delta p_{05} \rho_\ell} \cdot \qquad (5.1)$$

(a)

(b)

Figure 5-4   Upward Oriented Break, Liquid Entrainment Fluids:
Air-Water, T/S: 2-UP, p_0 = 285 kPa, h = 1.8 cm

(a)

(b)

Figure 5-5   Upward Oriented Break Two-phase Flow with Liquid
             Entrainment   T/S: 1B-UP, p_0 = 280 kPa, h = 1.6 cm

5-10

TABLE 5-2. Single Phase Cold Water Data
T/S: 1A-DN, $d_{(entrance)}$ = 3.62mm, d = 3.92mm,
L = 123.5mm, D = 102.2mm.

P_o (kPa)	Δp_{05} (kPa)	$G_\ell \times 10^{-4}$ (kg/m²s)	δG_ℓ (%)	C_D	$f^* \cdot \frac{L}{d}$	K	Re $\times 10^{-4}$
374	210.7	1.281	1.5	0.624	1.244	1.335	5.303
446	264.4	1.429	2.3	0.622	1.241	1.341	5.911
513	316.0	1.539	1.3	0.613	1.238	1.425	6.372
585	367.3	1.706	1.2	0.623	1.238	1.280	7.064
653	425.0	1.826	1.1	0.627	1.238	1.304	7.568
794	529.8	1.990	2.3	0.612	1.238	1.432	8.232
931	626.8	2.219	2.3	0.627	1.238	1.303	9.184
1069	724.8	2.437	2.2	0.637	1.238	1.194	10.083

* - Friction factor obtained directly from standard charts Ref. [26].

The average value of discharge coefficient was found to be $C_D = 0.62$.
Using the friction factor f, from the standard tables for the break
tube size used, the entry loss coefficient K was calculated as

$$K = \frac{2\Delta p_{05}\rho_\ell}{G_\ell^2} - f\frac{L}{d} \quad . \tag{5.2}$$

The values of K ranged between 1.19 to 1.48.

A summary of the single phase cold-water data for T/S 1-DN is shown in
Table 5-3. In this case f, the friction factor was determined from
the pressure gradient in the break tube measured experimentally.
Figure 5-6 shows the pressure profile for T/S 1-DN. The slopes
(dp/dz) of the pressure profiles are used to determine the friction
factor f, as

$$f = \frac{2\rho_\ell}{G_\ell^2}\left(\frac{dp}{dz}\right)d \tag{5.3}$$

and K, the entry loss coefficient was determined using equation (5.2).
Cavitation in this break tube was found to occur for $p_0 > 450$ kPa.

This was recognized from the pressure profile and as well from the
flow noise observed during the experiments. Using the mass flux and
the pressure drop data, we have correlated these two quantities with a
relation, as shown in Figure 5-7:

$$G_\ell = 30.32 \left(\Delta p_{05}\right)^{0.5} \tag{5.4}$$

where Δp_{05} is in Pascal units, and G_ℓ is in $kg/m^2 s$. The equivalent
discharge coefficient was calculated as $C_D = 0.678$ for this tube.

From the pressure profiles observed and the surface roughness, ε, shown
in Table 5-3 we find that the tube inner surface is close to that of
smooth tube. In fact this test section was machined to have sharp
edged entrance and smooth inside surface.

In Figure 5-8, the measured cold-water mass flux as a function of pipe
stagnation pressure is presented for different sizes of break tube.
The data shows that the hydraulic resistance of each tube is slightly
different from one another, and data in general are of good quality.

5.3.2 Saturated Water Flow

In Figure 5-8 the measured mass flow rates for different pipe pressure
are presented in terms of mass flux for the case of saturated water
single phase entrance flow through the break.

TABLE 5-3. Single Phase Cold Water Pressure Loss Summary
T/S: 1-DN, d = 3.96mm, l = 123.5mm, D = 102.2mm

Stagnation Pressure (kPa)	Re $\times 10^{-4}$	$\frac{dp}{dz}$ (kPa/cm)	$\frac{1}{2}\rho V^2$ (kPa)	$f = \frac{dp}{dz} \cdot \frac{d}{\frac{1}{2}\rho V^2}$	$\frac{\Delta P_{05}}{\frac{1}{2}\rho V^2} - f\frac{L}{d}$	$\varepsilon \times 10^3$ (cm)
141	2.228	1.291	15.20	0.0330	1.29	1.664
177	3.294	2.357	33.23	0.0279	1.36	0.8717
208	3.979	3.076	48.51	0.0251	1.40	0.4359
243	4.677	3.886	67.03	0.0229	1.41	0.2377
278	5.210	4.939	83.17	0.035	1.40	0.3566
308	5.878	5.800	105.9	0.0217	1.34	0.1506
342	6.265	7.020	120.4	0.0231	1.32	0.3685
382	6.558	8.003	131.8	0.0241	1.42	0.5547
417	7.179	9.302	157.9	0.0233	1.29	0.4755
444	7.432	10.14	169.3	0.0237	1.33	0.5547
523	8.071	-	199.6	-	-	-
570	8.230	-	207.7	-	-	-
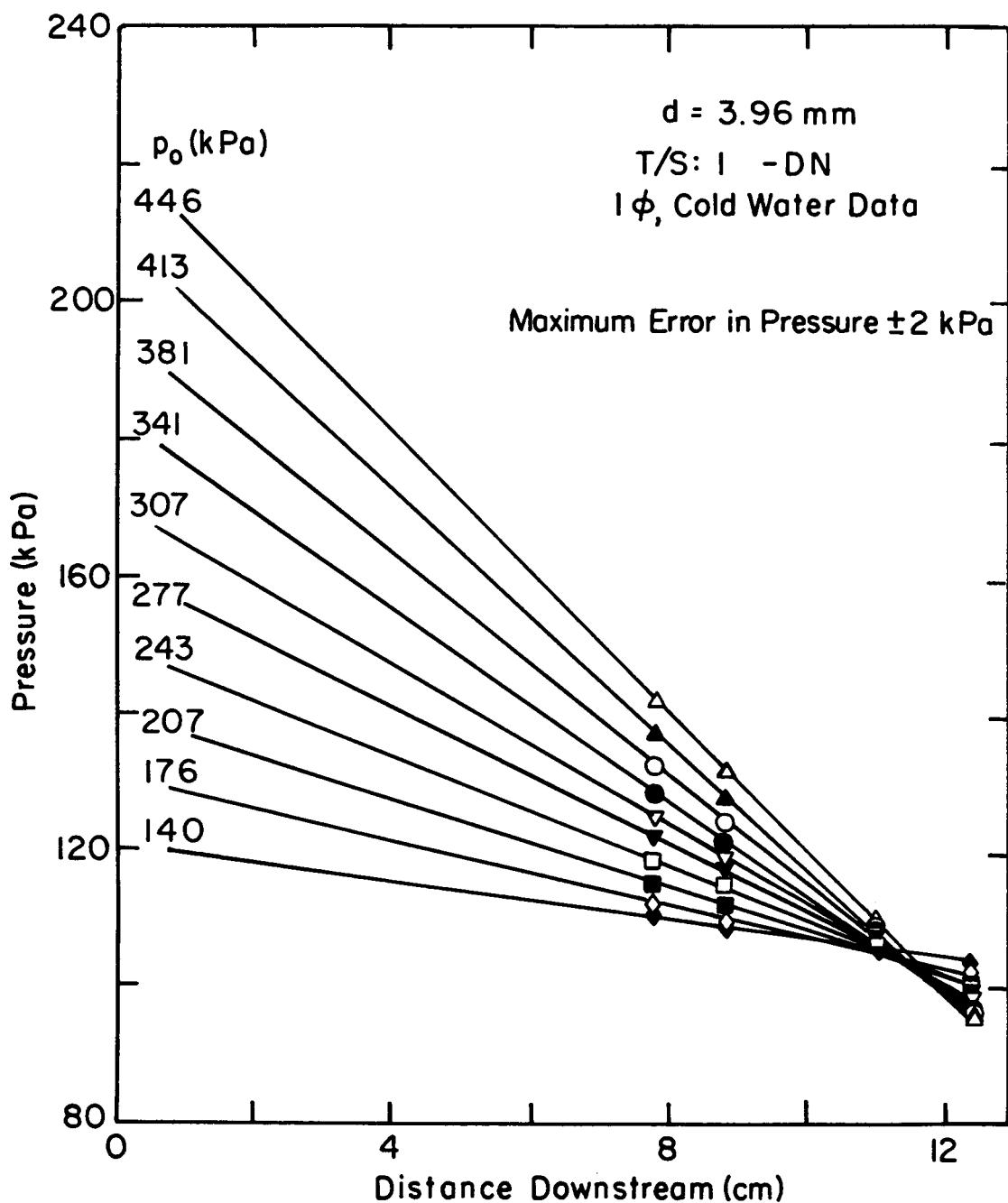
Figure 5-6   Pressure Profile in T/S: 1-DN,
             Cold-water Single-phase Flow

5-14
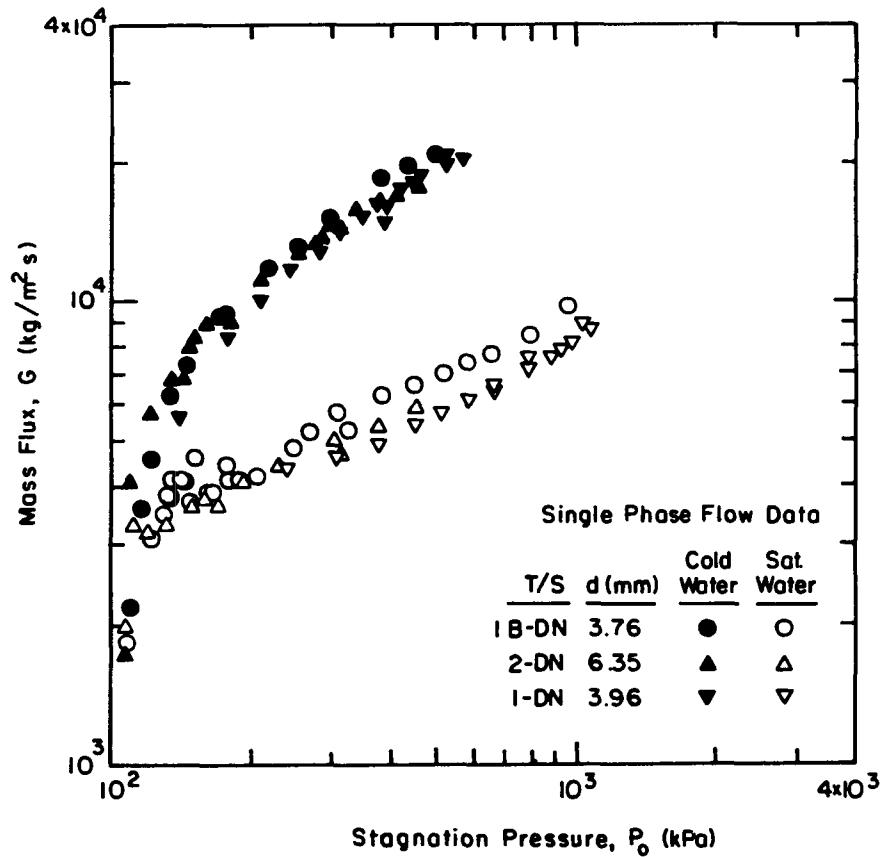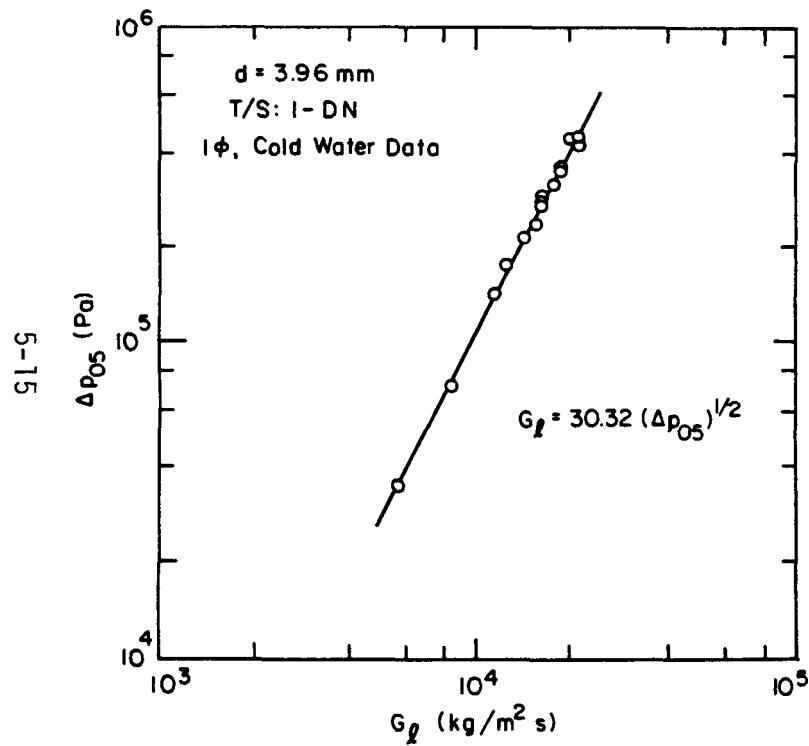
Figure 5-7   Pressure Loss vs Mass Flux for T/S:
1-DN Cold Water Single-phase Flow

Figure 5-8   Measured Mass Flux as a Function
of Stagnation Pipe Pressure for
Cold Water and Saturated Water
Entrance Conditions

5-15

Results of the pressure profiles obtained in T/S 1A-DN for nearly saturated water flow are shown in Figure 5-9. From pressure profiles we find that the larger pressure gradients are observed near the expansion at tube exit indicating that the choking occur at the exit plane. Since the subcoolings are small, from the pressure profile, it appears that the flashing occurs near the tube inlet. As there are no pressure taps close to tube inlet, it is difficult to identify the exact location of the flashing point. In fact this break tube had a smaller diameter at entrance making a orificed entrance that caused a larger pressure drop at the entrance.

In Figure 5-10, we have shown the pressure profiles for T/S 1-DN for single phase saturated water entrance flow. Here also we find that the flashing occurs near the tube inlet, because the pressure drop downstream of the inlet of tube is similar to two-phase pressure drop observed in two-phase steam-water tests. In Figure 5-9 and 5-10, two pressure points are shown at the tube exit. These two points are determined separately from absolute pressure readings at the upstream and the downstream side of the tube exit. Both pressure readings agree within the errors of the measurement indicated. In Figure 5-11, the pressure profiles for T/S: 2-DN are presented which show the same characteristics as indicated by the T/S: 1-DN. The choking of the flashed fluid occurs at the exit plane as evidenced by the large pressure gradient measured near the exit location. The critical pressure ratio as a function of stagnation pressure is presented in Figure 5-12. The present experimental results of single phase saturated water flow agree with the observations of Uchida and Nariai [28] for flow through pipes.

5.3.3 Air Flow

The measured mass flux of air for T/S: 1B-UP as a function of pipe stagnation pressure is shown in Figure 5-13. As the steam supply was not adequate to get critical flow through the break tube, the steam flow rate was theoretically calculated. Using the experimental mass flow rates of air flow the total pressure loss factor $(4f\ L/d)_T$ of the break tube was determined using standard gas dynamic equations [29] involving the Fanno process. As the entrance was sharp edged type the entrance loss was determined as the sum of isentropic contraction and a factor 0.5. Then the tube friction factor was determined as

$$f = \frac{d}{4L}\left[\left(4f\ \frac{L}{d}\right)_T - (\text{isentropic entrance loss} + 0.5)\right] \qquad (5.4)$$

Using this value of friction factor and the equations governing the Fanno process in the pipe, and taking into account the entrance loss the saturated steam mass flow rate was calculated by iterative method for an assumed pipe stagnation pressure. The results of these calculations are shown in Figure 5-13, in terms of steam mass flux as a function of stagnation pressure.
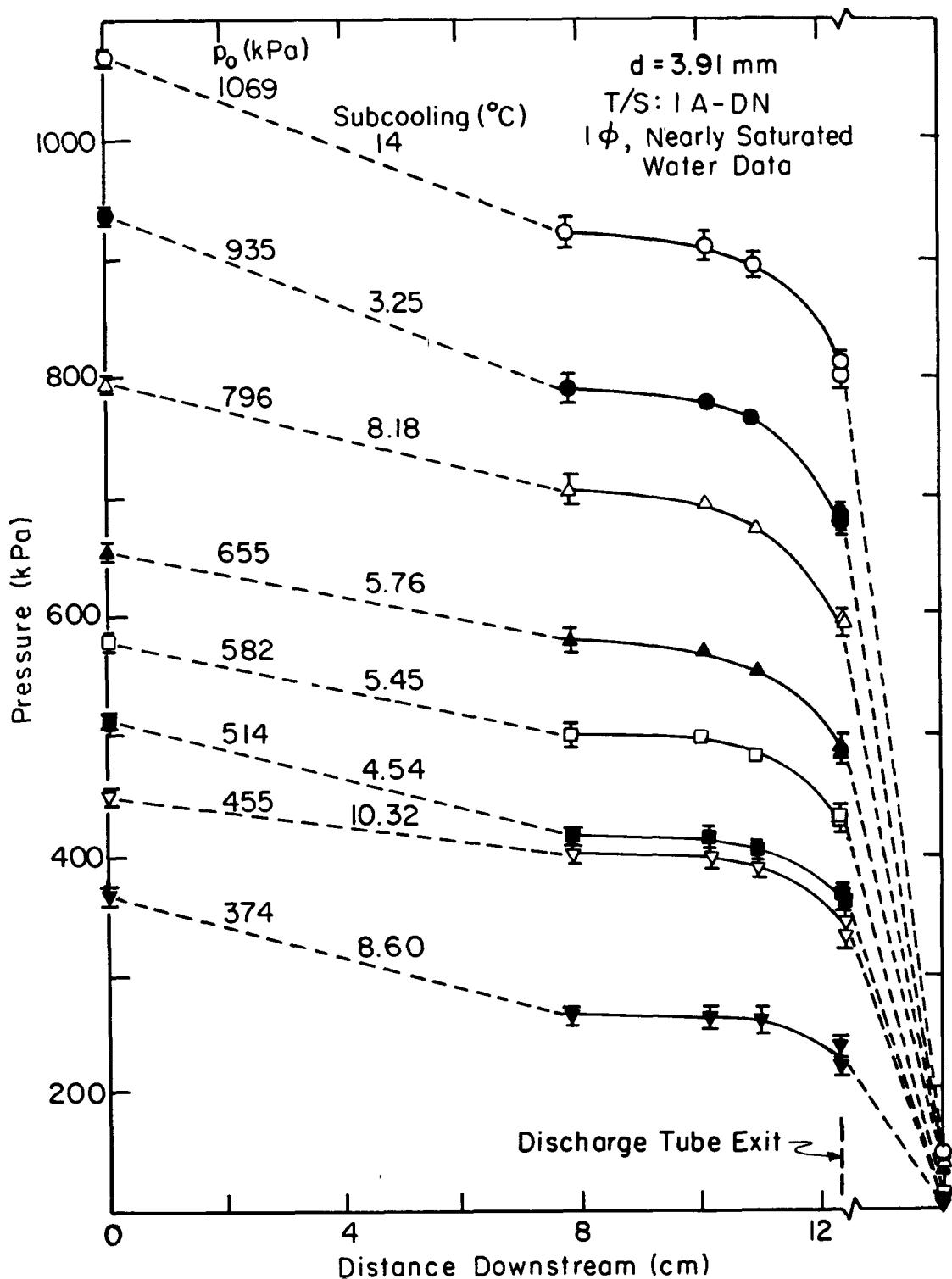
Figure 5-9   Pressure Profiles in T/S: 1A-DN, Nearly Saturated
Water Single-phase Entrance Flow
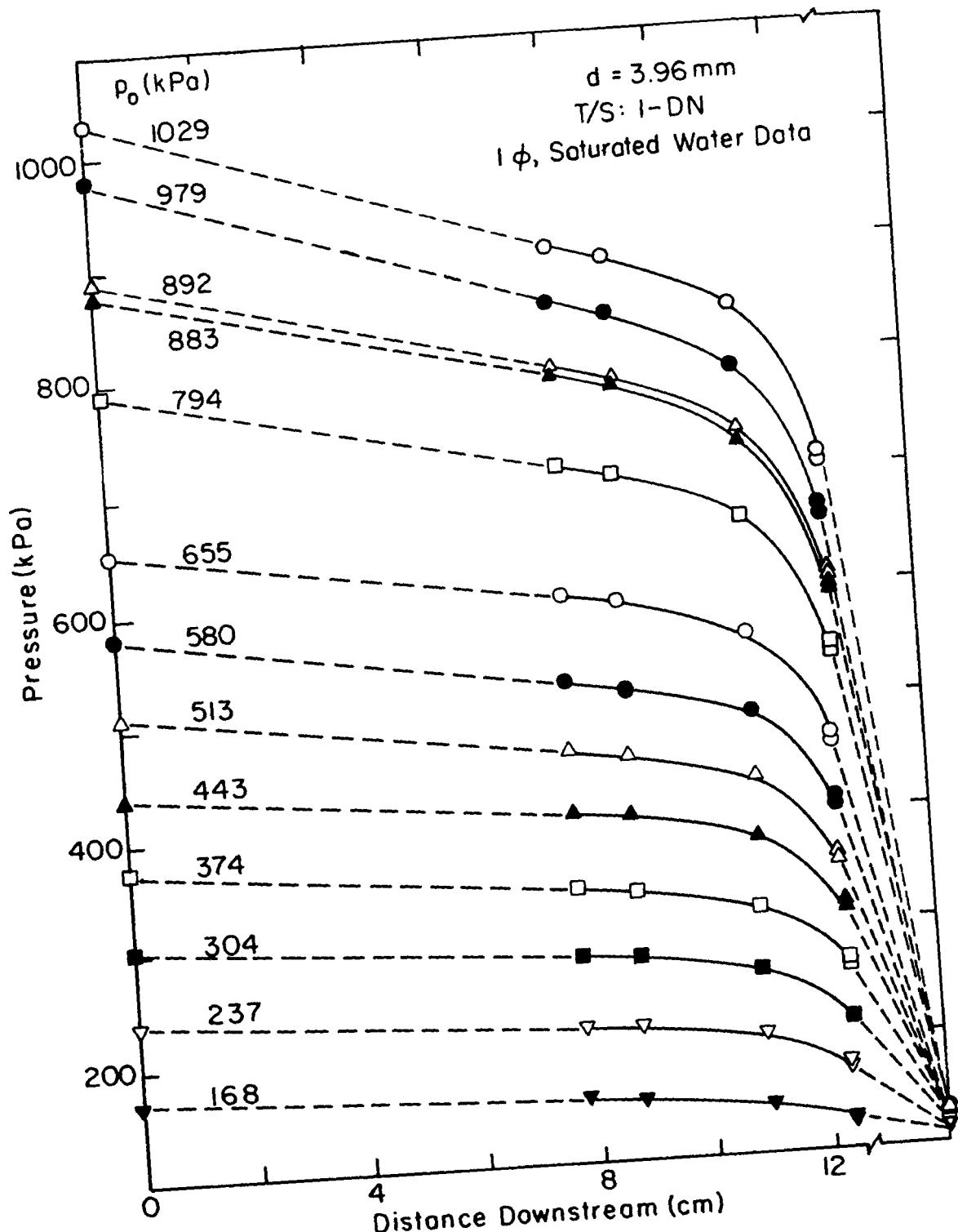
Figure 5-10   Pressure Profiles in T/S: 1-DN, Saturated Water, Single Phase Entrance Flow
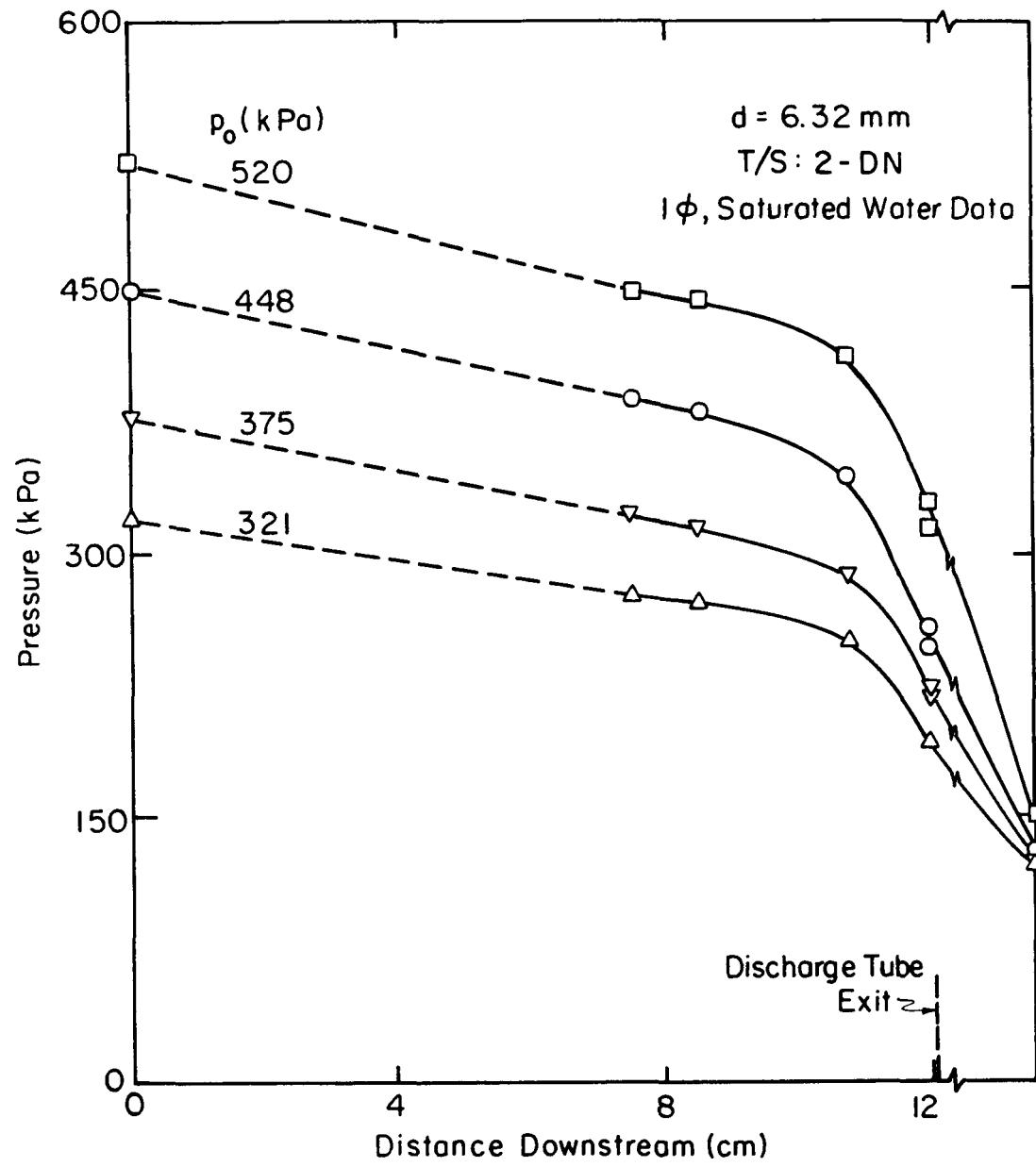
Figure 5-11   Pressure Profiles in T/S: 2-DN, Saturated Water,
              Single Phase Entrance Flow

5-19
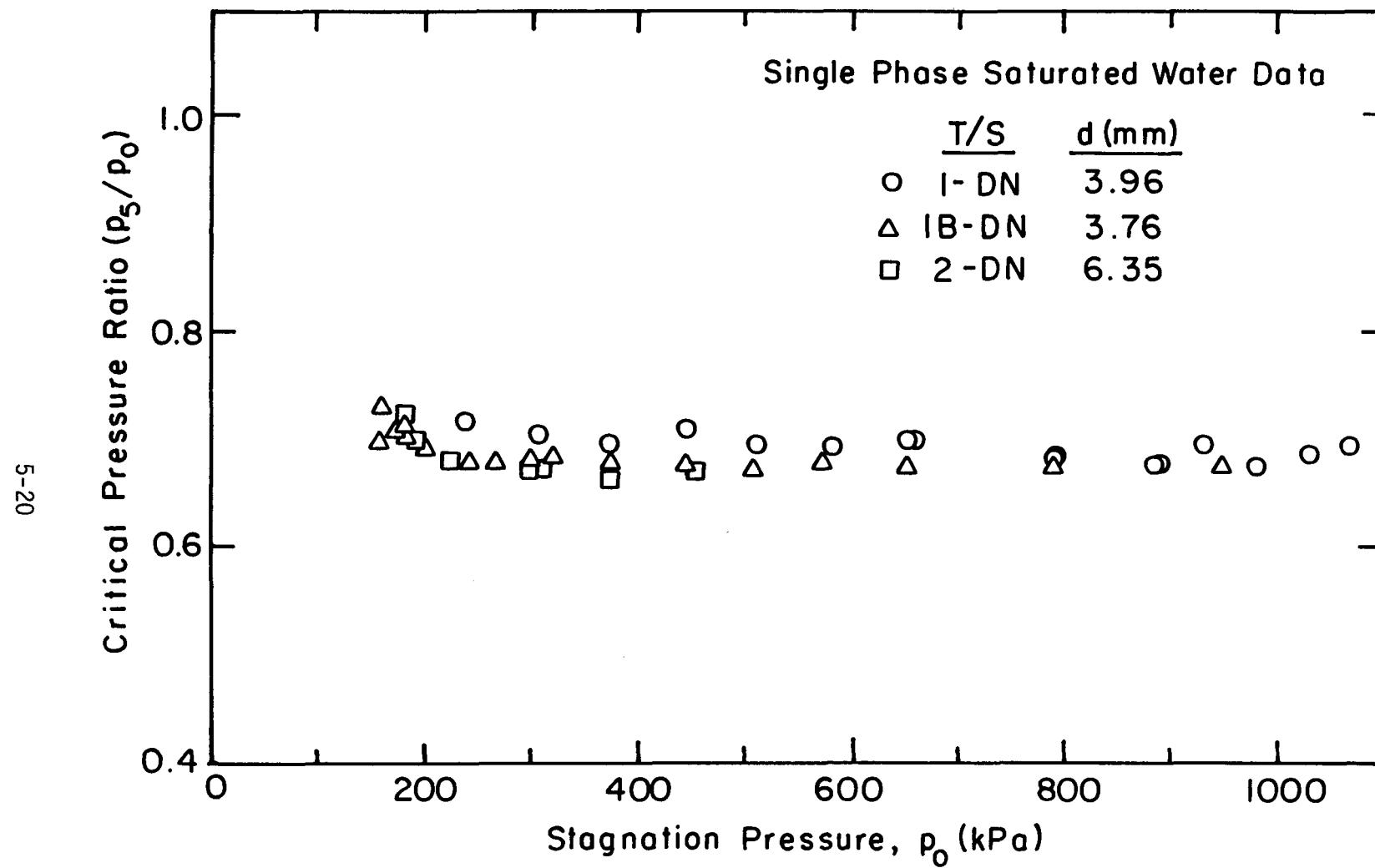
Figure 5-12   Critical Pressure Ratio vs Pipe Stagnation Pressure,
Saturated Water Single-phase Entrance Flow
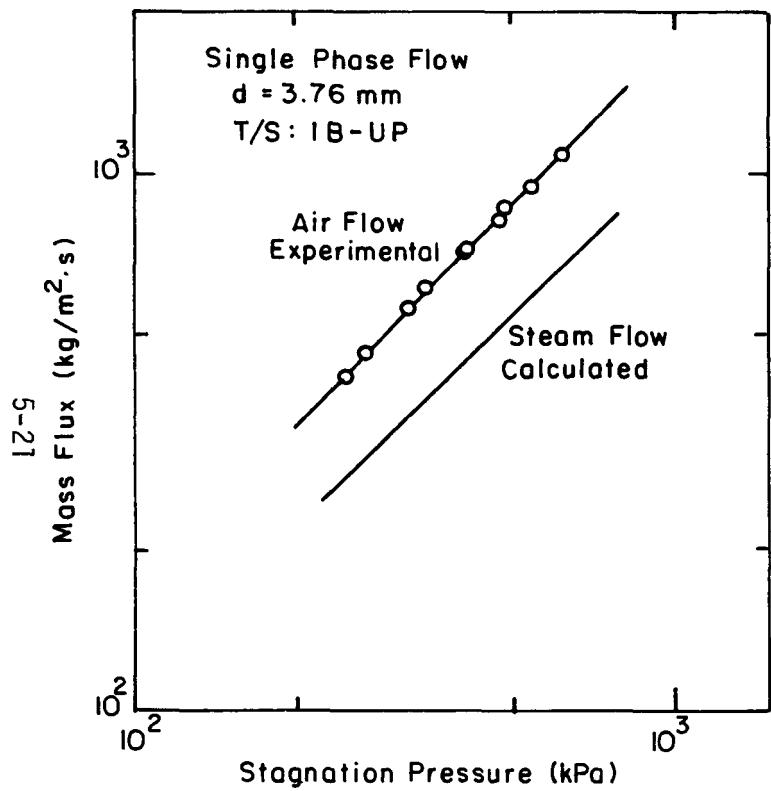
Figure 5-13   Single-phase Critical Mass Flux
as a Function of Pipe Pressure (p_o);
Air-Experimental Data; Steam-
Calculated Data; T/S: 1B-UP
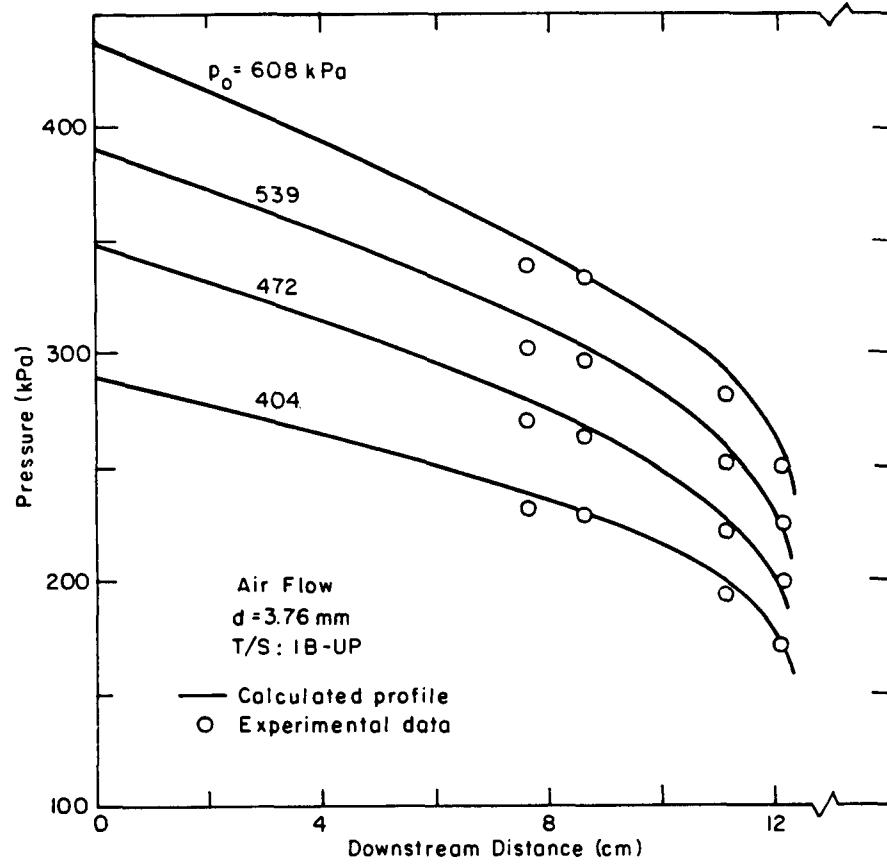
Figure 5-14   Pressure Profiles, Single
Phase Air Flow T/S: 1B-UP

The pressure profiles for air flow are shown in Figure 5-14. The measured and the calculated pressure profiles agree very well. The theoretical profiles were obtained using the measured mass flow rates. Again here, the entrance loss was calculated as a loss due to isentropic contraction loss plus a factor 0.5 for a given stagnation pressure for which the mass flow rate is known. Once the entrance pressure was calculated then the pressure profile along the tube length was generated using Fanno equations, assuming the flow is choked at the exit plane of the tube.

5.4 Inception Results

In this section the results of the inception of vapor pull-through and liquid entrainment phenomena are presented in terms of correlations relating the height of the interface with respect to break location and the discharge flow rate through the break.

5.4.1 Downward Orientation (Bottom Break)

Both air-water and steam-water flow system were studied to obtain the data on inception of vapor pull-through with downward oriented break of different sizes. The flow rate in the recirculation loop was maintained around 0.5 GPM to provide a superimposed velocity on the liquid flow in the pipe. The data for onset of (first bubble) pull-through and onset of continuous vapor pull-through are tabulated in Tables B-22 to B-25 in Appendix B. These data are presented in Figure 5-15 in terms of non-dimensional interface height and Froude number (discharge rate). The data are fitted with the relation

$$Fr_\ell \left(\frac{\rho_\ell}{\Delta \rho} \right)^{0.5} = B \left(\frac{h_b}{d} \right)^2 \tag{5.5}$$

where for the air-water flow system $B = 2.16$ for onset of first bubble pull-through, and $B = 1.47$ for onset of continuous vapor pull-through. For the steam-water flow system $B = 1.16$ for onset of first bubble pull-through and $B = 0.78$ for onset of continuous vapor pull-through. The INEL data are also shown in Figure 5-15. The present air-water data are compared with air-water data of KfK in Figure 5-16. We find from present data (UCB), that the air-water and steam-water data do not yield a single correlation in this representation, where the non-dimensional interface height is correlated with Froude number. A single correlation is desirable in general, which accounts for all the data available, namely, present (UCB), KfK and INEL, for the onset of vapor pull-through. Studies on this phenomenon by Easton and Catton [24] and Lubin and Hurwitz [25] have separately shown the effects of surface tension and of viscosity. A correlation was developed in the present work which takes into account both the viscosity and surface tension effects through viscosity number N_μ and Bond number Bo. In Figure 5-17 the data of INEL, KfK and UCB are
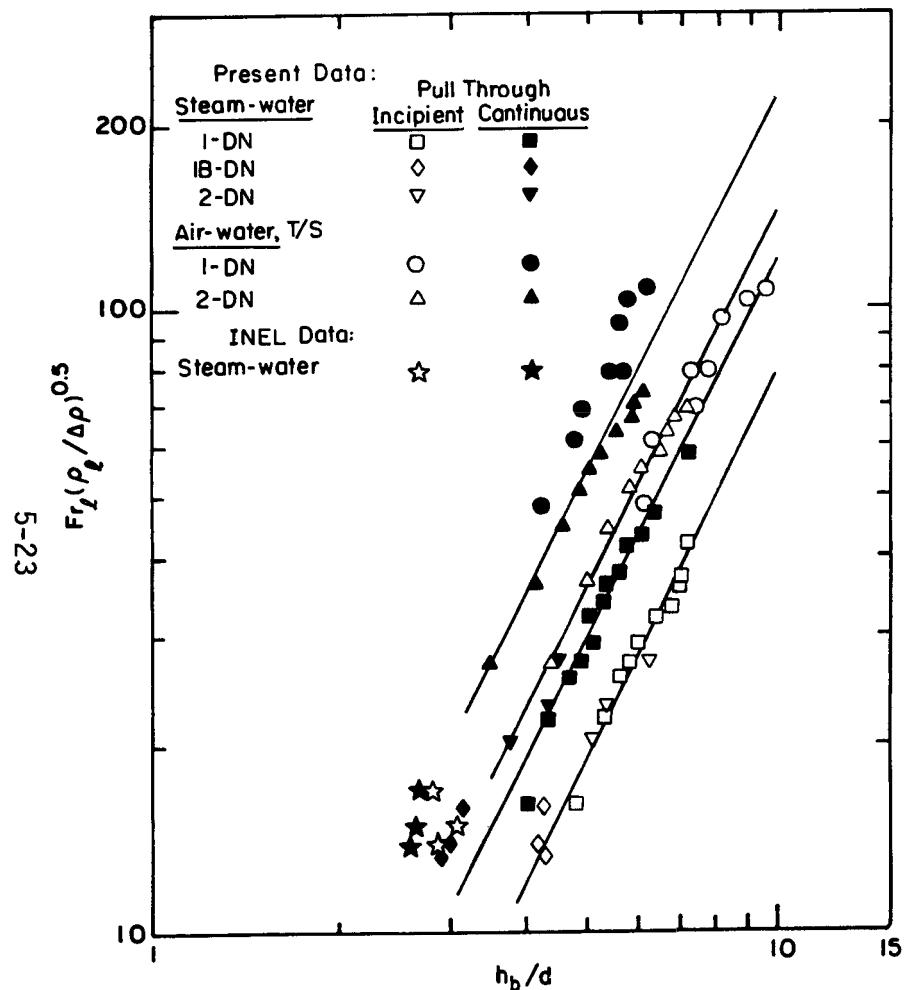
Figure 5-15   Inception Data of Vapor Pull-Through, Down Oriented Break for Air-Water and Steam-Water Flow System
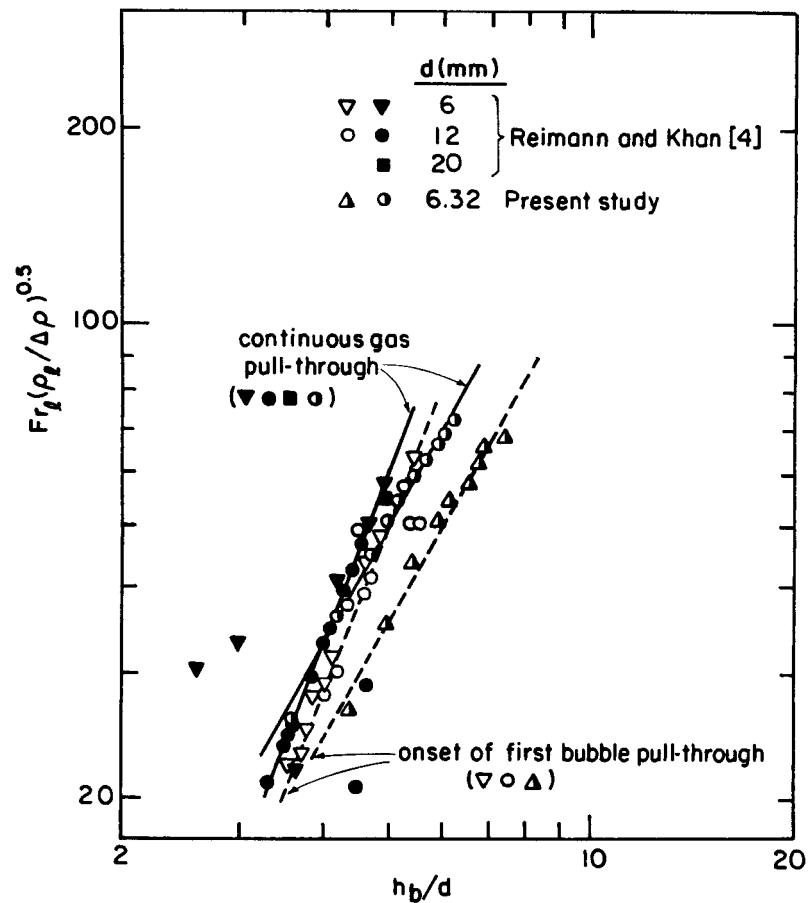
Figure 5-16   Comparison of Present Inception Data of Vapor Pull-Through with KfK Data for Air-Water System, Down Oriented Break

presented in this new representation for onset of first bubble pull-
through. The correlation which fits all the data is given as

$$Fr_\ell \ Bo^2 \ N_\mu^{-0.5} \ (\rho_\ell/\Delta\rho)^{0.5} = 19.4 \left[h_b/(\sigma/g\Delta\rho)^{0.5} \right]^{2.2} \qquad (5.6)$$

The INEL data were obtained based on the response of the differential
pressure transducer, where the change in noise level was designated
as the onset of pull-through. In the KfK and present (UCB) results,
visual observations were used to identify the height at which first
bubble-pull-through occurs. Hence more weight is given to KfK and
UCB data in obtaining the inception correlation shown in Figure 5-17.

5.4.2 Upward Orientation (Top Break)

For upward oriented break, the inception of liquid entrainment data
were obtained with test sections 1B-UP and 2-UP for air-water flow
system. As there was limited supply of steam with available power
supply units in the apparatus, the inception data for steam-water
system were obtained with the smaller test section 1B-UP. These data
are tabulated in Table B-26 to B-28 in Appendix B. The inception of
liquid entrainment data were well correlated in terms of gas Froude
number and non-dimensional interface height as shown in Figure 5-18
for both air-water and steam-water systems. The correlation that
fits the present data is given as

$$Fr_g \left(\frac{\rho_g}{\Delta\rho} \right)^{0.5} = 0.395 \left(\frac{h_b}{d} \right)^{2.5} \qquad (5.7)$$

The KfK data line is also shown in Figure 5-18 for comparison.
Larger inception heights were observed in KfK experiments than the
heights observed in present experiments for the same gas flow rates.

5.4.3 Side Orientation (Side Break)

For side oriented break, both the inception of vapor pull-through and
the liquid entrainment were studied. These data are tabulated in
Table B-29 to B-32 in Appendix B.

For inception of vapor pull-through phenomena, the data obtained with
and without superimposed flow velocity in the pipe, presented in
Figure 5-19, showed no influence of the superimposed flow velocity on
the inception data in the present experiments. The KfK data, however,
showed smaller effect of the superimposed liquid velocity on inception
data, but were not altogether conclusive. The data for steam-water
flow system and air-water flow system are shown in Figure 5-20 in the
representation of Froude number vs non-dimensional interface height.
Again in this representation the data for steam-water flow system and
air-water flow system yield two separate correlations similar to the
observations made with downward oriented break. Hence the correlation
developed earlier for downward oriented branch was used which takes

5-24
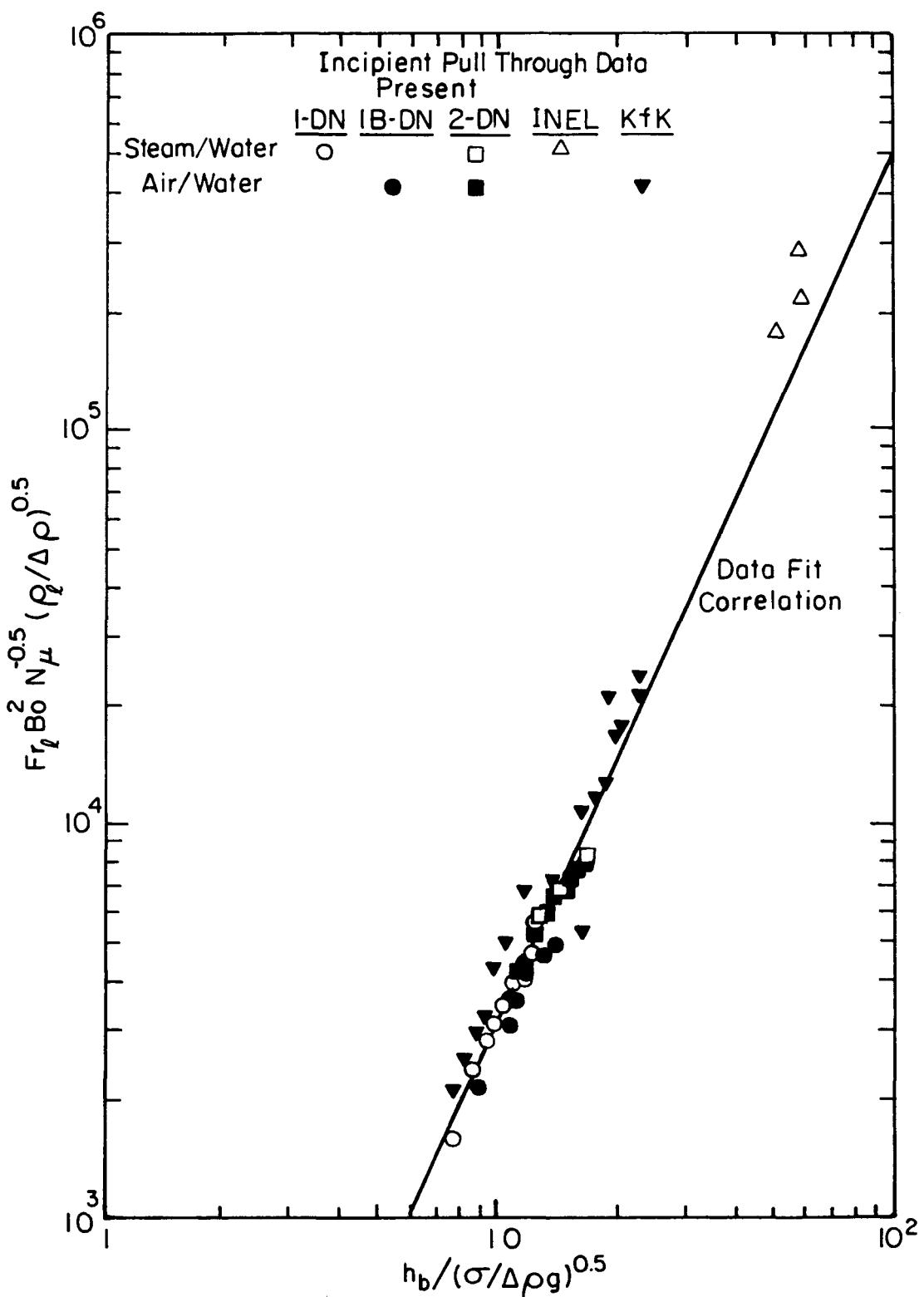
Figure 5-17   Correlation for Inception of First Bubble
Pull -Through Data of KfK, INEL and Present
(UCB) for Down Oriented Break
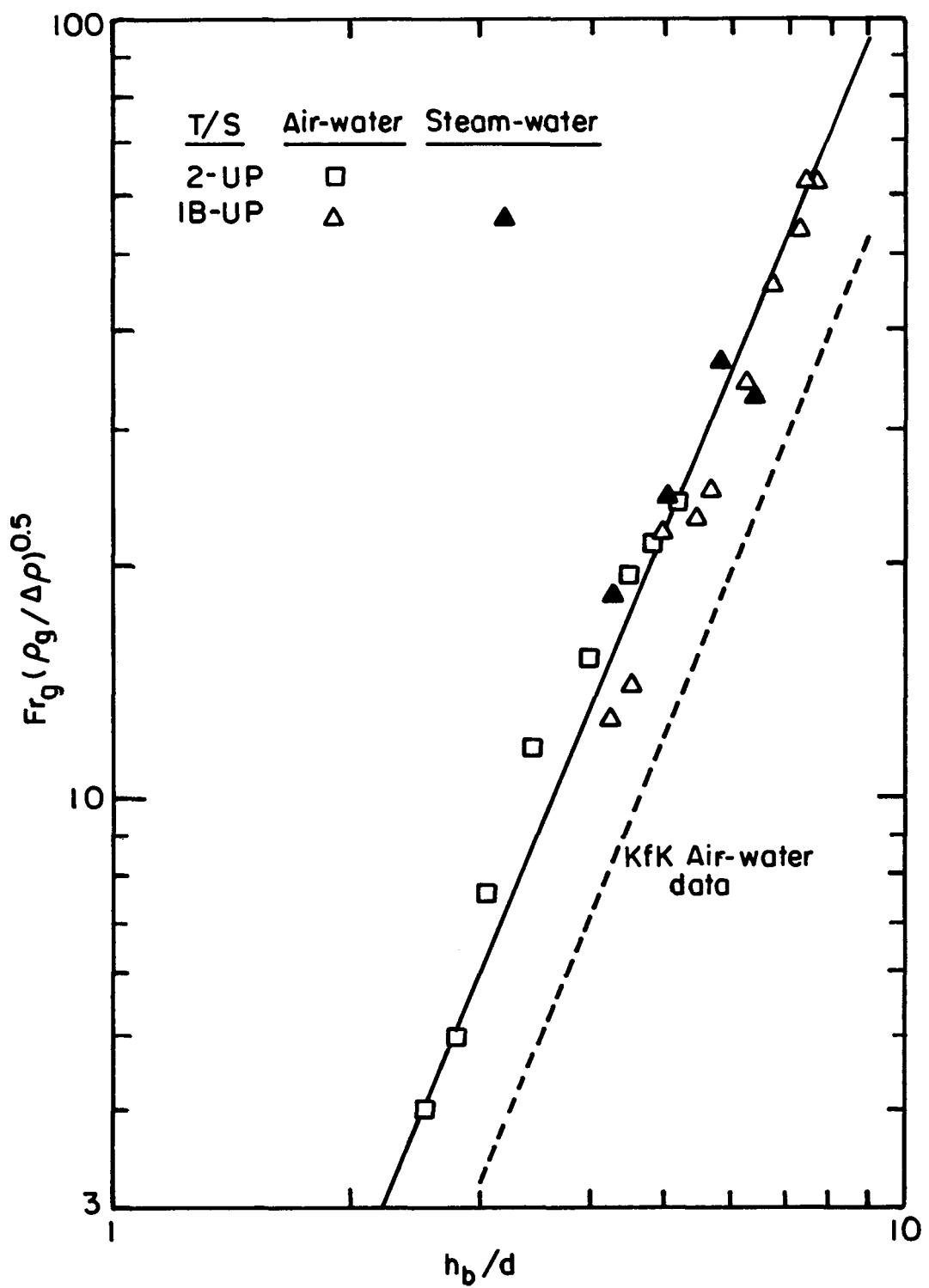
Figure 5-18   Inception Data of Liquid Entrainment,
Upward Oriented Break
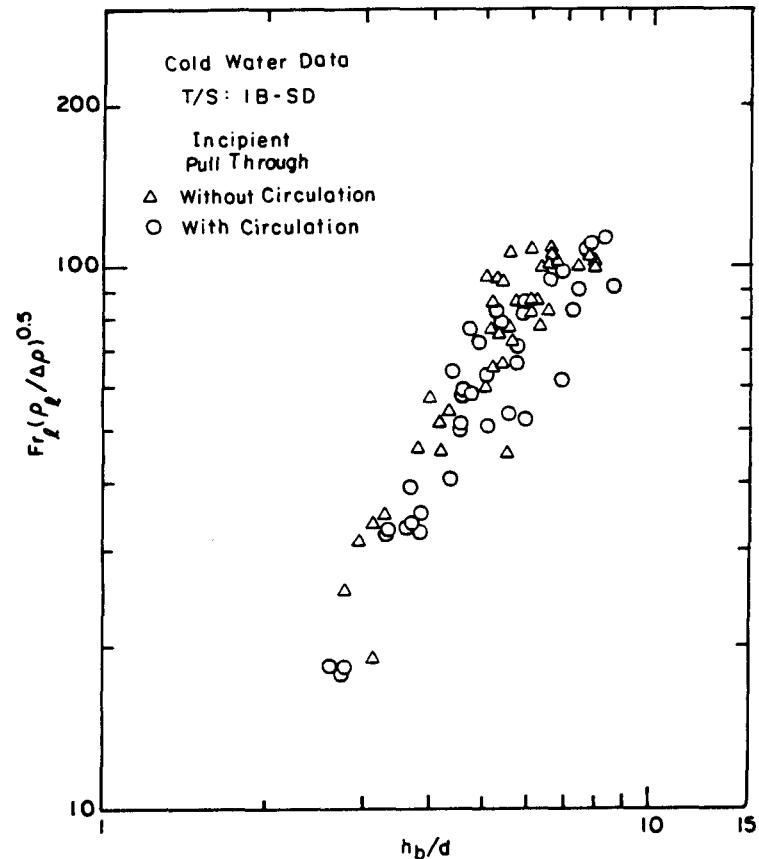
Figure 5-19   Inception Data of Vapor
Pull-Through with and without
Superimposed Liquid Velocity
for Side Oriented Break
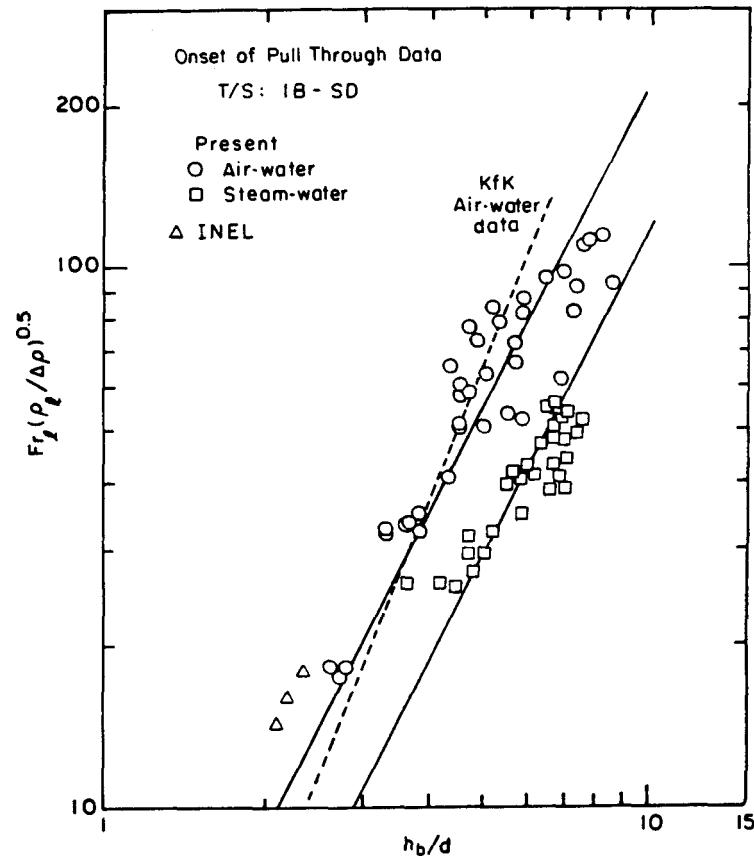
Figure 5-20   Inception Data of Vapor Pull-
Through for Air-Water and
Steam-Water Flow Systems,
Side Oriented Break

account of surface tension and viscosity effects through Bond number and viscosity number. The results of this new representation is shown in Figure 5-21 with present (UCB), KfK and INEL data. The correlation that fits all the data is given as

$$Fr_\ell \ Bo^2 \ N_\mu^{-0.5} \ (\rho_\ell/\Delta\rho)^{0.5} = 40.6 \left[\frac{h_b}{(\sigma/g\Delta\rho)^{0.5}} \right]^{2.1} \tag{5.8}$$

Again in obtaining this correlation more weight is given to KfK and present (UCB) data than the INEL data which were inferred from the differential pressure transducer response.

The data of inception of liquid entrainment for side oriented break are shown in Figure 5-22. The correlation that fits the data is given as

$$Fr_g \left(\frac{\rho_g}{\Delta\rho} \right)^{0.5} = 3.25 \left(\frac{h_b}{d} \right)^{2.5} \tag{5.9}$$

The INEL data and the KfK data line are also shown in Figure 5-22 for comparison. The INEL data agree well with the present (UCB) data. The KfK data show larger inception interface heights compared to present data for the same gas discharge through break. Similar observation was made in the case of results of upward oriented break when the inception data of the present and KfK experiments were compared.

5.5 Two-Phase Flow

5.5.1 Downward Orientation (Bottom Break)

The results of the air-water two-phase flow with vapor pull-through tests carried out on the glass test pipe are presented in Figure 5-23, 5-24 and 5-25 for two different stagnation pipe pressures. In Figure 5-23 and 5-24 the air-water mass flux shown as a function of non-dimensional interfact level, clearly indicate the height of interface at which inception of vapor pull-through occurs. The flow quality entering the break entrance shown in Figure 5-25 indicates an exponential relation with interface height. In Figure 5-26, 5-27 and 5-28, the mass flux measured with T/S: 1A-DN for air-water two phase flow are presented. From the pressure measurements it was observed that a larger pressure drop was measured across the exit of the break indicating that the choking of the flow occurred at the exit of the break. The break entrance quality shown in Figure 5-29 indicates an increase in quality with increase in stagnation pipe pressure for the same interface height.

The mass flux data of steam-water two phase entrance critical flow through break obtained with T/S: 1-DN are presented in Figures 5-30 to 5-37 for various stagnation pipe pressures varying from 370 kPa to
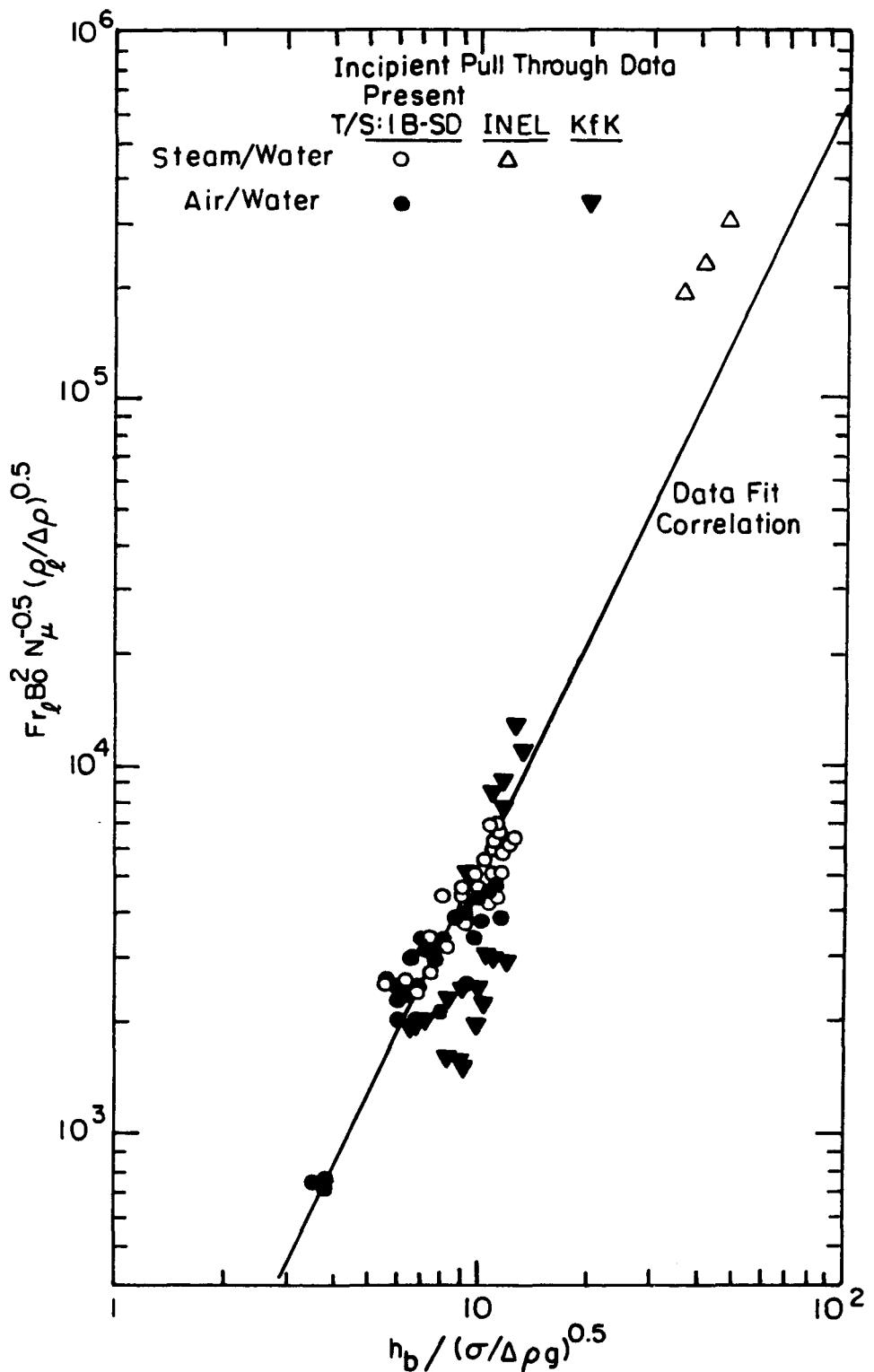
Figure 5-21 Correlation for Inception of Vapor Pull-Through
Data of KfK, INEL and present (UCB) for Side
Oriented Break
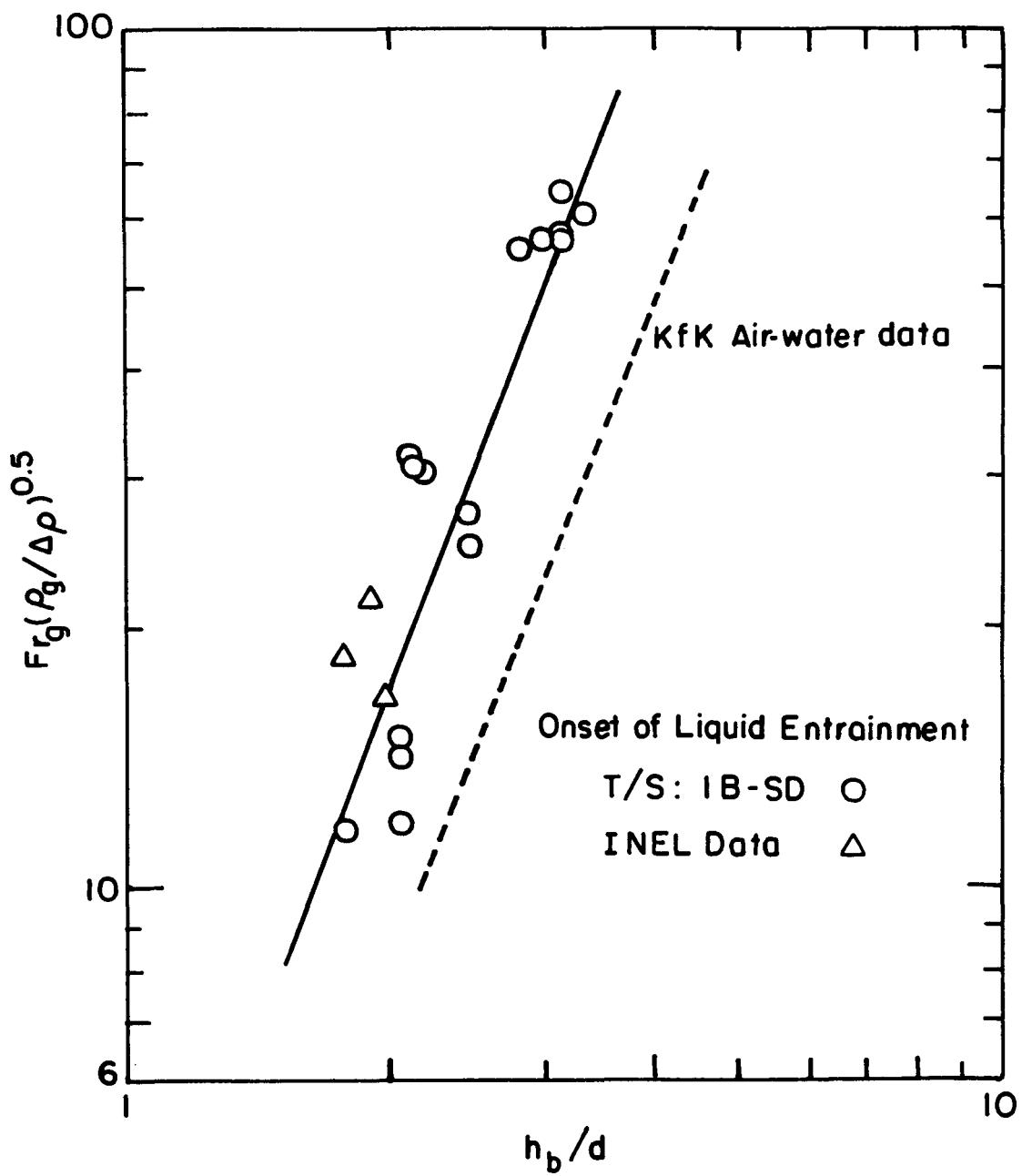
Figure 5-22 Inception Data of Liquid Entrainment,
Side Oriented Break

5-30
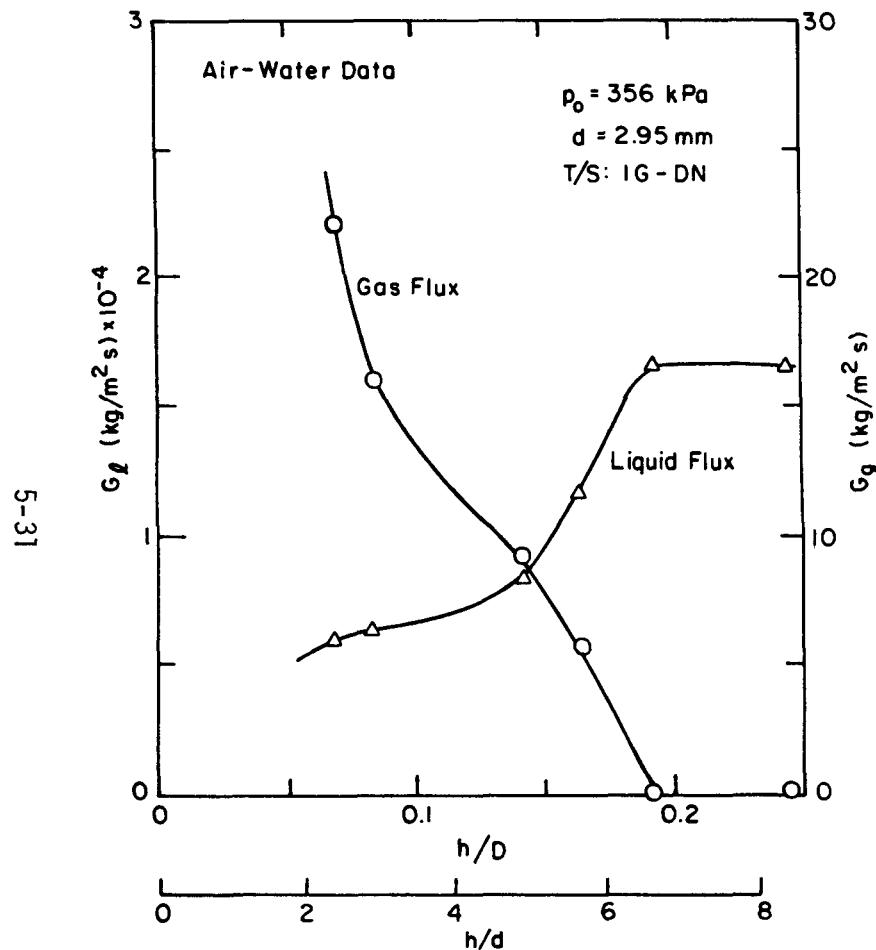
Figure 5-23   Break Liquid and Gas Mass
Flux for T/S: 1G-DN at $p_o =$
356 kPa, Air-Water Data,
Down Oriented Break
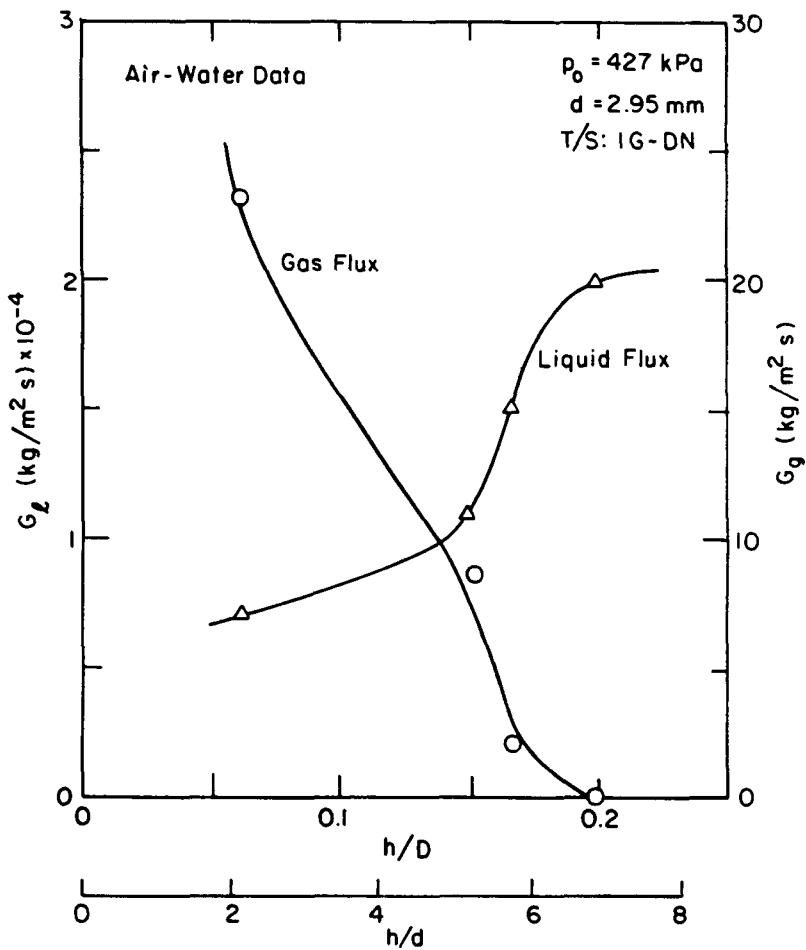
Figure 5-24   Break Liquid and Gas Mass
Flux for T/S: 1G-DN at $p_o =$
427 kPa, Air-Water Data,
Down Oriented Break
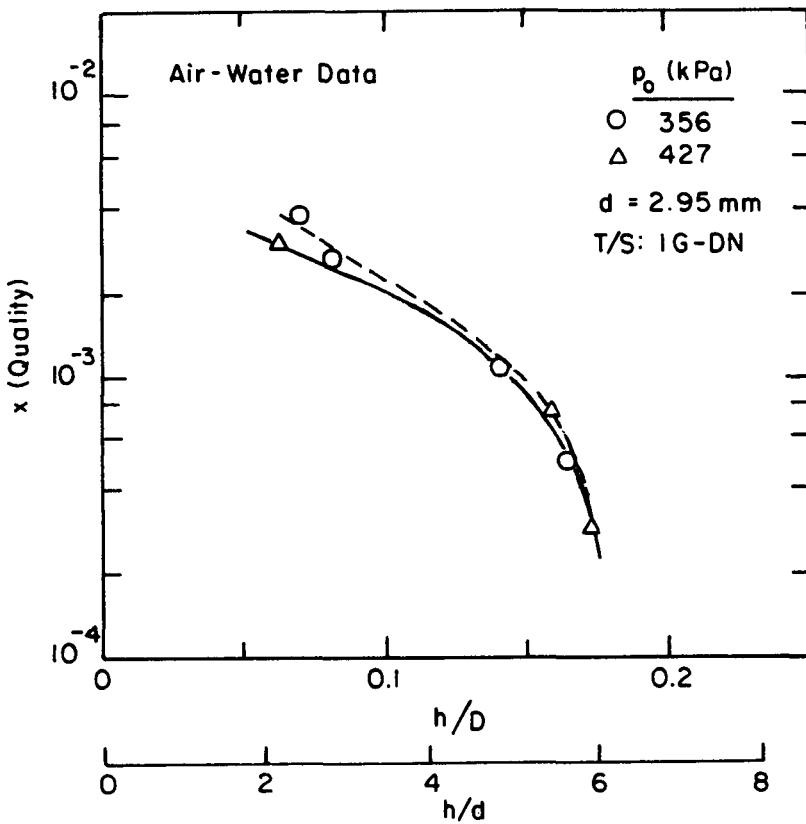
Figure 5-25   Break Entrance Quality x,
vs h/D for T/S: 1 G-DN,
Air-Water Data; Downward
Oriented Break
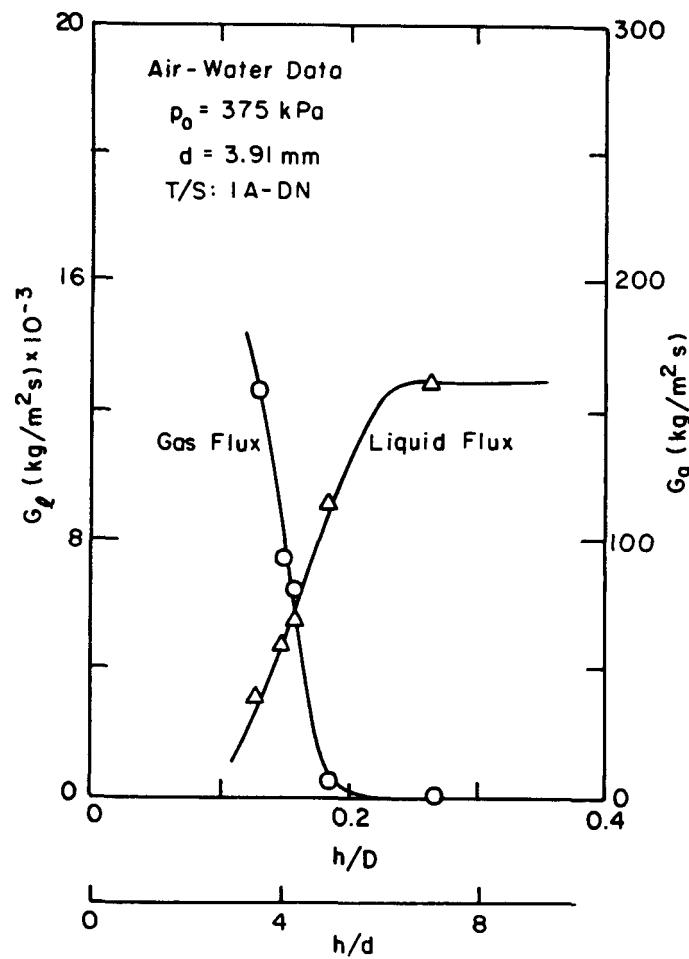
Figure 5-26   Break Liquid and Gas Mass
Flux for T/S: 1A-DN at p_o=
375 kPa Air-Water Data,
Down Oriented Break
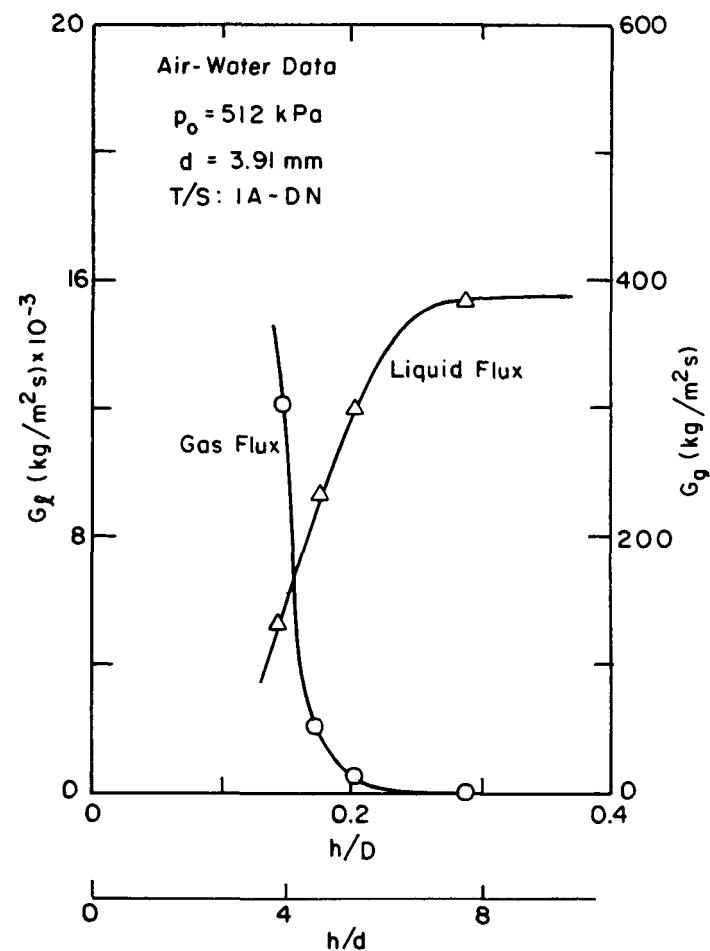
Figure 5-27   Break Liquid and Gas Mass
              Flux for T/S: 1A-DN at $p_0 =$
              512 kPa Air-Water Data,
              Down Oriented Break
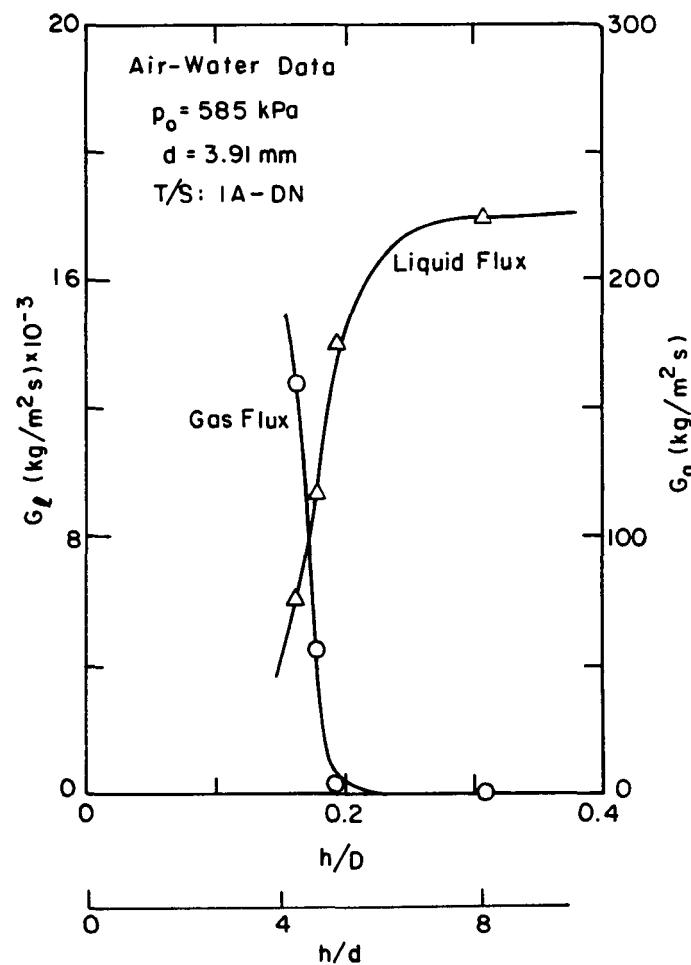
Figure 5-28   Break Liquid and Gas Mass
              Flux for T/S: 1A-DN at $p_0 =$
              585 kPa Air-Water Data,
              Down Oriented Break
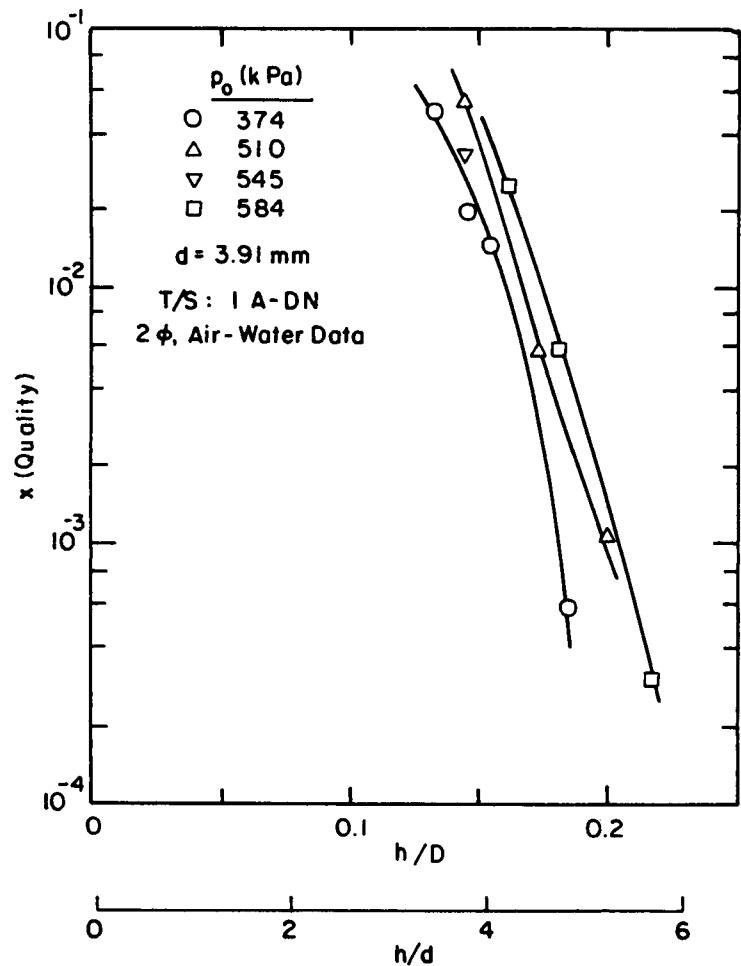
Figure 5-29 Break Entrance Quality x vs
h/D for T/S: 1A-DN Air-Water,
Down Oriented Break
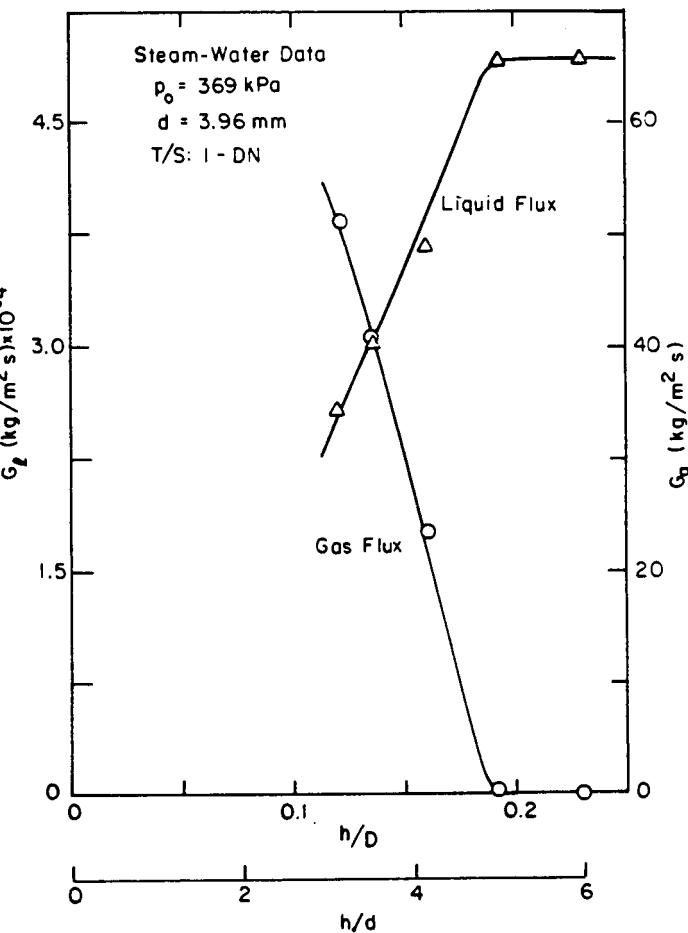
Figure 5-30 Break Liquid and Vapor Mass
Flux for T/S: 1-DN at p_0=
369 kPa, Steam-Water Data,
Down Oriented Break
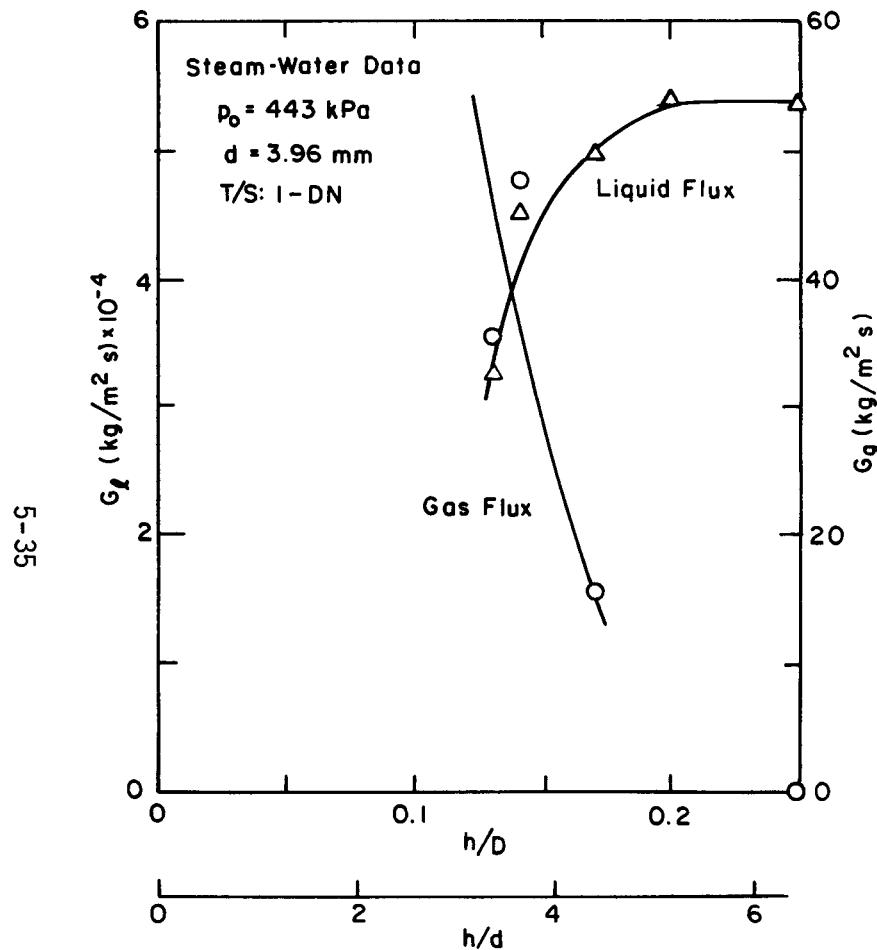
Figure 5-31   Break Liquid and Vapor Mass
Flux for T/S: 1-DN at p_o=
443 kPa, Steam-Water Data,
Down Oriented Break
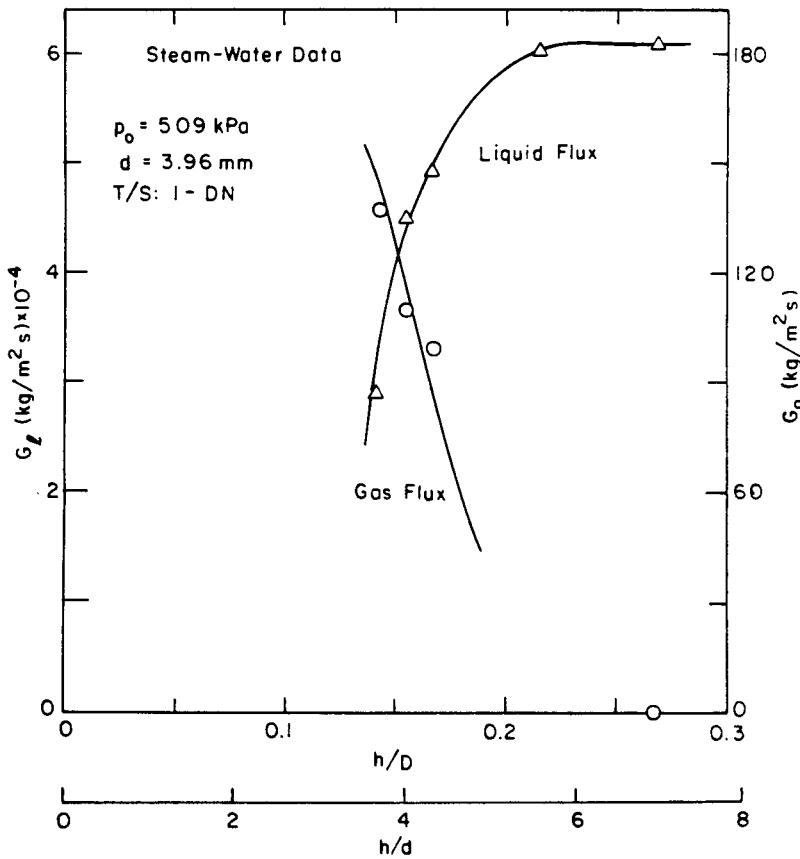
Figure 5-32   Break Liquid and Vapor Mass
Flux for T/S: 1-DN at p_o=
509 kPa Steam-Water Data,
Down Oriented Break
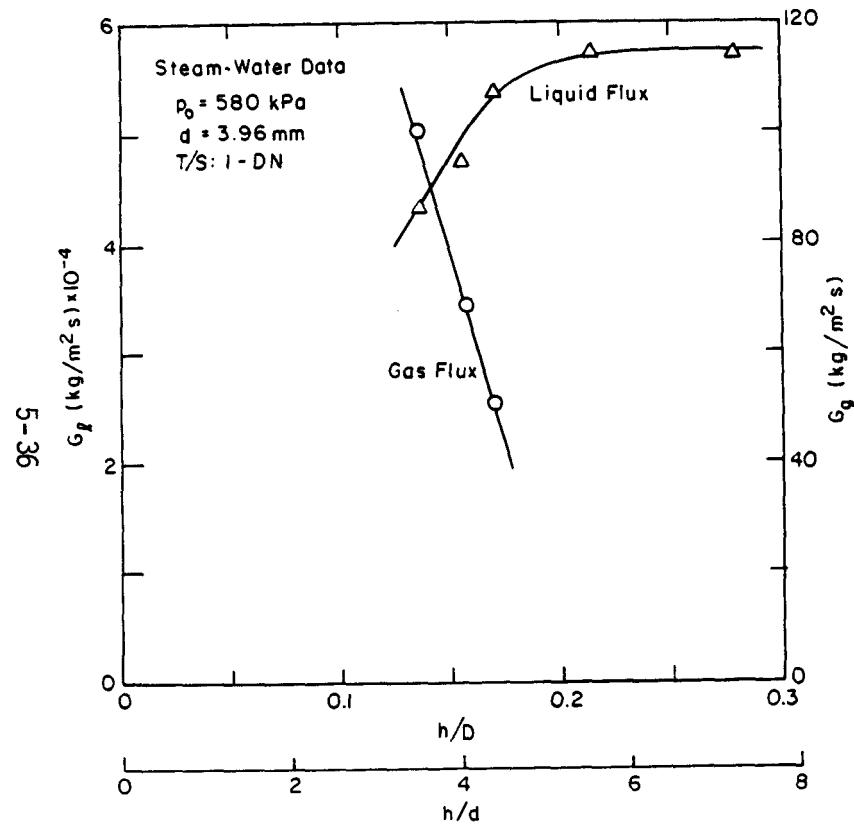
Figure 5-33   Break Liquid and Vapor Mass
Flux for T/S: 1-DN at p_o=
580 kPa Steam-Water Data,
Down Oriented Break
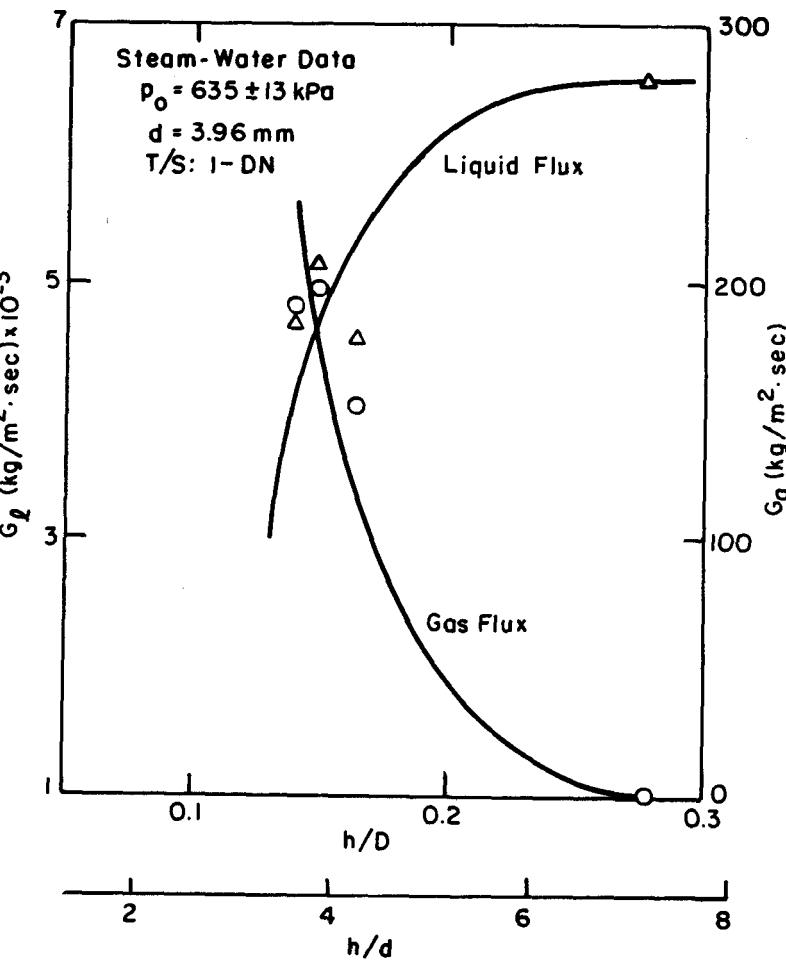
Figure 5-34   Break Liquid and Vapor Mass
Flux for T/S: 1-DN at p_o=
635 kPa, Steam-Water Data,
Down Oriented Break
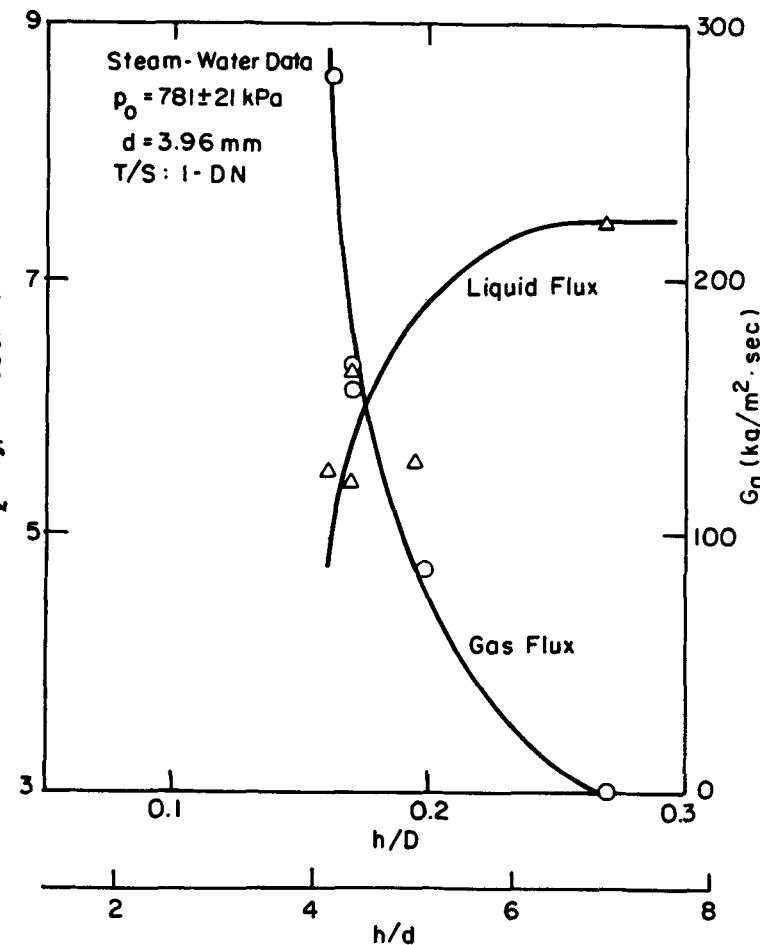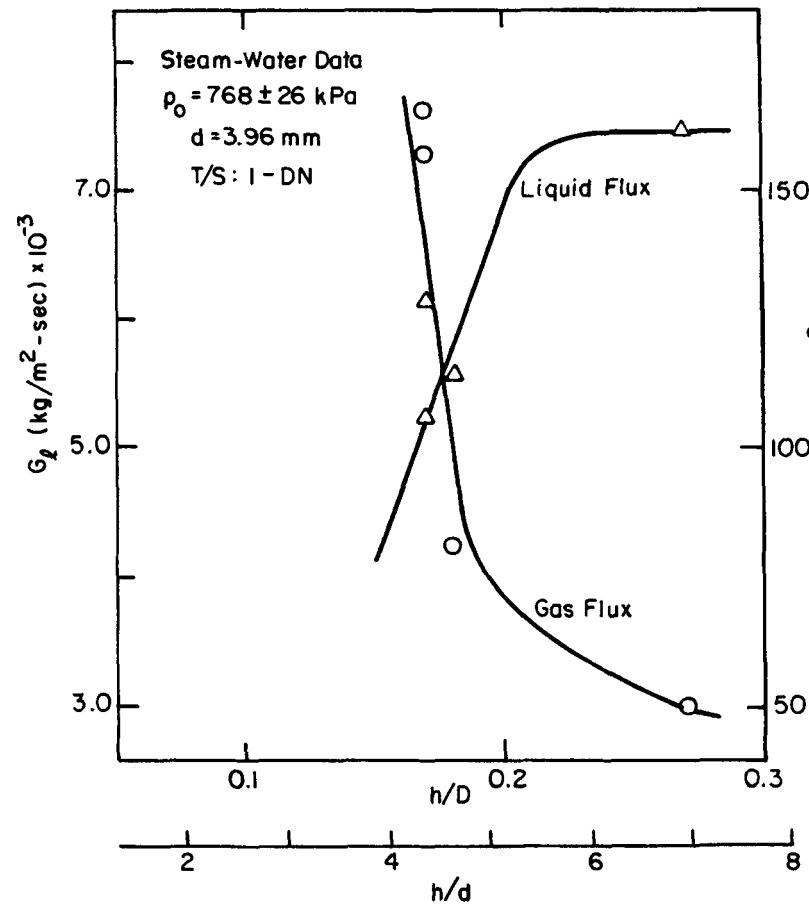
Figure 5-35   Break Liquid and Vapor Mass
             Flux for T/S: 1-DN at p_0 =
             768 kPa, Steam-Water Data,
             Down Oriented Break

Figure 5-36   Break Liquid and Vapor Mass
             Flux for T/S: 1-DN at p_0 =
             781 kPa, Steam-Water Data,
             Down Oriented Break
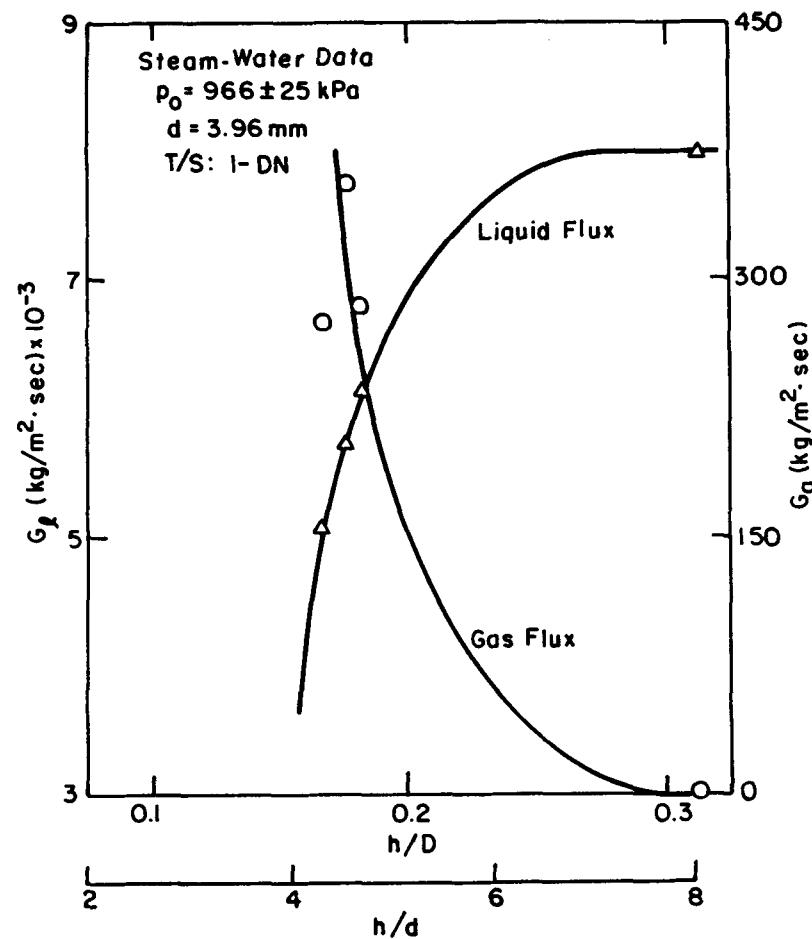
Figure 5-37　Break Liquid and Vapor Mass Flux for T/S: 1-DN at p_O = 966 kPa, Steam-Water Data, Down Oriented Break
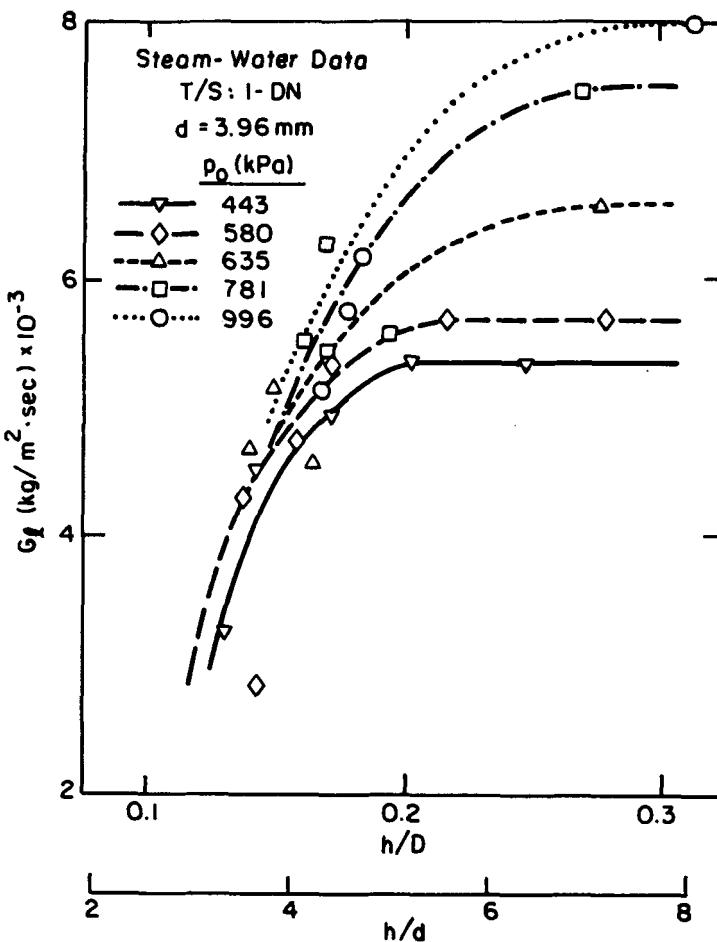
Figure 5-38　Break Liquid Mass Flux as Function of Stagnation Pressure for T/S: 1-DN, Steam-Water Data, Downward Oriented Break

970 kPa. The liquid flux results are shown in Figure 5-38 for different pipe stagnation pressure. From this figure we find that there is a sharp decrease in liquid flow rate with gas entrainment at different levels of liquid interface depending on the pipe stagnation pressure. The corresponding data for gas flux are summarized in Figure 5-39, which shows a sharp decrease in gas entrainment with increase in liquid interface.

The measured pressure profiles of two-phase steam-water critical flow in T/S: 1-DN are shown in Figure 5-40 through 5-45 for different stagnation pipe pressure varying from 370 kPa to 970 kPa. In each figure the liquid interface height and the measured entrance quality are indicated where it is observed that the two-phase pressure drop in the break tube increases with increase in the flow quality. From the pressure profiles it is evident that the flow choking occur at the exit of the break tube where large pressure gradients are measured.

The measured flow quality is presented in Figure 5-46 for different stagnation pipe pressure. For the same liquid interface height the flow quality is larger with higher pipe stagnation pressure.

The results of the measured mass flux of the critical two-phase steam-water flow with vapor pull-through for T/S: 2-DN are shown in Figure 5-47 through 5-50 for different stagnation pipe pressure. In Figure 5-51 the liquid mass flux are shown as function of different pipe pressure while in Figure 5-52, the entrained gas mass flux are shown. These figures show that the data trend obtained with the T/S: 2-DN are similar to those obtained with T/S: 1-DN. The measured pressure profiles as function of inlet flow quality are presented in Figures 5-53 through 5-56 for different pipe pressures. Here also we find from the pressure profiles that the choking occurs at the break tube exit and the two-phase pressure drop increases with increase in the entrance quality. The flow entrance quality as a function of the pipe stagnation pressure is shown in Figure 5-57, where again we find that the data trends are very similar to those obtained with T/S: 1-DN.

In order to achieve a single representation of quality data, the flow quality is correlated with the non-dimensional interface height. The interface height is non-dimensionalized with the interface height at which inception of first bubble pull-through occur. This process of non-dimensionalization of interface height conceals the pipe pressure effects on the measured quality. The quality correlation is shown in Figure 5-58. For each data point, in this figure, the value of h_b used was calculated from equation (5.6) for the pressure condition at which the particular quality and h were measured. The INEL data are also shown in this figure, where again the corresponding inception height h_b was calculated from equation (5.6). The present and INEL data agree well with each other in this representation. The correlating for quality which fits present data and INEL data is given as
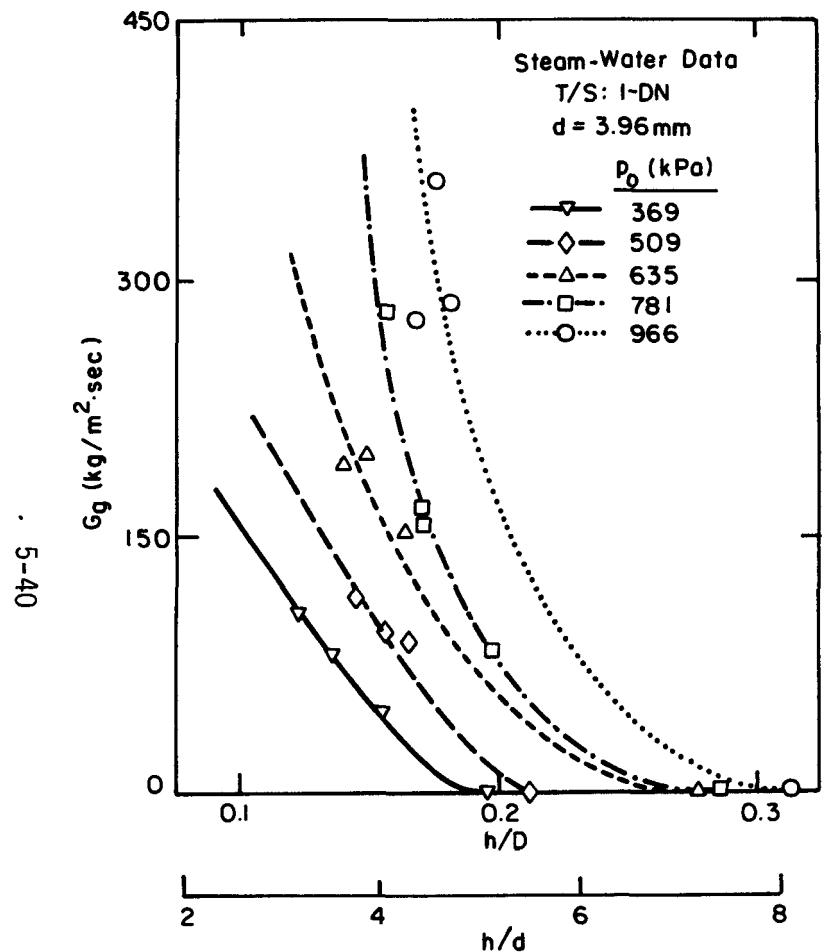
Figure 5-39   Break Vapor Mass Flux as
              Function of Stagnation
              Pressure for T/S: 1-DN,
              Steam Water Data,
              Downward Oriented Break
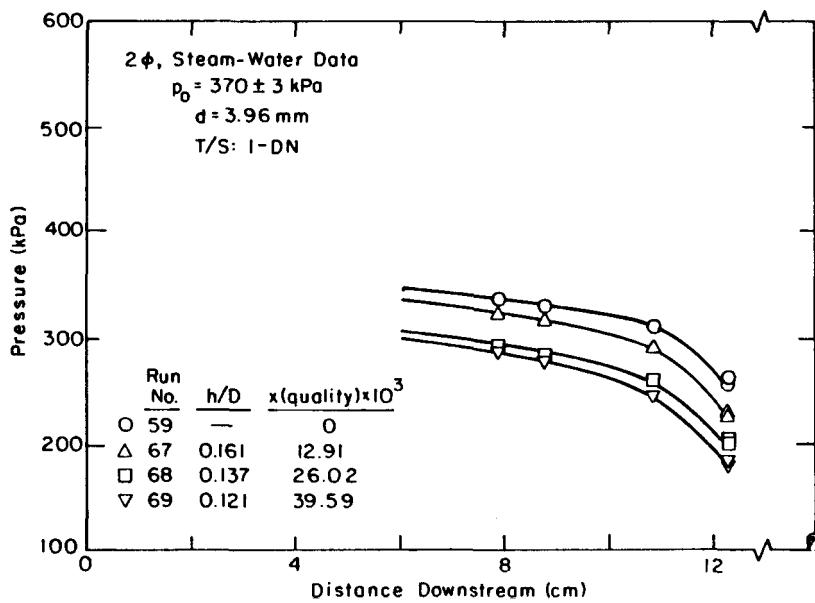
Figure 5-40   Pressure Profiles in T/S:
              1-DN, Two-phase Steam-Water
              Flow with Different Inlet
              Qualities p_0 = 370 kPa,
              Down Oriented Break
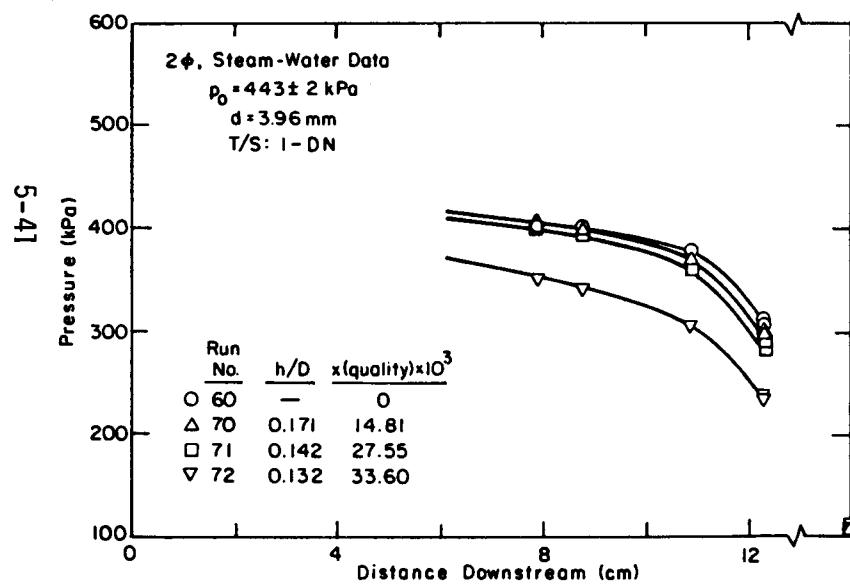
Figure 5-41   Pressure Profiles in T/S:
1-DN, Two-phase, Steam-Water
Flow with Different Inlet
Qualities, p_0 = 443 kPa,
Down Oriented Break
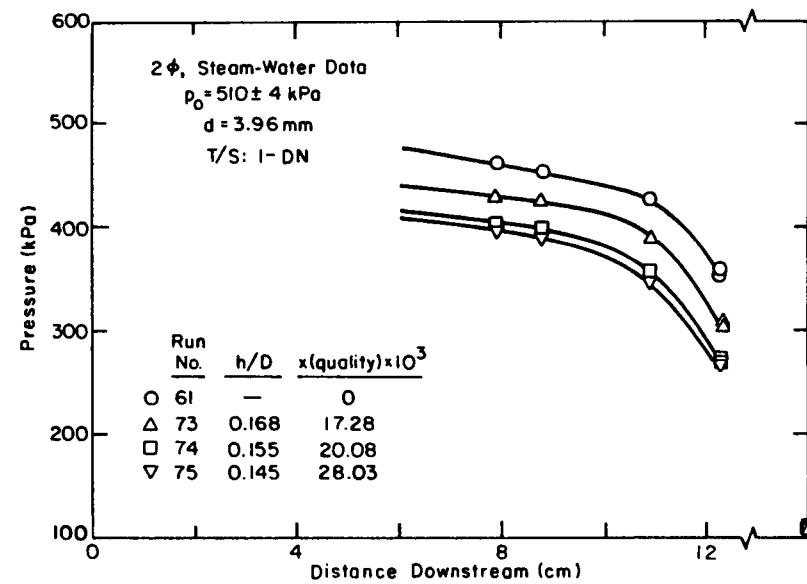
Figure 5-42   Pressure Profiles in T/S:
1-DN, Two-phase, Steam-Water
Flow with Different Inlet
Qualities, p_0 = 510 kPa,
Down Oriented Break
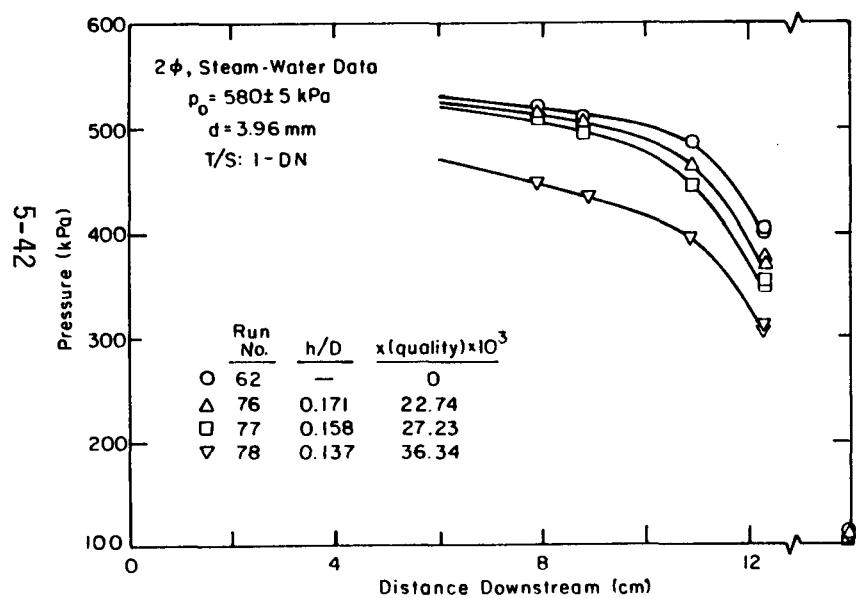
Figure 5-43 Pressure Profiles in T/S: 1-DN, Two-Phase, Steam-Water Flow with Different Inlet Qualities, p_0 = 580 kPa, Down Oriented Break
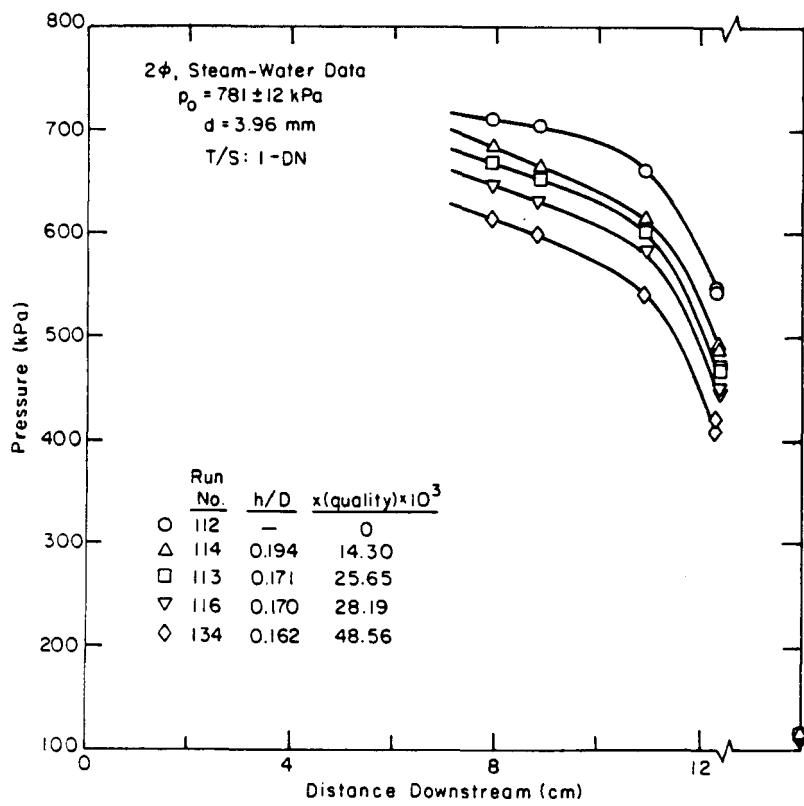
Figure 5-44 Pressure Profiles in T/S: 1-DN, Two-phase, Steam-Water Flow with Different Inlet Qualities, p_0 = 781 kPa, Down Oriented Break
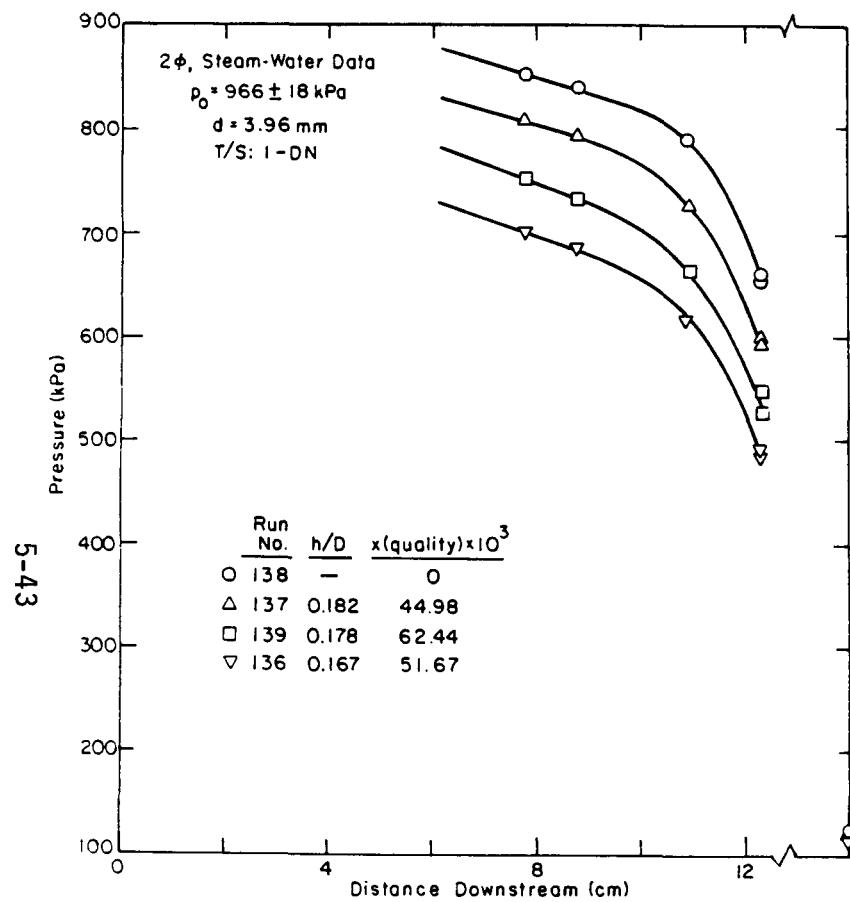
Figure 5-45   Pressure Profiles in T/S: 1-DN
               Two-phase, Steam-Water Flow
               with Different Inlet Qualities,
               p_0 = 966 kPa, Down Oriented
               Break
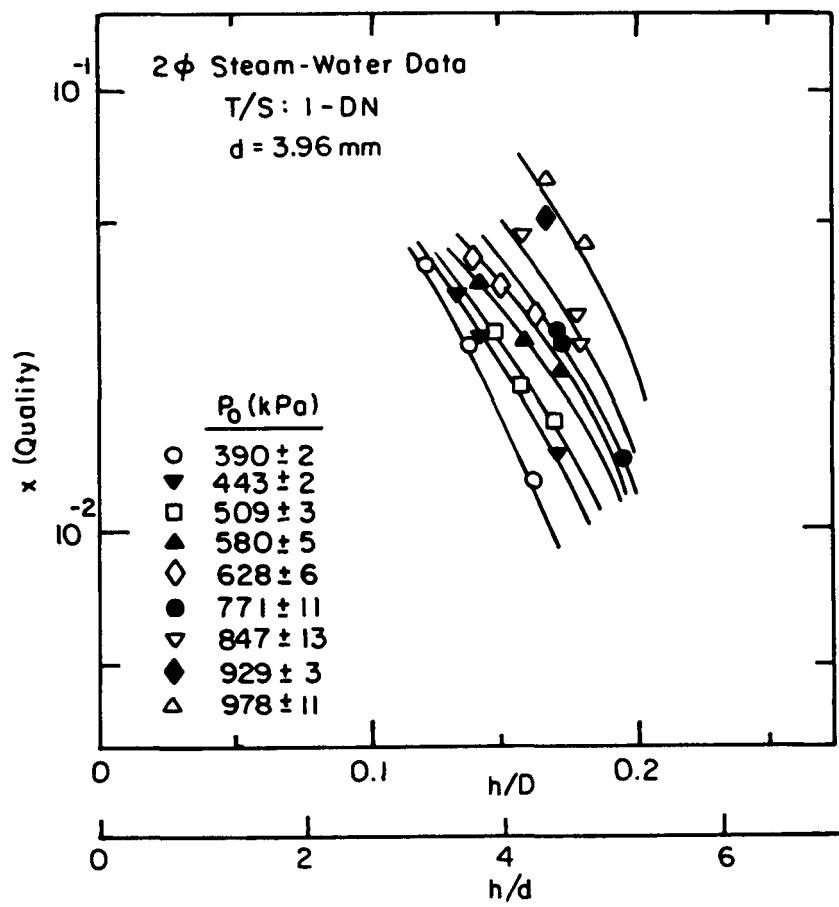
Figure 5-46   Break Entrance Quality vs
               h/D for T/S: 1-DN,
               Two-phase, Steam-Water Data,
               Down Oriented Break
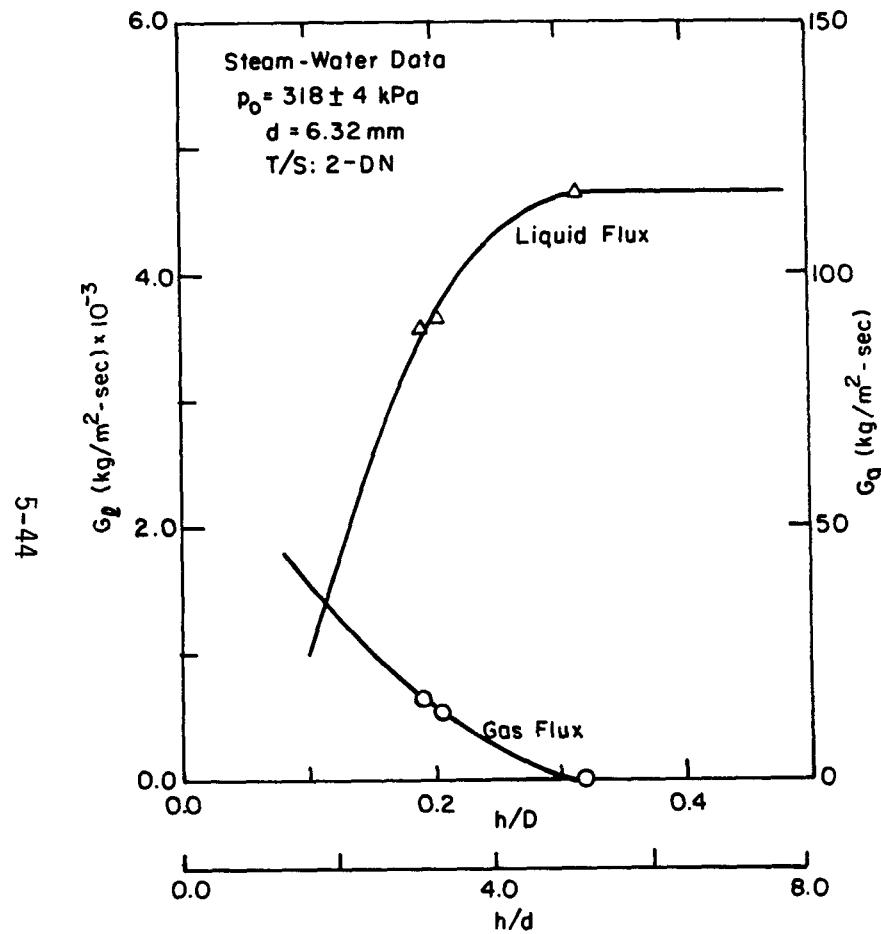
Figure 5-47 Break Liquid and Vapor Mass
Flux for T/S: 2-DN at
p_0 = 318 kPa, Steam-Water Data,
Down Oriented Break
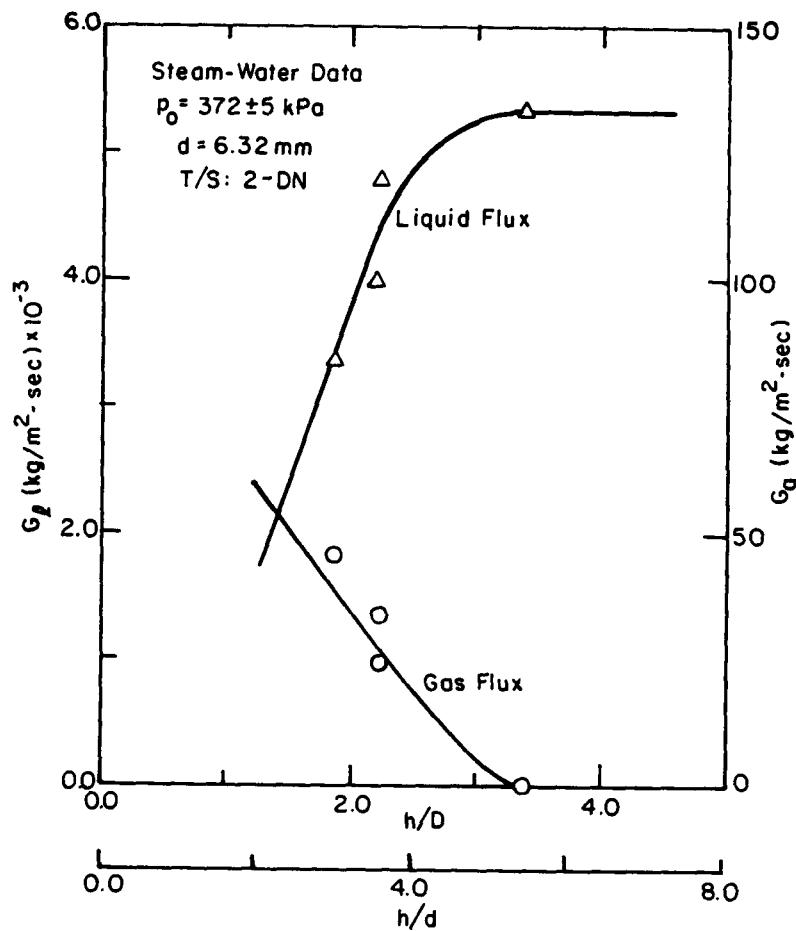
Figure 5-48 Break Liquid and Vapor Mass
Flux for T/S: 2-DN at
p_0 = 372 kPa, Steam-Water Data,
Down Oriented Break
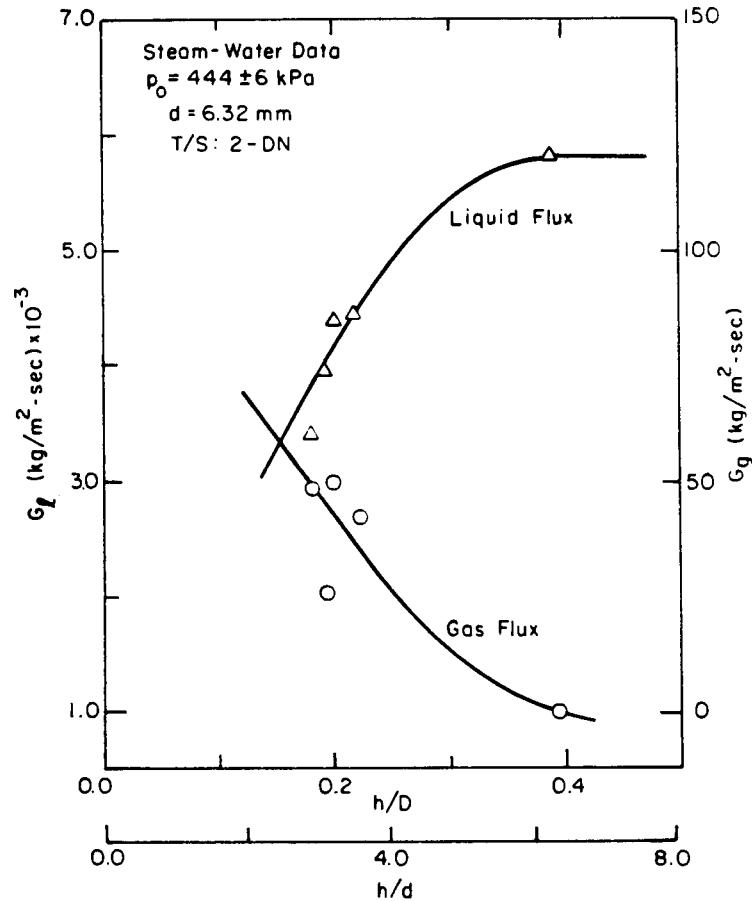
Figure 5-49   Break Liquid and Vapor Mass
               Flux for T/S: 2-DN at
               p_o = 444 kPa, Steam-Water Data,
               Down Oriented Break
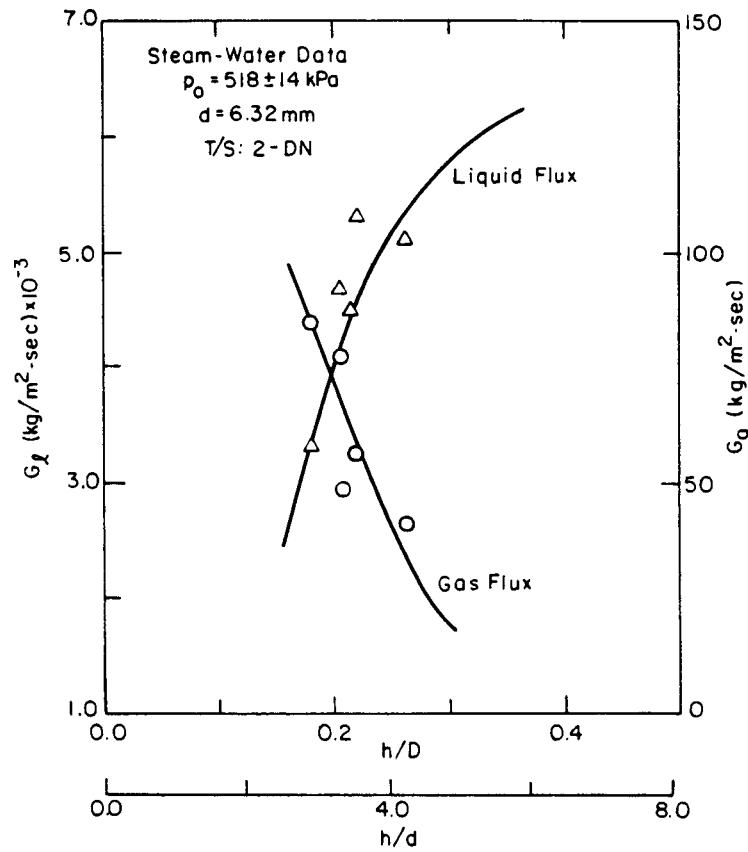
Figure 5-50   Break Liquid and Vapor Mass
               Flux for T/S: 2-DN at
               p_o = 518 kPa, Steam-Water Data,
               Down Oriented Break
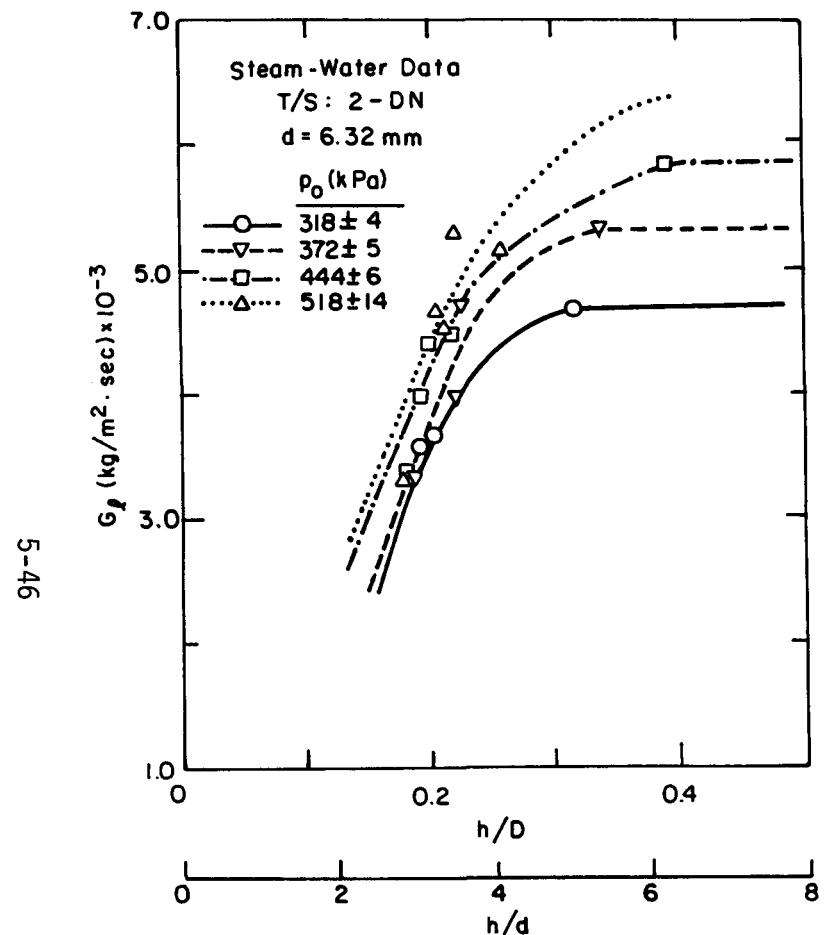
Figure 5-51 Break Liquid Mass Flux as
a Function of Stagnation
Pressure for T/S: 2-DN, Steam-
Water Data, Down Oriented Break
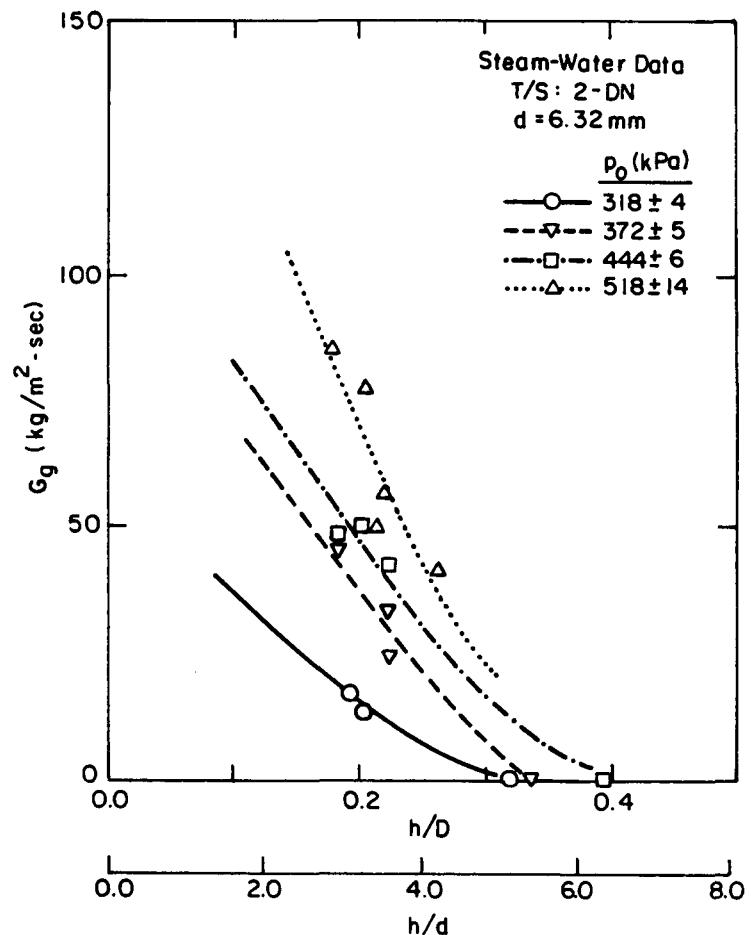
Figure 5-52 Break Vapor Mass Flux as a
Function of Stagnation
Pressure for T/S: 2-DN, Steam-
Water Data, Down Oriented Break
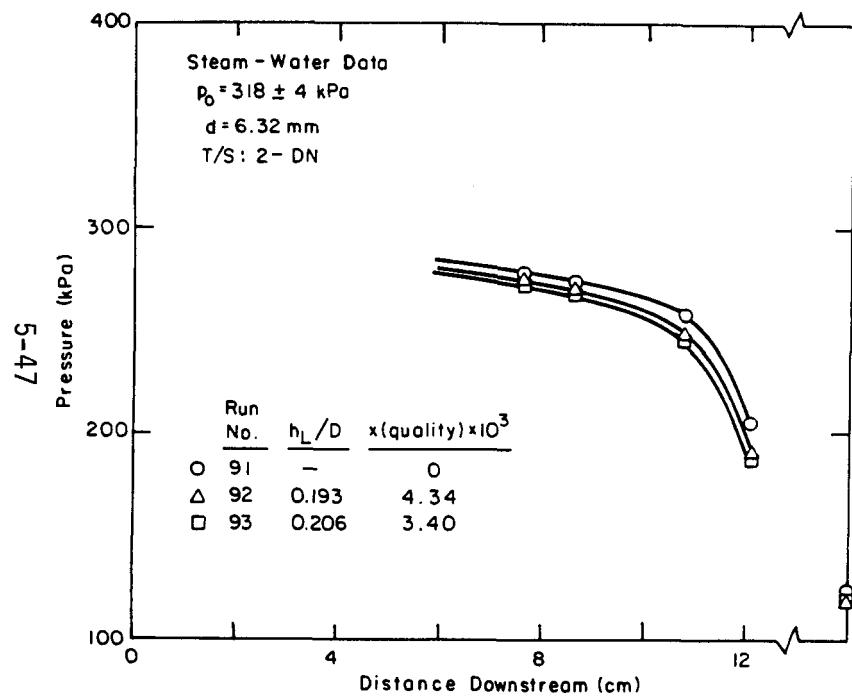
Figure 5-53 Pressure Profiles in T/S: 2-DN,
Two-phase Steam-Water Flow
with Different Inlet Qualities,
p_o = 318 kPa, Down Oriented
Break
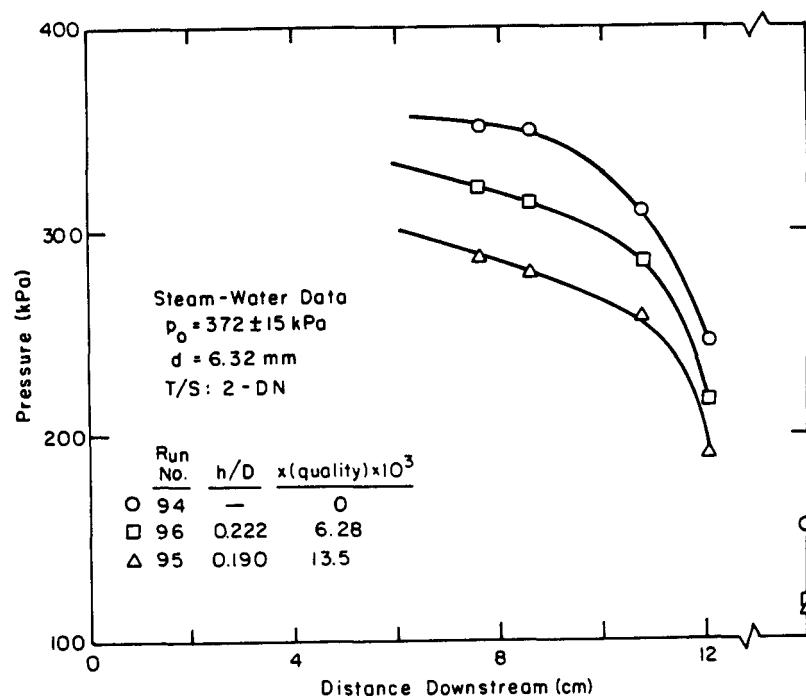
Figure 5-54 Pressure Profiles in T/S: 2-DN,
Two-phase Steam Water Flow
with Different inlet Qualities,
p_o = 372 kPa, Down Oriented
Break
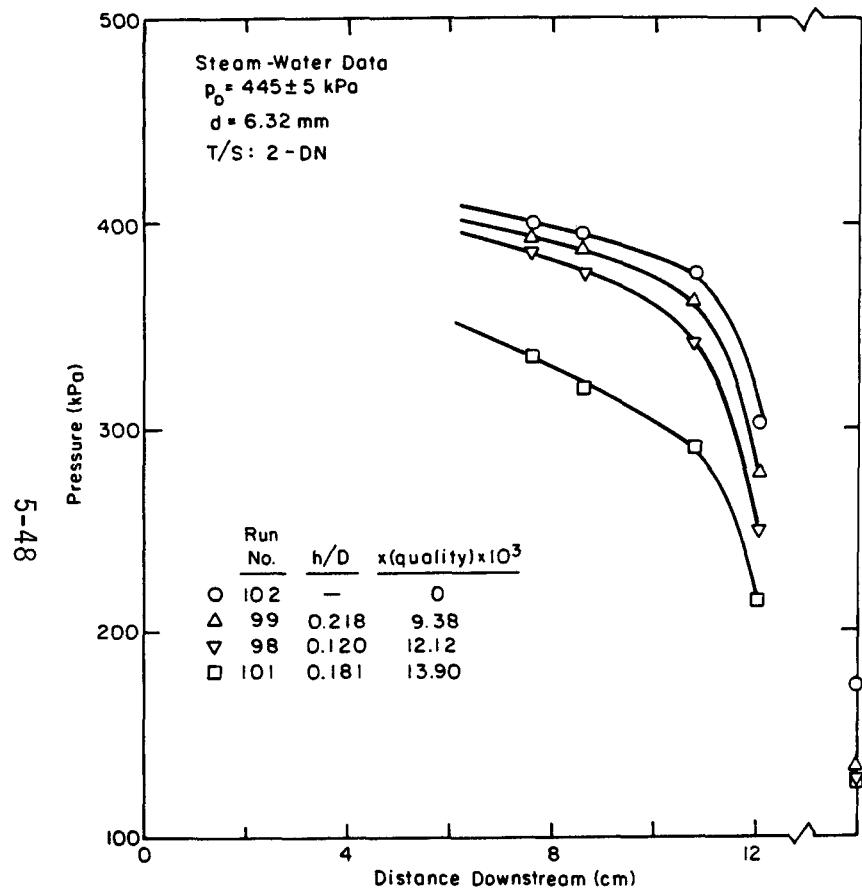
Figure 5-55   Pressure Profiles in T/S:
2-DN, Two-phase Steam-Water
Flow with Different Inlet
Qualities, p_0 = 445 kPa,
Down Oriented Break
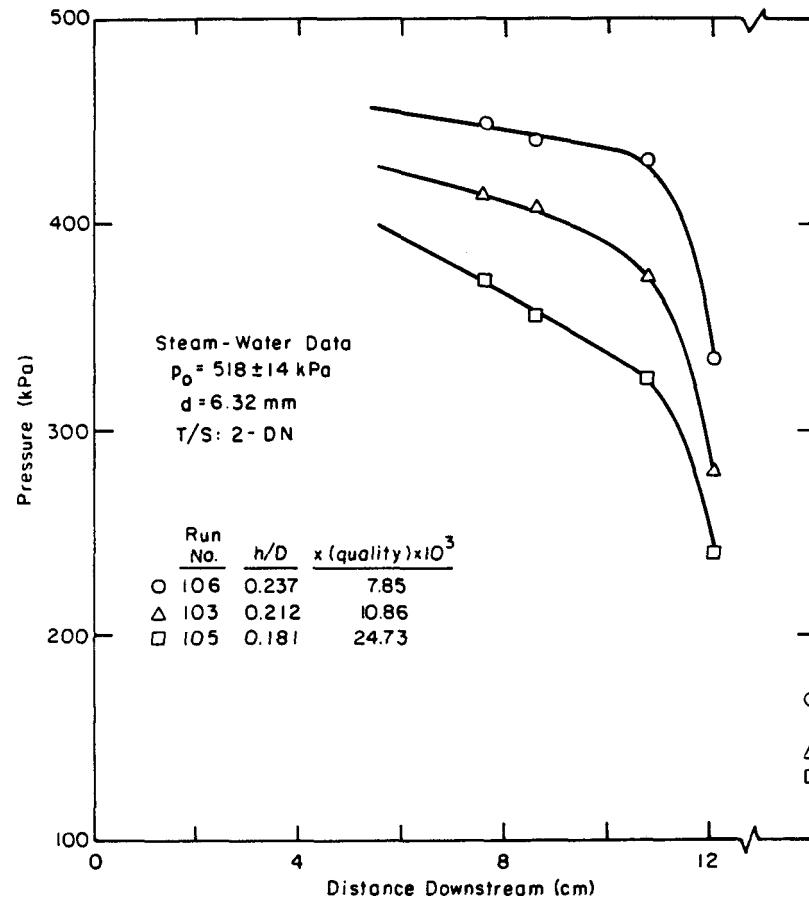
Figure 5-56   Pressure Profiles in T/S:
2-DN, Two-phase Steam-Water
Flow with Different Inlet
Qualities, p_0 = 518 kPa,
Down Oriented Break
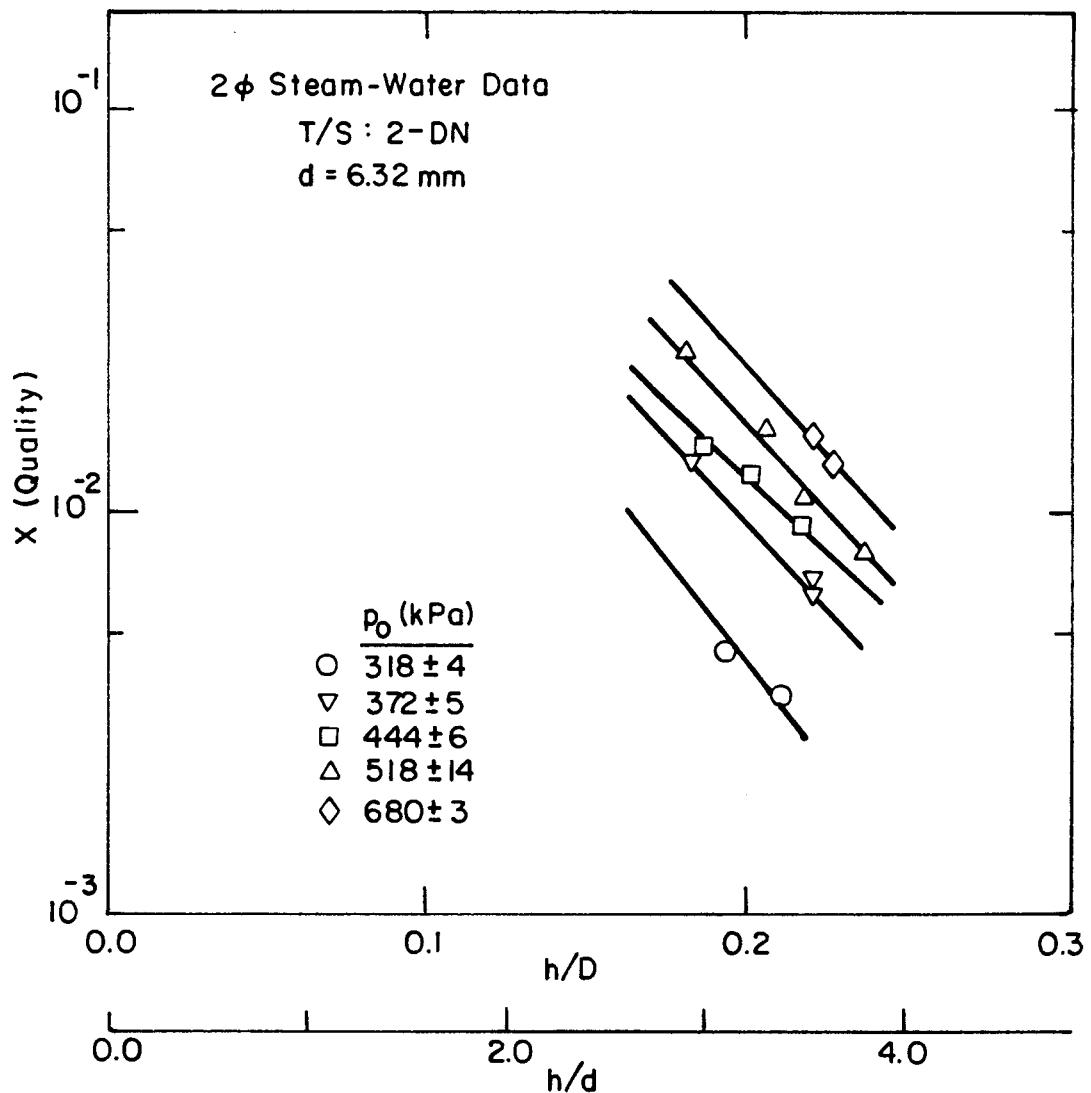
Figure 5-57   Break Entrance Quality vs h/D for T/S: 2-DN,
Two-phase Steam-Water Data, Down Oriented Break

5-49
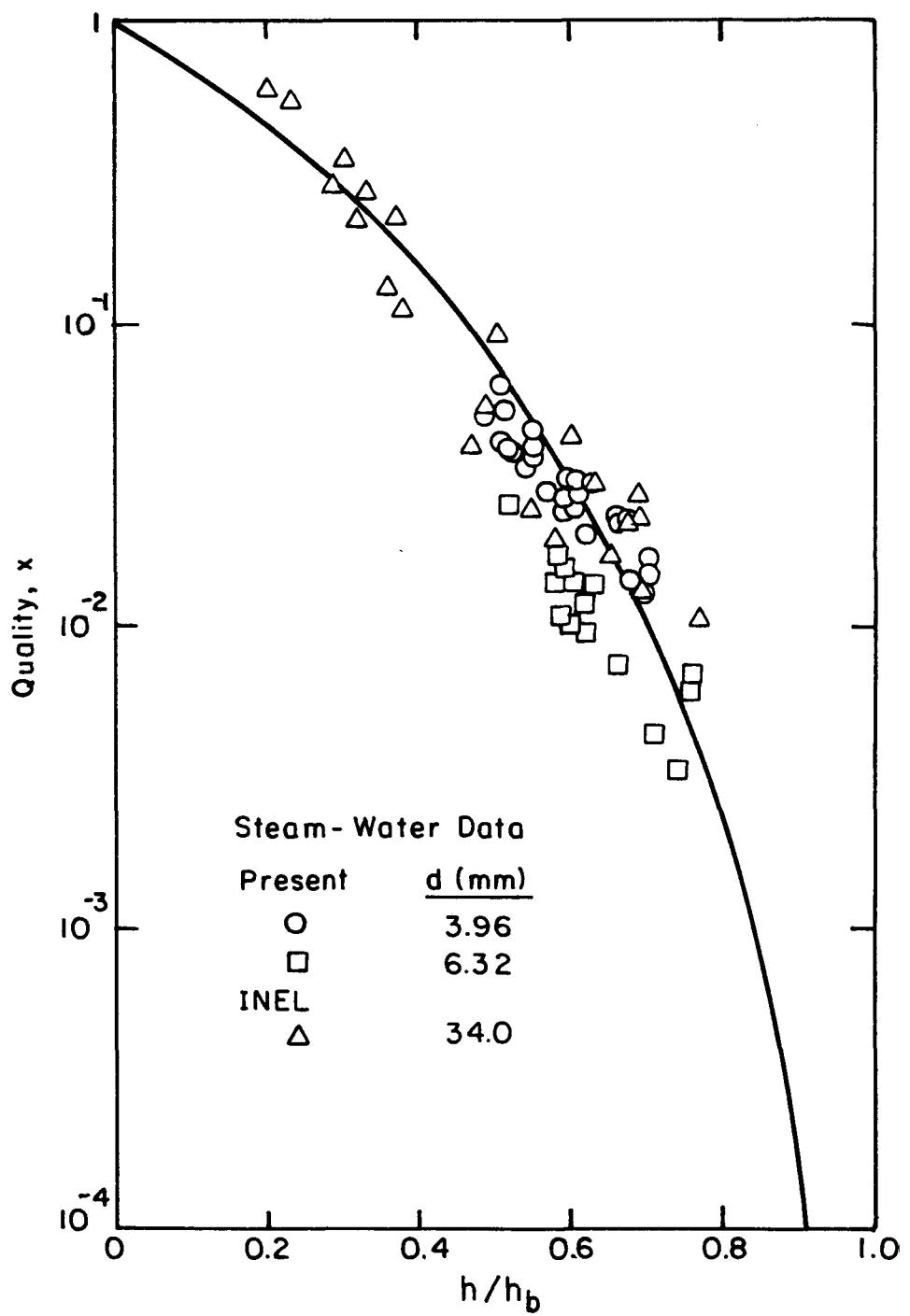
Figure 5-58   Break Entrance Quality Correlation for Two-phase
Steam-Water Flow with Vapor Pull-Through, Down
Oriented Break

$$x = e^{-3.1(\frac{h}{h_b})} \cdot \left[1- (\frac{h}{h_b})^2 \right]^{3.5} \qquad (5.10)$$

5.5.2 Upward Orientation (Top Break)

The results of two-phase discharge with liquid entrainment through the upward oriented break tube for air-water and steam-water system are summarized here. Typical mass flux measurements for steam-water and air-water flow system are presented in Figures 5-59 and 5-60. Liquid entrainment increases with decrease in the interface height h. From these figures, the interface height at which liquid entrainment begins can be identified as the height where the gas flux reaches a asymptotic value.

Typical pressure profiles for the steam-water system are shown in Figure 5-61 for a stagnation pressure of 400 kPa and for different interface heights and entrainment qualities. These two-phase pressure profiles are very similar to those observed in the case of two-phase discharges with vapor pull-through. This observation indicates that the flow patterns inside the break tube are similar for flow with vapor pull-through and liquid entrainment. The possible flow regime could be mixed type homogeneous two-phase flow and this explicitly excludes the separated flow; since in the latter case, the pressure drop associated with two-phase flow with vapor pull-through would be different from the pressure drop observed with two-phase flow with liquid entrainment.

The tube entrance quality results are presented in Figure 5-62. The quality measured for both steam-water and air-water are correlated with non-dimensional interface height. The present data extend over the quality range 10^{-2} to 0.95. The KfK data fit line is also shown in the figure. The KfK quality ranges only from 0.95 to 1. The present data compliment the KfK data in such a way that a consistent trend in the quality data versus h/h_b is observed. The present data were correlated by the relation

$$x = \left(\frac{h}{h_b} \right)^{3.25(1-h/h_b)^2} . \qquad (5.11)$$

5.5.3 Side Orientation (Side Break)

In the side oriented break, the two-phase discharge with vapor pull-through and liquid entrainment were both studied using the steam water system. In Figure 5-63, typical results of the mass flux are presented for two-phase with vapor pull-through, and in Figure 5-64 the corresponding pressure profiles are shown for different entrance qualities. The mass flux measured for two-phase entrance with liquid entrainment are shown in Figure 5-65 for a typical pressure of 198 kPa,
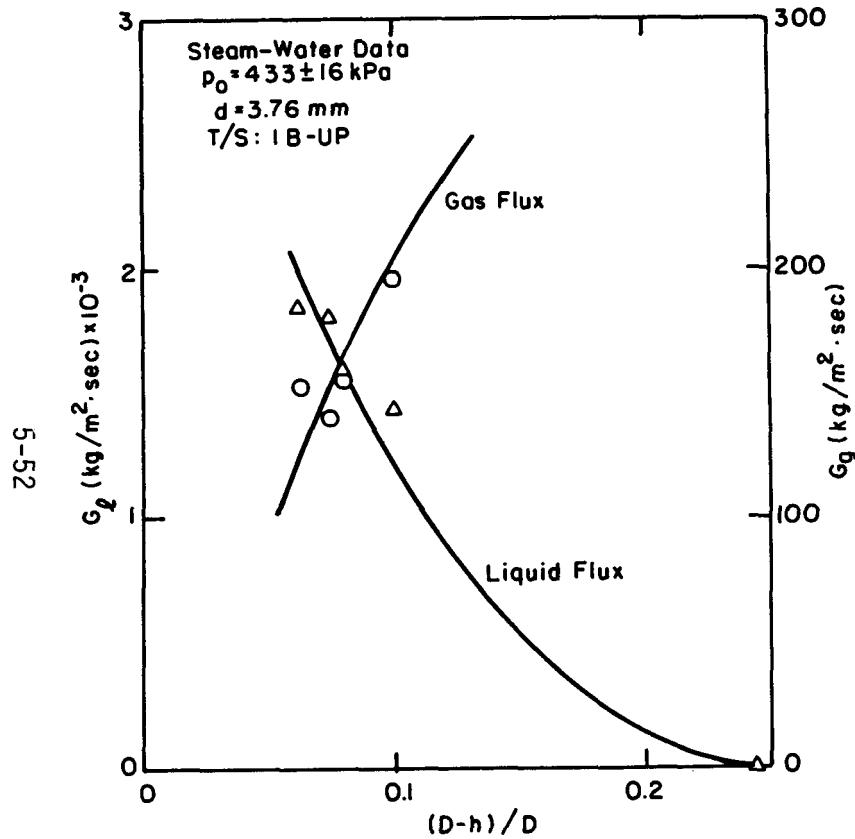
Figure 5-59   Break Liquid and Vapor Mass
Flux for T/S: 1B-UP at p_0 =
433 kPa, Steam-Water Data,
Up Oriented Break
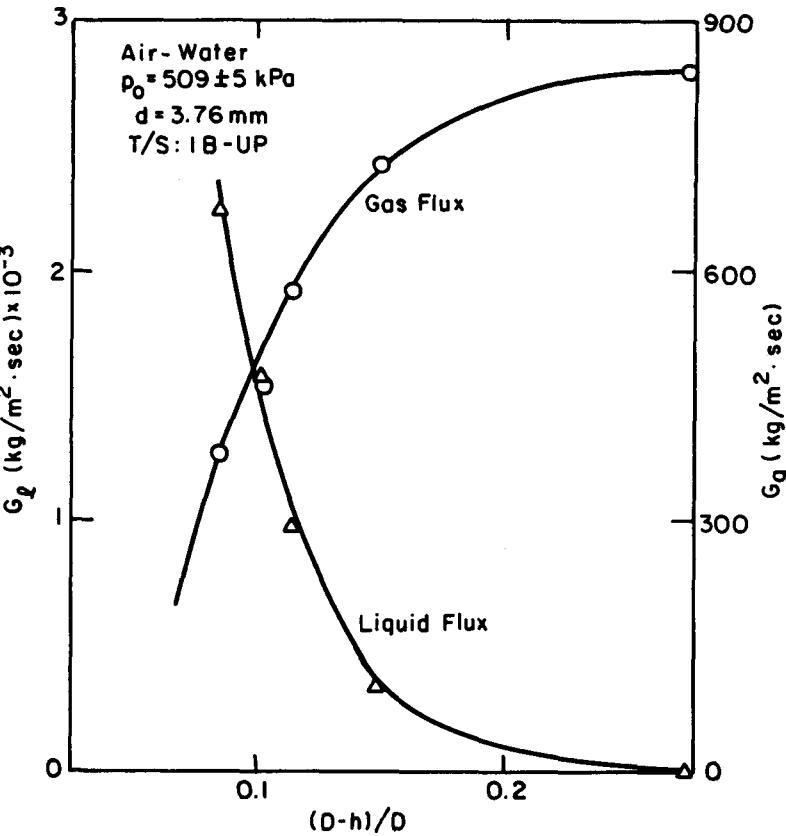
Figure 5-60   Break Liquid and Gas Mass
Flux for T/S: 1B-UP at
p_0 = 509 kPa, Air-Water Data,
Up Oriented Break
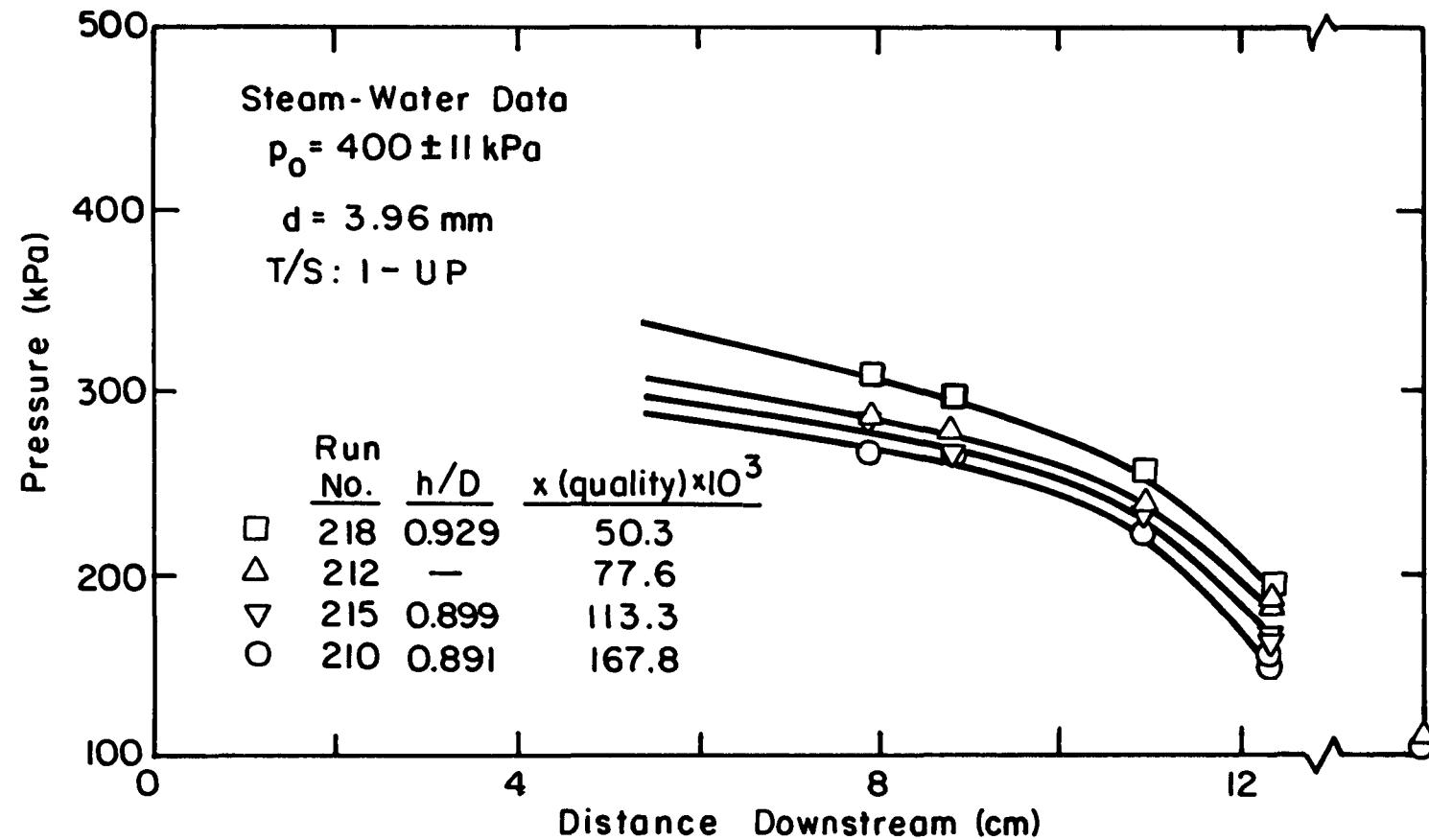
Figure 5-61   Pressure Profiles in T/S: 1-UP, Two-phase, Steam-Water Flow
with Different Inlet Qualities, p_o= 400 kPa, Up Oriented Break

Steam-Water Data

p_o = 400 ± 11 kPa

d = 3.96 mm

T/S : 1 - UP

	Run No.	h/D	x (quality)×10^3
□	218	0.929	50.3
△	212	—	77.6
▽	215	0.899	113.3
O	210	0.891	167.8
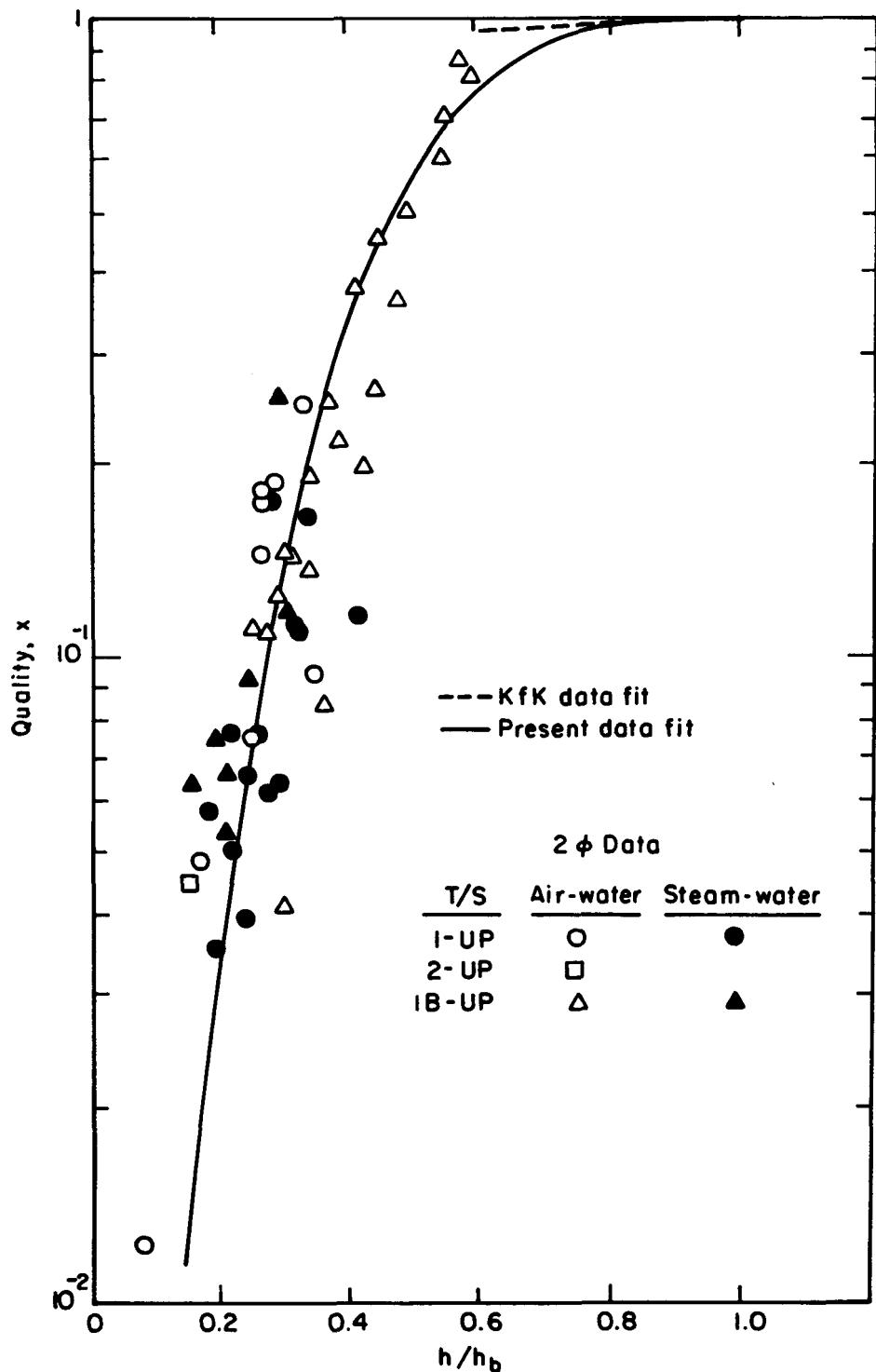
Figure 5-62   Break Entrance Quality Correlation for Two-phase
Steam-Water Flow with Liquid Entrainment,
Up Oriented Break
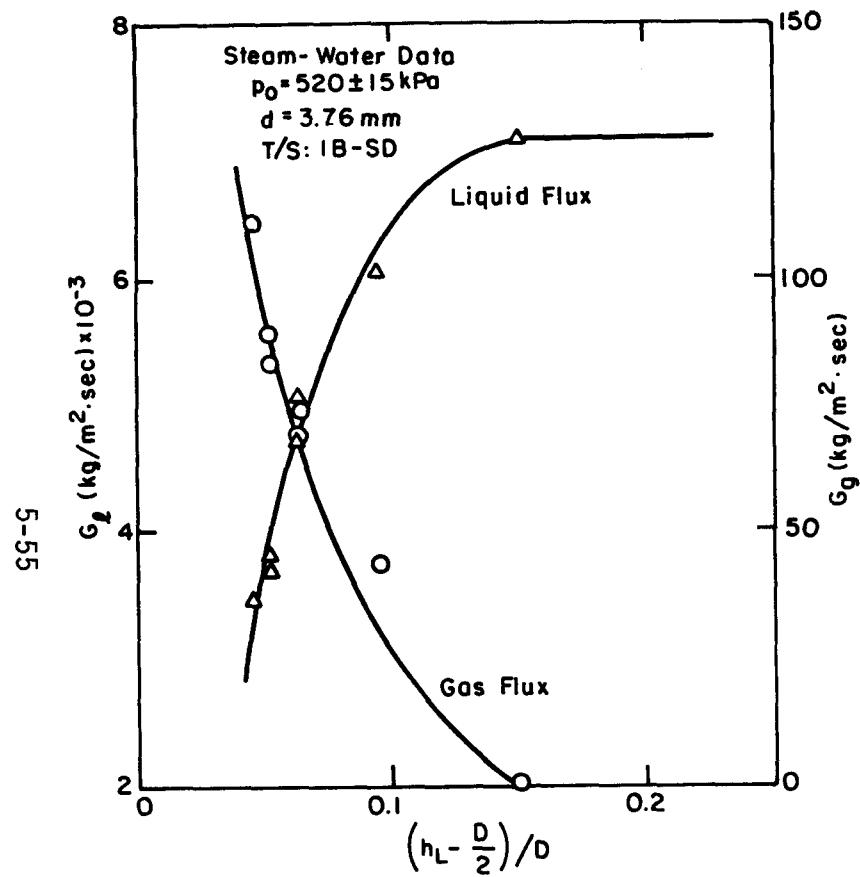
Figure 5-63 Break Liquid and Vapor Mass Flux for T/S: 1B-SD at p_0 = 520 kPa Steam-Water Flow with Vapor Pull-Through, Side Oriented Break
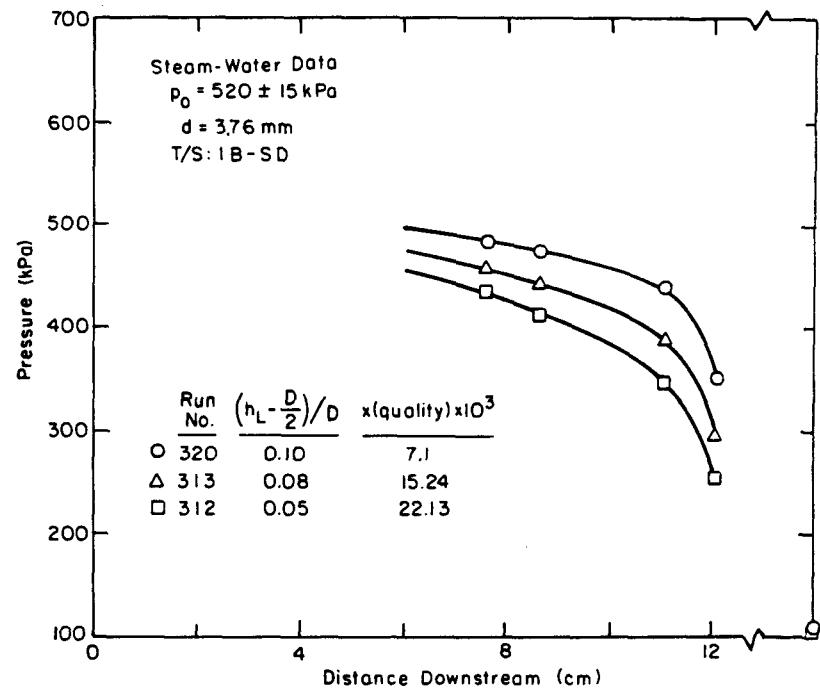
Figure 5-64 Pressure Profiles in T/S: 1B-SD, Two-phase Steam-Water Flow with Vapor Pull-Through, p_0 = 520 kPa, Side Oriented Break

and the corresponding pressure profiles are shown in Figure 5-66. From these figures we find that the observed mass flux and pressure profiles show the same data trend as observed in the downward oriented and upward oriented break flow measurements respectively for two-phase flow with vapor pull-through and liquid entrainment.

The measured entrance quality versus the non-dimensional interface height is shown in Figure 5-67 for pressure p_0 = 260 kPa. These data cover both the phenomena associated with two-phase flow viz., the liquid entrainment and vapor pull-through. In this figure the main test pipe center line is shown which separates the phenomena of liquid entrainment and the vapor pull-through. The heights for incipient liquid entrainment and vapor pull-through are also shown in Figure 5-67. In Figure 5-68, all the quality data measured in the steam-water system are presented in a general correlation that relates quality to the non-dimensional interface height h/h_b. In this figure the INEL data are also given. Both INEL and UCB (present) data are fitted with single correlation given as

$$x = x_0^{(1 + \frac{h}{h_b})^{0.7}} \left[1 - \frac{C}{2} \frac{h}{h_b} (1 + \frac{h}{h_b}) \right]$$ (5.12)

where

$$x_0 = 0.06$$

and
$$C = 1 \quad \text{for} \quad \frac{h}{h_b} \leq 0 \quad \text{liquid entrainment}$$

$$= 0 \quad \text{for} \quad \frac{h}{h_b} > 0 \quad \text{vapor pull-through} .$$

The line obtained with the correlation given by equation (5.13) is also shown in Figure 5-67.

5.6   Influence of Liquid and Gas Flow Rates in the Hozizontal Test Pipe

The superficial velocities of gas and liquid phases in the test pipe are presented in the Data Tables, Appendix B. The gas flow rates used in the present studies were small enough, not to produce significant drag on the liquid interface or to affect the onset of gas pull-through or liquid entrainment phenomena. For T/S: 1-DN the maximum steam flow rate in the test pipe for two-phase flow with vapor pull-through in terms of superficial velocity was 0.17 m/s with a liquid superficial velocity of 0.008 m/s.
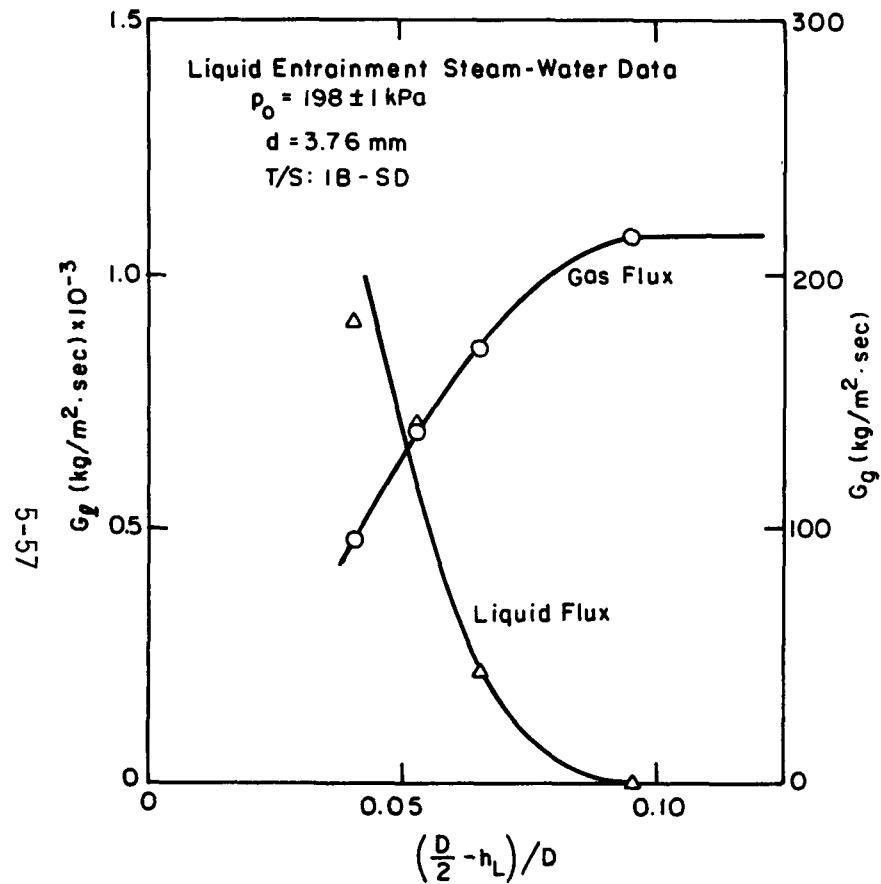
Figure 5-65   Break Liquid and Vapor Mass
Flux for T/S: 1B-SD at p_o = 198
kPa Steam-Water Flow with Liquid
Entrainment, Side Oriented Break
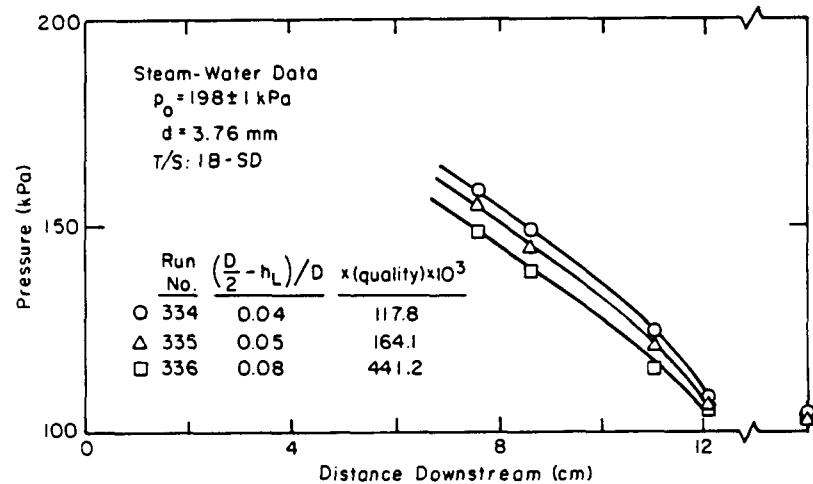
Figure 5-66   Pressure Profiles in T/S: 1B-SD,
Two-phase Steam-Water Flow with
Liquid Entrainment, p_o = 198 kPa,
Side Oriented Break
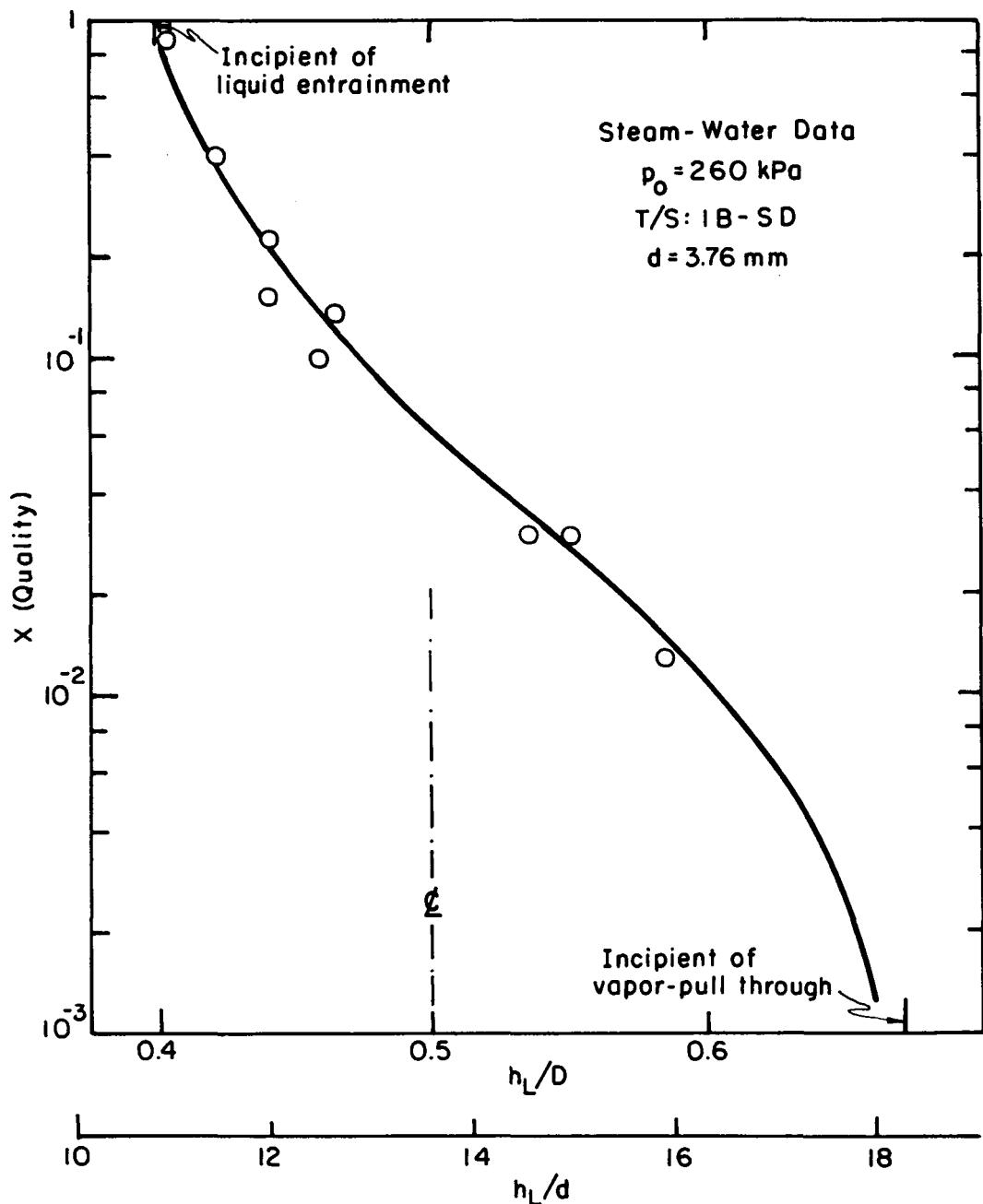
Figure 5-67 Break Entrance Quality vs h_L/D for T/S: 1B-SD,
Two-phase Steam-Water Data, p_0 = 260 kPa,
Side Oriented Break
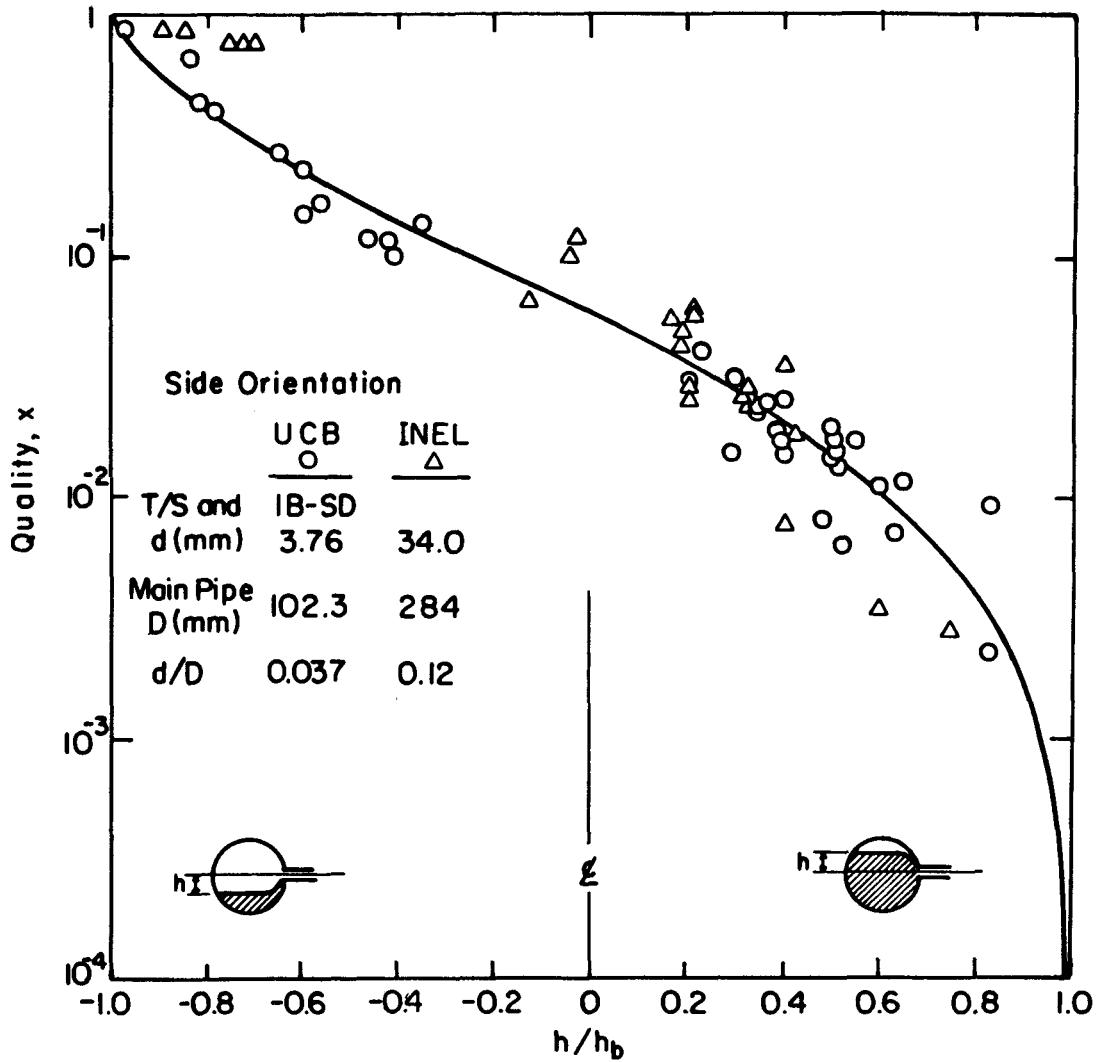
Figure 5-68   Break Entrance Quality Correlation for Two-Phase
Steam-Water Flow with Liquid Entrainment and
Vapor Pull-Through, Side Oriented Break

5-59

The experimental operational points were chosen such that the flow regime inside the test pipe was stratified and smooth. The liquid flow rates used in the test pipe, however, showed some influence on the formation/suppression of the vortex. For the case of two-phase flow with vapor pull-through, with the liquid cross flow in the horizontal test pipe, the liquid interface at the break showed flow patterns corresponding to flow geometries (b) and (c) of Reimann's categories depending on the interface level. Oscillation of vortex dominated gas pull-through was observed in tests done with steam water at higher interface levels. At low interface level the vortex free gas pull through was seen to be distorted in the downstream direction by liquid flow in the test pipe. The measurement of the liquid level made at upstream and downstream sides of test break showed a slope in the interface above the break. This slope was noticeable for large stagnation pressures, where the break mass flow rates are larger. Hence in the determination of interface level the average of the upstream and downstream interface level was calculated.

In case of two-phase flow with liquid entrainment, the maximum steam and liquid flow rates used for T/S: 1-DN, in terms of superficial velocity, were 0.22 m/s and 0.008 m/s. No influence of this gas and liquid cross flow was observed on the entrainment phenomena over the range of break flows studied.

5.7 Unsteady Vortex Gas Pull-Through

In case of flow geometry (b) for some of the test runs (e.g., run no. 8), carried out at a liquid height close to inception of continuous gas pull-through, an unsteady vortex was observed. For these runs it was found that during the gas pull-through the interface level at the break increased and decreased periodically, by a small amount ($\sim$2-3 mm) for fixed input flow rates of gas and liquid to the test pipe and pipe stagnation pressure. This periodic change of interface level was due to changes in mass flux rates through the break. An explanation for this observation may be the following. When there is increase in gas pull-through, the critical mass flux decreases. This decreases the liquid flow rate. Hence for the constant upstream conditions, some liquid accumulates in the pipe effectively increasing the liquid interface level. The increase in interface level decreases the vortex size and hence decreases the gas flow rate. This decrease in gas flow rate in turn increases the critical mass flux and the liquid flow rate. Increased liquid flow rate in turn decreases the interface level leading to increase in the size of the vortex and hence increases the gas flow rate, and the cycle repeats. This type of unsteady vortex was also observed in steam-water tests. In some cases, the vortex would appear and disappear intermittantly, and the gas pull-through often switched on and off.

6. CONCLUSIONS

Critical flow through small breaks on horizontal pipes carrying
stratified two-phase fluid was studied experimentally to investigate
the vapor pull-through and liquid entrainment phenomena and the effect
of these phenomena upon the mass flow rates and quality through the
small break. The present study (UCB), carried out with air-water and
steam-water systems, compliments the results of the air-water experi-
ments at KfK and the steam-water tests at INEL. The data presented
were obtained for downward, side and upward oriented break tubes of
diameter 3.76, 3.96, 6.32 and 10.15 mm at various stagnation pipe
pressures up to 1 MPa for flow with vapor pull-through and 0.5 MPa
for flow with liquid entrainment phenomena.

For the flow with vapor pull-through, in the present study both steam-
water and air-water incipience involved a vortex induced flow which
subsequently underwent transition to vortex free as the liquid level
was reduced. The superimposed velocity on the flow in the test pipe
affected the transition of vortex to vortex free flow.

In the present study, the steam-water level for incipient vapor pull-
through was higher than that for air-water in both downward and side
oriented breaks. This difference between air-water and steam-water
incipient results for vapor pull-through was attributed to the differ-
ence in physical properties. A new correlation form was developed
relating flow rate to liquid level that takes account of the surface
tension and viscosity effects through non-dimensional numbers (Bond
number and viscosity number in addition to the Froude number). The
new incipience correlation for vapor pull-through was successfully
used to fit the UCB, INEL and KfK data for both side and downward
oriented breaks. Using this new incipience correlation, the INEL qua-
lity data for downward oriented break were normalized and were found
to be in good agreement with the present steam-water quality data. A
single quality correlation was obtained for both INEL and UCB steam-
water data.

In the case of liquid entrainment at top oriented breaks the present
results showed no difference between air-water and steam-water incep-
tion data, however, the present data are a little higher in level at
the same Froude number than the KfK data. A quality correlation
obtained from the present data for liquid entrainment consistently
compliments KfK data.

A quality correlation was developed for the side oriented break where
both the phenomena of liquid entrainment and vapor pull-through were
observed depending on whether the interface height is below or above
the break location. Using the inception data calculated from the new
correlation for vapor pull-through and the correlation for liquid en-
trainment, the present quality correlation for side oriented break best
represents both INEL and the present steam-water data.

The present results are useful in the evaluation of critical flow in an LWR LOCA analysis. There are many methods available in the literature for the calculation of critical flow given the upstream stagnation state. The present study provides the means for obtaining the upstream stagnation state of the fluid entering the break channel when the upstream region is stratified. To utilize the incipient pull-through and entrainment correlations it is first necessary to apply the chosen critical flow model to obtain the break flow for single phase fluid (either saturated liquid or vapor, depending upon break location in relation to the liquid-vapor interface) entering the break. The appropriate incipience correlation is next used to obtain the incipient height h_b. With this information the corresponding quality correlation is used to obtain the break entrance quality corresponding to the actual interface height. Then the quality and pressure define the stagnation state for use in the critical flow model to obtain the actual break flow corresponding to the actual interface height.

7. REFERENCES

[1] Doa, L. T. C. and Carpenter, J. M., "Experiment Data Report for LOFT Nuclear Small-Break Experiment L-35/L3-5A," NUREG/CR-1695, EGG-2060, November 1980.

[2] Condie, K. G., "LOFT LOCE L3-5/L3-5A Result and Analysis," paper presented at the LOFT Review Group Meeting, Idaho Falls, Idaho, November 6, 1980.

[3] Burchill, E., "Physical Phenomena of Small Break Loss of Coolant Accident in PWR," Nuclear Safety, 23, Sept.-Oct. 1982.

[4] Zuber, N., "Problems in Modeling of Small Break LOCA," NUREG-0724, 1981.

[5] Crowley, C. J. and Rothe, P. H., "Flow Visualization and Break Mass Flow Measurements in Small Break Separate Effects Experiments," Small Break Loss-of-Coolant Accident Analysis in LWR's, EPRI WS-81-201, August 1981.

[6] Reimann, J. and Smoglie, C., "Flow Through a Small Pipe at the Top of a Large Pipe with Stratified Flow," presented at the annual meeting of the European Two-Phase Flow Group; Zurich, Switzerland, June 14-16, 1983.

[7] Smoglie, C., "Two-Phase Flow Through Small Branches in a Horizontal Pipe with Stratified Flow," Kernforschungszentrum Karlsruhe, (KfK) 3861, Dec. 1984.

[8] Smoglie, C., Reimann, J., and Muller, U., "Two-Phase Flow Through Small Breaks in a Horizontal Pipe with Stratified Flow," Proc. of Third Internat. Topical Meeting on Reactor Thermalhydraulics, Rhode Island, USA, Oct. 15-18, 1985, pp 13.A-1-13.A-8.

[9] Reimann, J. and Khan, M., "Flow Through a Small Break at the Bottom of a Large Pipe with Stratified Flow," Nucl. Sci. Eng., Vol. 88, pp. 297-310, 1984.

[10] Anderson, J. L. and Owca, W. A., "Data Report for the TPFL Tee/ Critical Flow Experiments," NUREG/CR-4164, EGG-2377, November 1985.

[11] Hall, D. G., "An Inventory of the Two-Phase Critical Flow Data Base," INEL, EGG-CAAP-5140, November 1980.

[12] Abdollahian, D., Healzer, J., Janssen, E. and Amos, C., "Critical Flow Data Review and Analysis, EPRI NP-2192, January 1982.

[13] Rouse, H., "Seven Exploratory Studies in Hydraulics," J. Hydr. Div. Proc. ASCE, HY4, pp (1038) 1-35, August 1956.

[14] Craya, A., "Theoretical Research in the Flow of Non-Homogeneous Fluids," La Houille Blanche, pp. 44-55, January-February 1949.

[15] Gariel, P., "Experimental Research on the Flow of Non-Homogeneous Gluids," La Houille Blanche, pp. 56-64, January-February 1949.

[16] Hardy, P. G. and Richter, H. J., "Critical Two-Phase Flow in Small Break Loss of Coolant Accidents," Final Report to EPRI NP-RP-2299-1. Dartmouth College, Hanover, CT, December 1983.

[17] Dagget, L. and Keulegan, G., "Similitude in Free Surface Vortex Formation," J. Hydr. Div. Proc. ASCE Vol. 100, HY11, pp. 1565-1581, Nov. 1974.

[18] Hattersley, J., "Hydraulic Design of Pump Intakes," J. Hydr. Div. Proc. ASCE, HY2, pp. 223-249, March 1965.

[19] Gordon, J. L., "Vortices at Intakes," Water Power, pp. 137-138, April 1970.

[20] Reddy, Y. R. and Pickford, J. A., "Vortices at Intakes in Conventional Pumps," Water Power, pp. 108-109, March 1972.

[21] Gluck, D. F., Gille, J. P., Zukoski, E. E., and Simkin, D. J., "Distortion of a Free Surface During Tank Discharge," J. Spacecraft, Vol. 3, pp. 1691-1692, Nov. 1966.

[22] Lubin, B. T. and Springer, G. S., "The Formation of a Dip on the Surface of a Liquid Draining from a Tank," J. Fluid Mech., Vol. 29 pp. 385-390, 1967.

[23] Lubin, B. T. and Hurwitz, M., "Vapor Pull-Through at a Tank Drain with and without Dielecrophoretic Buffling," Proc. Conf. Long Term Cryopropellant Storage in Space, NASA Marshall Space Centre, Huntsville, AL, pp. 173-180, 1966.

[24] Easton, C. R. and Catton, I., "Nonlinear Free Surface Effects in Tank Draining at Low Gravity," AIAA J. Vol. 8, Dec. 1970.

[25] Amos, C. and Schrock, V. E., "Critical Discharge of Initially Subcooled Water Through Slits," NUREG/CR-3475, LBL-16363, 1983.

[26] Engineering Div. of Crane Coy., "Flow of Fluids Through Valves Fittings and Pipe," Crane Co. Technical Paper No. 410, 1976.

[27] Young, H. D., "Statistical Treatment of Experimental Data," McGraw-Hill Book Co., New York, 1962.

[28] Uchida, H. and Nariai, H., "Discharge of Saturated Water Through Pipes and Orifices," Proc. of the 3rd Internat. Heat Transfer Conf., Chicago, USA, Vol. 5, pp. 1-12, 1966.

[29] Saad, M. A., "Compressible Fluid Flow," Prentice-Hall, Inc., New Jersey, 1985.

APPENDIX A

Data Reduction

In this appendix the methods applied for the reduction of raw data are described. The measured quantities forming the raw data were the responses of pressure transducer, load cell and thermocouple and the gas-liquid interface level in the test pipe. Data reduction procedure involved the conversion of raw data, in millivolts or volts, to pressures, weigh tank mass and temperatures. Then these quantities were used in calculation of mass flux, quality and other parameters of interest. Data reduction was done using a table programmable calculator. As the data obtained were for steady state phenomena, the actual calculations in data reductions were simple. Each measuring device was connected to specific channel of Auto-Data Eight and the responses were printed on paper tape for each channel. The channel numbers associated with each measuring device are indicated in Calibration Tables of Appendix D.

A.1 Reduction of Basic Measurements

The data printed on the paper tape, which are in terms of millivolts or volt readings were converted to pressure, differential pressure, weigh tank mass, equivalent mass discharged from the reservoir vessel or temperature according to the channel numbers, corresponding to each appropriate device. Since the experiments were steady state type, the average millivolt or volt readings from the multiple-sample data were taken for calculations, except for vessel level transducer and load cell readings which are transient variables. Fluctuations in the responses were used in the estimate of the uncertainty in the reading. These errors have been included in the Data Table Appendix B for pressure and temperature in stagnation state and as well in the pressure profiles. The pressure profiles within the discharge tube are obtained by adding or subtracting, as was appropriate, the differential pressures to the test pipe stagnation pressure. The pressure tap locations are given in Table 3-2.

Two absolute pressure transducers were used in the test section; one in the test pipe and another downstream of the break tube. Two pressure values were calculated for break tube tap number 5 using the upstream, and downstream absolute and appropriate differential pressures. These two values for p_5 are given in Data Tables in Appendix B.

To determine the time interval between the successive readings for particular channel (transient variables), the printouts were collected for five minutes for several times. The total number of prints was divided by the time, to obtain the value of the number of prints per second. The number of prints per second calculated ranged from 2.270 to 2.275 prints per second. This corresponds to 0.21% error in time measurement.

The liquid-gas interface height was determined as the average of the values read from the two level rods situated on either side of the break. This arrangement of two level readings on upstream and downstream of the break allows to estimate any slope on the interface in the vicinity of break.

A.2 Mass Flowrate Calculation

Weigh Tank Method

Liquid mass flow rate was calculated using two methods. One method used was to measure directly the mass of water collected in the weigh tank, using the measurements done with load cells. The other method employed was the mass discharge method, where the data of vessel level transducer was used.

Reduction of load cell data yielded mass of the weigh tank and its contents at any time t. Responses from both the load cells LC1 and LC2 were used and the average mass of the total discharged water was determined. The mass discharged up to time t in the weigh tank was

$$m_T = w_t - w_o \qquad (A.1)$$

In case of air-water tests, the total mass collected in the tank is water mass itself. But in case of steam-water system, the steam was condensed in the weigh tank and hence the total mass collected in the weigh tank is the sum of steam and water masses.

The mass discharged m_T at different times t was plotted against time and the slope of the best fit line was obtained to get the mass flow rate $\dot{m}$

In Figure A-1, we have shown the load cell responses with time recorded in earlier experiments with air-water in the glass test pipe. These data were collected by hand recording the readings from a analog milli-volt meter. Although the accuracy of these readings was not as good as those recorded by the Auto-Data system, the error in mass measurement was small (<4 percent). The mass flow rates calculated from both load cells agreed with one another in general.

Vessel Level Method

The vessel level transducer was calibrated for the volume of water (22°C) discharged from the reservoir, and the Table D-8 shows the calibration equation. Using the vessel level transducer readings the amount of the mass removed from the reservoir was calculated. This mass in the steam-water test is the sum of the steam and water removed from the reservoir. Once the flow was started, account was taken of the fact that water leaving the vessel was replaced by steam. The pressure and temperature of fluids inside the reservoir vessel were steady during
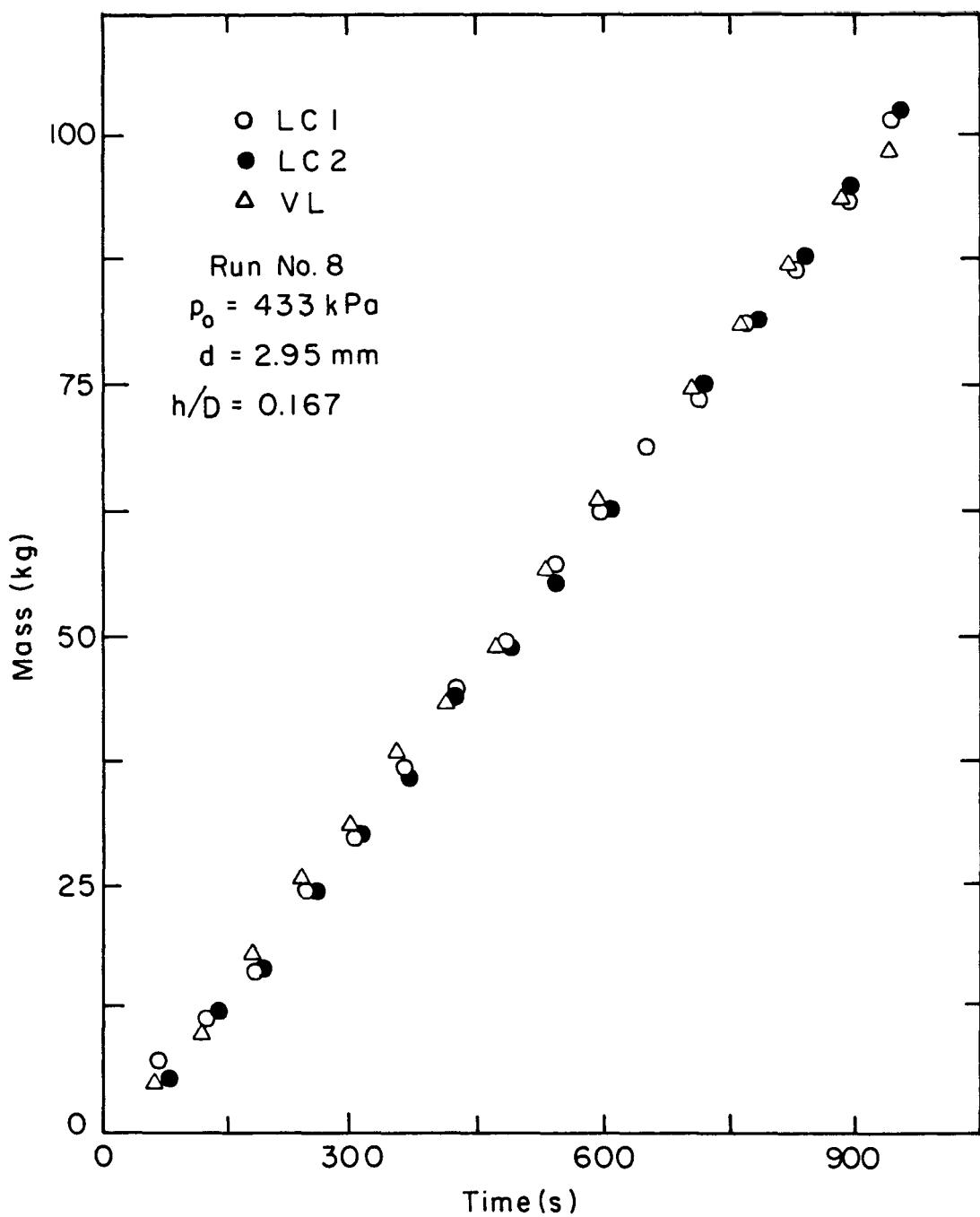
Figure A-1   Load Cell LC1 and LC2 and Vessel Level VL
Transducer Responses as Function of Time
Recorded Using Analog Voltmeter

A-3

the run. For v_0 as the initial volume of water in reservoir and v_t the volume after time t then the mass removed from the vessel was calculated as

$$m_T = (v_0 - v_t)(\rho_\ell - \rho_g) \tag{A.2}$$

In case of air water tests the water removed from the vessel was calculated as

$$m_T = m_w = (v_0 - v_t)(\rho_w - \rho_g) \tag{A.3}$$

Here again the mass flow rate was obtained as the slope of plot m_T versus time t.

Measurements from the reservoir vessel transducer for the mass dis-charged were of good quality with ms error less than 0.5% in general. For two phase flow with higher qualities, the weigh tank was sometimes subjected to sway. These oscillations affected the measurements of the load cell responses. For errors larger than 5% in mass measure-ment occurred, these readings were discarded and not used in mass flow rate calculations. Only the readings from reservoir vessel transducer were used. In absence of such oscillations, the mass measurements done with load cells gave very good results. The steam/gas flow rate from the break were calculated by measuring the steam/gas flow rates into and out of the pipe with the orifice meters. Initially on the glass system the air flow rate through the break tube was calculated using an air-water separator and manometer system described in Chapter 3. In the metallic system, two orifice meters were used. Using the standard orifice equation for compressible fluids, and the discharge coefficients presented in Table D-17, the mass flow rates of steam/air was calculated as

$$\dot{m}_i = YC_DA \sqrt{2\rho_i \, \Delta p} \tag{A.4}$$

where subscript i stands for gas (air, or nitrogen) and steam and

$$Y = 1 - (0.41 + 0.35\beta) \frac{\Delta p}{\gamma p} \tag{A.5}$$

Here all the notations are defined in nomenclature.

Using equation (A.4) & (A.5), the steam/air flow rate $\dot{m}_{gin}$ into the test pipe from reservoir vessel and $\dot{m}_{gout}$ the steam/air flow rate out of the test pipe through steam exit line are calculated. As the reservoir vessel pressure is maintained about 70-100 kPa higher than the test pipe pressure, the liquid entering test pipe may flash to produce steam. Also the enthalpy of the liquid in the recirculating

loop may not be same as in the test pipe. Hence a steam flow rate correction $\Delta\dot{m}_g$ was calculated for condensation/flashing effects from energy and mass balances (Refer Figure A-2).
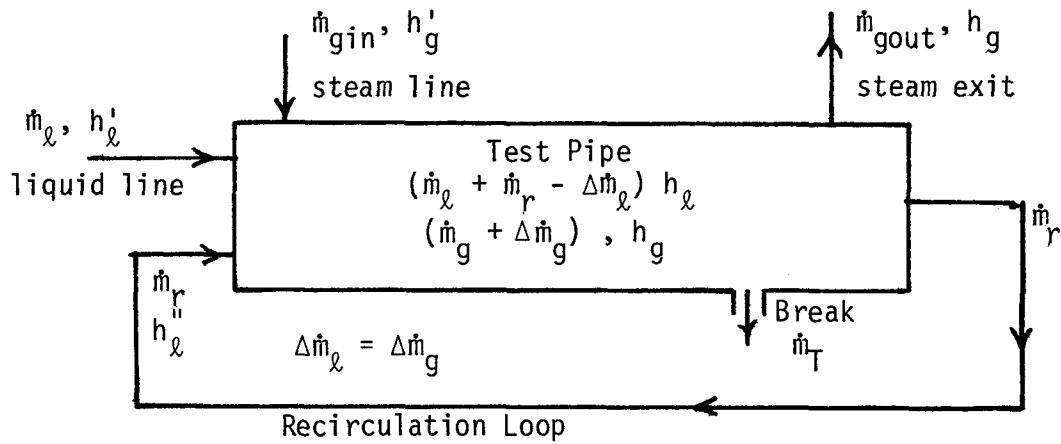
Figure A-2

The equation for $\Delta\dot{m}_g$ is given as

$$\Delta\dot{m}_g = \frac{1}{h'_{fg}}\left\{(h_{fg}- h'_{fg})\,\dot{m}_{gin} + (h_\ell- h'_\ell)\dot{m}_T + (h''_\ell - h'_\ell)\dot{m}_r + \dot{m}_{gout}(h_\ell- h'_\ell)\right\}$$

(A.6)

Then the steam flow rate at the break was calculated as

$$\dot{m}_g = \dot{m}_{gin} - \dot{m}_{gout} + \Delta\dot{m}_g \tag{A.7}$$

Heat loss test carried in the test pipe have shown that small amount of steam was condensed due to heat loss. In calculation of the steam mass flow rate, the rate of steam condensed $\dot{m}_{cond}$ was accounted as shown below.

$$\dot{m}_g = \dot{m}_{gin} - \dot{m}_{gout} - \dot{m}_{cond} + \Delta\dot{m}_g \tag{A.8}$$

Also in case of water flow rate calculated using volume discharge method, $\dot{m}_{cond}$ was accounted as

$$\dot{m}_W = \dot{m}_T - \dot{m}_g + \dot{m}_{cond} \, , \tag{A.9}$$

However, for the weigh tank method the water flow rate through break was given as

$$\dot{m}_W = \dot{m}_T - \dot{m}_g \tag{A.10}$$

In the air-water test carried out earlier on the glass system, the air mass flux through the break tube was given as [26]

$$G_g = 5.517 \ Y \ d_o^2 \left[\frac{\Delta p_{man}(14.69 + \Delta p_{man})}{KT \ S_g} \right]^{1/2} \frac{\rho_g}{A} \qquad (A.11)$$

where d_o is the diameter of the fitting through which air is discharged after being separated by air-water separator system. p_{man} is the differential pressure (in psi units) read by monometer. With the values of parameters used and for the ambient condition of 22^oC, the equation (A.11) reduces to the following equation which was used for calculation of air flux through break

$$G_g = 16.027 \left[\Delta p_{man} \ (14.696 + \Delta p_{man}) \right]^{1/2} \qquad (A.12)$$

A.3 Calculation of Other Quantities

The mass flux through the break was determined as

$$G_i = \dot{m}_i / A \qquad (A.13)$$

where $i = g, \ell$.

The quality entering the break tube was calculated as

$$x = \frac{G_g}{G_g + G_\ell} \qquad (A.14)$$

In case of inception data the non-dimensional numbers were calculated as follows.

Froude number:

$$Fr = \frac{G_\ell}{\rho_\ell \sqrt{dg}} \qquad (A.15)$$

Bond number:

$$B_o = d\sqrt{g\Delta\rho/\sigma} \qquad (A.16)$$

Viscosity number:

$$N_\mu = \mu_\ell / (\sigma\rho_\ell\sqrt{\sigma/g\Delta\rho})^{0.5} \qquad (A.17)$$

A-6

The liquid superficial velocity j_ℓ was obtained as

$$j_\ell = \left[\dot{m}_\ell + \dot{m}_r\right] \frac{1}{\rho_\ell A_p} \qquad (A.18)$$

where first term in the bracket is the break mass flow rate and the second term is mass flow rate in recirculation loop. A_p is the pipe cross section. The $\dot{m}_r$ is calculated from the orifice meter reading using the equation

$$\dot{m}_r = C_D \sqrt{2\rho_\ell \Delta p_{or}} \qquad (A.19)$$

The gas superficial velocity j_g was calculated as

$$j_g = \dot{m}_{gin}/\rho_g A_p \qquad (A.20)$$

where $\dot{m}_{gin}$ is the steam flow rate entering the test pipe.

APPENDIX B

Data Tables

In this appendix the data for all the tests carried out in the present experimental program are presented. Data tables are arranged according to the type of flow through break and the test section used. The run numbers were assigned according to the order of the tests. Runs 1 through 10 were carried out with the glass pipe system for air-water two-phase and single phase flow. The rest of the runs were done in the metal test pipe system. Tables B-2 through B-10 cover the data of flow with single phase entrance through break. Two-phase entrance flow data are presented in Tables B-11 to B-21. The inception data for gas pull-through and liquid entrainment are presented in Tables B-22 to B-32.

In each table the test section and the diameter of the break tube used are given at the heading. Test section 1G is the test break that was used with the glass pipe system. Test section 1A is the initial small ID test break tube used in the metallic system. This break tube was later machined to give a smooth inner surface and was then designated as 1. Test section 1B was used after test break 1 failed after long use. The notation - DN,-UP and -SD respectively correspond to the downward, upward and side oriented break. The details of the test break dimensions with the location of the pressure taps are given in Table 3-2. The break tube diameter, d, cross sectional area A, diameter of test pipe D, and the fluid flowing inside the test pipe and at the entrance of break tube are all given at the heading of each table. For the two-phase data tables, the type of flow at the break entrance is also given at the heading.

The data presented in the tables contain reduced data. As was explained in the data reduction procedure (Appendix A), except for mass measurements all the measurements are from steady state responses. Since each run lasted 2-4 minutes, the average value of each steady state measurement is reported here. The estimated error is given for each run. For main line conditions the errors are indicated in separate columns. For the branchline conditions, the errors associated with mass measurements are given in terms of percent error. The best value of mass flow rate was obtained in most of the cases with Mass Discharge Method (vessel level differential pressure measurement). The reported data for liquid mass flow rate was the average of the values obtained by both methods of measurement. Mass (volume) Discharge Method and the Weigh Tank Method, except for the runs where Weigh Tank Method had high errors (5%) due to weigh tank swaying. In such cases only the measured data from Mass Discharge Method is reported and was used for quality calculations.

The pressure profiles are presented along with errors associated with each in parentheses. For pressure p_5, two values are given which are calculated from two separate measurements as explained in the Data Reduction section (Appendix A). In the tables, when the measurements

were not made, or, when the entry does not apply to the case studied, the entry is given as "-". For some runs, when the transducers may have been subjected to a greater pressure than their range, malfunctioned, or may have been disconnected, the entry in the table is given as "na".

The data tables for inception of gas-pull-through or liquid entrainment contain the incipient liquid height h_b and the corresponding Froud number, and the stagnation pressure p_0. All the steam-water data refer to the saturated liquid state while air-water to that of room temperature conditions.

B-3

TABLE B-1   AIR-WATER 1ϕ and 2ϕ DATA WITH T/S: 1G-DN

$$d = 2.95 \text{ mm} \qquad A = 6.8183\times10^{-6} \text{m}^2 \qquad D = 101.6\text{mm}$$

Run No.		Mainline Conditions						Branchline Conditions						Flow Type at Entry
	h (cm)	P_o (kPa)	δP_o ($\pm$kPa)	T_o ($^\circ$C)	δT_o ($\pm^\circ$C)	j_ℓ (m/s)	j_g (m/s)	$G_\ell \times10^{-4}$ (kg/m^{2}s)	δG_ℓ (%)	δG_g (kg/m^{2}s)	δG_g (%)	x $\times10^3$	δx (%)	
1	16.7	349	3	22	0.3	0.010	–	1.172	2.9	5.64	7.8	0.48	5.6	Vortex 2φ
2	14.3	347	2	22	0.3	0.0068	–	0.831	2.9	9.12	3.2	1.10	6.7	Vortex 2φ
3	8.5	361	4	22	0.3	0.0052	–	0.624	3.6	15.94	2.2	2.65	4.1	Vortex free 2φ
4	7.0	365	3	22	0.3	0.0049	–	0.588	2.1	22.0	2.3	3.70	3.9	Vortex free 2φ
5	19.7	353	6	22	0.3	0.0141	–	1.671	2.3	–	–	–	–	1φ
6	25.0	351	8	22	0.3	–	–	1.655	2.4	–	–	–	–	1φ
7	20.2	436	6	22	0.3	–	–	2.031	2.2	–	–	–	–	1φ
8	17.1	434	5	22	0.3	–	–	1.517	2.2	2.12	12.9	0.13	10.1	Vortex, 2φ
9	15.3	429	5	22	0.3	0.0094	–	1.113	4.0	8.76	3.6	0.75	8.1	Vortex 2φ
10	6.2	421	5	22	0.3	0.0060	–	0.717	2.1	23.1	2.5	3.0	7.1	Vortex free 2φ

TABLE B-2   AIR-WATER   1ϕ DATA WITH T/S: 1A-DN

$d = 3.91$ mm $A = 1.2017 \times 10^{-5} m^2$ $D = 102.3$ mm

Run No.	Mainline Conditions						Branchline Conditions					
	p_o (kPa)	δp_o ($\pm$ kPa)	T_o (°C)	δT_o (°C)	$G_\ell \times 10^{-4}$ (kg/m².s)	δG_ℓ (%)	Pressure Profile (kPa)					
							p_1	p_2	p_3	p_4	p_5	p_6
11	374	4	25	0.3	1.3130	1.5	199.1 (4.9)	na	197.7 (5.0)	na	136.0(5.2) 142.2(0.7)	103.7 (0.0)
12	446	3	25	0.3	2.5241	2.3	226.1 (3.5)	na	225.4 (3.5)	na	145.3(2.7) 153.6(1.4)	104.2 (0.0)
13	513	3	25	0.3	1.5510	1.3	252.0 (5.4)	na	250.8 (5.6)	na	155.6(5.8) 161.6(0.7)	104.2 (0.0)
14	585	4	25	0.3	1.7250	1.2	279.7 (5.4)	na	277.9 (5.6)	na	161.8(5.7) 173.6(0.7)	104.2 (0.0)
15	653	4	24	0.3	1.8430	1.1	306.2 (6.4)	na	304.6 (6.4)	na	224.0(6.5) 231.2(1.4)	104.2 (0.0)
16	795	4	23.5	0.3	1.9890	2.3	363.8 (7.5)	na	360.9 (7.6)	na	262.3(7.8) 268.5(1.4)	104.8 (0.0)
17	932	4	23.5	0.3	2.2190	2.3	413.9 (4.4)	na	410.5 (4.4)	na	294.8(4.8) 309.2(6.9)	105.0 (0.0)
18	1069	2	23.5	0.3	2.4370	2.2	472.0 (4.7)	na	468.6 (4.7)	na	336.6(4.7) 347.0(2.1)	105.3 (0.0)

TABLE B-3   STEAM-WATER 1ϕ DATA WITH T/S: 1A-DN

$d = 3.91$ mm $A = 1.2017 \times 10^{-5} m^2$ $D = 102.3$ mm

	Mainline Conditions						Branchline Conditions					
							Pressure Profile (kPa)					
Run No.	P_0 (kPa)	δP_0 ($\pm$ kPa)	T_0 (^oC)	δT_0 (^oC)	$G_\ell \times 10^{-4}$ (kg/m^2.s)	δG_ℓ (%)	P_1	P_2	P_3	P_4	P_5	P_6
31	375	5	126.6	0.2	0.9580	0.86	266.6 (8.4)	na	265.6 (8.4)	265.6 (8.5)	239.2(9.0) 254.2(7.4)	113.1 (2.8)
32	455	4	145.1	0.3	0.5830	1.91	405.6 (4.6)	na	401.6 (4.7)	389.0 (4.9)	342.3(5.1) 335.0(5.0)	111.6 (1.4)
33	514	2	144.7	0.3	0.8040	0.03	418.5 (5.2)	na	406.0 (5.1)	406.9 (4.8)	361.4(4.3) 369.4(3.2)	117.9 (2.0)
34	582	2	151.9	0.2	0.799	2.05	501.2 (6.1)	na	500.0 (6.2)	488.4 (6.1)	433.1(6.1) 433.5(3.5)	120.8 (1.7)
35	655	6	156.8	0.2	0.715	0.96	581.1 (6.2)	na	572.4 (6.5)	556.4 (6.5)	491.7(6.6) 486.1(3.1)	118.8 (1.4)
36	796	6	165.7	0.3	0.7900	0.93	707.4 (6.5)	na	695.4 (6.5)	675.6 (6.7)	597.8(7.4) 597.3(6.4)	123.0 (1.4)
37	935	8	166.7	0.3	1.070	1.36	792.0 (8.4)	na	784.4 (7.4)	768.2 (3.3)	683.2(3.9) 690.2(7.2)	142.2 (3.1)
38	1074	3	174.4	0.2	1.101	1.02	925.1 (6.1)	na	915.3 (6.9)	896.1 (7.1)	799.2(6.8) 816.2(3.6)	148.5 (2.3)

TABLE B-4   AIR-WATER   1ϕ DATA WITH T/S: 1 -DN

d =   3.96 mm   A = $1.2331 \times 10^{-5} m^2$ D = 102.3 mm

Run No.	Mainline Conditions						Branchline Conditions					
							Pressure Profile (kPa)					
	P_0 (kPa)	δP_0 ($\pm$ kPa)	T_0 (°C)	δT_0 (°C)	$G_\ell \times 10^{-4}$ (kg/m^2.s)	δG_ℓ (%)	P_1	P_2	P_3	P_4	P_5	P_6
39	141	4	21	0.3	0.551	0.46	111.0 (1.4)	108.7 (1.4)	na	106.6 (2.2)	105.0 (1.4) 103.6 (0.3)	102.6 (0.3)
40	177	4	21	0.3	0.815	1.44	113.0 (3.1)	107.2 (3.2)	na	105.3 (3.4)	102.2 (2.1) 101.9 (0.1)	101.3
41	208	3	21	0.3	0.984	1.57	115.7 (2.6)	112.3 (2.6)	na	105.9 (2.8)	101.4 (2.6) na	na
42	243	6	21	0.3	1.157	0.90	118.9 (1.7)	114.7 (1.7)	na	106.3 (2.2)	100.3 (1.6) 97.1 (0.6)	102.8 (0.3)
43	278	2	21	0.3	1.289	0.36	121.7 (5.4)	116.9 (5.4)	na	106.2 (5.7)	99.0 (5.4) 97.5 (0.4)	103.6 (0.3)
44	308	8	21	0.3	1.454	0.33	122.3 (6.6)	115.2 (6.6)	na	103.0 (6.6)	94.8 (6.6) 90.8 (0.7)	96.6 (0.6)
45	342	2	21	0.3	1.550	2.25	126.3 (6.1)	118.6 (6.1)	na	104.6 (6.5)	95.3 (6.0) 90.6 (0.9)	96.9 (0.3)
46	382	9	21	0.3	1.622	2.09	131.7 (6.3)	123.2 (6.2)	na	107.4 (6.2)	96.0 (6.2) 90.6 (0.7)	97.6 (0.6)

$d = 3.96$ mm $A = 1.2331 \times 10^{-5} m^2$ $D = 102.3$ mm

Run No.	Mainline Conditions						Branchline Conditions					
							Pressure Profile (kPa)					
	P_o (kPa)	δP_o ($\pm$ kPa)	T_o (^oC)	δT_o (^oC)	$G_\ell \times 10^{-4}$ (kg/m^2.s)	δG_ℓ (%)	P_1	P_2	P_3	P_4	P_5	P_6
47	414	5	21	0.3	1.776	0.86	135.9 (4.9)	126.6 (5.2)	na	108.7 (4.9)	95.4 (4.7) 90.0 (0.7)	97.2 (0.6)
48	447	4	21	0.3	1.838	0.30	141.0 (7.8)	130.8 (7.8)	na	110.9 (2.7)	96.4 (7.7) 90.6 (0.6)	98.0 (0.3)
49	371	3	21	0.3	1.608	1.95	127.9 (6.2)	na	131.1 (6.6)	105.4 (7.9)	95.7 (3.9) na	na
50	382	5	21	0.3	1.486	0.90	123.0 (8.6)	na	126.1 (9.7)	99.1 (6.3)	87.2 (6.1) 88.9 (3.4)	97.0 (2.23)
51	383	5	21	0.3	1.621	2.11	123.7 (8.1)	114.9 (6.8)	na	99.4 (3.3)	87.8 (3.9) 106.5 (2.7)	97.0 (0.9)
52	526	7	21	0.3	2.092	1.39	11.5 (5.9)	na	13.6 (4.1)	97.5 (4.4)	84.0 (3.9) 114.7 (0.7)	105.3 (0.6)
53	452	4	21	0.3	1.861	0.45	132.2 (8.1)	na	124.5 (8.2)	105.9 (7.6)	89.6 (6.0) 113.2 (0.8)	105.3 (0.6)
54	523	6	21	0.3	1.996	0.37	10.7 (4.5)	na	14.1 (4.3)	97.6 (4.0)	83.0 (3.7) 113.7 (1.4)	104.7 (0.6)

TABLE B-4 (continued) AIR-WATER 1φ DATA WITH T/S: 1 -DN

d = 3.96 mm $\qquad$ A = $1.2331 \times 10^{-5} m^2$ $\qquad$ D = 102.3 mm

	Mainline Conditions						Branchline Conditions					
							Pressure Profile (kPa)					
Run No.	P_0 (kPa)	δP_0 ($\pm$ kPa)	T_0 (^oC)	δT_0 (^oC)	$G_\ell \times 10^{-4}$ (kg/m^2.s)	δG_ℓ (%)	P_1	P_2	P_3	P_4	P_5	P_6
55	570	7	21	0.3	2.036	2.11	11.6 (5.7)	na	13.2 (5.7)	96.4 (5.9)	83.6 (6.1) 114.5 (0.9)	104.4 (0.3)

TABLE B-5   STEAM-WATER   1ϕ DATA WITH T/S: 1 -DN

d = 3.96 mm A = $1.2331 \times 10^{-5} m^2$ D = 102.3 mm

Run No.	Mainline Conditions						Branchline Conditions					
							Pressure Profile (kPa)					
	p_0 (kPa)	δp_0 ($\pm$ kPa)	T_0 (^oC)	δT_0 (^oC)	$G_\ell \times 10^{-4}$ (kg/m^2.s)	δG_ℓ (%)	p_1	p_2	p_3	p_4	p_5	p_6
56	168	4	114.1	0.2	0.299	3.0	153.3 (3.2)	150.1 (2.1)	na	139.7 (2.2)	123.4 (2.0) 129.1 (6.3)	108.8 (0.6)
57	237	4	125.6	0.3	0.439	2.9	215.3 (0.4)	212.4 (3.4)	na	198.8 (3.5)	167.2 (3.2) 172.0 (0.3)	108.9 (0.2)
58	304	1	134.0	0.2	0.465	0.6	278.5 (2.0)	275.3 (3.0)	na	258.6 (2.0)	213.9 (2.9) 214.0 (0.9)	105.4 (0.3)
59	374	3	140.3	0.3	0.492	1.2	336.6 (3.9)	331.1 (4.2)	na	312.9 (3.6)	256.1 (3.4) 261.3 (1.6)	111.3 (0.6)
60	443	2	147.3	0.2	0.533	0.1	405.5 (2.8)	400.8 (2.5)	na	378.4 (3.2)	311.3 (0.8) 315.4 (2.7)	108.5 (0.6)
61	513	3	149.3	0.3	0.571	0.4	460.7 (5.9)	454.0 (4.8)	na	427.7 (6.2)	352.3 (4.4) 360.1 (1.6)	115.3 (0.9)
62	581	7	152.9	0.3	0.605	0.5	321.6 (4.9)	514.2 (5.2)	na	486.0 (4.5)	398.8 (4.2) 405.6 (1.8)	117.3 (0.6)
63	656	1	162.0	0.1	0.651	0.4	597.1 (5.0)	589.0 (4.8)	na	554.6 (4.7)	455.5 (2.7) 459.7 (3.1)	118.8 (0.9)
64	788	1	168.3	0.1	0.719	0.9	na	na	na	na	535.5 (0.3) 540.5 (3.4)	117.0 (0.9)

TABLE B-5 (continued) STEAM-WATER 1ϕ DATA WITH T/S: 1 -DN

$$d = 3.96 \text{ mm} \qquad A = 1.2331\times10^{-5} m^2 \qquad D = 102.3 \text{ mm}$$

Run No.	Mainline Conditions						Branchline Conditions					
	P_o (kPa)	δP_o ($\pm$ kPa)	T_o (°C)	δT_o (°C)	$G_\ell \times 10^{-4}$ (kg/m^2.s)	δG_ℓ (%)	Pressure Profile (kPa)					
							P_1	P_2	P_3	P_4	P_5	P_6
65	928	1	175.4	0.1	0.794	1.0	na	na	na	na	641.1 (6.9) 644.6 (5.0)	131.3 (0.9)
66	1065	6	177.9	0.2	0.883	0.1	na	na	na	na	732.9 (7.6) 739.9 (6.6)	138.5 (1.4)
108	653	6	155.7	0.4	0.657	0.6	394.5 (7.9)	585.6 (7.7)	na	552.7 (7.0)	454.2 (6.0) 456.2 (5.5)	117.9 (0.6)
112	794	4	169.8	0.4	0.746	0.7	710.9 (6.4)	700.4 (6.3)	na	660.5 (6.0)	542.1 (5.1) 545.9 (3.7)	118.8 (0.6)
115	883	4	174.6	0.2	0.758	0.4	788.3 (7.6)	775.1 (7.5)	na	726.5 (6.2)	592.6 (6.0) 598.5 (6.1)	123.4 (0.4)
133	892	16	174.6	1.4	0.756	0.3	790.7 (6.1)	779.8 (6.6)	na	734.6 (8.4)	599.7 (8.4) 607.9 (3.3)	123.9 (0.6)
135	1029	3	180.0	0.4	0.883	0.5	893.6 (6.1)	883.9 (6.1)	na	838.4 (6.0)	702.6 (6.0) 709.3 (3.3)	133.1 (2.3)
138	979	1	179.0	0.4	0.813	0.3	851.0 (3.7)	839.0 (3.6)	na	789.1 (3.6)	653.2 (3.8) 666.3 (50.7)	126.5 (1.4)

TABLE B-6   AIR-WATER   1φ   DATA WITH T/S: 2-DN

d =   6.32 mm   A =   3.13707x10^{-5}m^2 D = 102.3 mm

| Run No. | Mainline Conditions | | | | | | Branchline Conditions | | | | | |
| | P_o (kPa) | δP_o ($\pm$ kPa) | T_o (^{o}C) | δT_o (^{o}C) | G_ℓx10^{-4} (kg/m^2.s) | δG_ℓ (%) | Pressure Profile (kPa) | | | | | |
							p_1	p_2	p_3	p_4	p_5	p_6
79	143	1	22	0.3	0.6700	1.4	106.4 (1.8)	104.7 (1.8)	na	102.2 (1.8)	100.3 (1.8) 98.7 (0.5)	103.9 (0.3)
80	177	1	22	0.3	0.9060	1.2	110.4 (1.6)	107.7 (1.6)	na	102.4 (1.6)	98.0 (1.5) 95.8 (0.8)	105.1 (0.6)
81	212	1.4	22	0.3	1.1150	0.1	109.6 (2.8)	106.9 (2.8)	na	99.6 (2.8)	93.9 (2.7) 92.4 (0.8)	106.2 (0.6)
82	251	2	22	0.3	1.2800	0.2	44.7 (4.4)	41.6 (4.2)	na	42.2 (4.2)	91.8 (4.2) 92.1 (3.0)	107.6 (0.6)
83	281	3	22	0.3	1.3690	1.4	21.0 (4.0)	16.5 (3.9)	na	18.1 (3.9)	89.5 (3.5) 88.7 (2.3)	108.2 (0.6)
84	279	3	22	0.3	1.3680	1.5	20.6 (3.2)	17.7 (3.2)	na	19.2 (3.2)	89.7 (3.0) 87.6 (3.3)	107.9 (0.6)
85	302	1.4	22	0.3	1.4460	0.8	18.8 (4.5)	16.2 (4.5)	na	18.0 (4.5)	89.1 (4.3) 87.9 (2.4)	108.8 (0.9)
86	294	1	22	0.3	1.4630	0.5	6.4 (4.6)	3.5 (4.5)	na	3.8 (4.5)	76.2 (4.4) 88.4 (4.7)	109.1 (0.6)
87	336	2	22	0.3	1.5780	0.8	5.6 (5.8)	3.1 (5.7)	na	3.0 (5.7)	69.9 (5.5) 83.0 (2.4)	109.1 (0.1)

TABLE B-6 (continued) AIR-WATER 1φ DATA WITH T/S: 2 -DN

$d = 6.32$ mm $A = 3.13707 \times 10^{-5} m^2$ $D = 102.3$ mm

Run No.	P_0 (kPa)	δP_0 ($\pm$ kPa)	T_0 (°C)	δT_0 (°C)	$G_\ell \times 10^{-4}$ (kg/m^2.s)	δG_ℓ (%)	P_1	P_2	P_3	P_4	P_5	P_6
88	379	2	22	0.3	1.6490	1.3	3.4 (7.6)	-0.135 (7.5)	na	1.2 (7.4)	63.4 (6.7) 77.5 (3.0)	110.2 (1.1)
89	406	2.2	22	0.3	1.6960	1.2	2.5 (8.6)	-1.5 (8.3)	na	0.2 (8.3)	60.4 (5.9) 76.8 (6.8)	111.1 (5.9)
90	446	2.2	22	0.3	1.7990	0.8	6.2 (5.1)	4.5 (5.0)	na	2.9 (5.0)	56.6 (4.7) 71.4 (4.9)	111.1 (0.9)
191	160	2	20	0.3	0.8868	0.4	97.6 (1.6)	na	93.0 (1.6)	91.5 (1.6)	90.1 (1.6)	97.9 (0.3)
192	151	2	20	0.3	0.8088	0.5	90.7 (3.6)	na	86.6 (3.6)	85.2 (3.6)	84.1 (3.5)	97.3 (0.3)
193	147	1.9	20	0.3	0.7840	0.3	100.1 (11.0)	na	96.1 (11.0)	94.9 (11.0)	93.9 (11.0)	102.4 (0.3)
194	136	1.1	20	0.3	0.6784	0.6	100.6 (3.9)	na	97.4 (2.1)	96.3 (1.8)	95.6 (1.7)	97.6 (0.3)
195	122	0.8	20	0.3	0.5585	0.5	97.0 (1.2)	na	94.4 (1.2)	93.6 (1.2)	93.3 (1.2)	96.8 (0.3)

Mainline Conditions: P_0, δP_0, T_0, δT_0, $G_\ell \times 10^{-4}$, δG_ℓ

Branchline Conditions: Pressure Profile (kPa): P_1, P_2, P_3, P_4, P_5, P_6

$d = 6.32$ mm $\qquad$ $A = 3.1370 \times 10^{-5} m^2$ $\qquad$ $D = 102.3$ mm

Run No.	Mainline Conditions						Branchline Conditions					
	P_0 (kPa)	δP_0 ($\pm$ kPa)	T_0 (°C)	δT_0 (°C)	$G_\ell \times 10^{-4}$ (kg/m^2.s)	δG_ℓ (%)	Pressure Profile (kPa)					
							P_1	P_2	P_3	P_4	P_5	P_6
196	111	1	20	0.3	0.4065	0.2	98.6 (0.9)	na	96.5 (0.9)	95.9 (0.9)	95.9 (0.9)	97.6 (0.3)
197	106	0	20	0.3	0.1705	0.2	105.1 (0.3)	na	103.6 (0.3)	103.4 (0.3)	103.8 (0.3)	100.9 (0.3)

TABLE B-7 STEAM-WATER 1φ DATA WITH T/S: 2 -DN

$d = 6.32$ mm $A = 3.13707 \times 10^{-5} m^2$ $D = 102.3$ mm

Run No.	Mainline Conditions						Branchline Conditions					
							Pressure Profile (kPa)					
	p_0 (kPa)	δp_0 (± kPa)	T_0 (°C)	δT_0 (°C)	$G_\ell \times 10^{-4}$ (kg/m².s)	δG_ℓ (%)	p_1	p_2	p_3	p_4	p_5	p_6
91	310	4	135	0.4	0.4680	6.6	278.5 (6.1)	274.8 (3.5)	na	258.5 (4.1)	206.0 (3.1) 208.6 (1.3)	125.1 (1.2)
94	373	11	141.7	0.4	0.5310	3.9	326.4 (4.2)	323.0 (4.1)	na	309.3 (3.9)	244.8 (2.3) 247.5 (0.9)	130.2 (0.7)
102	448	3.3	148.3	0.2	0.5830	1.8	398.5 (4.1)	394.9 (4.0)	na	375.9 (3.6)	298.7 (3.3) 307. (3.8)	149.3 (2.7)
182	172	0	115.7	0.2	0.3600	1.5	156.2 (1.7)	na	149.8 (0.7)	144.9 (0.3)	124.0 (0.3)	106.8 (0.3)
183	227	3	124.1	0.2	0.4494	0.9	202.5 (3.9)	na	195.5 (3.4)	188.9 (3.0)	153.6 (3.0)	111.4 (0.3)
184	300	0	133.8	0.2	0.4998	1.7	264.9 (2.3)	na	258.9 (2.0)	250.8 (1.3)	199.7 (1.3)	121.9 (0.9)
185	120.2	0.8	104.4	0.2	0.3178	0.4	108.6 (2.1)	na	106.6 (1.2)	106.4 (1.2)	106.1 (1.0)	103.6 (0.3)
186	132.1	0.8	107.9	0.2	0.3283	0.8	117.8 (2.5)	na	115.9 (1.7)	113.4 (1.3)	108.1 (1.0)	103.6 (0.3)
187	158.9	0.6	113.0	0.2	0.3768	1.2	142.4 (1.5)	na	137.2 (1.3)	133.4 (1.0)	117.3 (0.7)	104.8 (0.3)

TABLE B-7 (continued) STEAM-WATER 1ϕ DATA WITH T/S: 2 -DN

d ≈ 6.32 mm A = 3.13707x10^{-5}m^2 D ≈ 102.3 mm

Run No.	Mainline Conditions						Branchline Conditions					
							Pressure Profile (kPa)					
	P_o (kPa)	δP_o ($\pm$ kPa)	T_o (^{o}C)	δT_o (^{o}C)	G_ℓx10^{-4} (kg/m^2.s)	δG_ℓ (%)	P_1	P_2	P_3	P_4	P_5	P_6
188	113.3	0.3	102.9	0.2	0.3294	0.8	106.3 (0.4)	na	104.8 (0.4)	104.5 (0.4)	104.0 (0.4)	103.1 (0.3)
189	149.3	1.1	110.7	0.2	0.3614	0.6	131.8 (4.7)	na	128.6 (4.1)	125.2 (4.0)	113.6 (1.3)	103.9 (0.3)
190	190.1	1.6	119.0	0.2	0.4122	0.2	170.3 (2.6)	na	164.2 (2.2)	159.1 (1.8)	132.6 (1.8)	107.1 (0.3)
198	107.0	1.4	100.9	0.2	0.2020	0.5	106.4 (1.4)	na	103.2 (1.4)	103.0 (1.4)	103.5 (1.4)	102.2 (0.6)

TABLE B-8   AIR-WATER 1ϕ DATA WITH T/S: 1B-DN

$d = 3.76$ mm $A = 1.1104 \times 10^{-5} m^2$ $D = 102.3$ mm

B-16

Run No.	Mainline Conditions						Branchline Conditions					
	P_o (kPa)	δP_o ($\pm$ kPa)	T_o (°C)	δT_o (°C)	$G_\ell \times 10^{-4}$ (kg/m^2.s)	δG_ℓ (%)	Pressure Profile (kPa)					
							P_1	P_2	P_3	P_4	P_5	P_6
140	175	6	20	0.3	0.9132	1.6	100.9 (6.3)	100.5 (6.3)	na	95.3 (6.3)	98.2 (6.3)	98.8 (0.3)
141	297	6	20	0.3	1.4753	1.3	103.7 (5.9)	100.5 (5.9)	na	87.9 (5.9)	95.8 (5.9)	97.1 (0.3)
142	380	11	20	0.3	1.8065	0.5	--	--	--	--	--	--
143	249	4	20	0.3	1.3160	0.5	101.6 (4.4)	100.4 (4.4)	na	93.8 (4.4)	98.8 (4.4)	97.1 (0.3)
144	437	10	20	0.3	1.9618	0.9	--	--	--	--	--	--
145	500	12	20	0.3	2.0782	0.8	--	--	--	--	--	--
146	217	4	20	0.3	1.1627	1.5	114.7 (4.0)	111.5 (4.0)	na	94.1 (3.9)	97.6 (3.7)	97.1 (0.3)
174	167	2	20	0.3	0.9015	1.2	96.7 (1.7)	96.2 (1.7)	na	91.9 (1.7)	94.0 (1.7)	96.5 (0.3)
175	144	2	20	0.3	0.6918	1.5	99.1 (1.4)	98.0 (1.4)	na	95.1 (1.4)	96.5 (1.4)	98.8 (0.3)

TABLE B-8 (continued) AIR-WATER 1ϕ DATA WITH T/S: 1B-DN

d = 3.76 mm   A = $1.1104 \times 10^{-5} m^2$ D = 102.3 mm

Run No.	Mainline Conditions						Branchline Conditions					
	p_o (kPa)	δp_o ($\pm$ kPa)	T_o (°C)	δT_o (°C)	$G_\ell \times 10^{-4}$ (kg/m^2.s)	δG_ℓ (%)	Pressure Profile (kPa)					
							p_1	p_2	p_3	p_4	p_5	p_6
176	133	1	20	0.3	0.5861	1.2	103.3 (1.5)	101.9 (1.5)	na	100.1 (1.5)	101.0 (1.4)	101.3 (0.3)
177	122	1	20	0.3	0.4386	1.0	105.9 (0.6)	104.1 (0.6)	na	103.1 (0.6)	103.7 (0.6)	101.9 (0.3)
178	116	1	20	0.3	0.3487	0.31	106.1 (0.4)	104.2 (0.4)	na	103.6 (0.4)	104.0 (0.4)	102.2 (0.3)
179	108	1	20	0.3	0.2111	0.6	105.7 (0.4)	103.8 (0.4)	na	103.7 (0.4)	103.9 (0.4)	101.9 (0.3)

TABLE B-9   STEAM-WATER 1ϕ DATA WITH T/S: 1B-DN

$d = 3.76$ mm $A = 1.1104 \times 10^{-5} m^2$ $D = 102.3$ mm

| Run No. | Mainline Conditions | | | | | | Branchline Conditions | | | | | |
| | P_o (kPa) | δP_o ($\pm$ kPa) | T_o (°C) | δT_o (°C) | $G_\ell \times 10^{-4}$ (kg/m².s) | δG_ℓ (%) | Pressure Profile (kPa) | | | | | |
							P_1	P_2	P_3	P_4	P_5	P_6
148	203	1	121.3	0.2	0.415	0.1	184.5 (2.3)	182.9 (1.9)	na	168.0 (1.4)	140.0 (0.7)	103.9 (0.1)
149	163	1	113.6	0.2	0.382	0.0	147.2 (2.8)	144.9 (2.3)	na	134.2 (2.0)	118.5 (1.6)	103.9 (0.3)
150	185	1	117.6	0.2	0.399	0.0	168.4 (1.9)	166.3 (1.8)	na	153.4 (1.0)	129.8 (0.6)	103.6 (0.3)
151	246	1	127.0	0.2	0.496	0.0	224.8 (2.1)	219.7 (1.8)	na	202.8 (1.1)	166.8 (0.7)	104.2 (0.3)
152	177	1	115.5	0.2	0.395	0.1	158.3 (2.8)	156.0 (2.7)	na	146.2 (2.4)	124.9 (2.2)	103.4 (0.3)
153	304	1	134.2	0.2	0.568	1.4	284.6 (3.4)	278.4 (3.2)	na	260.5 (2.5)	205.6 (1.6)	104.8 (0.3)
154	266	2	130.1	0.2	0.610	0.0	253.3 (4.1)	244.5 (4.0)	na	228.5 (2.5)	179.5 (3.3)	104.5 (0.3)
155	133	1	107.1	0.2	0.379	2.1	119.3 (1.7)	117.7 (1.6)	na	113.2 (1.3)	108.1 (1.1)	103.1 (0.3)

TABLE B-9 (continued) STEAM-WATER 1ϕ DATA WITH T/S: 1B-DN

d = 3.76 mm   A = $1.1104 \times 10^{-5} m^2$ D = 102.3 mm

Run No.	Mainline Conditions						Branchline Conditions					
							Pressure Profile (kPa)					
	P_0 (kPa)	δP_0 ($\pm$ kPa)	T_0 (°C)	δT_0 (°C)	$G_\ell \times 10^{-4}$ (kg/m^2.s)	δG_ℓ (%)	P_1	P_2	P_3	P_4	P_5	P_6
156	376	1	141.9	0.2	0.564	0.1	335.0 (4.5)	331.8 (4.1)	na	309.9 (3.2)	254.1 (1.9)	105.6 (0.3)
157	446	1	148.3	0.2	0.564	0.1	404.6 (4.8)	395.8 (4.3)	na	368.6 (3.4)	301.0 (1.7)	107.6 (0.3)
158	150	1	111.5	0.2	0.364	0.1	135.2 (1.2)	132.1 (1.1)	na	123.4 (1.0)	110.7 (0.6)	103.9 (0.3)
159	140	0	107.1	0.4	0.313	0.1	123.4 (1.4)	122.1 (1.4)	na	116.5 (0.8)	108.9 (0.4)	102.8 (0.1)
160	122	0	105.6	0.2	0.306	0.0	114.4 (2.1)	111.6 (2.0)	na	108.1 (1.3)	106.4 (0.6)	102.8 (0.3)
161	128	1	106.9	0.2	0.349	1.0	116.4 (1.2)	115.2 (1.2)	na	111.7 (0.9)	107.9 (0.9)	103.6 (0.3)
162	143	1	108.6	0.4	0.362	0.0	125.8 (1.4)	124.0 (1.8)	na	116.8 (1.0)	110.0 (0.6)	103.6 (0.3)
163	129	1	105.0	0.2	0.329	0.1	115.3 (1.3)	113.8 (1.2)	na	110.4 (0.9)	106.6 (0.4)	103.6 (0.1)

TABLE B-9 (continued)   STEAM-WATER   1ϕ DATA WITH T/S: 1B-DN

$d = 3.76$ mm $A = 1.1104 \times 10^{-5} m^2$ $D = 102.3$ mm

Run No.	Mainline Conditions						Branchline Conditions					
	P_0 (kPa)	δP_0 ($\pm$ kPa)	T_0 (^oC)	δT_0 (^oC)	$G_\ell \times 10^{-4}$ (kg/m^2.s)	δG_ℓ (%)	Pressure Profile (kPa)					
							P_1	P_2	P_3	P_4	P_5	P_6
164	180	0	116.9	0.2	0.369	0.0	162.9 (1.8)	160.6 (1.7)	na	149.4 (1.2)	127.5 (0.5)	103.4 (0.3)
165	107	1	100.4	0.2	0.184	0.5	106.7 (0.5)	105.7 (0.5)	na	105.6 (0.4)	105.0 (0.4)	102.8 (0.3)
166	161	1	113.0	0.2	0.382	2.0	139.9 (1.4)	138.4 (1.4)	na	127.5 (1.1)	111.7 (0.2)	103.6 (0.3)
167	508	2	152.7	0.2	0.709	0.0	454.0 (7.4)	449.2 (6.5)	na	418.4 (4.9)	339.7 (2.3)	108.5 (0.3)
168	145	1	109.4	0.2	0.285	0.2	131.5 (1.5)	130.4 (1.3)	na	122.3 (1.1)	111.7 (0.5)	103.6 (0.6)
169	573	2	156.2	0.2	0.631	0.1	515.8 (7.3)	506.1 (6.6)	na	474.4 (4.8)	387.8 (2.8)	110.8 (0.3)
170	159	1	113.6	0.2	0.423	0.0	144.8 (1.8)	143.2 (1.5)	na	132.9 (1.0)	117.0 (0.6)	103.1 (0.3)
171	653	1	161.0	0.2	0.772	0.0	588.9 (7.0)	578.9 (6.5)	na	539.5 (5.0)	439.4 (2.7)	113.4 (0.3)

TABLE B-9 (continued)   STEAM-WATER 1ϕ DATA WITH T/S: 1B-DN

d = 3.76 mm $A = 1.1104 \times 10^{-5} m^2$ D = 102.3 mm

Run No.	Mainline Conditions						Branchline Conditions					
	P_o (kPa)	δP_o ($\pm$ kPa)	T_o (°C)	δT_o (°C)	$G_\ell \times 10^{-4}$ (kg/m².s)	δG_ℓ (%)	Pressure Profile (kPa)					
							P_1	P_2	P_3	P_4	P_5	P_6
172	789	5	170.1	0.2	0.871	0.0	709.1 (5.1)	699.2 (4.8)	na	654.1 (4.0)	530.8 (3.4)	118.8 (0.3)
173	947	3	177.9	0.2	1.006	0.1	839.8 (7.3)	828.9 (7.1)	na	776.5 (6.4)	639.5 (5.5)	127.4 (0.3)
180	134.0	1.3	105.8	0.2	0.4209	1.0	118.2 (2.1)	117.0 (2.0)	na	113.6 (1.9)	107.3 (1.9)	103.4 (0.3)
181	321.4	0.6	136.2	0.2	0.6405	1.7	296.3 (3.4)	290.5 (3.2)	na	269.8 (2.4)	219.1 (1.5)	105.4 (0.3)

TABLE B-10 AIR FLOW 1ϕ DATA WITH T/S: 1B-UP

$$d = 3.76 \text{ mm} \qquad A = 1.1104\times10^{-5}\text{m}^2 \qquad D = 102.3 \text{ mm}$$

Run No.	Mainline Conditions						Branchline Conditions					
	P_o (kPa)	δP_o ($\pm$ kPa)	T_o (^{o}C)	δT_o (^{o}C)	$G_\ell \times 10^{-4}$ (kg/m^2.s)	δG_ℓ (%)	Pressure Profile (kPa)					
							P_1	P_2	P_3	P_4	P_5	P_6
240	404	4	20	0.3	711.80	0.9	231.7 (3.9)	227.8 (3.9)	na	193.3 (3.9)	173.9 (3.8)	103.9 (0.3)
241	472	4	20	0.3	810.03	1.1	266.2 (3.8)	262.6 (3.8)	na	222.3 (3.8)	199.7 (3.8)	104.2 (0.2)
242	539	4	20	0.3	940.92	0.9	300.3 (5.1)	296.6 (5.1)	na	251.0 (5.1)	225.6 (5.1)	104.8 (0.2)
243	608	5	20	0.3	1076.48	0.9	334.9 (4.8)	331.2 (4.8)	na	280.1 (4.7)	251.8 (4.7)	105.6 (0.2)

TABLE B-11   AIR-WATER   2φ   DATA WITH   T/S: 1A-DN, Gas Pull-through

d = 3.91 mm   A = 1.2017x10^{-5}m^2 D = 102.3 mm

| | Mainline Conditions | | | | | | | Branchline Conditions | | | | | | | | | | | |
| | | | | | | | | | | | | | | | Pressure | Profile | | (kPa) | |
Run No.	h (mm)	P_o (kPa)	δP_o (±kPa)	T_o (°C)	δT_o (±°C)	j_ℓ (m/s)	j_g (m/s)	G_ℓx10^{-4} (kg/m^{2}s)	δG_ℓ (%)	G_g (kg/m^{2}s)	δG_g (%)	xx10^3	δx (%)	P_1	P_2	P_3	P_4	P_5	P_6
19	18.9	376	3	25	0.3	0.0178	0.0557	0.911	2.0	5.18	4.6	0.57	5.0	210.4 (7.7)	na	195.3 (10.81)	190.7 (10.8)	169.0 (10.9) 174.9 (10.7)	105.9 (0.2)
20	15.9	378	3	25	0.3	0.0121	0.0382	0.539	2.0	79.60	8.7	14.50	15.5	233.7 (2.8)	na	204.2 (7.4)	195.7 (7.5)	173.8 (7.5) 176.8 (1.4)	108.5 (0.0)
21	15.1	380	2	25	0.3	0.0111	0.0415	0.464	2.3	92.30	6.6	19.50	11.8	236.1 (4.8)	na	208.4 (6.4)	201.0 (6.5)	176.1 (6.7) 178.6 (1.9)	108.3 (0.0)
22	13.7	369	1	25	0.3	0.0086	0.0515	0.317	3.1	157.35	10.9	47.30	19.4	251.3 (3.7)	na	202.2 (5.6)	212.7 (6.8)	188.8 (6.8) 185.0 (1.4)	107.6 (0.0)
23	17.6	517	3	25	0.3	0.0173	0.0207	0.918	2.4	52.41	5.5	5.68	10.0	282.2 (6.6)	na	247.7 (6.8)	237.6 (8.1)	202.0 (8.2) 209.0 (1.4)	107.0 (0.0)
24	20.6	517	3	25	0.3	0.0213	0.0197	1.192	1.8	13.13	5.2	1.10	9.4	275.7 (7.1)	na	257.0 (9.3)	254.7 (9.3	217.3 (11.7) 235.8 (12.3)	105.9 (6.7)
25	14.9	500	7	25	0.3	0.0107	0.0741	0.531	2.9	300.03	7.9	53.50	14.1	284.3 (12.4)	na	284.3 (12.4)	274.3 (12.5)	235.8 (12.7) 228.7 (12.8)	168.8 (6.7)
26	16.8	579	10	24	0.3	0.0127	0.0336	0.620	2.5	159.12	7.6	25.00	13.6	337.8 (11.7)	na	291.5 (11.9	272.4 (12.3)	234.8 (13.0) 232.3 (4.2)	108.1 (0.7)
27	18.4	587	7	24	0.3	0.0178	0.0246	0.988	2.0	56.69	6.5	5.71	6.8	315.7 (8.4)	na	278.2 (8.7)	267.8 (9.0)	224.3 (9.2) 324.9 (1.7)	106.5 (0.0)
28	22.2	589	6	24	0.3	0.0234	0.0134	1.397	2.2	3.85	4.7	0.27	8.6	313.0 (6.2)	na	298.9 (10.3)	298.9 (10.5)	249.3 (10.9) 252.3 (9.7)	105.0 (0.0)
29	27.9	661	3	24	0.3	0.0221	0.0207	1.366	2.1	28.65	6.0	2.09	10.7	349.4 (11.2)	na	328.0 (10.3)	320.6 (8.9)	267.0 (8.6) 265.7 (2.3)	104.2 (0.0)
30	14.9	647	14	24	0.3	0.0127	0.0495	0.579	3.5	192.23	7.3	32.20	13.4	390.11 (11.0)	na	331.4 (9.6)	317.2 (7.1)	266.1 (7.2) 268.0 (1.3)	108.5 (0.0)

TABLE B-12   STEAM-WATER   2φ   DATA WITH T/S: 1-DN, Gas Pull-Through

d = 3.96 mm   A = 1.2331x10^{-5} m^2 D = 102.3 mm

	Mainline Conditions							Branchline Conditions						Pressure Profile (kPa)					
Run No.	h_l (mm)	P_o (kPa)	δP_o (±kPa)	T_o (°C)	δT_o (±°C)	j_l (m/s)	j_g (m/s)	$G_l \times 10^{-4}$ (kg/m²s)	δG_l (%)	G_g (kg/m²s)	δG_g (%)	$x \times 10^3$	δx (%)	P_1	P_2	P_3	P_4	P_5	P_6
67	16.5	367	3	140.7	0.4	0.0096	0.0403	0.365	1.3	47.7	4.4	12.9	6.5	324.9 (5.2)	316.9 (2.4)	na	291.9 (4.2)	231.5 (1.8) 229.4 (5.1)	104.5 (0.2)
68	14.0	371	2	140.9	0.4	0.0096	0.0397	0.303	0.2	80.9	5.2	26.0	6.9	294.5 (3.1)	287.3 (2.9)	na na	257.8 (2.9)	199.5 (2.5) 198.1 (5.1)	103.3 (0.2)
69	12.4	369	1	140.9	0.1	0.0080	0.0724	0.251	3.1	103.3	4.4	39.6	7.3	286.8 (3.8)	278.1 (4.1)	na	245.4 (3.8)	185.2 (3.6) 182.0 (2.0)	103.5 (0.3)
70	17.5	444	5	148.1	0.4	0.0108	0.0446	0.492	3.0	74.0	4.2	14.8	6.0	409.5 (5.8)	400.0 (7.7)	na	370.4 (4.3)	299.2 (3.6) 303.9 (5.5)	107.9 (0.9)
71	14.6	441	8	147.5	0.1	0.0109	0.0474	0.454	4.7	128.8	7.5	27.6	8.8	400.2 (7.7)	393.5 (6.0)	na	362.4 (3.1)	288.4 (4.2) 281.3 (3.1)	108.2 (0.9)
72	13.5	445	5	147.9	1.0	0.0082	0.0537	0.321	4.3	111.5	5.2	33.6	7.6	353.2 (4.6)	342.9 (3.4)	na	307.4 (3.8)	237.1 (2.9) 239.4 (3.1)	106.5 (0.6)
73	17.2	511	6	152.1	0.4	0.0109	0.0671	0.491	0.7	86.4	3.6	17.3	5.9	429.7 (8.6)	425.5 (9.5)	na	386.5 (9.5)	303.3 (8.6) 309.1 (8.5)	109.1 (0.6)
74	15.9	510	5	152.5	0.1	0.0094	0.0639	0.459	5.2	93.6	4.7	20.1	6.9	404.2 (10.6)	397.5 (2.1)	na	356.6 (2.8)	278.1 (3.6) 271.1 (5.3)	108.8 (0.3)
75	14.8	506	3	151.9	0.4	0.0087	0.0784	0.388	1.2	112.4	4.1	28.0	6.9	397.9 (8.3)	390.3 (7.2)	na	350.5 (7.5)	272.0 (6.9) 273.2 (10.0)	108.2 (0.0)
76	17.5	582	8	158.2	0.4	0.0119	0.0422	0.533	3.6	124.0	2.9	22.7	4.6	517.9 (5.6)	505.4 (6.1)	na	465.2 (4.3)	370.4 (1.9) 380.5 (0.9)	111.6 (0.6)
77	16.2	584	4	158.4	0.2	0.0110	0.0431	0.477	4.1	133.5	4.5	27.2	6.1	510.2 (5.6)	495.1 (4.7)	na	447.6 (3.8)	352.2 (2.9) 356.7 (0.7)	111.0 (0.6)

TABLE B-12 (cont'd) STEAM-WATER 2ϕ DATA WITH T/S: 1 - DN, Gas Pull-Through

$d = 3.96$ mm $A = 1.2331\times10^{-5}$ m^2 $D = 102.3$ mm

| | | | | | | Mainline Conditions | | | | Branchline Conditions | | | | | | | | Pressure Profile (kPa) | | |
Run No.	h (mm)	P_o (kPa)	δP_o (±kPa)	T_o (°C)	δT_o (±°C)	j_ℓ (m/s)	j_g (m/s)	$G_\ell\times10^{-4}$ (kg/m²s)	δG_ℓ (%)	G_g (kg/m²s)	δG_g (%)	$x\times10^3$	δx (%)	P_1	P_2	P_3	P_4	P_5	P_6
78	14.0	575	6	157.8	0.2	0.0103	0.0602	0.428	4.5	161.2	3.7	36.3	5.8	452.6 (6.7)	438.0 (6.5)	na	396.3 (6.0)	305.4 (4.9) / 312.1(10.5)	109.6 (0.6)
109	16.8	634	1	155.1	0.2	na	na	0.460	8.4	151.6	10.0	32.0	13.1	561.6 (10.2)	549.0 (9.6)	na	498.6 (8.9)	393.1 (8.4) / 330.5 (1.9)	114.5 (0.9)
110	15.2	626	6	160.8	0.2	0.0126	0.0906	0.518	4.1	197.5	4.4	36.7	6.0	539.9 (7.0)	528.2 (6.7)	na	480.7 (3.8)	377.5 (3.0) / 384.9 (1.6)	111.1 (0.4)
111	14.2	625	4	160.6	0.2	0.0149	0.0878	0.470	0.8	191.3	13.0	40.7	13.0	527.1 (3.9)	512.7 (6.8)	na	462.4 (7.1)	359.3 (7.2) / 367.3 (3.5)	110.2 (0.1)
113	17.5	760	7	168.2	0.4	0.0136	0.0626	0.627	6.5	165.1	9.5	25.7	11.5	668.6 (7.8)	654.7 (4.1)	na	599.0 (3.9)	473.8 (3.0) / 468.6 (1.7)	114.2 (.14)
114	19.9	783	1	169.6	0.2	0.0125	0.0297	0.556	1.6	80.7	10.2	14.3	10.3	684.2 (6.9)	668.1 (4.3)	na	611.6 (3.9)	483.5 (3.1) / 491.01 (6.1)	114.2 (2.0)
116	17.4	762	6	168.0	0.4	0.0123	0.0593	0.541	5.7	157.0	9.4	28.2	12.4	646.9 (5.6)	629.9 (6.2)	na	572.6 (6.7)	447.2 (1.8) / 451.6 (9.1)	113.4 (1.1)
117	14.6	599	3	159.6	0.2	0.0084	0.1738	0.366	10.8	366.9	17.7	90.1	20.8	453.1 (7.1)	440.0 (6.7)	na	395.1 (6.5)	296.8 (6.3) / 301.4 (6.1)	111.4 (0.3)
118	16.3	664	3	163.7	0.4	0.0105	0.1223	0.447	5.6	283.4	23.7	59.6	25.0	525.6 (4.3)	512.0 (2.3)	na	463.7 (3.9)	355.4 (2.9) / 355.9 (1.8)	112.8 (0.9)
131	18.3	835	10	172.1	0.6	0.0136	0.0483	0.622	5.5	194.8	10.2	30.4	12.3	691.5 (4.4)	679.3 (3.9)	na	627.9 (3.2)	494.7 (3.9) / 506.9 (3.3)	116.5 (2.3)
132	18.1	860	5	174.0	0.6	0.0135	0.0379	0.621	7.0	167.9	8.5	26.4	11.0	725.6 (7.3)	710.0 (8.1)	na	648.7 (9.2)	514.5 (3.9) / 522.7 (3.8)	117.4 (2.3)

TABLE B-12 (cont'd) STEAM-WATER 2ϕ DATA WITH T/S: 1 - DN, Gas Pull-Through

$d = 3.96$ mm $A = 1.2331 \times 10^{-5}$ m^2 $D = 102.3$ mm

			Mainline Conditions							Branchline Conditions					Pressure Profile (kPa)				
Run No.	h (mm)	p_o (kPa)	δp_o ($\pm$kPa)	T_o (°C)	δT_o ($\pm$°C)	j_l (m/s)	j_g (m/s)	$G_l \times 10^{-4}$ (kg/m^{2}s)	δG_l (%)	G_g (kg/m^{2}s)	δG_g (%)	$x \times 10^3$	δx (%)	p_1	p_2	p_3	p_4	p_5	p_6
134	16.6	808	1	170.7	0.2	0.0082	0.0838	0.550	8.0	280.6	14.0	48.6	16.0	613.1 (3.8)	599.1 (3.0)	na	541.4 (3.0)	409.1 (2.8) 422.5 (1.3)	112.8 (0.6)
136	17.1	929	8	177.1	0.6	0.0118	0.0716	0.506	5.0	275.4	13.2	51.6	15.0	700.4 (4.3)	683.1 (4.4)	na	616.2 (4.5)	480.0 (4.7) 491.5 (3.1)	116.5 (0.9)
137	18.6	976	3	178.3	0.6	0.0146	0.0723	0.614	5.0	285.9	6.8	44.5	8.4	808.1 (4.5)	791.5 (6.1)	na	726.6 (3.9)	590.1 (5.3) 600.6 (5.1)	124.8 (4.3)
139	18.3	980	1	179.0	0.2	0.0192	0.0918	0.571	10.7	356.7	13.2	62.4	14.4	750.8 (5.1)	732.7 (5.2)	na	663.0 (3.6)	526.9 (3.9) 547.5 (0.1)	118.5 (0.3)

TABLE B-13 STEAM-WATER   2φ   DATA WITH T/S: 2-DN Gas Pull-Through

d = 6.32 mm   A = 3.13707×10^{-5} m^2 D = 102.3 mm

														Mainline Conditions				Branchline Conditions					Pressure Profile (kPa)					
Run No.	h_l (mm)	P_o (kPa)	δP_o (±kPa)	T_o (°C)	δT_o (±°C)	j_l (m/s)	j_g (m/s)	$G_l \times 10^{-4}$ (kg/m²s)	δG_l (%)	G_g (kg/m²s)	δG_g (%)	$x \times 10^3$	δx (%)	p_1	p_2	p_3	p_4	p_5	p_6
92	19.78	321	2	135.4	0.2	0.0333	0.0300	0.3627	1.6	15.808	7.6	4.339	7.79	276.3 (5.8)	270.4 (3.6)	na	248.2 (4.1)	189.8 (4.3) / 190.1 (2.2)	119.1 (2.3)
93	21.05	314	3	135.0	0.4	0.0171	0.0473	0.3670	6.4	12.49	6.9	3.395	9.4	270.0 (6.6)	264.0 (6.1)	na	245.1 (3.9)	188.3 (3.5) / 187.7 (6.1)	119.9 (2.0)
95	19.00	374	3	141.3	0.4	0.0156	0.0934	0.3350	2.9	45.75	6.3	13.50	6.9	287.8 (9.8)	278.9 (9.3)	na	258.0 (3.5)	190.6 (4.3) / 196.1 (9.0)	115.6 (1.2)
96	22.73	376	0.2	142.0	0.2	0.0184	0.1535	0.3920	1.9	24.80	0.3	6.282	1.9	319.7 (4.0)	313.3 (4.5)	na	286.0 (6.1)	213.8 (1.9) / 220.6 (3.1)	118.5 (3.1)
97	22.80	367	4	140.5	0.4	0.0218	0.1314	0.4740	6.2	32.39	3.4	6.787	7.1	324.8 (3.8)	322.8 (4.0)	na	302.8 (6.9)	235.6 (3.3) / 238.3 (4.1)	125.7 (3.4)
98	20.42	448	0.6	147.7	0.2	0.0193	0.0871	0.4040	7.4	49.60	4.1	12.12	8.4	386.5 (4.3)	377.1 (4.2)	na	341.6 (4.1)	254.6 (3.6) / 244.7 (8.1)	127.6 (1.4)
99	22.32	447	1	147.9	0.2	0.0209	0.1254	0.4440	0.55	42.01	1.0	9.380	1.1	393.5 (6.1)	387.6 (6.3)	na	362.5 (6.5)	274.0 (6.1) / 279.2 (6.2)	135.0 (3.4)
100	19.78	443	0.8	148.1	0.2	0.0188	0.0770	0.3950	3.3	25.37	2.4	6.38	3.3	366.8 (9.3)	357.1 (9.2)	na	323.7 (9.3)	242.8 (10.1) / 247.4 (6.9)	127.9 (1.4)
101	18.51	438	1.1	147.7	0.2	0.0165	0.0842	0.3380	11.6	47.66	5.3	13.90	12.7	334.5 (3.4)	324.4 (3.0)	na	291.3 (2.8)	213.4 (2.8) / 215.4 (3.9)	125.6 (1.1)
103	21.68	514	0.8	153.5	0.2	0.0213	0.0764	0.4480	6.0	49.21	3.0	10.86	6.7	414.0 (4.2)	407.3 (3.9)	na	373.1 (3.3)	272.3 (3.1) / 286.3 (4.3)	141.0 (2.9)

TABLE B-13 (cont'd) STEAM-WATER 2φ DATA WITH T/S: 2-DN Gas Pull-Through

d = 6.32 mm   A = 3.13707×10^{-5} m^2 D = 102.3 mm

| | Mainline Conditions | | | | | | | Branchline Conditions | | | | | | | Pressure Profile (kPa) | | | | | |
Run No.	h_L (mm)	P_o (kPa)	δP_o (±kPa)	T_o (°C)	δT_o (±°C)	j_ℓ (m/s)	j_g (m/s)	$G_\ell \times 10^{-4}$ (kg/m^{2}s)	δG_ℓ (%)	G_g (kg/m^{2}s)	δG_g (%)	$x \times 10^3$	δx (%)	P_1	P_2	P_3	P_4	P_5	P_6
104	22.20	520	4.4	152.7	0.4	0.0245	0.1158	0.5300	5.6	55.47	1.6	10.44	5.9	447.8 (6.1)	439.9 (6.8)	na	408.2 (7.1)	311.7 (7.1) 324.8 (6.3)	145.9 (3.4)
105	18.51	504	5.5	150.9	0.4	0.0166	0.1812	0.3337	0.43	84.64	7.1	24.73	7.1	372.7 (7.6)	361.3 (6.5)	na	324.1 (8.1)	236.8 (8.2) 241.5 (3.3)	131.4 (2.3)
106	24.23	532	2.8	152.9	0.2	0.0242	0.0982	0.5102	1.	40.499	8.2	7.84	8.2	474.3 (7.7)	464.6 (10.3)	na	430.4 (10.6)	330.5 (10.3) 336.4 (6.9)	151.7 (3.1)
107	21.05	519	0.8	151.9	0.2	0.0223	0.1109	0.4660	8.	76.91	2.6	16.25	8.4	447.8 (6.3)	437.6 (6.4)	na	401.2 (7.6)	300.7 (8.9) 305.6 (7.1)	142.8 (3.4)
129	22.64	678	4.4	163.7	0.2	0.0284	0.1178	0.6331	4.8	98.39	1.9	15.30	5.1	585.7 (6.9)	na	554.3 (7.3)	528.1 (7.5)	398.8 (8.1) 400.3 (1.9)	165.1 (1.4)
130	22.92	683	2.5	163.5	0.2	0.0301	0.1227	0.6617	1.8	98.47	3.8	14.88	4.2	599.7 (6.3)	na	571.2 (6.7)	550.8 (6.7)	430.2 (5.4) 430.0 (1.3)	176.8 (1.1)

TABLE B-14 STEAM-WATER 2ϕ DATA WITH T/S: 3-DN Gas Pull-Through

d = 10.15 mm   A = 8.09137×10^{-5} m^2 D = 102.3 mm

	Mainline Conditions							Branchline Conditions						Pressure Profile (kPa)					
Run No.	h_l (mm)	P_o (kPa)	δP_o ($\pm$kPa)	T_o (°C)	δT_o ($\pm$°C)	j_l (m/s)	j_g (m/s)	$G_l \times 10^{-4}$ (kg/m²s)	δG_l (%)	G_g (kg/m²s)	δG_g (%)	$x \times 10^3$	δx (%)	P_1	P_2	P_3	P_4	P_5	P_6
119	17.46	298	0.8	133.8	0.2	0.0274	0.6984	0.2080	3.1	115.80	4.2	52.74	5.3	204.2 (3.1)	196.8 (2.8)	na	171.8 (2.5)	139.3 (2.0) 140.5 (2.1)	137.4 (2.0)
120	19.37	281	0.8	132.1	0.2	0.0272	0.5009	0.2060	5.0	79.43	18.8	37.10	21.1	195.3 (3.5)	187.6 (3.0)	na	163.7 (2.5)	134.1 (2.0) 132.2 (12.1)	129.9 (0.2)
121	17.29	351	1.4	139.2	0.2	0.0291	0.3855	0.2350	8.1	75.02	19.1	30.90	22.6	233.3 (4.5)	208.3 (4.1)	na	176.2 (3.9)	152.8 (2.8) 150.4 (6.7)	150.8 (2.6)
122	16.83	363	5.5	139.6	0.2	0.0262	0.4328	0.2080	1.9	87.32	10.0	40.31	10.2	239.1 (7.1)	214.6 (6.4)	na	181.7 (6.3)	156.9 (5.9) 158.6 (2.8)	156.5 (1.4)
123	16.83	333	1.9	137.4	0.2	0.0284	0.4473	0.2310	3.7	83.02	14.5	34.63	16.2	226.8 (6.6)	219.0 (6.3)	na	188.9 (6.2)	151.3 (2.8) 135.3 (3.9)	146.5 (2.3)
124	16.52	361	1.9	140.5	0.4	0.0280	0.4710	0.2280	8.1	94.17	7.1	39.92	12.3	231.0 (4.0)	224.0 (3.5)	na	192.5 (3.1)	153.7 (2.6) 143.2 (3.4)	158.5 (0.9)
125	20.54	593	3.3	159.0	0.2	0.0240	0.2640	0.1910	1.31	25.68	8.7	12.89	8.8	588.4 (3.6)	585.7 (3.9)	na	584.9 (4.1)	577.8 (1.7) 581.0 (0.7)	156.8 (1.1)
126	20.13	344	3.0	138.6	0.2	0.0240	0.1655	0.1940	3.3	31.61	9.2	16.05	12.2	330.8 (3.4)	333.7 (4.1)	na	335.6 (4.3)	331.2 (4.4) 372.6 (6.9)	167.4 (5.6)
127	22.23	549	1.9	115.5	1.0	0.0275	0.1371	0.220	8.2	40.76	5.5	18.21	11.4	542.2 (3.6)	540.3 (3.3)	na	540.1 (3.1)	540.7 (2.1) 498.3 (4.2)	159.4 (2.3)
128	20.32	540	7.8	118.0	0.8	0.0272	0.0757	0.2090	3.8	21.97	17.5	9.914	18.5	524.0 (4.3)	524.4 (5.1)	na	522.4 (5.4)	525.5 (6.1) 495.7 (3.5)	156.8 (1.4)

TABLE B-15 AIR-WATER 2ϕ DATA WITH T/S: 1B-DN   Gas Pull-Through

d = 3.76 mm   A = 1.1104×10^{-5} m^2 D = 102.3 mm

	Mainline Conditions							Branchline Conditions						Pressure Profile (kPa)					
Run No.	h_L (mm)	P_o (kPa)	δP_o (±kPa)	T_o (°C)	δT_o (±°C)	j_ℓ (m/s)	j_g (m/s)	$G_\ell \times 10^{-4}$ (kg/m²s)	δG_ℓ (%)	G_g (kg/m²s)	δG_g (%)	$x \times 10^3$	δx (%)	P_1	P_2	P_3	P_4	P_5	P_6
400	12.7	150	0	20	0.3	0.0063	0.1543	0.1370	4.2	76.9	6.6	53.04	7.8	119.5 (1.4)	114.7 (1.2)	na	108.0 (0.9)	105.7 (0.2)	103.6 (0.1)
401	15.2	149	0	20	0.3	0.0075	0.1210	0.2210	0.1	32.2	7.7	14.35	7.7	116.7 (1.5)	113.3 (1.2)	na	107.7 (0.7)	105.8 (0.2)	103.6 (0.1)
402	16.5	150	0	20	0.3	0.0098	0.1003	0.3900	0.1	5.75	7.2	1.47	7.2	114.6 (2.4)	112.3 (2.0)	na	107.7 (1.5)	105.5 (0.2)	103.6 (0.1)
403	18.1	151	0	20	0.3	0.0100	0.1025	0.5190	0.1	9.52	5.3	1.83	5.3	110.7 (1.0)	108.6 (0.7)	na	105.9 (0.6)	105.3 (0.4)	103.9 (0.1)

TABLE B-16 AIR-WATER 2ϕ DATA WITH T/S: 1 - UP Liquid Entrainment

d = 3.96 mm $A = 1.2311 \times 10^{-5}$ m^2 D = 102.3 mm

Run No.	h_l (mm)	P_o (kPa)	δP_o ($\pm$kPa)	T_o (°C)	δT_o ($\pm$°C)	j_l (m/s)	j_g (m/s)	$G_l \times 10^{-4}$ (kg/m^{2}s)	δG_l (%)	G_g (kg/m^{2}s)	δG_g (%)	$x \times 10^3$	δx (%)	P_1	P_2	P_3	P_4	P_5	P_6
200	93.0	350	9	20	na	0.0079	0.0823	0.220	0.0	227.2	9.1	93.8	9.1	221.8 (3.9)	188.4 (3.1)	na	155.5 (3.0)	112.7 (2.3) 77.4 (1.1)	103.9 (0.3)
201	99.9	491	8	20	na	0.0163	0.0242	0.753	0.1	93.7	2.6	12.3	2.6	281.8 (1.1)	239.1 (1.0)	na	190.5 (0.7)	124.8 (2.1) 92.5 (3.3)	103.4 (0.3)
202	97.5	478	9	20	na	0.0115	0.0560	0.413	0.1	211.4	2.6	48.7	2.6	252.5 (5.4)	213.6 (5.9)	na	177.3 (5.3)	121.2 (5.1) 104.3 (3.1)	103.6 (0.3)
203	95.0	467	5	20	na	0.0088	0.0679	0.308	0.1	250.3	5.3	75.2	5.3	243.9 (3.6)	213.4 (3.6)	na	177.2 (8.9)	121.0 (4.1) 96.1 (1.6)	104.2 (0.6)
204	94.5	498	8	20	na	0.0079	0.1458	0.271	0.0	573.9	8.3	174.5	8.3	254.1 (3.1)	240.9 (4.2)	na	198.8 (4.6)	129.2 (6.1) 131.1 (1.1)	103.6 (0.3)
205	95.0	412	7	20	na	0.0074	0.1232	0.237	0.0	400.5	9.6	144.8	9.6	227.7 (3.3)	213.6 (3.7)	na	173.1 (3.8)	121.4 (3.9) 117.8 (0.9)	103.3 (0.3)
206	95.0	401	39	20	na	0.0072	0.1252	0.178	0.1	396.6	8.6	182.5	8.6	214.5 (4.9)	199.7 (3.8)	na	155.8 (3.9)	100.0 (3.3) 125.2 (1.0)	109.1 (0.3)
207	94.0	493	10	20	na	0.0080	0.1512	0.252	0.1	588.0	11.1	189.2	11.1	262.5 (9.1)	247.7 (9.2)	na	198.4 (9.5)	130.2 (10.1) 139.7 (3.0)	109.9 (0.3)
208	92.5	584	13	20	na	0.0087	0.1209	0.278	0.1	881.9	7.9	240.8	7.9	296.1 (8.9)	276.7 (8.9)	na	225.5 (13.1)	142.6 (1.6) 159.3 (1.4)	110.2 (0.3)

TABLE B-17   STEAM-WATER   2φ   DATA WITH T/S: 1 - UP Liquid Entrainment

$d = 3.96$ mm $A = 1.2331 \times 10^{-5}$ m^2 $D = 102.3$ mm

		Mainline Conditions						Branchline Conditions						Pressure Profile (kPa)					
Run No.	h_L (mm)	P_o (kPa)	δP_o (+kPa)	T_o (°C)	δT_o (±°C)	j_l (m/s)	j_g (m/s)	$G_l \times 10^{-4}$ (kg/m²s)	δG_l (%)	G_g (kg/m²s)	δG_g (%)	$x \times 10^3$	δx (%)	P_1	P_2	P_3	P_4	P_5	P_6
209	92.0	369	5	139.0	0.2	0.0063	0.1323	0.127	0.1	155.9	4.7	109.6	4.7	267.5 (11.1)	258.6 (11.7)	na	221.9 (11.9)	149.2 (6.9) 148.1 (3.0)	107.6 (0.6)
210	91.2	392	4	138.0	0.6	0.0066	0.1750	0.111	0.0	224.2	11.0	167.8	11.0	267.0 (6.9)	264.3 (8.9)	na	225.0 (10.1)	155.2 (11.3) 147.3 (5.6)	103.4 (0.3)
211	88.0	444	9	147.0	0.4	0.0079	0.1909	0.216	0.1	283.8	1.7	116.3	1.7	310.1 (6.7)	300.8 (8.1)	na	261.1 (8.1)	189.8 (7.9) 218.8 (3.5)	110.8 (0.9)
212	93.0	411	7	143.0	0.4	0.0080	0.1431	0.253	0.1	212.9	2.3	77.6	2.3	285.7 (7.6)	278.1 (6.1)	na	238.7 (8.2)	182.5 (11.3) 186.0 (3.5)	111.1 (1.4)
214	91.5	441	7	147.0	1.2	0.0085	0.1323	0.214	0.1	190.0	7.3	81.9	7.3	290.0 (9.5)	282.5 (9.4)	na	241.2 (4.8)	172.4 (5.1) 187.7 (3.3)	108.8 (0.3)
215	92.0	405	4	141.0	1.0	0.0080	0.1489	0.156	0.1	199.6	5.1	113.3	5.1	280.8 (7.1)	270.9 (7.3)	na	230.2 (7.5)	161.3 (6.9) 167.8 (3.3)	109.6 (0.3)
216	96.0	435	2	143.0	0.4	0.0087	0.0988	0.217	0.1	133.9	6.1	58.1	6.1	299.8 (9.0)	293.1 (9.2)	na	259.0 (10.1)	185.7 (11.2) 190.5 (3.8)	109.9 (0.3)
217	96.0	422	3	139.0	0.2	0.0082	0.0463	0.190	0.1	70.0	3.1	35.6	3.1	324.8 (6.0)	316.8 (6.1)	na	282.6 (6.5)	208.4 (6.4) 193.1 (1.7)	110.8 (0.3)
218	95.0	402	5	141.0	0.6	0.0074	0.0653	0.181	0.0	95.7	6.1	50.3	6.1	307.5 (5.1)	295.7 (5.3)	na	255.5 (5.6)	182.4 (5.9) 175.2 (5.3)	110.2 (0.3)
219	94.0	463	4	148.7	0.4	0.0084	0.0764	0.261	0.1	101.8	6.6	39.1	6.6	317.0 (11.6)	312.5 (11.7)	na	275.0 (12.2)	197.3 (12.4) 195.4 (4.3)	104.2 (0.3)
220	93.0	424	6	145.5	0.4	0.0074	0.0854	0.173	0.0	106.7	9.9	61.5	9.9	292.0 (7.7)	282.3 (8.1)	na	241.3 (8.3)	169.6 (8.4) 178.7 (2.4)	104.5 (0.3)

TABLE B-17 (cont'd) STEAM-WATER 2ϕ DATA WITH T/S: 1 - UP Liquid Entrainment

d = 3.96 mm   A = 1.2331x10^{-5} m^2 D = 102.3 mm

| | | Mainline Conditions | | | | | | Branchline Conditions | | | | | | | | Pressure Profile (kPa) | | | |
Run No.	h_l (mm)	p_o (kPa)	δp_o (±kPa)	T_o (°C)	δT_o (±°C)	j_ℓ (m/s)	j_g (m/s)	G_ℓx10^{-4} (kg/m^{2}s)	δG_ℓ (%)	G_g (kg/m^{2}s)	δG_g (%)	xx10^3	δx (%)	p_1	p_2	p_3	p_4	p_5	p_6
221	92.0	508	6	151.9	0.6	0.0079	0.0876	0.195	0.1	131.8	3.6	63.3	3.6	362.2 (6.1)	345.3 (6.2)	na	300.8 (6.4)	219.1 (6.6) 199.3 (2.3)	106.8 (0.3)
222	93.0	463	1	156.0	0.2	0.0077	0.1838	0.160	0.1	339.4	1.3	175.3	1.3	360.1 (4.9)	344.0 (4.5)	na	297.4 (4.3)	208.3 (4.2) 219.7 (2.1)	106.2 (0.3)

B-33

TABLE B-18 AIR-WATER 2φ DATA WITH T/S: 1B - UP Liquid Entrainment

d = 3.76 mm $A = 1.1104 \times 10^{-5}$ m^2 D = 102.3 mm

		Mainline Conditions						Branchline Conditions						Pressure Profile (kPa)					
Run No.	h (mm)	P_o (kPa)	δP_o (±kPa)	T_o (°C)	δT_o (±°C)	j_ℓ (m/s)	j_g (m/s)	$G_\ell \times 10^{-4}$ (kg/m²s)	δG_ℓ (%)	G_g (kg/m²s)	δG_g (%)	$x \times 10^3$	δx (%)	P_1	P_2	P_3	P_4	P_5	P_6
223	94.5	310	8	20	na	0.0075	0.0266	0.167	0.1	71.9	4.4	41.2	4.4	185.0 (11.1)	172.2 (10.0)	na	135.2 (9.2)	109.7 (8.4)	104.8 (0.3)
224	93.0	270	8	20	na	0.0063	0.0353	0.157	7.0	83.6	3.6	84.0	3.6	163.8 (10.7)	153.6 (7.0)	na	125.5 (6.4)	108.2 (5.3)	104.8 (0.3)
228	93.0	412	10	20	na	0.0062	0.0564	0.119	0.1	203.6	1.4	146.0	1.4	239.8 (15.4)	222.4 (12.7)	na	167.1 (9.6)	116.8 (7.1)	103.1 (0.3)
230	94.5	436	17	20	na	0.0086	0.0831	0.223	1.1	318.8	1.3	125.3	1.7	243.2 (5.6)	225.6 (3.1)	na	166.7 (3.9)	115.6 (1.4)	103.4 (0.3)
231	89.0	430	15	20	na	0.0064	0.7607	0.062	0.1	563.1	1.5	491.4	4.2	245.7 (9.9)	227.7 (6.1)	na	179.9 (4.3)	133.0 (3.3)	103.6 (0.3)
232	93.0	453	14	20	na	0.0084	0.4803	0.184	0.1	355.5	1.6	147.0	4.6	257.4 (11.8)	235.7 (9.2)	na	175.9 (3.6)	121.9 (1.0)	103.4 (0.3)
233	91.0	442	14	20	na	0.0077	0.5244	0.171	0.2	388.2	1.7	195.7	1.8	252.1 (3.9)	231.0 (1.8)	na	174.6 (0.3)	121.3 (0.3)	103.1 (0.3)
234	91.5	577	18	20	na	0.0074	0.7642	0.172	0.1	565.7	1.7	252.4	1.9	367.0 (6.6)	343.3 (6.9)	na	271.2 (3.4)	149.3 (2.1)	103.6 (0.1)
235	93.5	592	18	20	na	0.0089	0.6420	0.242	0.1	475.2	2.2	145.8	2.2	369.8 (8.6)	342.7 (8.1)	na	263.9 (3.6)	139.3 (0.6)	104.2 (0.1)
236	95.0	566	16	20	na	0.0094	0.5424	0.276	0.1	402.2	1.7	111.2	2.3	352.8 (10.1)	324.6 (9.3)	na	247.0 (6.1)	130.8 (3.2)	103.6 (0.1)
237	92.0	636	17	20	na	0.0083	0.7465	0.190	0.2	552.6	1.8	190.9	3.6	396.6 (8.0)	361.9 (5.1)	na	283.3 (4.4)	153.7 (3.3)	104.2 (0.1)

TABLE B-18 (cont'd) AIR-WATER 2ϕ DATA WITH T/S: 1B - UP Liquid Entrainment

d = 3.76 mm   A = 1.1104×10^{-5} m^2 D = 102.3 mm

			Mainline Conditions					Branchline Conditions						Pressure Profile (kPa)					
Run No.	h_l (mm)	P_o (kPa)	δP_o ($\pm$kPa)	T_o (^oC)	δT_o ($\pm^oC$)	j_l (m/s)	j_g (m/s)	$G_l \times 10^{-4}$ (kg/m^2s)	δG_l (%)	G_g (kg/m^2s)	δG_g (%)	$x \times 10^3$	δx (%)	P_1	P_2	P_3	P_4	P_5	P_6
238	94.0	647	17	20	na	0.0101	0.6077	0.313	0.2	449.8	1.3	109.9	1.8	368.9 (11.3)	346.1 (10.1)	na	271.3 (9.3)	143.8 (3.9)	103.9 (0.3)
239	86.5	458	13	20	na	0.0052	0.1682	0.012	0.1	675.7	1.7	845.6	12.0	249.7 (8.9)	241.8 (13.1)	na	200.3 (7.7)	168.2 (3.9)	104.2 (0.3)
244	87.0	355	12	20	na	0.0055	0.1700	0.013	0.1	528.7	1.7	797.6	1.7	200.7 (8.9)	189.6 (6.3)	na	156.8 (6.1)	126.6 (4.1)	103.4 (0.3)
245	90.0	367	15	20	na	0.0063	0.1217	0.070	0.1	392.3	2.0	358.8	2.0	214.0 (8.6)	199.5 (6.3)	na	154.6 (2.6)	113.6 (1.7)	103.4 (0.3)
246	89.0	642	20	20	na	0.0066	0.1387	0.096	0.1	780.9	2.2	447.6	2.2	334.0 (3.6)	320.6 (6.7)	na	252.1 (4.1)	188.6 (1.9)	104.6 (0.6)
247	87.0	505	17	20	na	0.0057	0.1643	0.033	0.1	728.0	1.5	690.4	1.5	268.3 (10.1)	262.6 (6.9)	na	211.7 (7.6)	169.7 (7.6)	105.1 (0.6)
248	89.0	592	18	20	na	0.0074	0.1206	0.156	0.1	553.4	1.1	261.9	1.1	327.3 (6.8)	301.9 (7.3)	na	232.6 (8.5)	157.8 (9.1)	104.5 (0.3)
249	86.0	594	20	20	na	0.0061	0.1859	0.059	0.1	855.4	1.9	593.4	1.9	316.6 (12.8)	305.2 (13.4)	na	249.0 (10.9)	202.8 (9.8)	105.9 (0.6)
255	90.5	503	18	20	na	0.0069	0.1307	0.096	0.1	576.4	1.3	376.1	1.3	283.0 (11.3)	265.8 (6.2)	na	212.9 (3.3)	145.5 (1.1)	103.9 (0.3)
256	91.5	514	15	20	na	0.0078	0.1023	0.167	0.0	461.8	1.7	217.0	1.7	287.8 (4.6)	265.5 (6.3)	na	199.5 (1.2)	135.6 (1.1)	103.6 (0.3)
257	93.5	512	16	20	na	0.0086	0.0847	0.225	0.0	380.7	1.6	144.6	1.6	288.1 (6.1)	261.5 (4.3)	na	198.6 (5.0)	132.6 (1.6)	103.6 (0.3)
258	96.0	417	11	20	na	0.0192	0.1392	0.382	0.1	178.6	1.7	44.6	1.7	195.7 (6.4)	159.6 (7.5)	na	148.0 (8.5)	112.6 (1.5)	109.6 (3.1)

TABLE B-19 STEAM-WATER 2φ DATA WITH T/S: 1B - UP Liquid Entrainment

d = 3.76 mm   A = 1.1104x10^{-5} m^2 D = 102.3 mm

	Mainline Conditions							Branchline Conditions						Pressure Profile (kPa)					
Run No.	h_l (mm)	P_o (kPa)	δP_o (±kPa)	T_o (°C)	δT_o (±°C)	j_l (m/s)	j_g (m/s)	$G_l \times 10^{-4}$ (kg/m²s)	δG_l (%)	G_g (kg/m²s)	δG_g (%)	$x \times 10^3$	δx (%)	P_1	P_2	P_3	P_4	P_5	P_6
225	94.6	412	10	164.0	0.2	0.0079	0.0871	0.186	0.1	131.5	3.3	66.2	3.3	271.5 (12.2)	257.1 (11.6)	na	201.9 (10.1)	152.9 (4.1)	103.9 (0.)
226	94.0	275	4	147.4	0.4	0.0070	0.2827	0.093	0.0	319.3	3.4	254.8	3.4	187.7 (6.3)	178.2 (5.1)	na	142.7 (3.1)	117.2 (1.9)	104.2 (0.6)
227	96.0	293	2	150.5	0.2	0.0076	0.2828	0.124	0.0	338.1	6.1	214.9	6.1	222.5 (10.6)	207.8 (6.6)	na	104.4 (6.5)	120.0 (3.8)	104.8 (0.3)
229	97.0	378	1	142.3	0.2	0.0076	0.1082	0.178	0.1	122.2	2.4	64.3	2.4	278.1 (11.1)	261.6 (10.9)	na	209.2 (9.6)	146.5 (3.8)	104.2 (0.3)
250	92.0	436	6	148.0	0.4	0.0076	0.1418	0.143	0.1	192.1	2.3	118.3	2.3	286.8 (11.5)	273.8 (9.3)	na	211.6 (7.7)	153.7 (6.5)	103.9 (0.3)
251	94.0	433	10	147.5	0.4	0.0077	0.1197	0.159	0.1	160.8	3.0	92.0	3.0	294.7 (13.5)	277.1 (11.5)	na	223.1 (6.9)	158.2 (3.3)	103.4 (0.3)
252	95.0	497	6	152.3	0.4	0.0087	0.0802	0.230	0.0	126.9	3.2	54.0	3.2	347.9 (7.9)	331.6 (6.3)	na	272.9 (4.1)	185.5 (3.2)	105.1 (0.3)
253	96.0	450	4	148.0	0.2	0.0087	0.0959	0.184	0.1	159.9	1.9	79.9	1.9	329.9 (8.9)	300.3 (6.3)	na	244.3 (2.1)	167.8 (11.9)	105.6 (0.1)
254	95.3	523	5	153.5	0.4	0.0087	0.0950	0.223	0.1	157.7	2.4	66.1	2.4	370.0 (6.5)	338.9 (3.8)	na	268.4 (3.6)	192.3 (9.3)	104.8 (0.3)

TABLE B-20 STEAM-WATER   2φ   DATA WITH T/S: 1B - SD Gas Pull-Through

d = 3.76 mm   A = 1.1104x10^{-5} m^2 D = 102.3 mm

	Mainline Conditions							Branchline Conditions						Pressure Profile (kPa)					
Run No.	h_L (mm)	P_o (kPa)	δP_o (±kPa)	T_o (°C)	δT_o (±°C)	j_ℓ (m/s)	j_g (m/s)	G_ℓx10^{-4} (kg/m^{2}s)	δG_ℓ (%)	G_g (kg/m^{2}s)	δG_g (%)	xx10^3	δx (%)	P_1	P_2	P_3	P_4	P_5	P_6
300	58.4	486	2	151.9	0.2	0.0107	0.0168	0.4000	0.1	32.22	7.2	8.00	7.2	410.9 (6.5)	395.0 (6.9)	na	340.6 (3.5)	255.3 (1.7)	105.9 (0.3)
301	58.4	415	6	143.5	0.2	0.0113	0.0384	0.4394	0.1	63.42	2.3	14.24	2.3	363.9 (6.1)	354.5 (6.9)	na	319.9 (3.6)	249.1 (1.0)	105.6 (0.3)
302	57.2	621	6	161.0	0.2	0.0114	0.0445	0.4310	0.1	107.7	3.7	24.38	3.7	519.4 (8.2)	490.0 (10.6)	na	407.3 (4.4)	298.3 (0.7)	108.5 (0.6)
303	55.9	532	2	154.9	0.2	0.0098	0.0530	0.3450	0.0	110.7	2.1	31.14	2.1	441.4 (7.1)	418.3 (6.0)	na	352.6 (3.3)	259.3 (1.7)	105.9 (0.3)
304	54.0	410	4	145.3	0.4	0.0085	0.0512	0.2710	0.2	83.83	4.0	29.96	4.0	339.1 (9.3)	321.2 (8.6)	na	270.2 (7.8)	198.7 (7.4)	105.1 (0.1)
305	55.9	444	3	148.1	0.4	0.0093	0.0481	0.3200	0.1	84.93	2.8	25.86	2.8	371.1 (6.9)	350.4 (6.4)	na	295.1 (5.9)	216.7 (5.1)	105.4 (0.3)
306	57.2	368	2	141.5	0.2	0.0109	0.0579	0.4270	0.1	85.5	3.3	19.65	3.3	308.8 (8.7)	295.5 (8.0)	na	253.4 (7.6)	189.0 (7.1)	103.9 (0.1)
307	59.1	375	1	141.9	0.2	0.0105	0.0313	0.4080	0.0	48.20	8.4	11.69	8.4	329.6 (10.1)	320.0 (9.7)	na	286.2 (7.1)	223.3 (1.9)	104.8 (0.3)
308	54.0	362	2	140.7	0.2	0.0082	0.0714	0.2489	0.0	103.9	3.8	40.05	3.8	294.7 (5.2)	277.1 (4.9)	na	230.8 (3.9)	167.8 (3.0)	104.2 (0.1)
309	59.8	264	1	129.7	0.2	0.0093	0.0199	0.3342	0.1	43.1	5.1	12.89	5.1	227.0 (6.5)	220.8 (5.5)	na	198.1 (4.4)	157.0 (3.9)	104.2 (0.3)
310	56.2	263	1	129.7	0.2	0.0084	0.0389	0.2772	0.0	42.0	1.8	14.96	1.8	221.2 (4.1)	210.9 (3.0)	na	182.6 (2.6)	141.7 (0.7)	104.2 (0.3)

TABLE B-20 (cont'd) STEAM-WATER 2φ DATA WITH T/S: 1B - SD Gas Pull-Through

d = 3.76 mm   A = 1.1104x10^{-5} m^2 D = 102.3 mm

				Mainline Conditions				Branchline Conditions							Pressure Profile (kPa)					
Run No.	h_l (mm)	P_o (kPa)	δP_o ($\pm$kPa)	T_o (°C)	δT_o ($\pm$°C)	j_l (m/s)	j_g (m/s)	G_lx10^{-4} (kg/m^{2}s)	δG_l (%)	G_g (kg/m^{2}s)	δG_g (%)	xx10^3	δx (%)	P_1	P_2	P_3	P_4	P_5	P_6
311	54.9	263	1	129.3	0.4	0.0084	0.0391	0.2760	0.0	42.2	3.7	15.06	3.7	219.8 (3.3)	208.8 (2.6)	na	179.8 (2.1)	129.1 (1.7)	104.2 (0.3)
312	56.5	520	1	153.9	0.2	0.0099	0.0407	0.3690	0.0	83.4	2.6	22.13	2.6	434.1 (10.4)	412.9 (8.8)	na	347.2 (8.2)	255.4 (7.7)	105.9 (0.1)
313	59.1	516	1	153.2	0.2	0.0114	0.0361	0.4700	0.0	73.5	6.3	15.42	6.3	454.5 (10.2)	440.1 (9.8)	na	387.6 (8.1)	295.5 (7.7)	106.5 (0.3)
314	59.1	500	3	152.3	0.4	0.0120	0.0346	0.5070	0.1	68.3	2.7	13.30	2.7	437.1 (6.1)	425.8 (6.3)	na	385.0 (4.0)	299.0 (3.2)	107.4 (0.3)
315	56.5	509	6	152.9	0.2	0.0101	0.0444	0.3800	0.1	89.2	2.2	22.91	2.2	423.9 (7.3)	400.8 (6.7)	na	336.9 (5.7)	247.8 (4.4)	105.9 (0.3)
316	61.0	638	1	162.0	0.2	0.0127	0.0261	0.5710	0.0	64.8	13.0	11.23	13.0	567.9 (7.4)	554.7 (7.3)	na	500.3 (7.2)	385.4 (6.6)	111.6 (0.3)
317	64.1	752	1	164.3	0.4	0.0166	0.0064	0.8120	0.0	18.42	6.3	2.27	6.3	646.8 (4.5)	637.5 (4.4)	na	596.0 (3.9)	490.4 (2.2)	121.4 (0.1
318	57.8	658	8	162.7	0.2	0.0114	0.0461	0.4580	0.1	118.0	3.5	25.1	3.5	554.6 (8.5)	527.2 (6.2)	na	440.8 (5.1)	321.6 (4.9)	108.5 (0.1)
319	59.4	682	1	164.7	0.2	0.0126	0.0358	0.5400	0.1	94.9	14.4	17.26	14.4	587.9 (3.3)	568.3 (3.6)	na	497.4 (3.6)	373.4 (3.1)	110.8 (0.3)
320	61.0	542	5	155.4	0.2	0.0136	0.0204	0.6050	0.1	43.3	4.6	7.10	4.6	480.8 (5.5)	473.1 (6.1)	na	438.2 (6.3)	351.8 (1.0)	109.4 (0.6)
321	57.8	612	2	159.8	0.2	0.0117	0.0351	0.4768	0.0	84.0	2.1	17.31	2.1	524.5 (7.2)	500.6 (6.8)	na	420.6 (6.0)	308.8 (5.3)	107.9 (0.3)

TABLE B-20 (cont'd) STEAM-WATER 2φ DATA WITH T/S: 1B - SD Gas Pull-Through

$d = 3.76$ mm $\qquad A = 1.1104 \times 10^{-5}$ m^2 $\qquad D = 102.3$ mm

														Mainline Conditions			Branchline Conditions			Pressure Profile (kPa)					
Run No.	h_L (mm)	P_o (kPa)	δP_o (±kPa)	T_o (°C)	δT_o (±°C)	j_L (m/s)	j_g (m/s)	$G_L \times 10^{-4}$ (kg/m²s)	δG_L (%)	G_g (kg/m²s)	δG_g (%)	$x \times 10^3$	δx (%)	P_1	P_2	P_3	P_4	P_5	P_6
322	59.70	820	3	171.7	0.2	0.0135	0.0314	0.5641	0.0	99.0	5.8	17.26	5.8	702.1 (9.4)	677.6 (11.7)	na	579.1 (6.1)	445.5 (1.1)	139.6 (0.3)
323	57.20	783	2	169.9	0.2	0.0129	0.0356	0.5440	0.1	107.5	5.6	19.36	5.6	675.0 (8.4)	650.2 (7.8)	na	558.9 (6.8)	426.7 (6.6)	138.5 (0.3)
324	64.2	794	2	170.7	0.2	0.0159	0.0230	0.7411	0.1	70.2	6.2	9.39	8.2	721.5 (5.4)	713.3 (.50)	na	664.1 (4.4)	540.6 (3.8)	146.8 (0.3)

TABLE B-21 STEAM-WATER   2φ DATA   WITH   T/S: 1B - SD Liquid Entrainment

d = 3.76 mm   A = 1.1104x10^{-5} m^2 D = 102.3 mm

	Mainline Conditions							Branchline Conditions						Pressure Profile (kPa)					
Run No.	h_l (mm)	p_o (kPa)	δp_o (±kPa)	T_o (°C)	δT_o (±°C)	j_l (m/s)	j_g (m/s)	$G_l \times 10^{-4}$ (kg/m²s)	δG_l (%)	G_g (kg/m²s)	δG_g (%)	$x \times 10^3$	δx (%)	p_1	p_2	p_3	p_4	p_5	p_6
325	42.6	281	4	131.9	0.4	0.0051	0.2107	0.0124	0.1	241.8	0.8	661.9	0.8	187.2 (3.6)	173.5 (3.5)	na	140.1 (3.3)	110.1 (2.7)	103.9 (0.1)
326	46.4	284	2	131.7	0.4	0.0063	0.1162	0.0998	0.2	134.7	1.4	119.5	1.4	220.1 (2.1)	204.8 (2.2)	na	162.6 (1.8)	119.4 (1.1)	103.6 (0.3)
327	44.5	282	3	131.9	0.4	0.0058	0.1786	0.0567	0.1	205.6	1.0	266.1	1.0	207.7 (2.8)	191.9 (2.8)	na	150.8 (2.6)	113.8 (2.1)	103.9 (0.3)
328	47.0	259	2	129.2	0.2	0.0049	0.0975	0.0930	0.2	103.9	2.2	100.8	2.2	204.7 (1.8)	191.8 (1.7)	na	160.0 (1.6)	113.7 (1.1)	103.4 (0.3)
329	45.1	254	4	128.6	0.2	0.0049	0.1318	0.0776	0.1	137.9	1.7	151.0	1.7	195.4 (3.6)	182.7 (3.6)	na	151.8 (3.4)	109.5 (2.5)	102.8 (0.6)
330	43.2	259	2	129.2	0.2	0.0055	0.2033	0.0323	0.2	216.8	1.7	401.9	1.7	188.1 (2.5)	175.7 (2.5)	na	149.3 (2.2)	106.8 (1.5)	103.9 (0.6)
331	47.6	240	3	126.2	0.6	0.0061	0.1508	0.0955	0.1	149.4	2.4	135.3	2.4	196.7 (6.8)	184.0 (6.7)	na	149.5 (6.7)	118.3 (6.6)	105.4 (0.3)
332	45.1	247	0	127.6	0.2	0.0056	0.1757	0.0623	0.1	179.7	1.6	223.8	1.6	191.4 (1.8)	177.6 (1.6)	na	141.4 (1.6)	113.2 (1.2)	105.1 (0.3)
333	41.3	240	3	126.4	0.4	0.0048	0.2747	0.0037	0.1	273.7	1.4	878.9	1.4	150.2 (4.1)	142.1 (3.8)	na	118.9 (3.7)	107.9 (2.6)	105.4 (0.3)
334	47.0	199	1	120.4	0.2	0.0062	0.1429	0.0906	0.1	120.9	3.8	117.8	3.8	158.8 (2.0)	148.5 (1.8)	na	123.2 (1.7)	108.2 (1.3)	105.9 (0.3)
335	45.7	198	1	120.0	0.2	0.0059	0.1665	0.0703	0.2	137.9	2.8	164.1	2.8	155.9 (2.1)	145.7 (2.0)	na	121.0 (1.9)	107.3 (1.7)	104.5 (0.3)
336	43.2	198	1	120.0	0.2	0.0052	0.2065	0.0217	0.1	171.1	2.3	441.2	2.3	148.4 (1.7)	138.7 (1.6)	na	116.8 (1.3)	106.4 (0.9)	104.8 (0.1)

TABLE B-22   INCEPTION DATA FOR GAS PULL-THROUGH
AIR-WATER SYSTEM   T/S: 1B-DN, d = 3.76 mm

p_0 (kPa)	First bubble Pull-Through		Continuous gas Pull-Through		$Fr_\ell\left(\dfrac{\rho_\ell}{\Delta\rho}\right)^{0.5}$
	h_b(mm)	Error(%)	h_b(mm)	Error(%)	
175	23.3	6.2	16.5	4.4	48.29
217	23.7	6.3	18.0	4.8	61.76
249	27.9	7.4	18.4	4.9	68.90
297	27.7	7.3	20.3	5.4	79.74
297	29.2	7.7	22.4	5.9	79.74
380	30.8	8.2	20.9	5.5	95.32
437	33.7	8.9	21.6	5.7	102.59
500	36.2	9.6	23.3	6.2	108.72

TABLE B-23   INCEPTION DATA FOR GAS PULL-THROUGH
AIR-WATER SYSTEM   T/S: 2-DN, d = 6.32 mm

p_0 (kPa)	First bubble Pull-Through		Continuous gas Pull-Through		$Fr_\ell\left(\dfrac{\rho_\ell}{\Delta\rho}\right)^{0.5}$
	h_b(mm)	Error(%)	h_b(mm)	Error(%)	
143	27.4	5.0	22.3	6.3	27.00
177	31.2	4.3	26.1	5.3	36.52
212	33.8	4.0	29.3	4.7	44.92
251	36.9	3.6	30.6	4.4	51.58
281	38.2	3.5	31.8	4.3	55.18
302	41.4	3.2	33.1	4.1	58.30
336	42.0	3.2	35.0	3.8	63.64
379	43.3	3.1	36.9	3.6	66.51
406	46.5	2.9	37.6	3.6	68.42
446	na	na	38.8	3.4	72.58

TABLE B-24   INCEPTION DATA FOR GAS PULL-THROUGH
STEAM-WATER SYSTEM   T/S: 1-DN; d = 3.96 mm

P_o (kPa)	First bubble Pull-Through		Continuous gas Pull-Through		$Fr_\ell \left(\dfrac{\rho_\ell}{\Delta\rho}\right)^{0.5}$
	h_b (mm)	Error(%)	h_b (mm)	Error(%)	
170	19.1	6.7	15.9	8.0	16.12
234	20.9	6.1	17.2	7.4	22.23
305	22.2	5.7	18.4	6.9	25.38
372	23.5	5.4	19.1	6.7	26.88
441	24.1	5.0	20.3	6.3	29.32
519	25.4	4.7	20.1	6.1	32.19
556	27.0	4.4	20.9	5.9	33.49
543	27.9	4.3	21.6	5.6	35.87
653	27.9	9.0	22.2	12.5	36.89
794	28.5	8.5	22.5	11.0	42.28
883	na	na	24.1	10.5	43.16
891	na	na	24.4	10.3	43.02
925	na	na	25.1	9.0	46.79
1016	na	na	28.5	10.0	58.79

TABLE B-25   INCEPTION DATA FOR GAS PULL-THROUGH
STEAM-WATER SYSTEM   T/S: 2-DN; d = 6.32 mm

P_o (kPa)	First bubble Pull-Through		Continuous gas Pull-Through		$Fr_\ell \left(\dfrac{\rho_\ell}{\Delta\rho}\right)^{0.5}$
	h_b (mm)	Error(%)	h_b (mm)	Error(%)	
310	32.5	5.0	24.2	6.8	20.22
373	34.4	4.8	27.3	6.4	23.07
448	40.1	4.3	28.6	6.9	27.10

TABLE B-26 INCEPTION DATA FOR LIQUID ENTRAINMENT
AIR-WATER SYSTEM, T/S: 1B-UP; d - 3.76 mm

P_0 (kPa)	Onset of Liquid Entrainment		Error(%)	$Fr_g\left(\dfrac{\rho_g}{\Delta\rho}\right)^{0.5}$
	h_L (mm)	$h_b = (h_L - \dfrac{D}{2})$ (mm)		
112	67.0	15.8	3.2	12.58
114	68.0	16.8	3.0	13.92
118	72.1	21.0	2.0	24.72
120	71.3	20.1	2.5	22.87
128	69.5	18.3	2.7	21.91
172	74.5	23.3	2.0	33.98
290	76.5	25.3	2.0	45.89
420	78.5	27.3	1.8	53.07
529	80.0	28.8	2.0	62.03
543	79.5	28.3	1.8	62.10

TABLE B-27 INCEPTION DATA FOR LIQUID ENTRAINMENT
AIR-WATER SYSTEM, T/S: 2-UP; d = 6.32 mm

P_0 (kPa)	Onset of Liquid Entrainment		Error(%)	$Fr_g\left(\dfrac{\rho_g}{\Delta\rho}\right)^{0.5}$
	h_L (mm)	$h_b = (h_L - \dfrac{D}{2})$ (mm)		
104	66.8	15.6	3.2	3.95
105	68.5	17.3	2.9	4.89
109	70.0	18.8	2.7	7.52
115	72.5	21.3	2.4	11.59
125	76.5	25.3	2.0	15.04
133	79.5	28.3	1.8	19.32
149	81.5	30.3	1.7	21.12
170	83.8	32.6	1.5	23.67

TABLE B-28   INCEPTION DATA FOR LIQUID ENTRAINMENT
STEAM-WATER SYSTEM, T/S: 1B-UP, d = 3.96 mm

P_o (kPa)	Onset of Liquid Entrainment		Error(%)	$Fr_g\left(\dfrac{\rho_g}{\Delta\rho}\right)^{0.5}$
	h_L (mm)	$h_b = (h_L - \dfrac{D}{2})$ (mm)		
117	67.0	16.0	3.6	18.05
128	70.0	18.8	3.4	24.20
159	72.8	21.6	3.1	36.19
164	75.1	24.0	2.8	32.93

TABLE B-29   INCEPTION DATA FOR GAS PULL-THROUGH
AIR-WATER SYSTEM (NO CROSS FLOW IN PIPE)
T/S: 1B-SD; d = 3.76

P_o (kPa)	Onset of Gas Pull-Through		Error(%)	$Fr_\ell\left(\dfrac{\rho_\ell}{\Delta\rho}\right)^{0.5}$
	h_L (mm)	$h_b = \left(h_L - \dfrac{D}{2}\right)$ (mm)		
117	62.9	11.7	2.8	18.80
125	61.6	10.5	2.9	25.58
130	62.2	11.1	2.8	31.33
135	62.9	11.7	2.8	33.42
138	63.5	12.3	2.7	34.98
157	71.8	20.6	2.7	45.43
161	65.4	14.3	2.8	46.48
163	66.7	15.5	2.8	45.43
185	66.7	15.5	2.7	52.23
195	67.3	16.2	2.8	54.84
203	66.0	14.9	2.8	57.46
209	69.8	18.7	2.7	60.07
233	70.5	19.3	2.6	65.31
237	71.1	20.0	2.5	66.35
270	72.4	21.2	2.5	73.16
276	71.1	20.0	2.5	74.73
282	70.5	19.3	2.5	77.35
286	71.8	20.6	2.4	77.87

TABLE B-29 (Cont'd) INCEPTION DATA FOR GAS PULL-THROUGH
AIR-WATER SYSTEM (NO CROSS FLOW IN PIPE)
T/S: 1B-SD; d = 3.76

p_0 (kPa)	Onset of Gas Pull-Through		Error(%)	$Fr_\ell \left(\dfrac{\rho_\ell}{\Delta\rho}\right)^{0.5}$
	h_L (mm)	$h_b = \left(h_L - \dfrac{D}{2}\right)$ (mm)		
302	74.9	23.8	2.4	78.40
313	73.7	22.5	2.4	82.59
322	75.6	24.4	2.5	83.64
330	70.5	19.3	2.4	86.25
330	74.3	23.2	2.4	86.25
330	72.4	21.2	2.5	84.69
341	72.4	21.2	2.4	87.30
342	73.7	22.5	2.6	87.30
373	71.1	20.0	2.7	95.17
380	71.1	20.0	2.4	94.12
385	69.8	18.7	2.3	96.74
416	79.2	28.0	2.1	100.42
419	74.9	23.8	2.0	101.99
424	76.2	25.0	1.8	102.00
425	81.2	30.0	1.6	102.00
425	78.7	27.6	1.8	102.00
430	75.6	24.4	1.7	102.00
435	81.2	30.0	1.6	103.00
441	80.1	29.0	1.7	105.67
458	76.2	25.0	1.8	106.20
464	71.8	20.7	2.4	107.25
466	73.7	22.6	2.2	109.87
493	76.2	25.0	1.8	109.89

TABLE B-30   INCEPTION DATA FOR GAS PULL-THROUGH
             AIR-WATER SYSTEM   T/S: 1B-SD; d = 3.76 mm

p_0 (kPa)	Onset of Gas Pull-Through h_L (mm)	$h_b = (h_L - \frac{D}{2})$ (mm)	Error(%)	$Fr_\ell \left(\frac{\rho_\ell}{\Delta\rho}\right)^{0.5}$
114	61.0	9.9	3.2	17.75
114	61.6	10.5	3.2	18.25
115	61.6	10.5	3.2	18.27
132	63.5	12.4	3.1	32.11
133	65.4	14.3	3.0	32.48
134	63.5	12.4	3.1	32.89
135	64.8	13.7	3.1	33.42
135	64.8	13.7	3.1	33.42
138	65.4	14.3	3.0	34.98
146	64.8	13.7	3.0	39.16
149	66.0	14.9	2.9	39.69
151	67.3	16.2	2.8	40.73
176	67.9	16.8	2.8	50.14
180	73.0	21.9	2.5	52.23
183	67.9	16.8	2.8	51.18
191	71.6	20.5	2.6	54.84
198	69.9	18.8	2.7	51.00
200	67.9	16.8	2.7	57.46
208	68.6	17.5	2.7	58.51
211	67.9	16.8	2.7	60.07
222	69.9	18.8	2.7	62.69
222	76.8	25.7	2.2	62.17
236	67.3	16.2	2.7	65.31
248	72.4	21.3	2.5	66.35
265	72.4	21.3	2.5	72.11
274	69.2	18.1	2.7	73.16
284	68.6	17.5	2.7	76.82
291	71.1	20.0	2.6	78.92

TABLE B-30 (cont'd)   INCEPTION DATA FOR GAS PULL-THROUGH
AIR-WATER SYSTEM T/S: 1B-SD; d = 3.76 mm

p_0 (kPa)	Onset of Gas Pull-Through h_L (mm)	$h_b = (h_L - \frac{D}{2})$ (mm)	Error(%)	$Fr_\ell\left(\frac{\rho_\ell}{\Delta\rho}\right)^{0.5}$
297	73.0	21.9	2.5	81.01
312	70.5	19.4	2.6	83.63
318	78.1	27.0	2.1	83.63
322	73.0	21.9	2.4	83.64
351	78.7	27.6	2.1	91.49
356	83.2	32.1	2.0	93.06
380	75.6	25.5	2.2	95.17
387	76.8	25.7	2.2	97.79
460	79.5	28.4	2.0	107.25
515	80.2	29.1	2.0	112.51
600	81.7	30.6	2.0	115.19

TABLE B-31   INCEPTION DATA FOR GAS PULL-THROUGH
STEAM-WATER SYSTEM T/S: 1B-SD; d = 3.76 mm

p_0 (kPa)	Onset of Gas Pull-Through h_L (mm)	$h_b = (h_L - \frac{D}{2})$ (mm)	Error(%)	$Fr_\ell\left(\frac{\rho_\ell}{\Delta\rho}\right)^{0.5}$
237	68.0	16.9	2.8	25.99
240	66.7	15.6	2.8	26.16
243	64.8	13.7	3.1	26.28
256	69.2	18.1	2.8	27.27
289	69.9	18.7	2.8	29.05
291	68.6	17.5	2.8	29.06
345	68.6	17.5	2.8	32.03
356	70.5	19.4	2.7	32.34
400	72.4	21.3	2.6	34.85
408	73.0	21.9	2.5	35.04
464	72.4	21.3	2.5	42.09

TABLE B-31 (cont'd) INCEPTION DATA FOR GAS PULL-THROUGH
STEAM-WATER SYSTEM T/S: 1B-SD; d = 3.76 mm

| p_o (kPa) | Onset of Gas Pull-Through | | Error(%) | $Fr_\ell \left(\dfrac{\rho_\ell}{\Delta\rho} \right)^{0.5}$ |
	h_L (mm)	$h_b = (h_L - \dfrac{D}{2})$ (mm)		
488	75.9	24.8	2.3	38.70
505	77.5	26.4	2.0	39.33
517	71.8	20.7	2.7	39.93
525	73.0	21.9	2.5	40.53
544	76.8	25.7	2.2	41.17
550	74.3	23.2	2.3	41.47
593	76.2	25.1	2.2	43.32
603	73.7	22.5	2.5	43.58
619	77.5	26.4	2.0	44.27
706	74.9	23.8	2.3	47.48
726	77.5	26.4	2.0	48.47
735	76.2	25.1	2.1	48.73
776	78.7	27.6	1.9	49.85
791	76.2	25.1	2.2	51.06
846	79.4	28.3	1.9	52.52
857	76.8	25.7	2.2	53.43
877	77.5	26.4	2.0	53.78
888	76.2	25.1	2.1	54.40
904	76.2	25.1	2.1	54.92
913	75.6	24.5	2.2	55.13

TABLE B-32   INCEPTION DATA FOR LIQUID ENTRAINMENT, SIDE ORIENTATION
AIR-WATER SYSTEM, T/S: 1B-SD; d = 3.76 mm

p_o (kPa)	Onset of Liquid Entrainment		Error(%)	$Fr_g\left(\dfrac{\rho_g}{\Delta\rho}\right)^{0.5}$
	h_L (mm)	$h_b= (\frac{D}{2} - h_L)$ (mm)		
106	44.5	6.7	3.4	11.68
107	43.2	7.9	3.4	14.80
110	44.5	6.7	3.4	4.71
110	43.2	7.9	3.4	11.91
116	44.5	6.7	3.4	6.79
118	43.2	7.9	3.5	14.24
127	41.9	9.3	3.6	24.94
153	41.9	9.3	3.6	27.40
161	42.2	9.0	3.6	30.58
166	45.6	5.6	3.2	30.97
179	45.5	5.5	3.2	32.54
368	40.0	11.2	3.7	56.04
387	39.4	11.8	3.7	56.82
403	39.4	11.8	3.7	64.23
434	40.6	10.6	3.7	55.02
448	39.4	11.8	3.8	57.87
503	38.7	12.5	3.8	61.51

APPENDIX C

Error Analysis

In this appendix the uncertainties involved in the experimentally mea-
sured quantities and the calculated parameters are considered. The
uncertainties in the experimental data come from measuring devices and
recording systems. In measuring quantities such as test pipe stagna-
tion pressure and temperature, a multi-sample data is used. The error
involved in these measurements, when calculated assuming the constant
stagnation condition, is the dynamic error. This dynamic error is
associated with measured quantities in addition to the errors due to
calibration and recording system. In the present study, the steady
state data were collected for 2-4 minutes. Hence they involve uncer-
tainty due to dynamic error. The errors involved in reduced quantities
were evaluated using the standard error propagation method [27].

C.1 Errors in Basic Measurements

In these experiments the basic measured quantities are pressures,
temperatures, differential pressures, and forces (load cells). For a
given measured quantity, there are essentially three factors which
contribute to the error in measurement. These factors are dynamic
error, calibration error and error in recording the measurement. The
calibration error is the difference between the actual response of the
measuring device and the response predicted by the calibration equa-
tion. In Appendix D, the calibration equation, the rms error between
the data and the calibration curve, and the maximum error are presented.
In all the cases we find that the maximum error is less than three
times the rms error. Hence a calibration error can be taken to be the
larger of these two quantities with a confidence of interval of 99%.
As the calibration error is systematic, it is added directly to other
errors.

The recording error in the present case is the difference between the
actual emf output of the measuring device and the emf recorded by the
Auto-Data. The Auto-Data has an accuracy of ±1 in the last significant
bit, according to the manufacturer. By using a standard cell, emf
readings for about five minutes (total of 741 readings) were recorded
and it was found that less than 38 of the total readings were more
than ±0.001 V (the value of the least significant bit) different from
the mean 1.016 V, and none of the readings were more than ±0.002 V
different. The error of ±1 in the last significant bit has been con-
sidered with estimated uncertainty interval of 99% confidence. These
errors are presented in Appendix D.

The dynamic error associated with multiple-sample data has been calcu-
lated as the rms error between data and its mean. To the dynamic
error calibration error should be added to include all the errors
associated with measurements made of the multi-sample data. In the

data tables Appendix B we have presented the dynamic error for each run for temperature and pressure measurements. Since this error is stochastic, the calculated error is approximately the standard derivation. Three times this calculated value can be taken as the estimated uncertainty in measurement with 99.7% confidence level.

C.2 Errors in Reduced Quantities

The calculated parameters are mass flow rates, quality and other parameters based on one or more basic measurements. The standard error propagation method is used for calculation of the errors associated with reduced quantities.

For a function $R (a_1, a_2, a_3 \ldots a_n)$ with a_i, $i = 1, \ldots n$, as independent variables, having uncertainty for each variable a_i as δa_i, the uncertainty δR is given as

$$\delta R = \left[\left(\frac{\partial R}{\partial a_1} \delta a_1 \right)^2 + \left(\frac{\partial R}{\partial a_2} \delta a_2 \right)^2 + \ldots + \left(\frac{\partial R}{\partial a_n} \delta a_n \right)^2 \right]^{1/2} \qquad (C.1)$$

The percent of error is then given as $100 \times \frac{\delta R}{R}$.

The relative error associated with mass flow rate measured from the orifice meter is calculated as

$$\frac{\delta \dot{m}_i}{\dot{m}_i} = \left[\left(\frac{\delta Y}{Y} \right)^2 + \left(\frac{\delta C_D}{C_D} \right)^2 + \left(\frac{1}{2} \frac{\delta \rho_i}{\rho_i} \right)^2 + \left(\frac{1}{2} \frac{\delta \Delta P}{\Delta P} \right)^2 \right]^{1/2} \qquad (C.2)$$

with $i = g, \ell$ for gas and liquid respectively.

In equation (C.2) the δ's indicate the absolute uncertainty in each of the individual uncertainty components.

The uncertainty in $\Delta \dot{m}_g$ is given as

$$\delta \Delta \dot{m}_g = \frac{1}{h_{fg}} \left\{ \left[(h_{fg} - h'_{fg}) \delta \dot{m}_{gin} \right]^2 + \left[(h_\ell - h'_\ell) \delta \dot{m}_T \right]^2 + \left[(h''_\ell - h'_\ell) \delta \dot{m}_r \right]^2 \right.$$
$$\left. + \left[(h_\ell - h'_\ell) \delta \dot{m}_{gout} \right]^2 \right\}^{1/2} . \qquad (C.3)$$

In equation (C.3) the thermodynamic properties of fluid were read directly from the standard tables. The errors in the thermodynamic properties were calculated using the uncertainties in the temperature

and pressure. These are given in Table C-1. As the relative error in enthalpy is negligible in comparison with the relative error in mass measurement, the errors associated with enthalpies are not shown in equation (C.3).

The uncertainty in steam and water mass flow rates are

$$\delta \dot{m}_g = \left[(\delta \dot{m}_{gin})^2 + (\delta \dot{m}_{gout})^2 + (\delta \Delta \dot{m}_g)^2 + (\delta \dot{m}_{cond})^2 \right]^{1/2} \qquad (C.4)$$

$$\delta \dot{m}_w = \left[(\delta \dot{m}_T)^2 + (\delta \dot{m}_g)^2 \right]^{1/2} \qquad (C.5)$$

The uncertainty in mass flux in

$$\delta G_i = \delta G_i / A \qquad (C.6)$$

The error propagated in quality is

$$\delta x = \left[\left(\frac{\delta G_g}{G_g} \right)^2 + \left(\frac{\delta G_T}{G_T} \right)^2 \right] \qquad (C.7)$$

The errors associated with G_ℓ, G_g, and x are presented in Data Tables Appendix B. Table C-1 also gives the values of errors associated with parameters not covered in Data Tables.

TABLE C-1

Source of Uncertainty	Uncertainty	
Time (t)	0.22 %	
Water Level (h_L)	1.27 mm.	
Tube Diameter (d)	0.64 %	for d = 3.96 mm
	0.40 %	for d = 6.2 mm
	0.10 %	for d = 10.2 mm
Vapor density (ρ_g)	0.7 %	
liquid density (ρ_ℓ)	0.03%	
Vapor Enthalpy (h_g)	0.012%	
Liquid Enthalpy (h_ℓ)	0.08%	

APPENDIX D

Calibration of Instrumentation

D.1 Thermocouple Calibration

The iron-constantan thermocouples and the copper-constantan thermo-
couples were both calibrated at two known temperature points, viz,
freezing point of water and boiling point of water. For other tempera-
ture values the tabulated millivolt temperature charts supplied by the
manufacturer (Omega Engg. Inc.) were used to check the calibration.

For the calibration an ice junction was made with crushed ice and dis-
tilled water in an insulated thermos bottle. Both J-and T-type thermo-
couples were wired exactly as in the experimental setup. Two junctions
of the thermocouple were immersed in the $0^{\circ}C$ ice bath and were allowed
to settle to equilibrium for 5 minutes. The thermobouple responses
were recorded by the Auto-Data Eight system. The Auto-Data has resolu-
tion of 0.01 millivolts in the 0-100mV range. This corresponds to an
uncertainty in the measurement between ±0.18 and $\pm0.19^{\circ}C$ for J-type
thermocouples and between ±0.17 and $\pm0.24^{\circ}C$ for T-type thermocouples.
Both thermocouples showed no zero offset when both junctions were
immersed in the ice bath. For $100^{\circ}C$ reference point, distilled water
was boiled in a 250m beaker vigorously and the thermocouple probes
were immersed inside the boiling water with tip held 3 to 4cm above
from the bottom of beaker. The readings were observed to remain stable
and were then recorded. A higher temperature bath was created using a
heated bath of Linseed Oil. All thermocouples were calibrated for
various temperature level using a calibrated thermocouple and a preci-
sion thermometer as references in addition to the standard charts for
T-type and J-type thermocouples. For each type of thermocouple, a
calibration equation was formulated. Two sets of six thermocouples,
each for T and J-type agreed with the calibration equation within the
uncertainty of Auto-Data measurement.

D.2 Pressure Transducers

Two Statham absolute pressure transducers having range 0-790 kPa, one
Statham pressure transducers with range 0-20 MPa and two Validyne
differential pressure transducers having ranges $\pm$ 345 kPa and ±827 kPa
were all calibrated using a Crosby dead weight tester, model CD-1M.
The tester applies fluid pressure to the instrument being calibrated
and this pressure is then read directly from a balanced beam scale.
The smallest division on the beam scale is 6.89 kPa. The accuracy in
reading is estimated as ±3.45 kPa.

Calibration of each of the above transducers was started by setting

zero on the pressure scale and recording the transducer voltage output as read by the Auto-Data. The Crosby fluid pressure was then increased in a steps of size suitable for making at least fifteen readings over that transducer range. Auto-Data and Crosby pressure scale readings were recorded for each steps. The results are shown for each trans-ducer mentioned above in Tables A-1, A-2, A-3, A-7 and A-11.

The reservoir vessel level transducer had a full scale range of ±25 kPa, therefore, a different method other than the Crosby pressure scale was employed for calibration. The calibration of this transducer was done with the device installed on the reservoir. The reservoir was filled with cold (21°C) water up to the top of its constant area section. Starting with the vessel full, water was drained in units of 19.1 litres into a graduated water bottle. Transducer response was recorded as a function of the total amount of water discharged from the vessel. The graduated water bottle had a maximum uncertainty in volume measure-ment of 0.05 litres. The calibration of the reservoir vessel trans-ducer is shown in Table A-8. Six Data Sensor ±103 kPa differential pressure transducers were calibrated using an open ended mercury mano-meter. Pressure was established by setting up a pressurized air feed line with regulating valve for control of pressure. Each transducer was connected downstream of this valve via a tee, with another branch of the tee connected to the manometer. The maximum uncertainty in reading the differential height of mercury columns in the manometer was ±1.6 mm Hg corresponding to a pressure uncertainty of ±0.27 kPa. The calibration tables for these pressure transducers are presented in Tables A-4, A-5, A-6, A-12, A-13 and A-14.

D.3 Weigh Tank Load Cells

As in the case of reservoir vessel level transducer, the load cells were calibrated in-situ. Mass was added to the tank by a measured quantity of water using graduated bottle of volume 19.10 liter. Read-ings of the output of each load cell were recorded on the Auto-Data for each addition of mass of about 19.06 kg of cold water. Calibrations for each load cell are presented in Table A-9 and A-10. The readings of the two load cells LC1 and LC2 and the reservoir vessel level trans-ducer VL offer two separate methods for calculating the total dis-charged mass flow rates as described in Appendix A.

D.4 Orifice Meter Calibration

All the three orifice meters used were sharpe edged type and were identical in design. In calibrating these orifice meters cold water was used to determine the discharge coefficient C_D associated with each orifice plate. For calibration the orifice meters were hooked up with the identical set-up as was used in the experimental apparatus. The cold water from the laboratory tap supply was passed through the

orifice meter and the response of the differential pressure transducer
was recorded with Auto-Data. The water flow rate was determined by
collecting the water in a graduated bottle downstream of the orifice
meter for a interval of time measured with stop watch. Using the
standard orifice equation, the discharge coefficient for various ori-
fice plate diameters, were obtained. Table D-17 present the discharge
coefficient for different orifice plates calibrated.

For each tables of data reported in Appendix D, a quadratic calibration
equation was developed using a HP-67 programmable calculator. A least-
square fitting algorithm was employed to obtain a + bx + cx^2 calibra-
tion equations listed in the tables. These equations were used in the
data reduction program. Tables D-1 through D-16 also show the dis-
crepancy between the values of the pressure predicted by the calibra-
tion equation and that determined by the calibration instrument used;
this discrepancy is referred to as the calibration error. Also listed
are the root mean square (rms) values of calibration error. The
probable error in the measured quantity due to uncertainty in the
calibration instrument used and the error in transducer output voltage
are also presented in the tables.

TABLE D-1
Calibration of Stagnation Pressure Transducer
Gould-Statham Model PA 822-100, s/n 21442
Auto-Data Ch 1

Pressure (KPa)	Amplifier Output (mV)	Calibration Error (KPa)
101.32	0.40	3.44
135.79	1.49	-0.92
170.27	2.78	-0.28
239.21	5.21	-1.55
273.69	6.48	-0.92
308.16	7.67	2.49
377.11	10.27	0.46
445.06	12.76	1.40
480.53	14.04	1.35
515.00	15.23	-0.18
583.05	17.70	-0.75
652.90	20.21	-0.19
687.37	21.50	1.08
721.85	22.70	-0.15
790.70	25.22	0.75
825.27	26.46	0.64
859.75	27.71	0.82
928.69	30.24	2.05
997.64	32.63	-0.59
1032.11	33.93	0.74
1066.58	35.20	1.80
1135.53	37.56	-1.62

Probable Error in Pressure Reading = 3.45 KPa
Probable Error in Transducer Output Reading = 0.01 mV
Equivalent to 0.28 percent KPa
    Calibration Equation:
$P(KPa) = a+b(mV)+c(mV)^2$
    where
a = 93.714
b = 27.619
c = 0.002
The maximum error between the measured absolute pressure in the above
calibration and the prediction of the calibration equation was
3.44 KPa (= 0.30% full scale).   rms Error = 1.36 kPa.

TABLE D-2
Calibration of Differential Pressure Transducer
Validyne Model DP-15,125psid diaphram, s/n 50140
Auto-Data Ch 2

Pressure (KPa)	Amplifier Output (V)	Calibration Error (KPa)
0.00	0.000	1.37
34.47	0.194	0.24
68.95	0.397	0.53
103.42	0.591	-0.82
137.89	0.787	-1.93
206.84	1.200	-1.93
241.32	1.407	-0.53
275.79	1.617	0.27
344.74	2.027	0.94
379.21	2.241	0.94
413.68	2.451	1.26
482.63	2.868	1.03
551.58	3.283	0.00
586.05	3.492	-0.60
620.53	3.704	0.53
689.47	4.139	0.72
723.95	4.343	1.02
758.42	4.565	0.00
827.37	5.000	0.21

Probable Error in Pressure Reading = 3.45 KPa
Probable Error in Transducer Output Reading = 0.001 V
Equivalent to 0.17 KPa
    Calibration Equation:
$P(KPa) = a+b(V)+c(V)^2$
    where,
a = 1.374
b = 172.091
c = -1.370
The maximum error between the measured differential pressure in the above calibration and the prediction of the calibration equation was 1.37 KPa (= 0.17 percent full scale). rms Error = 0.82 kPa.

TABLE D-3
Calibration of Differential Pressure Transducer
Validyne Model DP-15,50psid diaphram, s/n 50139
Auto-Data Ch 3

Pressure (KPa)	Amplifier Output (V)	Calibration Error (KPa)
0.00	0.000	-0.32
13.79	0.205	0.10
34.47	0.503	0.06
68.95	1.001	0.06
82.74	1.204	0.30
103.42	1.499	0.01
137.89	1.997	0.08
158.58	2.299	0.08
172.37	2.501	0.22
206.84	2.997	-0.07
227.53	3.290	-0.27
241.32	3.495	-0.27
275.79	4.001	0.67
289.58	4.205	0.28
310.26	4.506	0.26
344.74	5.003	-0.12

Probable Error in Pressure Reading = 3.45 KPa
Probable Error in Transducer Output Reading = 0.001 V
Equivalent to 0.07 KPa
    Calibration Equation:
$P(KPa) = a+b(V)+c(V)^2$
    where
a = -0.319
b = 69.327
c = -0.076
The maximum error between the measured differential pressure in the
above calibration and the prediction of the calibration equation was
0.67 KPa (= 0.19 percent full scale). rms Error = 0.32 kPa.

TABLE D-4
Calibration of Differential Pressure Transducer
Data Sensor Model PB413B-17, s/n 434
Auto-Data Ch 4

Pressure (KPa)	Amplifier Output (mV)	Calibration Error (KPa)
0.00	3.00	0.07
4.66	3.94	0.03
10.16	5.03	-0.10
12.28	5.46	-0.09
17.78	6.59	-0.01
24.55	7.94	-0.10
33.02	9.74	0.37
42.96	11.66	0.00
53.12	13.66	0.16
59.47	14.93	-0.15
67.73	16.60	-0.15
78.73	18.77	-0.07
89.10	20.84	0.04
100.32	23.07	0.15
105.19	24.00	0.02
109.85	24.88	-0.15

Probable Error in Pressure Reading = 0.21 KPa
Probable Error in Transducer Output Reading = 0.01 mV
Equivalent to 0.05 KPa
    Calibration Equation:
$P(KPa) = a+b(mV)+c(mV)^2$
    where,
a = -14.634
b = 4.888
c = 0.004
The maximum error between the measured differential pressure in the above calibration and the prediction of the calibration equation was 0.37 KPa (= 0.34 percent full scale). rms Error = 0.13 kPa.

TABLE D-5
Calibration of Differential Pressure Transducer
Data Sensor Model PB413B-17, s/n 429
Auto-Data Ch 5

Pressure (KPa)	Amplifier Output (mV)	Calibration Error (KPa)
0.00	7.57	1.45
15.66	10.12	-2.80
20.32	11.87	0.43
27.09	13.34	0.34
35.56	15.17	0.24
42.96	16.83	0.49
51.01	18.44	-0.09
59.05	20.29	0.52
64.76	21.32	-0.35
77.89	24.11	-0.26
83.81	25.40	-0.01
91.64	27.04	0.04
98.84	28.53	0.04
106.46	30.08	-0.04

Probable Error in Pressure Reading = 0.21 KPa
Probable Error in Transducer Output Reading = 0.01 mV
Equivalent to 0.04 KPa
    Calibration Equation:
P(KPa) = $a+b(mV)+c(mV)^2$
    where,
a = -31.653
b = 4.301
c = 0.001
The maximum error between the measured differential pressure in the
above calibration and the prediction of the calibration equation was
2.8 KPa (= 2.63 percent full scale). rms Error = 0.89 kPa.

TABLE D-6
Calibration of Differential Pressure Transducer
Data Sensor Model PB413B-17, s/n 320
Auto-Data Ch 6

Pressure (KPa)	Amplifier Output (mV)	Calibration Error (KPa)
0.00	4.87	-0.31
3.81	5.82	0.45
9.95	7.00	-0.01
17.14	8.52	0.11
23.92	9.96	0.26
32.17	11.55	-0.33
40.85	13.33	-0.44
49.74	15.20	-0.32
58.63	17.23	0.57
64.55	18.29	-0.24
74.08	20.28	-0.17
79.16	21.48	0.54
86.99	22.97	-0.11
88.89	23.48	0.45
95.03	24.62	-0.18
101.17	25.91	-0.10
108.15	27.34	-0.17

Probable Error in Pressure Reading = 0.21 KPa
Probable Error in Transducer Output Reading = 0.01 mV
Equivalent to 0.05 KPa
    Calibration Equation:
P(KPa) = a+b(mV)+c(mV)^2
    where,
a = -23.726
b = 4.806
c = 0.000
The maximum error between the measured differential pressure in the
above calibration and the prediction of the calibration equation was
0.57 KPa (= 0.53 percent full scale). rms Error = 0.32 kPa.

TABLE D-7
Calibration of Differential Pressure Transducer
Gould Statham Model PA822-100, s/n 21455
Auto-Data Ch 7

Pressure (KPa)	Amplifier Output (mV)	Calibration Error (KPa)
101.32	1.70	1.45
122.00	2.39	0.49
135.79	2.81	-1.30
156.48	3.55	-0.84
170.27	4.08	0.52
190.95	4.78	-0.16
204.74	5.25	-0.52
225.43	6.02	0.79
239.21	6.46	-0.42
273.69	7.66	-0.61
308.16	8.91	0.63
342.64	10.06	-1.00
377.11	11.32	0.53
411.58	12.51	0.05
446.05	13.72	0.13
515.00	16.14	0.31
583.95	18.52	-0.67
652.90	20.98	0.63
721.85	23.41	1.06
790.79	25.75	-1.07

Probable Error in Pressure Reading = 3.45 KPa
Probable Error in Transducer Output Reading = 0.01 mV
Equivalent to 0.29 KPa
    Calibration Equation:
$P(KPa) = a + b(mV) + c(mV)^2$
    where,
a = 54.194
b = 28.580
c = -0.001
The maximum error between the measured differential pressure in the
above calibration and the prediction of the calibration equation was
1.45 KPa (= 0.18 percent full scale). rms Error = 0.75 kPa.

TABLE D-8
Calibration of Differential Pressure Transducer
Gould Statham Model PM8142-3.6, s/n 621
Auto-Data Ch   0

Volume Discharged (litre)	Amplifer Output (mV)	Calibration Error (litre)
0.00	15.00	0.56
19.17	13.75	0.51
57.37	11.10	0.83
76.47	9.68	0.10
95.57	8.25	0.98
114.67	6.93	0.16
152.87	4.18	0.48
172.04	2.72	0.01
191.165	1.28	0.08
210.30	-0.19	0.34
220.85	-0.96	0.13

Probable Error in Volume Discharge Reading = 0.05 1
Probable Error in Transducer Output Reading = 0.01 mV
Equivalent to 0.13 1
    Calibration Equation:
$V_c(Kla) = a+b(mV)+c(mV)^2$
   where,
a = 208.144
b = -12.144
c = -0.046
The maximum error between the measured volume discharge in the above
calibration and the prediction of the calibration equation was
0.98 1 (= 0.44 percent full scale). rms Error = 0.49 litre.

TABLE D-9
Calibration of Weigh Tank Load Cell
Gould Statham Model UC3 with UC4 Adapter
Auto-Data Ch 9

Mass Added (Kg)	Load Cell 1 Output (mV)	Calibration Error (Kg)
0.00	-29.00	-0.86
19.06	-27.30	0.65
38.12	-25.75	0.35
57.18	-24.20	0.06
76.24	-22.63	0.00
95.30	-21.05	0.06
114.36	-19.47	0.13
133.42	-17.91	0.05
152.53	-16.35	-0.28
171.64	-14.77	0.26
190.70	-13.20	-0.32
209.76	-11.61	-0.14
228.82	-9.98	0.53

Probable Error in Mass Added (rms) = 0.38 Kg
Probable Error in Transducer Output Reading = 0.01 mV
Equivalent to 0.12 Kg
    Calibration Equation:
$M(Kg) = a+b(mV)+c(mV)^2$
    where,
a = 350.152
b = 12.104
c = -0.000
The maximum error between the mass added reading in the above
calibration and the prediction of the calibration equation was
0.86 Kg (= 0.38 percent full scale).

TABLE D-10
Calibration of Weigh Tank Load Cell
Gould Statham Model UC3 with UC4 Adapter
Auto-Data Ch   10

Mass Added (Kg)	Load Cell 2 Output (mV)	Calibration Error (Kg)
0.00	-10.00	0.75
19.06	-8.51	-0.71
38.12	-6.87	-0.44
57.18	-5.23	-0.22
76.24	-3.58	0.06
95.30	-1.94	0.16
114.36	-0.29	0.33
133.42	1.34	0.21
152.53	2.98	0.11
171.64	4.59	-0.39

Probable Error in Mass Added (rms) = 0.41 Kg
Probable Error in Transducer Output Reading = 0.01 mV
Equivalent to 0.12 Kg
 Calibration Equation:
$M(Kg) = a+b(mV)+c(mV)^2$
 where,
a = 118.066
b = 11.632
c = -0.010
The maximum error between the mass added reading in the above calibration and the prediction of the calibration equation was 0.75 Kg (= 0.44 percent full scale).

TABLE D-11
Calibration of Absolute Pressure Transducer
Gould Statham Model PA822-3M, s/n 26888
Auto-Data Ch 11

Pressure (KPa)	Amplifier Output (mV)	Calibration Error (KPa)
101.32	-0.01	-1.26
170.27	0.07	-0.98
239.21	0.15	-0.68
308.16	0.23	-0.38
377.11	0.31	-0.05
446.06	0.39	0.29
515.00	0.47	-1.05
583.95	0.55	1.44
652.90	0.63	1.86
721.85	0.71	1.86
790.79	0.79	2.31
859.74	0.87	2.76
928.69	0.95	3.24
997.64	1.03	3.73
1066.58	1.11	4.25
1135.53	1.18	3.91
1204.48	1.26	-3.36
1273.42	1.34	2.79
1342.37	1.42	-2.21
1411.32	1.50	-1.61
1480.27	1.58	-0.99
1549.21	1.66	-0.34
1618.18	1.74	0.30
1687.11	1.82	0.99
1756.06	1.90	1.68
1825.00	1.98	2.40

Probable Error in Pressure Reading = 3.45 KPa
Probable Error in Transducer Output Reading = 0.01 mV
Equivalent to 8.65 KPa
    Calibration Equation:
P(KPa) = a+b(mV)+c(mV)^2
    where,
a = 108.721   b = 865.157   c = 1.447
The maximum error between the measured absolute pressure in the above
calibration and the prediction of the calibration equation was
4.25 KPa (= 0.23 percent full scale). rms Error = 2.13 kPa.

TABLE D-12
Calibration of Differential Pressure Transducer
Data Sensor Model PB413B-17, s/n 433
Auto-Data Ch 12

Pressure (KPa)	Amplifier Output (mV)	Calibration Error (KPa)
0.00	-0.61	-0.18
6.56	0.62	-0.83
12.06	1.76	-0.88
19.26	3.27	-0.87
25.19	4.66	-0.20
33.23	6.30	-0.47
43.18	8.51	-0.01
55.88	11.24	-0.08
63.07	12.95	-0.88
68.15	13.91	0.22
73.87	15.20	0.47
82.12	16.95	0.29
89.95	18.60	0.02
96.30	20.02	0.16
105.19	21.85	-0.40

Probable Error in Pressure Reading = 0.21 KPa
Probable Error in Transducer Output Reading = 0.01 mV
Equivalent to 0.05 KPa
   Calibration Equation:
$P(KPa) = a+b(mV)+c(mV)^2$
   where,
a = 2.752
b = 4.801
c = -0.006
The maximum error between the measured differential pressure in the above calibration and the prediction of the calibration equation was 0.88 KPa (=0.84 percent full scale). rms Error = 0.50 kPa.

TABLE D-13
Calibration of Differential Pressure Transducer
Data Sensor Model PB413B-17, s/n 342
Auto-Data Ch 13

Pressure (KPa)	Amplifier Output (mV)	Calibration Error (KPa)
0.00	0.02	-0.01
5.50	1.22	0.06
9.95	2.11	-0.27
18.20	3.97	0.12
25.61	5.60	0.29
39.16	8.47	0.10
40.46	8.74	0.06
52.07	11.20	-0.07
60.53	12.99	-0.16
68.36	14.65	-0.22
74.50	16.04	0.15
84.02	18.06	0.11
90.59	19.46	0.11
98.21	21.08	0.11
105.40	22.55	-0.16

Probable Error in Pressure Reading = 0.21 KPa
Probable Error in Transducer Output Reading = 0.01 mV
Equivalent to 0.05 KPa
    Calibration Equation:
$P(KPa) = a+b(mV)+c(mV)^2$
    where,
a = -0.098
b = 4.632
c = 0.002
The maximum error between the measured differential pressure in the above calibration and the prediction of the calibration equation was 0.29 KPa (= 0.28 percent full scale). rms Error = 0.15 kPa.

TABLE D-14
Calibration of Differential Pressure Transducer
Data Sensor Model PB4138-17, s/n 489
Auto-Data Ch 14

Pressure (KPa)	Amplifier Output (mV)	Calibration Error (KPa)
0.00	1.30	-0.08
5.72	2.57	0.18
10.37	3.51	-0.03
17.57	5.00	-0.20
24.34	6.46	-0.06
31.11	7.95	0.23
37.25	9.23	0.17
41.69	10.11	-0.08
49.74	11.80	-0.08
59.05	13.75	-0.08
66.03	15.75	-0.17
73.44	16.79	-0.09
83.39	18.86	0.08
90.59	20.36	0.10
99.05	22.07	-0.10
105.19	23.36	-0.01

Probable Error in Pressure Reading = 0.21 KPa
Probable Error in Transducer Output Reading = 0.01 mV
Equivalent to 0.05 KPa
   Calibration Equation:
$P(KPa) = a+b(mV)+c(mV)^2$
   where,
a = -6.188
b = 4.697
c = 0.003
The maximum error between the measured differential pressure in the
above calibration and the prediction of the calibration equation was
0.23 KPa (= 0.22 percent full scale). rms Error = 0.13 kPa.

TABLE D-15
Calibration of T-Type Thermocouples
Auto-Data Ch   15-20

Temperature (°C)	Amplifier Output (mV)	Calibration Error (°C)
98.3	4.1	-0.28
100.3	4.2	-0.16
111.1	4.7	-0.44
113.3	4.8	-0.55
141.9	6.2	-0.44
170.0	7.6	-0.81
171.7	7.7	0.40
212.2	9.8	-1.43
220.8	10.4	0.89

Probable Error in Temperature Reading (rms) = 0.67 °C
Probable Error in Thermocouple Output Reading = 0.01 mV
Equivalent to 0.23 °C
    Calibration Equation:
$T(°C) = a + b(mV) + c(mV)^2$
    where,
a = 6.82
b = 23.276
c = -0.252
The maximum error between the measured temperature in the above calibration and the prediction of the calibration equation was 1.43 °C (= 0.65 percent full scale).

TABLE D-16
Calibration of J-Type Thermocouples
Auto-Data Ch 21-26

Temperature ($^\circ$C)	Amplifier Output (mV)	Calibration Error ($^\circ$C)
81.7	4.3	0.69
83.6	4.4	0.57
96.7	5.1	-0.06
99.0	5.2	-0.58
100.1	5.4	0.11
111.4	5.9	-0.45
113.3	6.0	-0.56
138.4	7.4	-0.44
142.0	7.6	-0.42
170.0	9.2	0.68
211.4	11.4	-0.28
220.8	11.9	-0.42

Probable Error in Temperature Reading (rms) = 0.48 $^\circ$C
Probable Error in Thermocouple Output Reading = 0.01 mV
Equivalent to 0.17 $^\circ$C
    Calibration Equation:

$$T(^\circ C) = a + b(mV) + c(mV)^2$$
    where,
a = 6.95
b = 17.324
c = 0.051
The maximum error between the measured temperature in the above calibration and the prediction of the calibration equation was 0.69 $^\circ$C (= 0.31 percent full scale).

TABLE D-17
Discharge Coefficients for Orifice Meters

Orifice Plate Diameter (mm)	C_D	Standard Deviation (percent)
2.56	0.999	1.21
3.86	0.785	1.07
5.03	0.754	1.93
6.37	0.877	2.75